AD-A065 410 FEDERAL AVIATION ADMINISTRATION WASHINGTON D C SYSTE--ETC F/G 4/1
FEDERAL AVIATION ADMINISTRATION - FLORIDA INSTITUTE OF TECHNOLO--ETC(U)
MAR 79

UNCLASSIFIED FAA-RD-79-6 NL

1 OF 2
AD A065410

REPORT NO. FAA-RD-79-6

LEVEL II

12

B.S.

AD A065410

DDC FILE COPY

FEDERAL AVIATION ADMINISTRATION-FLORIDA INSTITUTE OF TECHNOLOGY WORKSHOP ON GROUNDING AND LIGHTNING TECHNOLOGY

MARCH 6-8, 1979
MELBOURNE, FLORIDA

Prepared By

U.S. DEPARTMENT OF TRANSPORTATION
FEDERAL AVIATION ADMINISTRATION
Systems Research & Development Service
Washington, D.C. 20590

NOTICE

This document is disseminated under the sponsorship of the Department of Transportation in the interest of information exchange. The United States Government assumes no liability for its contents or use thereof.

Technical Report Documentation Page

1. Report No.	2. Government Accession No.	3. Recipient's Catalog No.
(14) FAA-RD-79-6 ✓		

4. Title and Subtitle	5. Report Date
(6) Federal Aviation Administration -Florida Institute of Technology Workshop on Grounding and Lightning Technology Held on 6-8 March 1979, Melbourne, Florida.	(11) Mar 79
	6. Performing Organization Code
7. Author(s)	8. Performing Organization Report No. (12) 157p.
9. Performing Organization Name and Address Florida Institute of Technology ✓ Department of Electrical Engineering Melbourne, Florida 32901	10. Work Unit No. (TRAIS)
	11. Contract or Grant No.
12. Sponsoring Agency Name and Address Department of Transportation Federal Aviation Administration Washington, DC 20590	(13) Type of Report and Period Covered Final rept. March 6-8, 1979
	14. Sponsoring Agency Code ARD-350

15. Supplementary Notes

A043 708

16. Abstract

A state-of-art review and background research reveals a number of opinions as to the preferred techniques for providing grounding and lightning protection of electronic equipment and systems. The Systems Research and Development Service and the Flight Standards Service of the Federal Aviation Administration in conjunction with the Florida Institute of Technology conducted a workshop which brought together distinguished experts in the fields of grounding, lightning phenomenology and transient protection. This year the format of the workshop was expanded to include the effects of direct strikes and induced lightning on aircraft and their contents as well as lightning detection and warning systems. This report contains the papers presented at the workshop. A supplementary report will be issued containing the papers which were not available for printing before the workshop.

17. Key Words	18. Distribution Statement
Grounding, lightning protection, lightning detection, EMP, Transient protection, aircraft.	Document is available throught the National Technical Information Service, Springfield, VA 22151.

19. Security Classif. (of this report)	20. Security Classif. (of this page)	21. No. of Pages	22. Price
UNCLASSIFIED	UNCLASSIFIED	153	

Form DOT F 1700.7 (8-72) Reproduction of completed page authorized

METRIC CONVERSION FACTORS

Approximate Conversions to Metric Measures

Symbol	When You Know	Multiply by	To Find	Symbol
		LENGTH		
in	inches	*2.5	centimeters	cm
ft	feet	30	centimeters	cm
yd	yards	0.9	meters	m
mi	miles	1.6	kilometers	km
		AREA		
in^2	square inches	6.5	square centimeters	cm^2
ft^2	square feet	0.09	square meters	m^2
yd^2	square yards	0.8	square meters	m^2
mi^2	square miles	2.6	square kilometers	km^2
	acres	0.4	hectares	ha
		MASS (weight)		
oz	ounces	28	grams	g
lb	pounds	0.45	kilograms	kg
	short tons (2000 lb)	0.9	tonnes	t
		VOLUME		
tsp	teaspoons	5	milliliters	ml
Tbsp	tablespoons	15	milliliters	ml
fl oz	fluid ounces	30	milliliters	ml
c	cups	0.24	liters	l
pt	pints	0.47	liters	l
qt	quarts	0.95	liters	l
gal	gallons	3.8	liters	l
ft^3	cubic feet	0.03	cubic meters	m^3
yd^3	cubic yards	0.76	cubic meters	m^3
		TEMPERATURE (exact)		
°F	Fahrenheit temperature	5/9 (after subtracting 32)	Celsius temperature	°C

*1 in = 2.54 (exactly). For other exact conversions and more detailed tables, see NBS Misc. Publ. 286, Units of Weights and Measures, Price $2.25, SD Catalog No. C13.10:286.

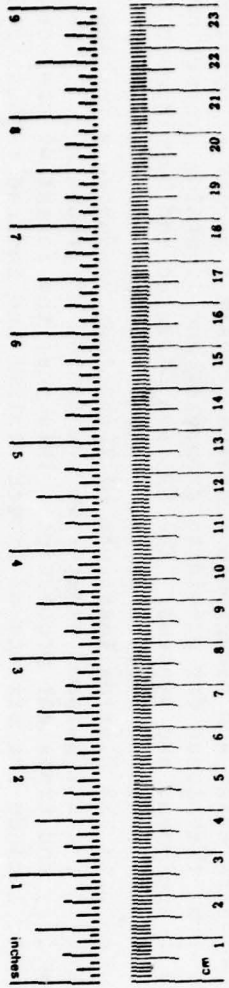

Approximate Conversions from Metric Measures

Symbol	When You Know	Multiply by	To Find	Symbol
		LENGTH		
mm	millimeters	0.04	inches	in
cm	centimeters	0.4	inches	in
m	meters	3.3	feet	ft
m	meters	1.1	yards	yd
km	kilometers	0.6	miles	mi
		AREA		
cm^2	square centimeters	0.16	square inches	in^2
m^2	square meters	1.2	square yards	yd^2
km^2	square kilometers	0.4	square miles	mi^2
ha	hectares (10,000 m^2)	2.5	acres	
		MASS (weight)		
g	grams	0.035	ounces	oz
kg	kilograms	2.2	pounds	lb
t	tonnes (1000 kg)	1.1	short tons	
		VOLUME		
ml	milliliters	0.03	fluid ounces	fl oz
l	liters	2.1	pints	pt
l	liters	1.06	quarts	qt
l	liters	0.26	gallons	gal
m^3	cubic meters	35	cubic feet	ft^3
m^3	cubic meters	1.3	cubic yards	yd^3
		TEMPERATURE (exact)		
°C	Celsius temperature	9/5 (then add 32)	Fahrenheit temperature	°F

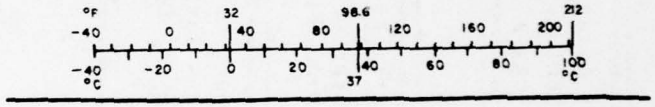

CONTENTS

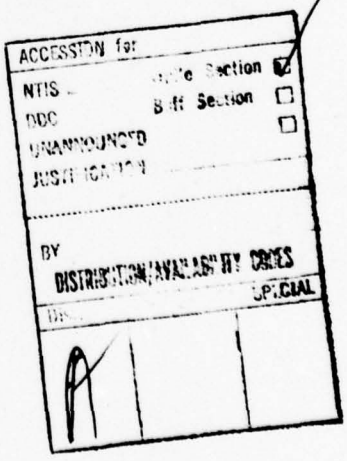

RETURN STROKE LIGHTNING CHANNEL MODEL

DENNIS W. QUINN
Mathematician
Applied Mathematics Group
Structures Division
Flight Dynamics Laboratory
Wright-Patterson AFB, OH 45433

BIOGRAPHY

Dennis W. Quinn is a mathematician in the Applied Mathematics Group in the Structures Division of the Flight Dynamics Laboratory at Wright-Patterson Air Force Base. He received his B.A. in 1969, M.S. in 1971 and Ph.D. in 1973 in mathematics at the University of Delaware. Between May, 1969 and September, 1971, he worked as a mathematician in the Elastomers Laboratory of the E. I. DuPont Company at Chestnut Run, Wilmington, Delaware. Between September, 1973 and November, 1974, he was a Resident Research Associate of the National Research Council at the Aerospace Research Laboratories, Wright-Patterson AFB. Between November, 1974 and June, 1975, he was a mathematician in the Applied Mathematics Laboratory of the Aerospace Research Laboratories. Since June, 1975 he has been in the Applied Mathematics Group in the Flight Dynamics Laboratory.

ABSTRACT

In this paper, transmission line theory is used to model the current waveform in a lightning flash to ground. By adjusting the resistance, inductance, capacitance, and the initial voltage distribution within the channel, all within reasonable limits, we are able to construct waveforms with rise times of between 1 and 10 microseconds and times to one half of peak value of between 10 and 250 microseconds. These waveforms are then used to compute electrical and magnetic fields to determine indirect as well as direct effects on aircraft.

I. INTRODUCTION

In this paper we investigate the behavior of the lightning current waveform and voltage distribution as functions of both time and altitude. The approach is to use a mathematical model of a lightning stroke which reduces to the transmission line equation and then to solve these equations. Three different solutions are presented and analyzed. If the resistance, conductance, inductance and capacitance are constant and the boundary data are suitable, a closed form exact solution exists. An alternative computational method is to use a fourier series approach. However, this method has serious drawbacks which will be discussed. A third possibility, and one which works in the case of non-constant coefficients and the most general boundary data, is a finite difference method. In Section II the basic equations will be exhibited. In Sections III, IV and V, we will derive and discuss successively the exact solution, the finite difference solution and the fourier series solution. In Section VI, the three methods will be compared.

It is generally agreed (see Bewley[1], Uman[2], Wagner[3]) that a typical lightning stroke begins with the propagation of a negatively charged channel or streamer, called the stepped leader, from the cloud to the ground. When the leader reaches the ground or joins with a second leader propagating up from the ground, the heavy current which characterizes the main stroke (also called the return stroke) begins. Until recently, a model developed by Bruce and Golde[4] has had widespread use. However, this model describes the current flowing in the main stroke as only a function of time which is of the form

$$i = i_0 \left(e^{-\alpha t} - e^{-\beta t}\right).$$

The Bruce-Golde model is plotted in figure 1 for representative values of α and β.

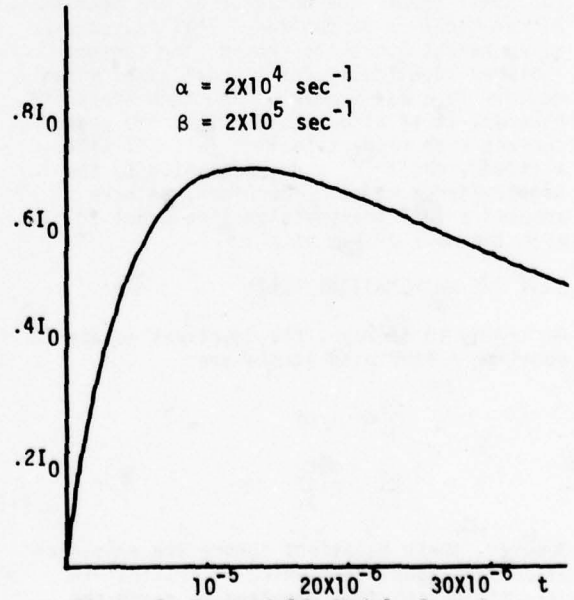

Figure 1 Bruce-Golde Model, I vs t

As a generalization of the Bruce-Golde model, Dennis and Pierce[5] considered the current in the main stroke to be of the form

$$i = i_0 \left(e^{-\alpha(t-x/u)} - e^{-\beta(t-x/u)}\right).$$

Although this modification corrects the defect of the Bruce-Golde model of no dependence on height, the Dennis-Pierce model has its own defects. In figure 2, the Dennis-Pierce current function is plotted for representative values of α, β and u.

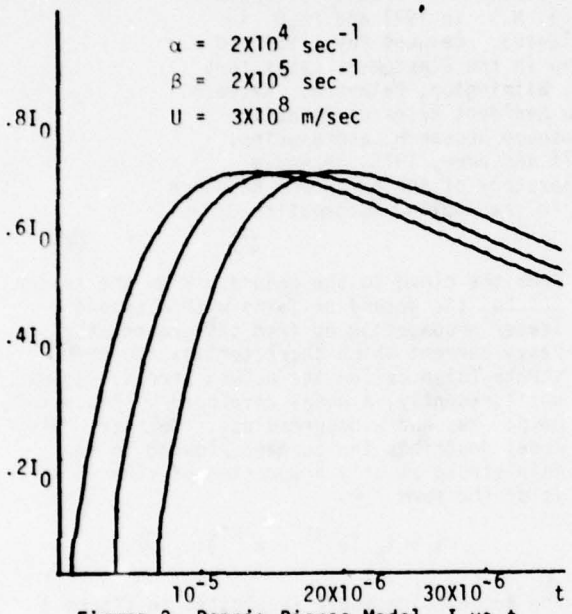

Figure 2 Dennis-Pierce Model, I vs t

For small times, the behavior of the Dennis-Pierce model is as desired. That is, at a given height above the ground, the current vanishes identically for a short time, rises rapidly to a maximum value and then drops off. However, it is also required that the peak current with respect to time fall off with altitude, and this is not satisfied by the Dennis-Pierce model. Therefore, we have adopted a full transmission line model in line with the work of Kim et al[6].

II. THE MATHEMATICAL MODEL

According to Bewley[1], the equations to use in modeling a lightning stroke are:

$$\frac{\partial v}{\partial x} = - Ri$$

$$\frac{\partial i}{\partial x} = C \frac{\partial v}{\partial t} \qquad (1)$$

However, these equations ignore the existence of an inductance term which is critical in determining the time required to reach the initial peak current. Therefore, following Kim et al[6] we propose to use the telegraph equation with all terms included.

$$\frac{\partial v}{\partial x} + L \frac{\partial i}{\partial t} + Ri = 0 \qquad (2a)$$

$$\frac{\partial i}{\partial x} + C \frac{\partial v}{\partial t} + GV = 0 \qquad (2b)$$

We now assume that the energy loss due to the conductance term is small compared to the other equations, so that G = 0.

If equations (2) are combined, then both i and v satisfy the equation:

$$\frac{\partial^2 w}{\partial x^2} - LC \frac{\partial^2 w}{\partial t^2} - RC \frac{\partial w}{\partial t} = 0 \qquad (3)$$

Again following Kim et al[6], we note that at or near peak current $\frac{di}{dt} \simeq 0$ and equation (3) for the current reduces to the wave equation:

$$\frac{\partial^2 i}{\partial x^2} - LC \frac{\partial^2 i}{\partial t^2} = 0$$

so that LC is related to the speed of propagation of the peak current. In fact, we have $V = 1/\sqrt{LC}$. Therefore, we agree with Kim et al that the inductance term should be included.

The boundary condition at X = 0, the ground, and at x = H, the cloud height and the initial condition at t = 0 need to be specified. First, the voltage at the ground is assumed to be zero while the current at the cloud is assumed to be a small constant value which is taken to zero.

Hence, the boundary conditions are:

$$v\ (0, t) = 0 \qquad (4a)$$

$$i\ (H, t) = 0 \qquad (4b)$$

At the initial time t = 0, the voltage distribution is assumed to be a known constant except at the ground where it rapidly decreases to zero, while the time derivative of the current at t = 0 is assumed be vanish identically. Hence, the initial conditions are:

$$v\ (x, 0) = V_o \qquad (5a)$$

$$\frac{\partial i}{\partial t}\ (x, 0) = 0 \qquad (5b)$$

If equation (2a) is evaluated at x = H and (4b) is used, then we have:

$$\frac{\partial v}{\partial x}\ (H, t) = 0 \qquad (6)$$

Now, evaluating equation (2a) at t = 0 and substituting in equation (5a) and (5b), one obtains that $i(x, 0) \simeq 0$ except at the ground. If this is now substituted into equation (2b), which has been evaluated at t = 0, one obtains that

$$\frac{\partial v}{\partial t}\ (x, 0) = 0 \qquad (7)$$

We now have that v satisfies the differential equation (3), initial conditions (5a) and (7) and boundary conditions (4a) and (6). For ease of later reference, we now write these as:

$$\frac{\partial^2 v}{\partial x^2} - LC\,\frac{\partial^2 v}{\partial t^2} - RC\,\frac{\partial v}{\partial t} = 0 \qquad (8a)$$

$$v\,(x, 0) = V_o \qquad (8b)$$

$$\frac{\partial v}{\partial t}\,(x, 0) = 0 \qquad (8c)$$

$$v\,(0, t) = 0 \qquad (8d)$$

$$\frac{\partial v}{\partial x}\,(H, t) = 0 \qquad (8e)$$

These constitute a well-posed initial-boundary value problem for a hyperbolic partial differential equation. Once we have solved for v, we can then integrate equation (2b) to determine i(X, t), using equation (4b) as an initial (or final) condition.

III. THE EXACT SOLUTION

In this section we will use the Rieman Method[7] to obtain an exact closed form solution to the problem described by equations (8) in the case of constant coefficients. We follow the development of reference (8). If constants K and α are defined by $K = \frac{R}{L}$ and $\alpha = 1/\sqrt{LC}$ then a new function U(X, t) is defined by:

$$U(X, t) = v(X, t)\, e^{\frac{K}{2}t},$$

and U satisfies the equations

$$\frac{\partial^2 U}{\partial t^2} - \frac{K^2}{4}\,U - \alpha^2\,\frac{\partial^2 U}{\partial x^2} = 0 \qquad (9a)$$

$$U(X, 0) = V_o \qquad (9b)$$

$$\frac{\partial U}{\partial t}\,(X, 0) = \frac{K}{2}\,V_o \qquad (9c)$$

$$U\,(0, t) = 0 \qquad (9d)$$

$$\frac{\partial U}{\partial x}\,(H, t) = 0 \qquad (9e)$$

Let (X_o, t_o) be a point in $[(X, t);\ X > 0,\ t > 0]$ such that $X_o - \alpha t_o \geq 0$. If equation (9a) is multiplied by an arbitrary function W(x,t) having two continuous derivatives and integrated on the domain of dependence then we have

$$0 = \int_o^{t_o}\int_{X_o+\alpha(t-t_o)}^{X_o+\alpha(t_o-t)} W\left[\frac{\partial^2 U}{\partial t^2} - \alpha^2\,\frac{\partial^2 U}{\partial X^2} - \frac{K^2}{4}U\right] dX\, dt$$

$$= \iint\left[\frac{\partial}{\partial t}\left(W\,\frac{\partial U}{\partial t} - \frac{\partial W}{\partial t}\,U\right) + \alpha^2\,\frac{\partial}{\partial X}\left(\frac{\partial W}{\partial X}\,U - W\,\frac{\partial U}{\partial X}\right)\right.$$

$$\left. + U\left[\frac{\partial^2 W}{\partial t^2} - \alpha^2\,\frac{\partial W}{\partial X^2} - \frac{K^2}{4}\,W\right]\right\} dX\, dt \qquad (10)$$

But if W also satisfies equation (9a) then equation (10) reduces to

$$0 = \int_o^{t_o}\int_{X_o+\alpha(t-t_o)}^{X_o+\alpha(t_o-t)} \left[\frac{\partial}{\partial t}\left(W\frac{\partial U}{\partial t} - \frac{\partial W}{\partial t}\,U\right)\right.$$

$$\left. + \alpha^2\,\frac{\partial}{\partial X}\left(\frac{\partial W}{\partial X}\,U - W\,\frac{\partial U}{\partial X}\right)\right] dX\, dt \qquad (11)$$

If we now make the change of variables

$$\xi = X - \alpha t$$

$$\eta = X + \alpha t$$

then equation (11) becomes

$$0 = \int_{\eta_1}^{\eta_2}\int_{\xi_1}^{\eta} \frac{\partial}{\partial \xi}\left(U\,\frac{\partial W}{\partial \eta} - W\,\frac{\partial U}{\partial \eta}\right) d\xi\, d\eta$$

$$+ \int_{\xi_1}^{\xi_2}\int_{\xi}^{\eta_2} \frac{\partial}{\partial \eta}\left(U\,\frac{\partial W}{\partial \xi} - W\,\frac{\partial U}{\partial \xi}\right) d\eta\, d\xi \qquad (12)$$

where the limits of integration are indicated in the diagram

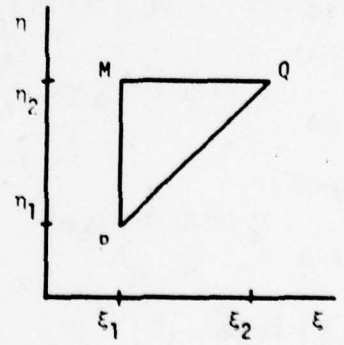

Now if $\frac{\partial W}{\partial \eta} = 0$ on the line $\xi = \xi_1$ and $\frac{\partial W}{\partial \xi} = 0$ on the line $\eta = \eta_2$ then, after performing the integration of exact differentials, equation (12) becomes

$$W(M)\,U(M) = [W(P)\,U(P) + W(Q)\,U(Q)]/2$$

$$+ \int_P^Q \left(W\,\frac{\partial U}{\partial \eta} - U\,\frac{\partial W}{\partial \eta} + U\,\frac{\partial W}{\partial \xi} - W\,\frac{\partial U}{\partial \xi}\right) dS \qquad (13)$$

where S is arc length along the line segment $\overline{PQ}$.

In ξ, η coordinates W must satisfy the equations:

$$\frac{\partial^2 W}{\partial \xi \partial \eta} + \frac{K^2}{16\alpha^2} W = 0$$

$$\frac{\partial W}{\partial \eta} = 0 \text{ on } \xi = \xi_1$$

$$\frac{\partial W}{\partial \xi} = 0 \text{ on } \eta = \eta_2 \qquad (14)$$

But if a new variable τ is introduced to be

$$\tau = \frac{K}{2\alpha} (\xi - \xi_1)^{1/2} (\eta - \eta_2)^{1/2}$$

then W satisfies the equation

$$\frac{d^2 W}{d\tau^2} + \frac{1}{\tau} \frac{dW}{d\tau} + W = 0$$

so that

$$W(\xi,\eta) = J_o(\frac{K}{2\alpha} (\xi - \xi_1)^{1/2} (\eta - \eta_2)^{1/2})$$

satisfies equation (14) and is the desired function for equation (13). Moreover W(M) = W(P) = W(Q) = 1 so that equation (13) becomes

$$U(M) = [U(P) + U(Q)]/2$$

$$+ \int_P^Q (J_o \frac{\partial U}{\partial \eta} - U \frac{\partial J_o}{\partial \eta} + U \frac{\partial J_o}{\partial \xi} - J_o \frac{\partial U}{\partial \xi}) \, dS$$

If we now transform back to X, t coordinates we arrive at the result

$$U(X, t) = (U(X - \alpha t, 0) + U(X + \alpha t, 0))/2$$

$$+ \frac{1}{2\alpha} \int_{X-\alpha t}^{X+\alpha t} J_o(\hat{\sigma}) \frac{\partial U}{\partial t} (S, 0) \, dS$$

$$- \frac{K^2 t}{8} \int_{X-\alpha t}^{X+\alpha t} J_o'(\hat{\sigma})/\hat{\sigma} \, U(S, 0) \, dS$$

where $\hat{\sigma} = \frac{K}{2} \left[\frac{(S-X)^2}{\alpha^2} - t^2 \right]^{1/2}$

However, since $X - \alpha t \leq S \leq X + \alpha t$, $(S- X)^2/\alpha^2 - t^2 < 0$, so we will define

$\sigma = \frac{K}{2} (t^2 - \frac{(S-X)^2}{\alpha^2})^{1/2} = i\hat{\sigma}$ and the representation for U becomes

$$U(X, t) = (U(X - \alpha t, 0) + U(X + \alpha t, 0))/2$$

$$+ \frac{1}{2\alpha} \int_{x-\alpha t}^{X+\alpha t} I_o(\sigma) \frac{\partial U}{\partial t} (S, 0) \, dS$$

$$+ \frac{K^2 t}{8C} \int_{X-\alpha t}^{X+\alpha t} U(S, 0) I_1(\sigma)/\sigma \, dS \qquad (15)$$

where I_o and I_1 are standard modified bessel functions.

In order for equation (15) to be a solution of equation (8) U(S, 0) must have two continuous derivatives and $\frac{\partial U}{\partial t}$ (S, 0) must have one continuous derivative. Moreover, for $X - \alpha t < 0$, we need to know U(S, 0) and $\frac{\partial U}{\partial t}$ (S, 0) for $S < 0$. To accomplish this we define V_o of equation (8b) to be $V_o(X)$ where

$$V_o(X) = V_o X^2 (3-2X/100)/10000 \text{ for } 0 \leq X \leq 100 \text{ meter}$$

$$= V_o \text{ for } 100 \leq X_o$$

$$= -V_o(-X) \text{ for } X < 0 \qquad (16)$$

Then $U(X, 0) = V_o(X)$ and $\frac{\partial U}{\partial t} (X, 0) = \frac{K}{2} V_o(X)$ in equation (9b) and (9c). In this section we will restrict (X, t) so that $X + \alpha t \leq H$ so boundary condition (9e) will not be a concern. In Section VI we will show that the finite difference method gives results identical with the exact solution of this section, so that for computational purposes one can use finite differences. With the inclusion of equation (16), equation (15) may now be evaluated for particular values of (X, t) satisfying $X + \alpha t < H$. One then obtains a solution of equations (8) by using the fact that $v(X, t) = U(X, t) e^{-\frac{K}{2}t}$, that $K = \frac{R}{L}$ and that $\alpha^2 = 1/LC$.

IV. FINITE DIFFERENCE SOLUTION

For a background of finite difference theory, we recommend Reference (9) Chapter 9. We will briefly describe our derivation.

If we expand the functions V(X + h, t) and V(X - h, t) a Taylor series about h = 0 we obtain

$$V(X+h,t) = V(X,t) + h \frac{\partial V}{\partial X} (X,t) + \frac{h^2}{2} \frac{\partial^2 V}{\partial X^2} (X,t) + O(h^3)$$

$$V(X-h,t) = V(X,t) - h \frac{\partial V}{\partial X} (X,t) + \frac{h^2}{2} \frac{\partial^2 V}{\partial X^2} (X,t) + O(h^3)$$

Now if we subtract V(X-h,t) from V(X+h,t) we obtain

$$V(X+h,t) - V(X-h,t) = 2h \frac{\partial V}{\partial X} (X,t) + O(h^3)$$

Therefore we have that

$$\frac{\partial V}{\partial X}(X,t) = (V(X+h,t) - V(X-h,t))/2h + O(h^2)$$

What this tells us is that the difference quotient $(V(X+h,t) - V(X-h,t))/2h$ is a second order approximation of the derivative $\frac{\partial V}{\partial X}$ and that the truncation error is of the order h^2. Similarly we can approximate second derivatives by

$$\frac{\partial^2 V(X,t)}{\partial X^2} = \frac{V(X+h,t) - 2V(X,t) + V(X-h,t)}{h^2} + O(h^2)$$

so that equation (8a) may be written as

$$\frac{V(X+\Delta X,t) - 2V(X,t) + V(X-\Delta X,t)}{\Delta X^2} + O(\Delta X^2)$$

$$-LC\left[\frac{V(X,t+\Delta t) - 2V(X,t) + V(X,t-\Delta t)}{\Delta t^2} + O(\Delta t^2)\right]$$

$$-RC\left[\frac{V(X,t+\Delta t) - V(X,t-\Delta t)}{2\Delta t} + O(\Delta t^2)\right] = 0$$

Therefore, if we drop the $O(\Delta X^2)$ and $O(\Delta t^2)$ terms and simplify, we have

$$V(X,t+\Delta t)\left(1+\frac{R\Delta t}{2L}\right) = 2V(X,t) + V(X,t-\Delta t)$$

$$\left(\frac{R\Delta t}{2L} - 1\right) + \frac{\Delta t^2}{LC\Delta X^2}[V(X+\Delta X,t) - 2V(X,t)]$$

$$+ V(X-\Delta X,t)$$

Since this is an explicit scheme, for stability reasons (see [9, p489]), we must restrict Δt so that $\Delta t \leq \Delta X\sqrt{LC}$. We choose $\Delta t = \Delta X\sqrt{LC}$ so that $\frac{\Delta t^2}{LC\Delta X^2} = 1$ and equation (17) becomes

$$V(X,t+\Delta t)\left(1+\frac{R\Delta t}{2L}\right) = V(X,t-\Delta t)\left(\frac{R\Delta t}{2L} - 1\right)$$

$$+ V(X+\Delta X,t) + V(X-\Delta X,t) \qquad (18)$$

This equation may now be used to generate a solution of equations (8). The results will be discussed in Section VI.

V. FOURIER SERIES SOLUTION

A third alternative for solving equations (8) is to use separation of variables. If we assume $V(X,t)$ is the produce of a function of X and a function of t, then

$$V(X,t) = f(X)\,g(t)$$

and equation (8a) becomes

$$f''(X)g(t) - LCf(X)g''(t) - RCf(X)g'(t) = 0$$

or

$$f''/f = LC\,g''/g + RC\,g'/g = -\lambda_n^2$$

where λ_n is a separation constant to be determined.

Therefore f and g satisfy

$$f''(X) + \lambda_n^2 f(X) = 0$$

and

$$g''(t) + R/L\,g'(t) + \lambda_n^2/LC\,g(t) = 0$$

Because of boundary condition (8d) and (8e)

$$f(X) = A_n \sin \lambda_n X$$

where $\lambda_n = \frac{(2n+1)\pi}{2H}$ for $n=0, \pm1, \pm2, \cdots$

Also, because of initial condition (8c),

$$g(t) = B_n\left[e^{(-R/2L+S)t} + (S-R/2L)e^{(-R/2L-S)t}/(S+R/2L)\right]$$

where $S = (R^2/4L^2 - \lambda_n^2/LC)^{1/2}$

Therefore, a function of the form

$$V(X,t) = \sum_{n=0}^{\infty} A_n \sin \lambda_n X\left[e^{(S-R/2L)t} + (S-R/2L)\,e^{(-S-R/2L)t}/(S+R/2L)\right] \qquad (19)$$

satisfies conditions (8c), (8d) and (8e) and if the series converges after two derivatives are taken under the summation, it also satisfies (8a). To satisfy condition (8b) we use the orthogonality of the sine function. That is,

$$\int_0^H \sin \lambda_n X \sin \lambda_k X = 0 \text{ if } k \neq M$$

$$= H/2 \text{ if } k = M$$

Hence, if equation (19) is evaluated at t=0 and then multipled by $\sin \lambda_k X$ and integrated from 0 to H we obtain

$$\int_0^H V(X,0) \sin \lambda_k X\,dX = A_k \frac{H}{2}\left[1+(S-R/2L/(S+R/2L)\right] \qquad (20)$$

Equation (20) is used to determine the coefficients A_k.

VI. COMPARISON OF THE METHODS

In figure 3, $V(X,t)$ is plotted versus t for three different values of X using the exact solution method of Section III. The integrals were evaluated using a 40 point trapazoidal

rule. This number of points was needed to avoid spurious oscillations in the solution for values of t greater than 7×10^{-6}. This is due to the fact that the interval of integration is $(X-\alpha t, X+\alpha t)$ and therefore increases in length as t increases. Each integration required approximately one minute of calculation time on the Hewlett Packard 9830, so a plot consisting of 20 points required 20 minutes and figure 3 together required 1 hour to generate.

The finite difference solutions corresponding to figure 3 are depicted in figure 4. To compute the finite difference solutions, a grid of 81 points in the X-direction and points spaced Δt apart in the t-direction with $\Delta t = [LC]^{1/2}\ \Delta X = [LC]^{1/2}\ H/80$ was used. The computational time for the entire finite difference grid of 79 different heights and 50 time steps required only 20 minutes, so figure 4 was generated in only 20 minutes compared to 60 minutes for 3.

The Fourier Series solution is depicted in figure 5. To obtain a relatively accurate solution, 80 terms of the fourier series were required. Consequently, each of figure 5 required 33 minutes of computation time for a total of 1 hour 39 minutes for all three.

Table 1 summarizes the comparison of these methods. The conclusion to be drawn is that for computational purposes the finite difference method is the one to use.

In figure 6 we plotted the current distribution obtained from finite differences as a function of time for several heights as indicated. From these plots one reaches the conclusion that, at height X, the current remains zero from t=0 until t=X/C at which time the current rises abruptly to its maximum value and then decreases to zero. The maximum value of the current is greatest close to the ground and this maximum value falls off rapidly with height.

REFERENCES

1. L. V. Bewley, Traveling Waves on Transmission Systems, John Wiley & Sons, New York, 1951.

2. M. A. Uman, Lightning, McGraw-Hill, New York, 1969.

3. C. F. Wagner, "The Lightning Stroke as Related to Transmission Line Performance, Part I," Electrical Engineering, May, 1963, pp. 339-347.

4. C. E. R. Bruce and R. H. Golde, "The Lightning Discharge," J. Inst. Elect. Engrs. (London) 88, 1941, pp. 487-524.

5. A. S. Dennis and E. T. Pierce, "The Return Stroke of a Lightning Flash to Earth as a Source of VLF Atmospherics," Radio Sci., 68D, 1964, pp. 777-794.

6. D. G. Kim, G. A. Dubro, L. P. Tessler, and R. L. Boggess, "Transmission Line Theory Applied to Aircraft Lightning Interactions" Proceedings of IEEE 1977 International Symposium on Electromagnetic Compatibility, Seattle, Washington, August 2-4, 1977, IEEE Publishers, 77CH1231-0 EMC.

7. A. N. Tychanov and A. A. Samarski, Partial Differential Equations of Mathematical Physics, Volume I, Holden-Day, San Francisco, 1951, pp. 107-110.

8. N. S. Koshlyakov, M. M. Smirnov and E. B. Gliner, Differential Equations of Mathematical Physics, North-Holland Publishing Company, Amsterdam, 1964, pp. 72-74.

9. E. Isaacson and H. B. Keller, Analysis of Numerical Methods, John Wiley & Sons, New York, 1966, pp. 442-530.

TABLE 1

I. METHOD - Exact
ACCURACY - Exact
COMPUTATIONAL TIME - One hour for 20 points on each of 3 plots.

II. METHOD - Finite Difference
ACCURACY - 81 grid points in X direction yield nearly exact solutions.
COMPUTATIONAL TIME - 20 minutes for 3950 points to be computed although only 150 were plotted.

III. METHOD - Fourier Series
ACCURACY - 80 terms in the series yielded reasonable accuracy although spurious oscillations typical of fourier series were still there.
COMPUTATIONAL TIME - One hour 39 minutes.

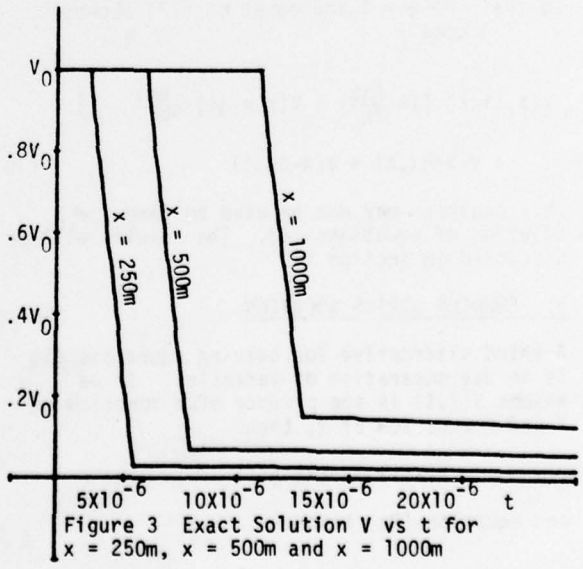

Figure 3 Exact Solution V vs t for x = 250m, x = 500m and x = 1000m

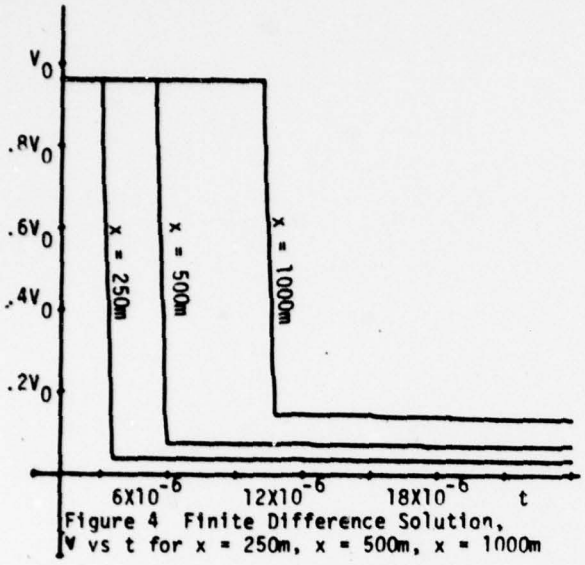

Figure 4 Finite Difference Solution, V vs t for x = 250m, x = 500m, x = 1000m

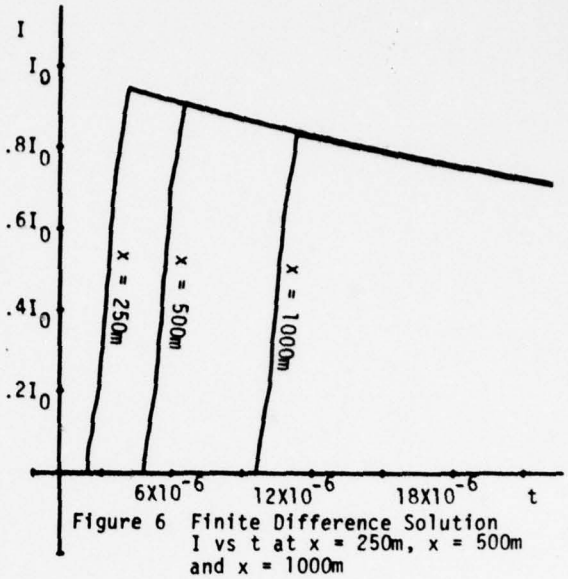

Figure 6 Finite Difference Solution I vs t at x = 250m, x = 500m and x = 1000m

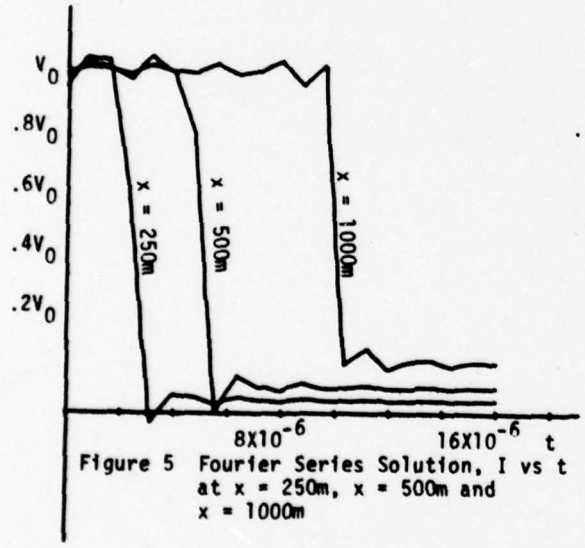

Figure 5 Fourier Series Solution, I vs t at x = 250m, x = 500m and x = 1000m

NON-LINEAR MODELING OF LIGHTNING RETURN STROKES

Dr. David F. Strawe

Technical Advisor for the Electromagnetic Effects
Organization of the
Boeing Aerospace Company
P.O. Box 3999
Seattle, WA 98124

BIOGRAPHY

David F. Strawe is an electromagnetics analyst working in the field of electromagnetic pulse (EMP) transients analysis. He received the Ph.D degree in electrical engineering from Michigan State University in 1967. Since then he has worked at Boeing developing analytical techniques and computer codes for the prediction of electrical transients produced in electronic equipment by nuclear EMP and lightning threat environments. Both airborne and ground systems have been modeled. During the past two years, he has been engaged in the development of analytical models for lightning discharge current transients and their associated electromagnetic fields.

ABSTRACT

This paper describes a transmission line model of a cloud-to-ground return stroke in which the non-linear breakdown physics is included. Consistent channel and line parameters are determined from the past current time history using a shock wave (Braginskii type) model of the channel arc. The model shows peak currents, decay times, and scale heights (lengths) similar to linear models. It also provides current rise times and rise rates well in accord with measured data. It indicates that the velocity of propagation of the current wave declines with elevation, as observed photographically, even when the line model is initially uniform in temperature and channel diameter. Most importantly, it predicts a substantial decline in current rise rate with elevation or distance from the discharge initiation. The rise time increases faster with elevation than the amplitude declines. The rise rate declines much faster than current amplitude.

BACKGROUND

Most analytical models[1,2,3] of lightning return strokes have either assumed current time histories impressed upon assumed discharge geometries or have involved linear charged transmission line models from which currents and fields are calculated. The line models predict reasonable peak currents, pulse durations, and propagation velocities provided the proper time independent lightning channel (and line) parameters are chosen. The channel expands in diameter by over an order of magnitude during the initial 100 microseconds of the return stroke so that constant parameters cannot adequately represent the entire pulse period. Further, the usual linear time independent line model produces a step rise in current and, hence, contains no information on the current rise rate which determines the level of induced lightning transients in exposed equipment.

Detailed numerical studies[4-8] of arc development have been carried out in cylindrical and spherical symmetry for assumed current time histories. These analyses have established the time and spatial development of the related plasma parameters, i.e., temperature, pressure, particle densities, conductivity, arc radius, etc., for specified currents but not for natural self consistent ones. The actual current and the channel arc interact in a lightning discharge to a high degree especially in the early phase when both the current and arc plasma are building. A self consistent model is needed to describe the buildup phase which determines such important current parameters as maximum rate of rise (or rise time) and propagation velocity.

The close agreement between the step excited currents on vertical conducting wires over conducting ground and those on a transmission line has been established[9]. This forms a justification for the economical and traditional line model of the return stroke.

TECHNICAL APPROACH

It is assumed that the branched structure of the charged cloud-to-ground leader system can be represented for channel current calculations as a network of transmission line segments. The current so obtained can be used with an assumed channel geometry to calculate the resultant electromagnetic fields. Only the current calculation is addressed here.

In the models solved to date only the equivalent line resistance per unit length (R) is considered non-linear and time varying. In principle, since the channel radius changes significantly with time and the channel is geometrically more nearly a vertical monopole[9,10] than a linear transmission line, the inductance (L) and capacitance (C) per unit length should

1.

also be time functions. These involve logs of time varying terms and are themselves weak time functions[10,11]. Inclusion of this time dependence is planned for later models. The channel tortuosity (random path bending) and corona sheath charge storage effects are included as modifications to the L and C values or equivalently as modification to the hot channel (R = 0) velocity factor (v_f) and characteristic impedance (Z_0). Some of the charge stored in the sheath during leader formation is retrievable during the return stroke. This is accounted for by assuming a larger effective conductor radius for capacitance calculation than the sub-centimeter current carrying core.

Two line model configurations have been used. One has uniform ladder sections of constant parameter values and represents a channel about 2 kilometers (km). The second has non-uniform section definitions representing progressively longer channel lengths and propagation times. This one represents a total channel length of 9.6 km. This telescoping of section lengths more efficiently utilizes the limited number of sections permitted by the analysis code used to solve this network. Telescoping is justified by the natural increase in rise time with propagation distance. In each of these configurations, the discharge is assumed to start when a groundward propagating negative leader from the cloud meets an upward positive leader from the ground. The height of the merger point was taken as 100 meters. The first configuration model is shown in Figure 1. The charge on the channel is discharged after merger by propagating current waves which spread out from the merger point.

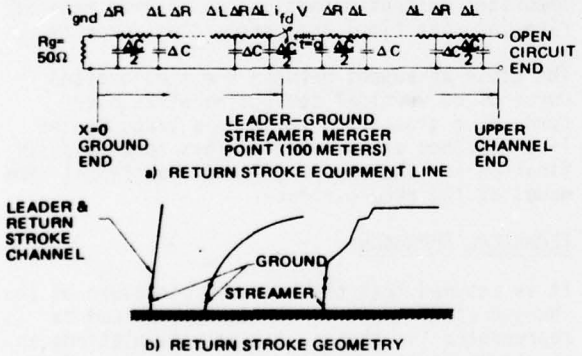

Figure 1: Lightning Model Geometry and Configuration

The model networks were solved with the time domain code CIRCUS II[12]. At each time step in the calculations, a model subroutine calculates the channel resistances and corresponding section resistances for each section from the past current time history and feeds them to CIRCUS for the next time step calculation.

The resistance models developed for use here are based on the spark channel model of Braginskii[13]. This relatively simple model assumes that a conducting channel has been established prior to the initiation of the spark by prebreakdown, streamer, and/or leader processes. The resultant arc radius, temperature, pressure, etc. are determined from the spark current time history. The current is assumed to heat (i^2R loss) the initially conducting arc plasma to higher temperatures and tens of atmospheres of pressure. This condition produces a hydrodynamic shock wave in the air surrounding the spark channel resulting in rapid channel expansion. Braginskii uses the strong shock approximation to simplify the physical picture of the expansion process. This picture produces an essentially uniform electrical conductivity determined from channel temperature and pressure which is nearly constant in time. The channel resistance per unit length is determined from the conductivity and the arc radius.

Assuming that the conductivity (σ) is time dependent, Braginskii's solutions for radius (a) and channel resistance can be cast in the form:

$$a^2(t) = a_0^2 + \beta \int_0^t \left(\frac{i^2(t')}{\sigma(t')} \right)^{1/3} dt \qquad (1)$$

$$R(t) = \pi \sigma(t) a^2(t)^{-1} \qquad (2)$$

Here a_0 is the radius at the current arrival or starting time; it is an initial condition for the program. This form allows "updating" of model segment resistances from local current values. If, as Braginskii did, we take σ to be time independent, (1) and (2) represent the complete resistance model. If not, the temperature and pressure must be explicitly calculated so that the conductivity can be determined from them.

THE ARC MODEL OF THE LIGHTNING CHANNEL

The channel geometry is assumed to be axisymmetric or locally of cylindrical symmetry. The channel parameters are described in terms of a deposited energy rate set by the local current time history (i^2R loss). Detailed analyses[4-8] have established representative radial contours of these parameters for lightning-like currents as shown in Figure 2a. The Braginskii idealization of this picture is illustrated in Figure 2b.

The referenced analyses solve, in cylindrical or spherical[7] symmetry, the hydrodynamic equations of continuity of mass, momentum, and energy (transfer) together with two equations of state relating pressure, temperature, mass density, internal energy density, etc. In Braginskii's model, the numerical gridding in radius of the detailed analyses is replaced by definition of three radial regions. The central "channel" region contains the hot low density plasma. The channel is assumed to have all of the shock system internal energy but negligible kinetic energy of translation. The "shell" region contains the mass excluded from the channel

during its expansion. It has negligible thickness, is relatively cool containing all the kinetic energy of the shock, but negligible internal energy. The "ambient" region comprises everything beyond the shock or shell radius a(t). It is completely unperterbed since the shock velocity ȧ(t) is supersonic.

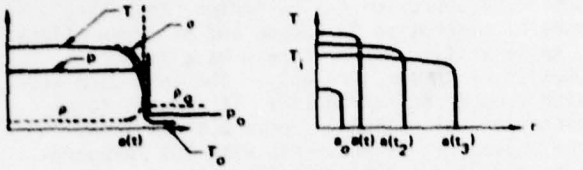

a) TYPICAL ARC CHANNEL RADIAL PROFILES

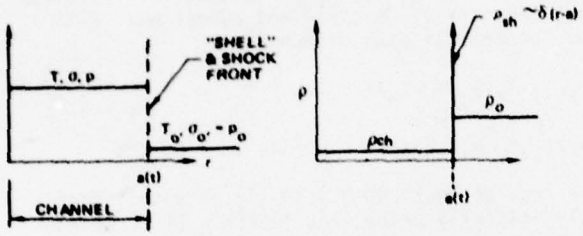

b) BRAGINSKII'S MODEL IDEALIZATION

T TEMPERATURE
P PRESSURE
σ ELECTRICAL CONDUCTIVITY
ρ MASS DENSITY
a CHANNEL OR SHOCK RADIUS
r CYLINDRICAL RADIAL DIMENSION

Figure 2: Arc Channel Radial Geometry

Braginskii further assumes that no net energy is lost by the shock system through thermal radiation or conduction. All such losses from the shell are negligible, and all energy lost from the channel is re-absorbed in shell and returned to the channel as hot plasma. The latter is a result of assuming the internal energy of the shell to be negligible. Braginskii uses the piston approximation for determining the channel and shell pressure from the shock velocity.

$$p = K_p \rho_o \dot{a}^2 \tag{3}$$

Here ρ_o is the ambient air mass density and K_p is an efficiency factor slightly less than unity. This form is approximately valid when p is much larger than the ambient p_o. The use of (3) with the channel-shell segmentation of Figure 2b constitutes the strong shock approximation.

With the preceding assumption, the equations describing the channel development are:

$$\frac{dW_c}{dt} + p\frac{d}{dt}(\pi a^2) = i^2 R \tag{4}$$

$$\varepsilon \frac{dM}{dt} = Q_t + Q_r \tag{5}$$

$$p = (n_e + n_i + n_o)kT = \frac{(Z+1)\rho kT}{m_a} \tag{6}$$

$$\varepsilon = \frac{3p}{2\rho} + \frac{I}{m_a} \doteq \frac{p}{(\gamma-1)\rho} \tag{7}$$

Where the channel parameters used are:

W_c	internal energy (εM)
p	pressure
ε	internal energy per unit mass
M	channel mass ($\pi a^2 \rho$)
Q_t	rate of heat conduction to shell
Q_r	rate of heat radiation to shell
n_e, n_i, n_o	electron, ion, neutral particle density
k	Boltzmann's constant (1.38×10^{-23} joule/°K)
T	Kelvin temperature (T_k = T/1000)
ρ	mass density
m_a	average atomic mass (kg)
I	average energy of dissociation and ionization per atom
γ	the specific heat ratio for ionized air (C_p/C_r)

The continuity of mass condition is contained in the model form assumption as applied to equations (3) and (4). Momentum is conserved in the derivation of equation (3) for the pressure-velocity relation. Equations (4) and (5) constitute the energy balance equations, while equations (6) and (7) are the thermal and caloric equations of state, respectively. The second form of (7) is used by Braginskii and is reported to be a good approximation with constant γ for T greater than 8000 - 10,000°K (K°K)[4,13,14].

Braginskii ultimately assumes σ to be independent of time and temperature so that only a(t) need be determined to calculate R. Equation (5) is unnecessary except where temperature is desired. He neglects radiation in favor of conduction since the former is "difficult to compute accurately". However, radiation dominates at practical temperatures (>15 K°K) and his temperature estimates are excessively high. As will be seen, when radiation is properly entered into (5), realistic temperatures result as in Model II.

The equations now can be combined to form Braginskii's equation:

$$\frac{i^2}{\sigma} = 2\pi^2 \rho_o K_p \left[a^3 \dot{a}^3 + \frac{a^3 \dot{a}}{2(\gamma-1)} \frac{da^2}{dt^2} \right]$$

$$= 2\pi^2 \rho_o K_p \xi (a\dot{a})^3 ; (\dot{a} \equiv \frac{da}{dt}) \tag{8}$$

Strickly, ξ is a function of radius and time, but for power law currents and constant σ, a becomes a power law and ξ becomes a constant. This is the assumption Braginskii makes in obtaining his analytical solution.

$$\xi = 1 + \frac{1}{2(\gamma-1)\dot{a}^2} \frac{d^2 a^2}{dt^2} = 1 + \frac{(2-k)}{\gamma-1} \tag{9}$$

$$\text{where } i = Rt^n;\ a \sim t^k;\ k = \frac{2n+3}{6} \tag{10}$$

so that, integrating (10)

$$a^2 = a_o^2 + \beta \int_o^t \left[\frac{i^2}{\sigma}\right]^{1/3} dt \tag{11}$$

where $\beta = \frac{2}{\sqrt[3]{2\pi K_p \rho_o \xi_n}} = \beta_n$ (12)

Using (10) in (11) and dropping a_o as small, Braginskii's famous analytical solution results:

$$a_n = \alpha_n i^{1/3} t^{1/2} \quad (13)$$

where $\alpha_n^2 = \frac{3\beta}{(2n+3)\sqrt[3]{\sigma}}$ (14)

Agreement with measured data on laboratory arcs and lightning is also good [15,16,17,18]. Equation (11) is numerically convenient and is used in Model I with the constant Braginskii σ (2.22×10^4 mhos/meter nominal).

Model II is developed from Model I by modification of equations (4) and (5) to include the effect of lost and reabsorbed thermal radiation from the channel, temporal variation of thermal and electrical conductivity, and low pressure momentum transfer. The resulting equations are solved numerically without approximation at each time step of the CIRCUS transmission line solution.

The revised pressure-radius relation is obtained by applying Newton's second law to the shell with the ambient and shell pressures in opposition.

$$(p-p_o)\, 2\pi a = \Delta F = \frac{d}{dt}(\text{momentum}) =$$

$$= \frac{d}{dt}(\text{shell mass} \times \dot{a}) = \frac{d}{dt}\left[K_p \rho_o \pi (a^2 - a_o^2)\dot{a}\right] \quad (15)$$

$$\frac{p}{p_o} = 1 + \frac{G}{a}\frac{d}{dt}(a^2 - a_o^2)\dot{a} \quad (16)$$

where $G = \frac{K_p \rho_o}{6 p_o}$

Equation (16) improves on (3) by returning p to p_o at initial and late times. It also takes the shell mass to be zero at initial time consistent with an equipressure hot channel. It bridges the gap between the weak and strong shock regimes.

In equation (5), Q_r is the ultraviolet (u.v.) radiation from the channel which is reabsorbed in the shell and returned as plasma to the channel. It depends on that radiated; i.e., on channel T,p, and a^2, as well as the optical thickness of the shell [19,20,21]. This term is formulated as the product of the total channel radiation and a re-absorption factor f_a.

$$Q_r = Q_{tot.\,rad} \cdot f_a$$

The remainder of $Q_{tot.rad}$ is considered lost from the system and subtracted from the source term i^2R in (4).

$$i^2R \rightarrow i^2R - Q_{tot.rad}(1-f_a) \quad (17)$$

The total radiated power in Model II was treated as transparent radiation [20,22] proportional to the channel mass and a radiation factor.

$$Q_{tot\cdot rad} = p\, a^2\, F_r(T) \quad (18)$$

The absorption factor, in general, depends on the shell mass, i.e., on $\rho_o a^2$, as well as wavelength. However, if the radiation spectrum is considered approximately Planckian, the sharp onset of absorption in oxygen and nitrogen allows f_a to be written approximately as a simple function of temperature only. The form used was taken from Brode[7] and Hill[6]. It assumes total absorption below 1860 Å (above 6.67e.v.) and none above. It is monotonic with 10% reabsorption at 8K°K and 90% at 50 K°K. The function $F_r(T)$ is a fit to the measured data for radiated power density of Devoto[19] and agrees well with the theoretical data of Bond[22].

$$F_r(t) = K_r T^n \varepsilon^{-T_r/T} \quad (19)$$

where $K_r = 2.2 \times 10^5$, $n = 4$, $T_r = 20$ K°K

The heat conduction term in (7) is significant only initially below, say 15 K°K. It is related to the heat conductivity K_T at the channel edge.

$$Q_t = -2\pi a \left.\frac{\delta T}{\delta r}\right|_{r=a} K_T(a) = 2\pi a\, mTK \quad (20)$$

Evaluation of this term is tricky in that there is nothing in the model to specify $\frac{\delta T}{\delta r}$. It has maximum magnitude at r=a. A value of m=2 to 3 with $K_T = K_T(r=0)$ seems appropriate from previous studies. Undoubtedly m changes with a. The value K_T is a function of T and p. It has an electronic constituent, dominant for T above 15K°K, related to the electrical conductivity through the Wiedemann-Franz Law and another due to neutrals and recombination effects[23]

The forms used for both σ and K_T are curve fits to detailed results of Plooster[4].

$$\sigma = \sigma(p,T) = \frac{1.52 \times 10^4 p^{.22}}{1+\left(\frac{13.4}{T_k}\right)^6 p^{.54}} \quad (21)$$

$$K_T = K_T(p,T) = \sqrt{\frac{T_k}{10} + \frac{(\sigma T \times 10^{-4})^2}{29.1}} + \frac{4}{1+10^3(1-T_k/6)^4} \quad (22)$$

Also, these functions agree well with measured data of Devoto[19]. It is planned, in a later model, to add a magnetic pressure (pinch effect) term to the pressure relation (16). This effect appears to be significant at large currents of the order of 100KA and at smaller radii.

RESULTS

Model I has been applied to configurations 1 and 2 for a number of initial conditions. Figures 3 and 4 shows time histories of currents versus altitude for configuration 2 using Braginskii's constant conductivity of 2.22×10^4 mhos/meter.

Figure 5 shows the effect of reduced constant conductivity of 10^4 mhos/meter. The most significant effect shown in the figures, from an electrical transient point of view, is the rapid reduction in peak current rise rates with elevation or distance from the discharge initiation point. As expected, the peak amplitude declines slowly and the rise time increases with elevation. An additional effect of reduced conductivity is a slowing of the propagation velocity of the current wave. The hot column velocity ($\sigma = 2.22 \times 10^4$) was set to 0.5 c_o, but the observed velocity of the current peaks ranged from 0.2 - 0.3 c_o. Plots of rise rate and velocity for these cases are shown in Figure 6. Velocity here is defined in terms of the arrival of the 63% of peak current point.

The value of the column open circuit voltage V was set at 10^7 volts to produce the approximately 10-20 Kilo Amperes (KA) at ground level observed in the figures. When V was increased to 10^8, the peak currents increased to approximately 250 KA (Figure 7) and the rise portion was speeded up in terms of rise time and propagation velocity (~.4 c_o). Rise rate and velocity data are shown in Figure 8. The initial radius used in all of the calculations described in this paper was 1 millimeter.

In Model II both channel radius and temperature are initialized. The latter was chosen to be 10 K^oK in the case displayed. Figure 9 shows current time history versus altitude for configuration 2 and $V = 10^7$. This is the counterpart of the Model I run shown in Figure 3. Its rise rate and velocity dependence are shown in Figure 10. The lower rise rates and slower velocities result from the decreased channel development rate caused by the initially lower electrical conductivity.

The most significant result from the model data obtained thus far is the rapid decline in the current rise rate with elevation. This would indicate that cloud-to-ground lightning return strokes represent a much greater electrical transient threat at ground level than to aircraft at elevation. Measured "ground current" would produce very pessimistic transient estimates to aircraft in flight. It is easy to imagine that the leader attachment phase or intracloud lightning represent a more severe threat even with their lower (on the average) peak currents. This is because of the closer proximity to the discharge initiation point. The model current shows a smooth increase from zero current with all lower order derivatives apparently vanishing at current onset. This smoothing effect increases rapidly with elevation. It may explain why little VHF energy is detected in the radiated fields of cloud-to-ground return strokes[24,25]. Most of the observed VHF energy appears to be associated with leader development and intracloud discharges whose high current rise rate discharge initiation points are elevated and hence more readily observed at a distance.

In order that the channel model used here might be compared to others and to measured data, it was used with the Pierce[26] lightning current. This current has double exponential form with a peak of 20 KA at 1.5 μs and a half value fall time of 40 μs. The current is shown with the resulting channel temperature, pressure, and radius in Figure 11.

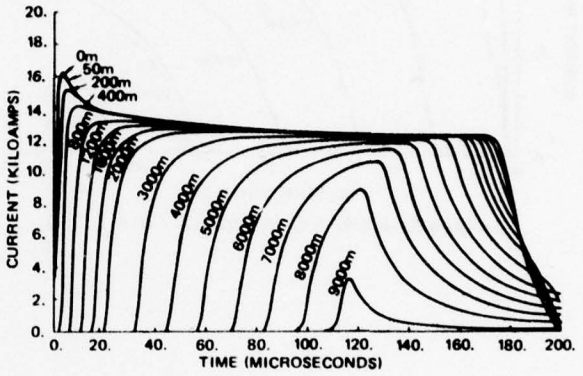

Figure 3: Model I, Configuration 2 ($\sigma = 2.22E4$)

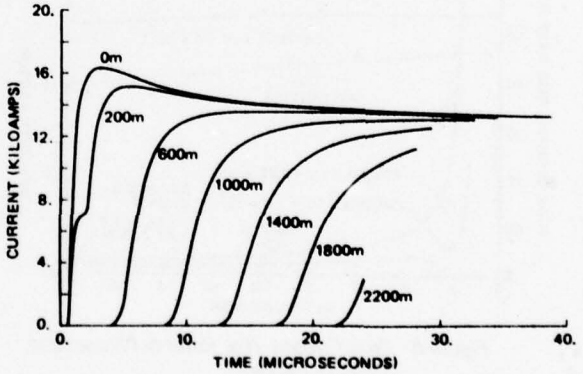

Figure 4: Model 1, Configuration 1 ($\sigma = 2.22E4$)

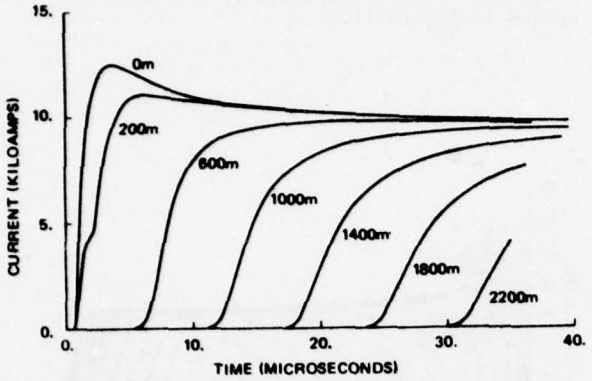

Figure 5: Model I, Configuration 1 (σ = 1.0E4)

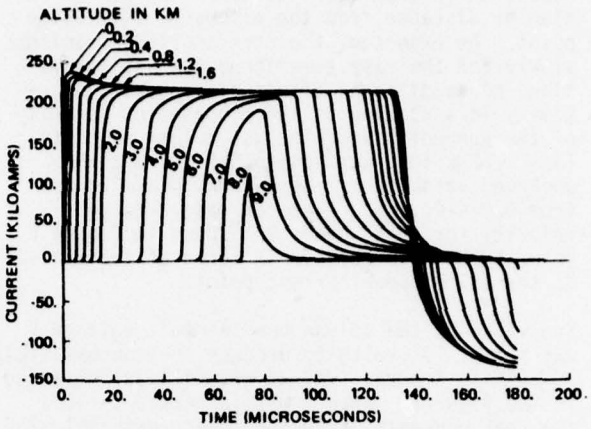

Figure 7: Model 1, Configuration 2, Vmax = 1.E8, σ = 2.22E4

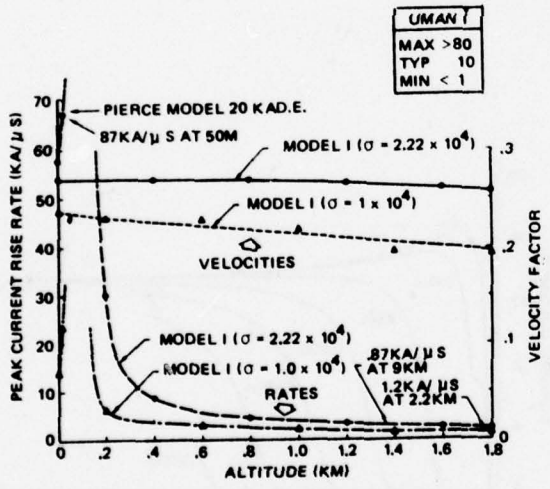

Figure 6: Peak Current Rise Rates & Propagation Velocity Factors

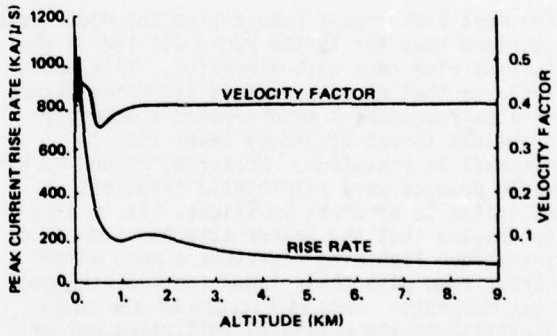

Figure 8: Peak Rise Rates & Propagation Velocity Factors (Model 1, Conf. 2, Vmax 1.E8)

NOTE: Figures 9 and 10 were distributed at workshop.

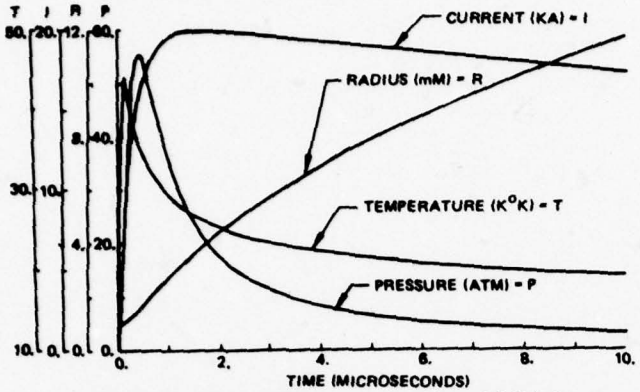

Figure 11: Channel Parameters for Pierce 20 KA Current

ACKNOWLEDGMENT

The Author would like to thank D. G. Chapman for programming the equations and for helpful discussions during model development. Thanks also go to Ms. C. J. Romani for typing the manuscript.

REFERENCES

1. Bruce, C.E.R., and Golde, R. H., "The Lightning Discharge", J. Institute Elec. Eng, London, 88, 1941.

2. Price, G. H., and Pierce, E. T., "The Modeling of Channel Current in the Lightning Return Stroke", Radio Science, May-June 1977.

3. Uman, M. A., and McLain, D. K., "Magnetic Field of Lightning Return Stroke", J. Geophysical Res., 74, 1969.

4. Plooster, M. N., "Numerical Simulation of Spark Discharges in Air", Phys. Fluids 14, 2111, 1971.

5. Plooster, M. N., "Numerical Model of the Return Stroke of the Lightning Discharge", Physics of Fluids, 14, 2124, 1971.

6. Hill, R. D., "Channel Heating in Return Stroke Lightning", J. Geophysical Res., 76, 637, 1971.

7. Brode, H. L., "Review of Nuclear Weapons Effects", Ann. Rev. Nucl. Sci., 18, 153, 1968.

8. Brode, H. L., "Review of Nuclear Weapons Effects", Ann. Rev. Nucl. Sci., 18, 153, 1968.

9. Strawe, D. F., "Lightning Source Model Development Program", Boeing Document D180-22936-1, January 1978.

10. King, R.W.P., and Schmitt, H. J., "The Transient Response of Linear Antennas and Loops", IRE Trans. Ant. Prop., May 1962.

11. Shen, L. C., et al, "A Simple Formula of Current in Dipole Antennas", IEEE Trans. Ant. Prop., Sept., 1968.

12. *PRESTO Digital Computer* Code Users Guide, Volume 4, CIRCUS-II, Final Report, Defense Nuclear Agency, Contract DNA001-75-C-0225, December 1975.

13. Braginskii, S. I., "Theory of the Development of a Spark Channel", Soviet Physics, JETP, 7, 1068, 1958.

14. Predvoditelev, A. S., et. al., "Tables of Thermodynamic Functions of Air", English Translation, Associated Technical Services, INC, 1962.

15. Jones. R. C., "Return Stroke Core Diameter", J. Geophysical Res., 73, 809, 1968.

16. Uman, M. A., "The Diameter of Lightning", J. Geophysical Res., 69, 583, 1964a.

17. Uman, M. A., "The Peak Temperature of Lightning", J. Atmos. Terr. Phys., 26, 123, 1964b.

18. Uman, M. A., "Lightning", McGraw Hill, N.Y., 1969.

19. Devoto, R. S., et. al., "Air Transport Coefficients from Electric Arc Measurements", Phys. Fluids, 21(4), April 1978.

20. Griem, H. R., "Plasma Spectroscopy, McGraw Hill, New York, 1965.

21. Kivel, B., and Bailey, K., "Tables of Radiation from High Temperature Air", AVCO-Everett Research Report RR-21, Everett, Mass, Dec. 1957.

22. Bond, J. W., et. al., "Atomic Theory of Gas Dynamics", Addison-Wesley, Reading, Mass, 1965.

23. Spitzer, L., and Harm, R., Phys. Review, 89, 977, 1953.

24. Uman, M. A., et. al., "An Unusual Lightning Flash at Kennedy Space Center", Science, Vol. 201, No. 4350, July 7, 1978.

25. Proctor, D. E., "A Hyperbolic System for Obtaining VHF Radio Pictures of Lightning", J. Geophysical Research, Vol. 76, No. 6, Feb. 20, 1971.

26. Cianos, N. and E. T. Pierce, "A Ground-Lightning Environment for Engineering Use", Stanford Research Institute, Project 1834, August 1972.

ELECTRIC FIELDS IN THUNDERCLOUDS

W.P. WINN
C.B. MOORE
C.R. HOLMES
Department of Physics
New Mexico Institute of Mining and Technology
Socorro, New Mexico 87801

L.G. BYERLEY, III
Lightning Location & Protection
2030 E. Speedway Blvd., Suite 210
Tucson, Arizona 85719

ABSTRACT

The electric field inside thunderclouds in central New Mexico appears to be closely coupled to the winds and radar echo structure. These relationships are revealed by measurements with a balloon-borne electric-field meter made simultaneously with a high-resolution vertically scanning radar and a variety of other ground-based instruments.

BACKGROUND

For several years we have been conducting measurements to delineate the structure of the isolated, relatively small thunderstorms over Langmuir Laboratory in central New Mexico. The main objective of our work is to learn how thunderstorms produce the intense electrification that causes lightning and to find out the connection between winds, precipitation, space charge, and lightning. Although the basic questions (e.g., What causes electricity in thunderclouds?) are still unanswered, we are beginning to learn some interesting things.

We shall begin with a brief description of the balloon-borne electric field meter, and then present some results from its use on both captive and free balloons.

ELECTRIC FIELD METER

Two copper spheres serve both as sensors and as a telemetry antenna for the electric field meter.[1] The electronic circuits and batteries are located inside the spheres. This arrangement avoids sharp metallic protrusions that would give rise to corona discharges in the intense electric fields inside thunderclouds. The spheres are attached to a horizontal dielectric shaft that rotates about its axis as shown in Figure 1. The shaft precesses slowly about a vertical axis. The spheres are electrically connected to each other through circuits that detect the charge induced on them by the thunderstorm's electric field. The orientation of the instrument in space is given by sensors of gravity and/or magnetic fields. All signals are telemetered to ground. With this data it is possible to determine all three components of the electric vector.

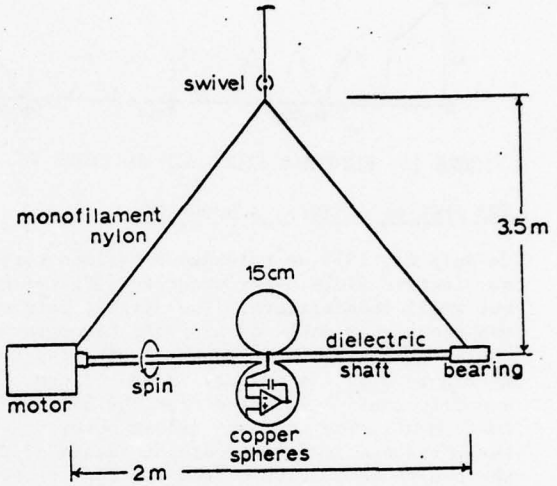

FIGURE 1. BALLOON-BORNE ELECTRIC FIELD METER

SPACE CHARGE NEAR THE GROUND

One of the most characteristic features of our electric field records is a rapid increase in electric field strength soon after the balloon leaves the ground. This rapid increase is caused by a space-charge layer just above the ground that comes from corona discharges at the tips of the leaves and other sharp protrusions attached to the earth. The upper graph in Figure 2 compares the electric field record from an instrument carried on a captive balloon with the record from a ground-based instrument.[2] The electric field was intense enough to cause substantial corona from pointed objects attached to the earth, but it was nearly constant during the first two-thirds of the interval shown. There were no lightning flashes during this interval. The lower graph shows the altitude of the balloon vs. time. Notice how the electric field increased by a factor of four in the first 200 meters above the ground. This implies a space charge density of about 0.5 nanoCoulombs per cubic meter. The electric field at the ground became less intense near the end of the interval shown as it changed polarity. As a result, the corona became less intense, the space-charge layer cleared, (by advection or other transport mechanisms) and the electric field was no longer a strong function of altitude.

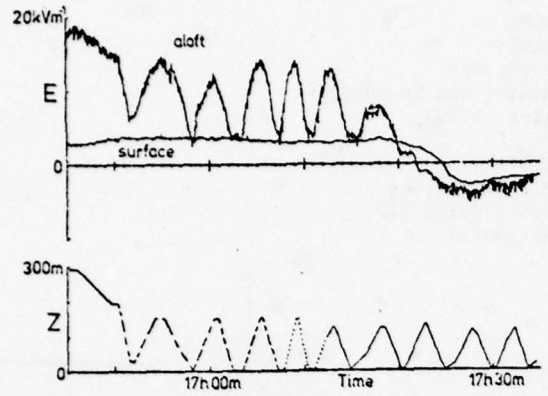

FIGURE 2. ELECTRIC FIELD AND ALTITUDE VS. TIME

THE EDGE OF A STORM, A SOUNDING

On July 16, 1975 we released a balloon carrying an electric field meter under the edge of mature but small thunderstorm. The visible rain shaft was about 7 km north of Langmuir Laboratory, where the balloon was launched. The top trace in Figure 3 is the primary record of the electric field E vs. time from the balloon-borne instrument. The next two traces below it are the horizontal and vertical components of E, which have been deduced from the top trace.

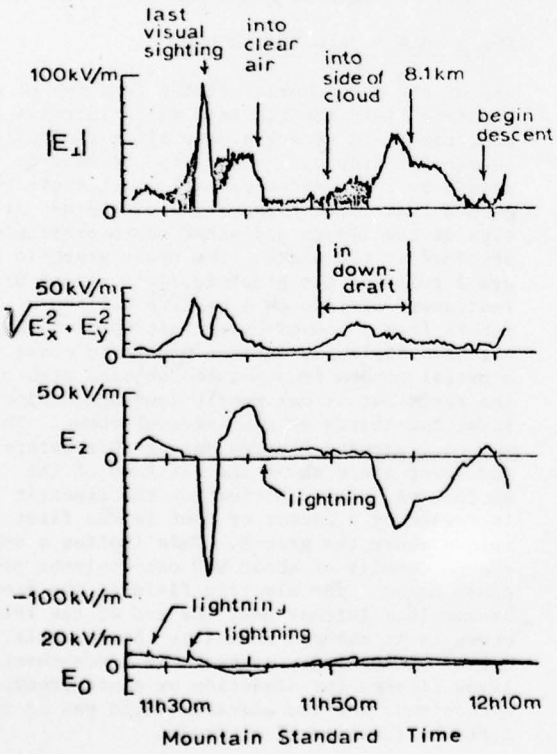

FIGURE 3. ELECTRIC FIELD VS. TIME

The bottom trace is the electric field at the ground. The same vertical scale has been used for E in all four traces to facilitate comparisons; it is apparent that the electric field strength can be very much greater inside a thundercloud than it is at the ground. The most intense field encountered during this flight was about 100 kV/m, or about 1000 Volts per centimeter.

Figure 4 is an interpretive drawing of the storm, incorporating electric field data from the balloon-borne instrument, wind data deduced from the motion of the balloon, and radar data showing echos from the cloud. The space-charge layer near the ground had a density of about .25 nanoCoulombs per cubic meter, somewhat less than in the example discussed above.

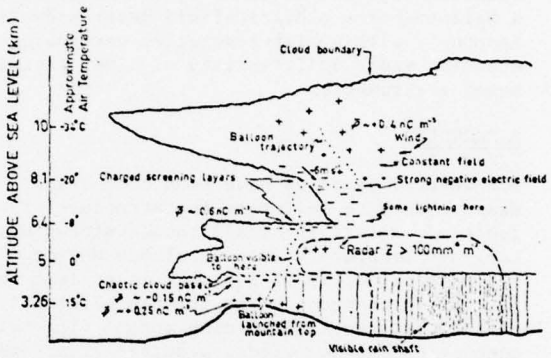

FIGURE 4. INTERPRETATIVE DRAWING OF A THUNDERSTORM ON JULY 16, 1975.

The cloud base was chaotic and not well defined where the balloon entered it on the outskirts of the storm. The electric field was intense near the cloud base, and the winds suggested that the space charge causing the field may have come from the central part of the storm to the north. The cloud base is identified in Figure 3 by the note "last visual sighting".

At an altitude of 6.4 km above sea level, the balloon rose into a layer of clear, stable air that had inhibited convection except in the vigorous, central part of the storm. As the balloon rose into the clear air, the electric field indicated by the instrument it was carrying declined abruptly, as shown in Figure 3, at the time labeled "into clear air". The abrupt decline can be explained by a charged screening layer (of finite thickness) of density 0.6 nanoCoulombs per cubic meter. This layer of charge "screens" the charge inside the cloud so that its electric field is not as strong as it otherwise would be in the clear air outside the cloud.

The balloon rose in clear air until it encountered a slanted downdraft beneath an anvil (Figure 4). The downdraft's velocity cancelled the balloon's upward motion relative to ground and carried the balloon several kilometers horizontally toward the center of the storm.

The electric field pattern in the vicinity of the downdraft suggests (not conclusively) that the downdraft was carrying negative charge. We do not have enough data to speculate on where that charge went after it entered the main part of the cloud.

The last feature of interest during this flight occurred at the layer of strong shear where the balloon rose out of the slanted downdraft (blowing toward the north) into wind that caused the anvil (blowing toward the south). The electric field shows an abrupt discontinuity in slope at that altitude (8.1 km, see Figure 3) indicating a change in space-charge density. It is not surprising that air coming from different parts of a storm should each carry different amounts of space charge, but it is satisfying to see this effect so clearly. The space charge in the winds coming from the central part of the storm and causing the anvil had a density of about 0.4 nanoCoulombs per cubic meter.

A pressure-activated switch released the instrument from the balloon before it passed through the top of the cloud. The trajectory of the instrument during descent showed that the slanted downdraft was still present; it was a very persistent feature of this storm.

THE CENTER OF A STORM, ANOTHER SOUNDING

In 1977, a free balloon carrying an electric-field meter and a standard meteorological radiosonde rose into the central, active part of a small, isolated thunderstorm over Langmuir Laboratory. Electric field at the balloon vs. altitude for this flight is shown in Figure 5.

Again notice the initial rapid rise in electric field just after launch, indicative of the space charge layer arising from corona discharges on the ground. The electric field soon became far more intense as it approached the main negative charge center inside the cloud. The occasional abrupt decreases in electric field strength were the result of lightning flashes. The electric field (which was mostly vertical) passed through zero and became intense with the opposite polarity as it passed and rose above the negative charge center. The electric field intensity reached about 140 kV/m (1400 Volts per centimeter) both above and below the negative charge center. We have seldom seen fields more intense than this with balloon-borne instruments carried into thunderclouds. This value is approximately one-third the value believed to be necessary to support the initial growth of a lightning flash,[3] about 400 kV/m. The probability of encountering a field strength of 400 kV/m is very low because such a field would last only for a short time and it would be present over a relatively small volume. We have never observed such a strong field with our balloon-borne meter, although we do have an indication of such a value (somewhat suspect) from our earlier experiments using the instrumented rockets.[4]

There is no distinctive feature in the radar echoes at the altitude of the negative charge center.

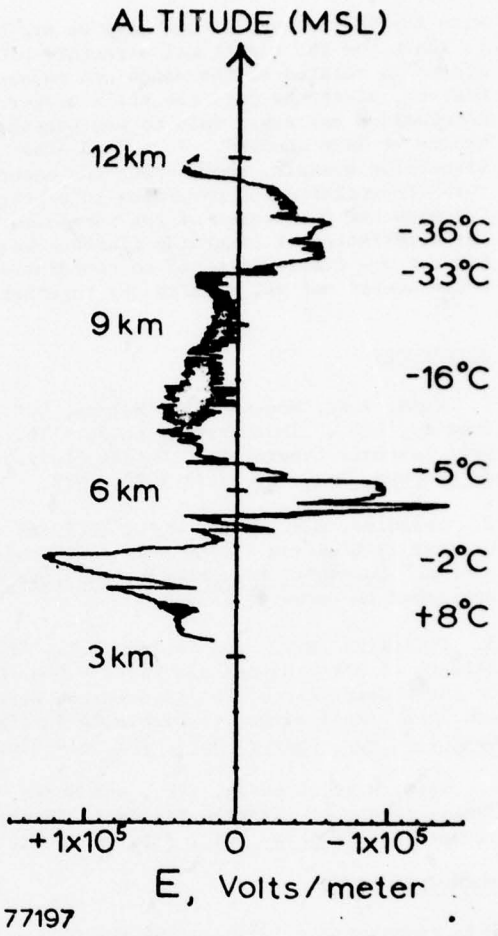

FIGURE 5. ELECTRIC FIELD VS. ALTITUDE FROM A SOUNDING ON JULY 16, 1977.

As the balloon rose farther above the negative charge center, the electric field strength became less intense and more horizontal than vertical. The horizontal direction of the field is indicated in Figure 5 by the noise-like trace above and below 9 km. At higher resolution it can be seen that the trace is not noisy, but rather it is sinusoidal--a result of the horizontal direction of the field and the precession of the horizontal shaft of the instrument (Figure 1). The radar profiles of this storm show that the weak, horizontal field occurred when the balloon was near the edge of the cloud. As the balloon rose into the anvil at about 10 km, the field became more intense and vertical in a direction that would result from positive charge overhead. At about 11.5 km above sea level the balloon had passed above most of the positive charge in the anvil.

The instrument was released from the balloon before it rose into the clear air at the top of the storm.

SUMMARY

With the instruments we now have we are beginning to learn how the electrical structure of thunderstorms is related to the winds and radar echoes. However, since the data are still meager our conclusions may apply only to the particular storms we have studied. To answer other questions--for example, those about the nature and role of precipitation particles in electrification and the causes of the particular characteristics of lightning flashes--we need to develop new instruments and to coordinate measurements not yet carried out together.

REFERENCES

1. Winn, W.P., Moore, C.B., Holmes, C.R., Byerley, L.G., "Thunderstorm on July 16, 1975, Over Langmuir Laboratory: A Case Study," J. Geophys. Res., 83, 3079-3092, 1978.

2. Standler, R.B., Winn, W.P., "Effects of Coronae on Electric Fields Beneath Thunderstorms," Quart. J. Roy. Meteor. Soc., to be published in January, 1979.

3. Griffiths, R.F., and Phelps, C.T., "The Effects of Air Pressure and Water Vapour Content on the Propagation of Positive Corona Streamers, and Their Implications to Lightning Initiation," Quart. J. Roy. Meteor. Soc., 102, 419-426, 1976.

4. Winn, W.P., Schwede, G.W., and Moore, C.B., "Measurements of Electric Fields in Thunderclouds," J. Geophys. Res., 79, 1761-1767, 1974.

ACKNOWLEDGMENTS

This research was supported by the Office of Naval Research and by the Atmospheric Research Section of the National Science Foundation.

THE AUTHORS

W.P. Winn: Chairman of the Physics Department at New Mexico Tech; Ph.D., University of California at Berkeley.

C.B. Moore: Professor of Atmospheric Physics at New Mexico Tech; B.Ch.E., Georgia Institute of Technology

C.R. Holmes: Professor of Physics at New Mexico Tech; Ph.D., Pennsylvania State University.

L.G. Byerley, III: Research Engineer at Lightning Location and Protection, Inc.; B.S., New Mexico Tech.

MEASUREMENTS ON NATURAL AND TRIGGERING LIGHTNING

par Jean-Louis BOULAY and Pierre LAROCHE

Office National d'Etudes et de Recherches Aérospatiales (ONERA)
92320 Châtillon (France)

ABSTRACT

A station for triggering lightning has been installed in mid-France in 1973. Several organizations are cooperating in measurements of triggered and natural lightning. These measurements are made either in proximity to the point of impact or at distant stations. They are intended for the determination of several parameters (optical, acoustic and electromagnetic) related to the lightning discharge. We present, first of all, a brief description of the experiments carried out by the ensemble of all of the cooperating organizations.

A particular investigation performed by ONERA will then be presented in detail. It concerns the setting-up of a network of electrostatic field sensors on the ground, intended for localizing the atmospheric electrical charges neutralized in a lightning stroke.

1. EXPERIMENTAL STATION OF ST-PRIVAT D'ALLIER

An experimental station for the study of lightning was installed in 1973 near St-Privat d'Allier, a town in the approximate center of France. The ensemble of experiments and observations was intended essentially for the study of triggered lightning. However, the objectives of the series of experiments in 1978 were, for the first time, shared between natural lightning and triggered lightning phenomena. The many scientists and engineers, assembled in 1978, belonged to eight groups and to six organizations ✱ .

✱ *EDF* *(Electricité de France) Direction des Etudes et Recherches - Paris.*

CEA *(Commissariat à l'Energie Atomique) Centre de Saclay et de Grenoble.*

LDG *(Laboratoire de Détection et de Géophysique) CEA - Bruyères Le Chatel.*

CNET *(Centre National d'Etudes des Télécommunications) Centre de Lannion.*

IOPG *(Institut et Observatoire de Physique du Globe) Clermont-Ferrand.*

LPA *(Laboratoire de Physique Atmosphérique) Université de Toulouse.*

ONERA *(Office National d'Etudes et de Recherches Aérospatiales) Châtillon-sous-Bagneux.*

1.1. General Characteristics of the Station

The lightning strokes were triggered by the firing of a rocket fitted with a conducting wire, the end of which was connected to ground. This type of triggering was first employed successfully by M.M. Newman[1,2]. The rockets used at St-Privat d'Allier are of the type "Counter-Hail" (diameter : 70 mm, length : 847 mm, weight at launching : 2.7 kg). The metal wire, steel 0.2 mm diameter, is fed out from a spool ; this system limits the maximum speed of the rocket to approximately 180 m/s. The rocket, braked by the wire, attains an altitude of 700 m in 5 seconds and is destroyed at the end of its trajectory by an explosive charge.

Two methods for firing the rocket are available (Fig.1). The first is situated on a platform installed at the top of a pylon and consists of six rocket launching pads. The second is located on the ground and consists of four rocket launching pads.

Fig. 1 – Station for triggering lightning (photo EDF).

The preparations for triggering are predicated on information furnished by an X-band radar concerning local storm cloud formations and also by the readings of a lightning detector (antenna CIGRE) which has a range of approximately 5 km.

The choice of the instant of firing is then determinated from the reading furnished by an electrostatic field detector, installed in close proximity to the firing station.

During the six years of use of this station, 114 firings have been made during 34 storms ; 84 lightning strokes have been triggered. Twenty-seven lightning flashes have occured with persistent currents of long duration and of feeble amplitude, while 57 lightning flashes have shown one or several high current pulses (more than 1 kA). For the majority of the successfull firings, the field at the ground is negative (the charges induced on the ground are positive), and the field amplitude is close, on the average, to 10 kV/m. The altitude attained by the rockets at the moment of the lightning stroke is between 100 and 300 m.

1.2. General Recapitulation of Measurements Carried out[3,4,5]

The overall assembly of measurements carried out on the ground is shown in Fig.3.

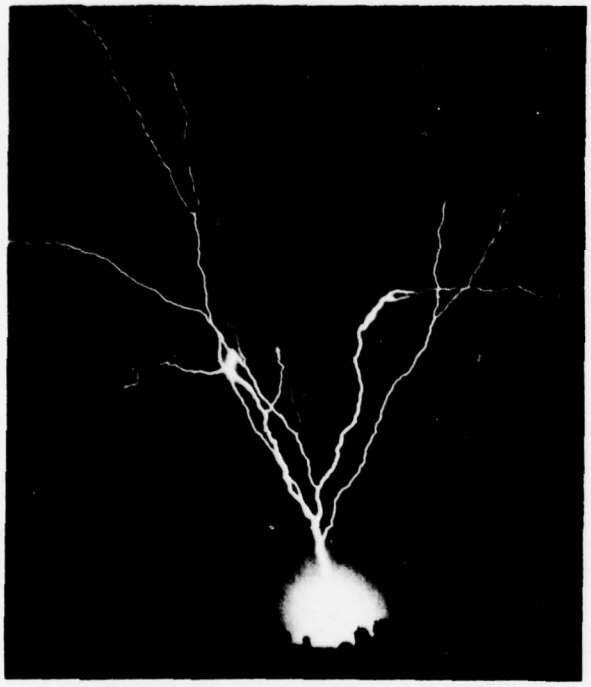

Fig. 2 – Triggered lightning flash seen at a distance of 2.7 kilometers (photo EDF).

a) measurement of discharge current for triggered lightning flash

The current in a lightning flash is measured by means of a coaxial resistive shunt with a time response of 10 ns. The signals are recorded, both on a transient oscilloscope and on a magnetic recorder. One can therefore analyze both high speed phenomena (rise times as short as 200 ns) and slow phenomena (such as the persistent currents of lightning).

b) optical measurements

The photography at the foot of the triggered lightning arc is performed with cinematographic equipment (high speed moving picture cameras at 54 frames/s and 150 frames/s), installed at 100 m from the pylon and 70 m from the ground launching pad.

The visualization of the triggered lightning flashes is obtained by means of additional equipment (photographic cameras, cine cameras at 48 and 500 frames/s and streak cameras) assembled at another station located 2.7 km, south of the firing pad. An example of lightning stroke visualization is given in fig.2.

c) acoustic measurements

Pressure sensitive probes are installed in the vicinity of the ground firing pads (at distances from 0.6 m to 200 m), in order to analyze the characteristic acoustic wave produced by the lightning flash.

d) electromagnetic measurements

Several measurements of the electromagnetic field are made at a number of points on the site (Fig.3). In general, the measurements are applicable to natural lightning as well as to triggered lightning.

. Wide band measurements

These are intended for the study of the electrical impulse produced by the lightning-flash. They are made in proximity to the firing pads and in a zone located about 3 km south-east of the station.

The electric and magnetic sensors used have a passband between 150 Hz and 20 MHz.

. Localization of UHF sources

ONERA has set up a phased array located 7 km North of and oriented towards the triggering station. This system is composed of an ensemble of 36 dipole antennas tuned to 0.9 Ghz and positioned on a plane reflecting panel (6 m x 6 m), inclined at 60° to the horizontal (Fig.4). The disposition of the dipoles was determined in order to permit, in optimal fashion, the restitution of the azimuthal and vertical positions of the U.H.F. electromagnetic sources created by the discharge. The antennas were connected to 36 synchronized receivers, the outputs of which were fed to a 14 channel analog magnetic recorder.

The data reduction of the measurements is made at a later time by computer numerical analysis. These procedures are currently being worked out.

e) detection of atmospheric conditions

A 10 cm radar, operated by IOPG, is installed 12 km south of the station. This radar detects the approach of cloud formations. In complementing thus the classic meteorological infor-

mation, it contributes to the determination of the favorable times for triggering the lightning.

During storms, the reflection ratio of the cloud cells is measured and recorded in a manner to permit the determination of their structure.

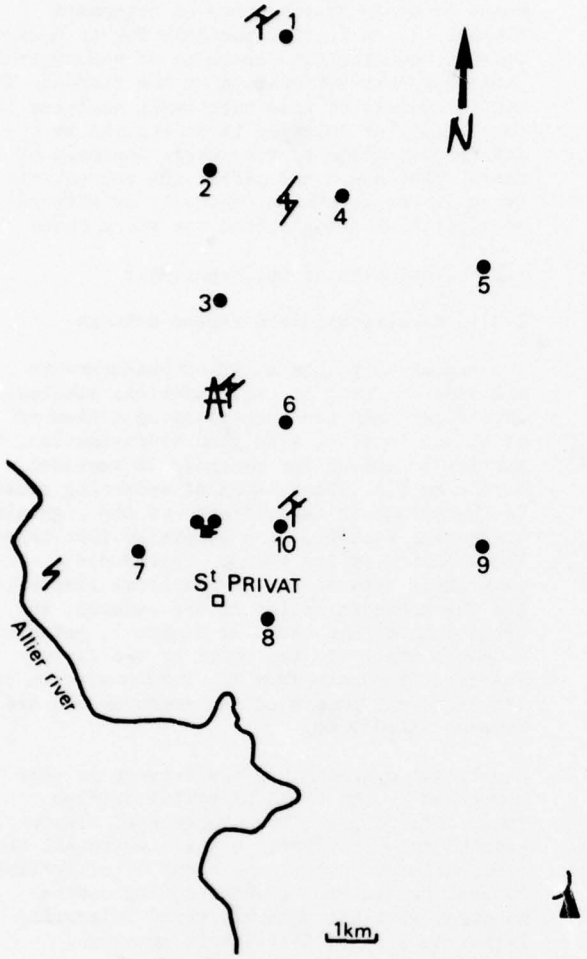

Fig. 3 – Disposition of experimental site.

Legend :

- ● Electrostatic field sensor
- Electromagnetic field measurement
- Station for triggering lightning
- Optical measurements
- Radar 10 cm

Triggered lightning flash A :

- Negative charge neutralized (Z = 6 km)
- Positive charge neutralized (Z = 7.2 km)

f) electrostatic field measurements

The horizontal and vertical components of the electrostatic field are measured at altitude by probe-equipped balloons. The field on the ground and the variations during the lightning are measured at 10 distant sites by means of a network of detectors. The objectives of this measurement are, on the one hand, to follow the evolution of electricity in the atmosphere during periods of storm activity and, on the other hand, to localize the electric charges neutralized during the natural and triggered lightning discharges. The following presentation is devoted entirely to the description and analysis of the preliminary results of these experiments.

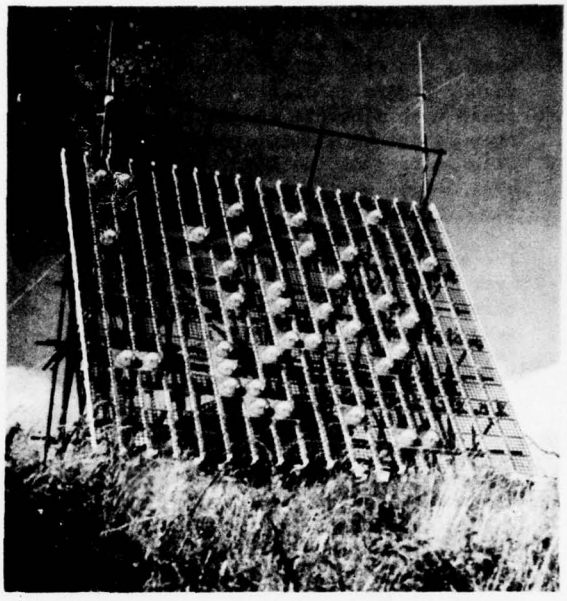

Fig. 4 – Phased antenna array.

2. NETWORK OF ELECTROSTATIC FIELD SENSORS

2.1. Electrostatic Field at Ground During Storm[6,7]

Separated electrical charges inside connective clouds induce, at ground, high electrostatic fields, which can be as large as several times 10^4 kV/m beneath important cloud cells.

a) The relatively slow variations of the field, at ground, without lightning strokes, are caused either by cloud cell movements or by local variations of electrification mechanisms. These evolutions, detected simultaneously, at different points on the ground, permit one to find, under some conditions, the geographical position of a single particular storm-cloud cell. Several investigators have desmonstrated that the electrical field induced at ground by the cells would be represented by a vertical distribution of point charges above a conductive plane.

It should be noted that this kind of an electrical model cannot describe completely the exact physical nature of cell electrification. The use of these models which show generally the axial symmetry of the field at ground

and define the localization of storms may be used also for the definition of warning systems (i.e. short time prediction of the field increase at ground or of the arrival of storms).

b) The rapid variations of electrostatic field are produced by lightning strokes. The measurements of these variations give much information on the nature and the development of the phenomena.

Figure 5, taken from the work of R.H. Golde,[6] shows the variation of the electrical field during two typical discharges between cloud and earth. Figure 5a corresponds to an impulse flash with discrete components. Every field step is due to a return-stroke which induces illumination of the stroke channel, and the neutralization of a part of the charge inside the cloud.

The second picture (Fig.5b) corresponds to a hybrid flash which is characterized by persistent illumination of the channel, and by several successive return-strokes. The persistent component causes, under those conditions, a progressive variation of the electric field at ground.

The exploitation of the measurements of these variations, at several points, together with the use of the electrostatic models, permits the determination of the electrical charges neutralized by the return-strokes, and also the determination of the whole charge dissipated by the flash.

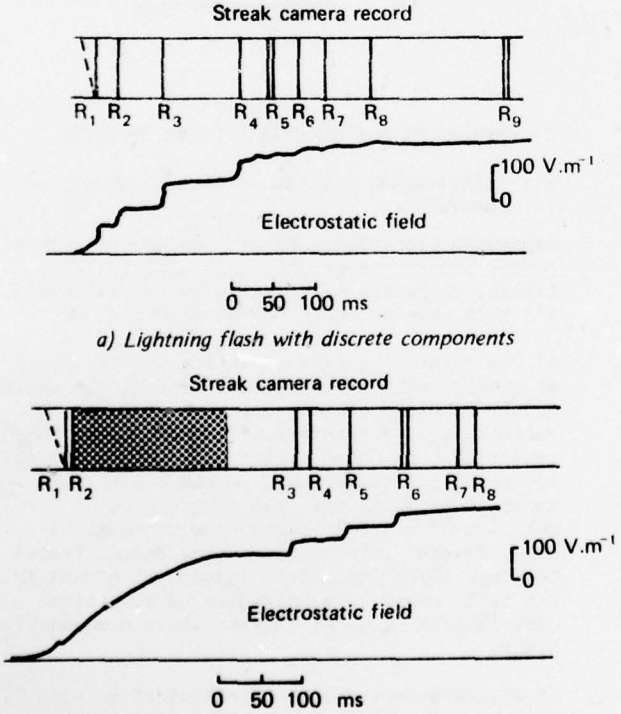

a) Lightning flash with discrete components

b) Hybrid lightning flash

Fig. 5 – Typical electric field variations during lightning flash (Kitagawa 1962).

2.2. Purpose of Measurements

The purpose of the measurements is to localize the cloud cells and also the charge centers neutralized by the lightning flashes.

This method of localization is validated by means of other measurements on triggered flashes. It is in fact possible, for triggered flashes, to calculate the value of the neutralized charge by integration of the current. The other interest of this experiment concerns the possibility of relating these results to the information given by the radar. Analysis of these relations would permit the characterization of the electrical activity of different precipitation areas within the storm cloud.

2.3. Description of the Experiment

2.3.1. Electrical field sensor network

The number of points at which measurements are made is fixed at ten. Numerical simulations have shown that the corresponding system of equations is able, with good approximation, to furnish solutions for monopole or vertical dipole models. The network of measuring sensors is installed, in the vicinity of the lightning triggering station, on a generally flat terrain. The location of the sensors represents a compromize between the geographical limitations and the characteristics of the sensors. The final disposition, shown in figure 3, extends from the north to the south of the firing station. Distances from the firing station to the different points of the measurements are between 1 and 9 km.

Functional operation of the network is telecommanded by the ONERA principal station (point n°1, fig.3). The sequence of events is started from the firing station where all the information on storm conditions is centralized. Natural events are recorded during several minutes, with the possibility of triggering lightning strokes within this interval.

2.3.2. Electrical field measurement stations

The stations are automatic and consist of an electrical field sensor (cf. 2.3.3.) and of command and recorder systems inside a metallic shelter (Fig.6). This shelter is located at about 50 meters from the sensor, to avoid electrical configuration modification in the vicinity of the measurement point. The functional states of the station (start, stop and record) are indicated by a signal transmitted to the principal station n°1. Measurements are recorded at each station on magnetic tape in two forms : one form is by frequency modulation (FM channel pass band 0-5 kHz) for the analog signal and for the time base ; the second form is direct recording (pass band 100 Hz-75 kHz) for the digitilized signal.

Fig. 6 – Station for measurement of atmospheric electric field.

2.3.3. Electrical field sensor

This sensor is a type of electrostatic field-mill : the design has been defined and optimized for both of the following objectives :

a) measurements of slow variations of the electrical field

b) measurements of rapid changes of the field during lightning.

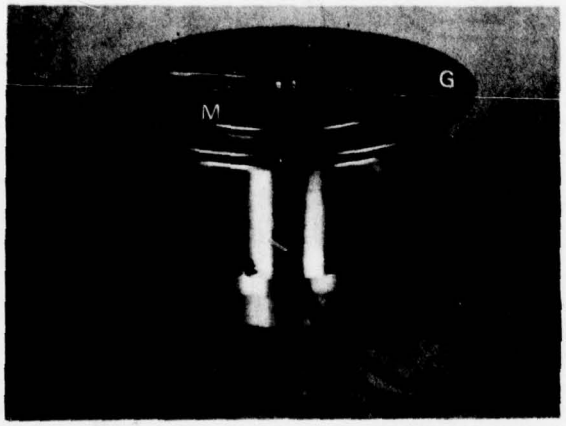

Fig. 7 – Electrostatic field sensor.

The sensor, shown in figure 7, has a detection unit and an electronic unit for signal treatment. A rotating electrode M, driven at 62.5 Hz by a DC motor, shields periodically a fixed electrode G. Both electrodes G and M have the same number of sectors (20). Another sensing electrode receives an induced 1250 Hz signal.

It can be shown that this configuration,, together with suitable electronics, is capable of detecting a step of the electric field with a rise time as shorter than one millisecond.

The electronics include principally a preamplifier which gives a measurement signal *independent of* the speed of the field mill motor. A synchronous detector is commanded by an in-phase signal formed by an optoelectronic device. The sensor gives directly an analog signal and also a digital signal composed of 12 bit words delivered 2 500 times per second. These two signals are transmitted to the shelter by cables. The threshold of the measurement is about 15 Vm^{-1} and the whole range is ± 30 kVm^{-1}.

2.4. Methods for Determining the Location of the Electrical Charges

2.4.1. Analytical solution of system of equations

The single charge model can describe correctly, in general, the neutralization of charges by cloud to ground discharge. This mathematical model can be solved analytically[8]. Let Q denote the equivalent charge at Z km above ground, X and Y the coordinates of its position at ground and X_o, Y_o the coordinates of the point where the measurement is made; then the equivalent electrostatic field is :

$$\Delta E_{co} = \frac{-QZ}{2\pi\varepsilon_o\left[(X-X_o)^2+(Y-Y_o)^2+Z^2\right]^{3/2}}$$

The system of equations obtained with four measurements can be solved by means of a change of variables. When one has more than four measurements, combinations of these measurements, four at a time, permit one to obtain a set of X, Y, Z, Q solutions. The dispersion of the solutions depends upon the measurement errors and on the validity of the model.

2.4.2. Numerical computer solution of system of equations

Intra cloud or cloud to cloud discharges are often well represented by a vertical dipole charge model. The parameters of this model are the charges Q_1 and Q_2 situated at Z_1 and Z_2 km above a conducting plane simulating the ground. The field variation at a point X_o, Y_o is

$$\Delta E_{co} = -\sum_{i=1}^{2} \frac{Q_i Z_i}{2\pi\varepsilon_o\left[(X-X_o)^2+(Y-Y_o)^2+Z_i^2\right]^{3/2}}$$

The system of equations formed from these field measurements cannot be linearized. For this reason it is necessary to perform a numerical computer calculation which is based on a least squares method[9]; one looks for Q_1, Z_1

Q_2, Z_2, X and Y which minimize the following function :

$$F = \sum_{i=1}^{N} (\Delta E_{Mi} - \Delta E_{Ci})^2$$

where : N is the total number measurements (e.g. 10)

ΔE_{Mi} is the field value measured at station "i"

ΔE_{Ci} is the field value for the i^{th} station as calculated by the mathematical model.

2.5. Preliminary Results of the Experiment

Between July and September 1978, measurements were recorded for 310 lightning flashes ; 13 of these were triggered strokes during 5 storm events. The electrical fields were measured simultaneously at 6 or more stations, for a period of one hour and 17 minutes.

The reduction of the data was started in October 1978 and is not yet completed. The results presented in this paper are necessarily preliminary and do not give the entire synthesis of the measurements performed at St-Privat d'Allier.

2.5.1. Slow field variations

Storm cloud cells show electrical activity with varying amplitudes. Typical field variations, shown in figure 8a over a two minute interval, are characteristic of an active storm. On the average, strokes are detected every five seconds. The record in figure 8b shows field variations due to a storm cloud of small activity. Five strokes are detected during three minutes but points A and B correspond to triggered lightning strokes.

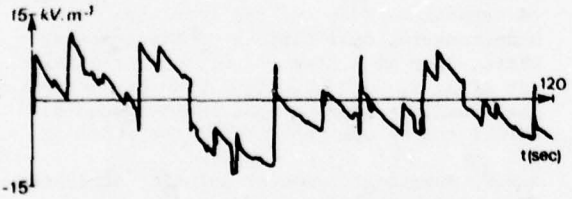

a – High activity cloud

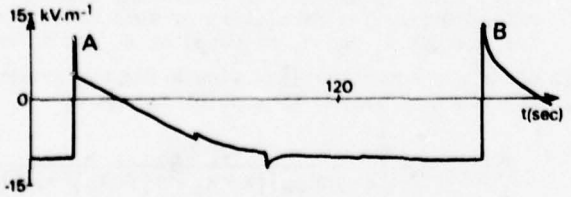

b – Low activity cloud.

Fig. 8 – Typical electric field variations.

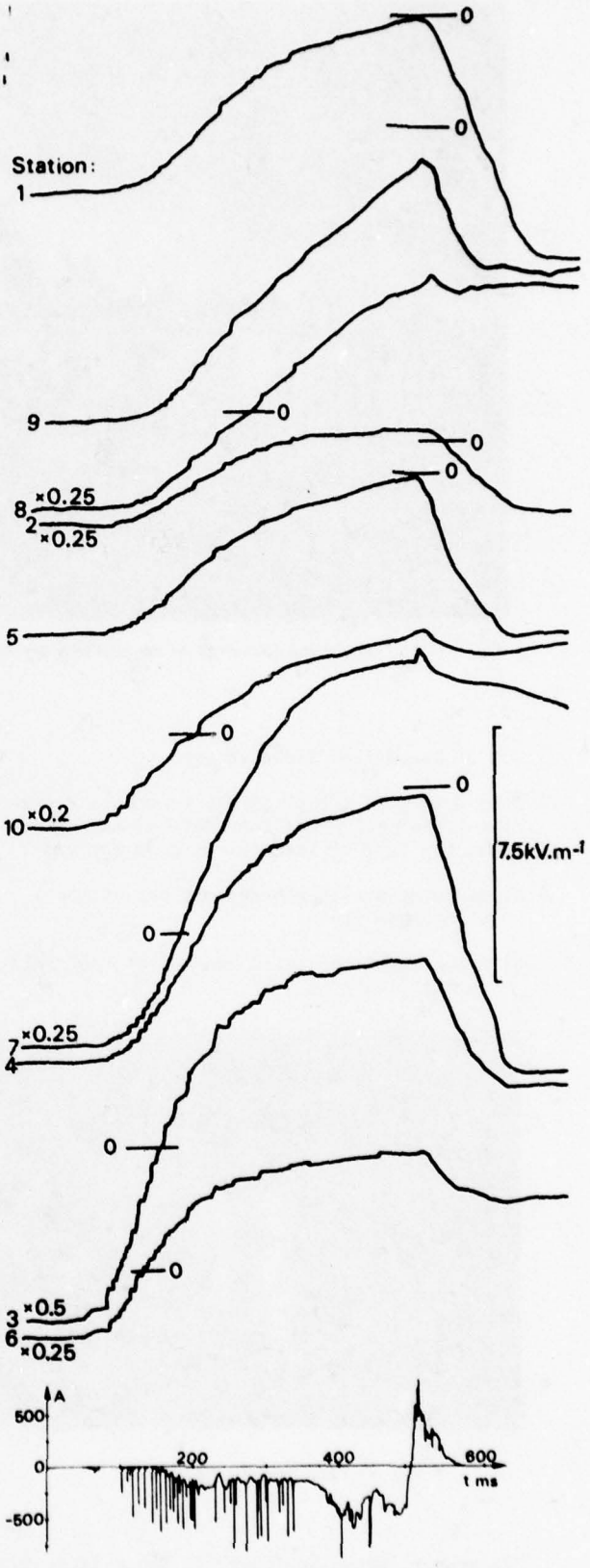

Fig. 9 – Variations of the electrostatic field due to the triggered lightning flash, A.

2.5.2. Rapid field variations during lightning

There is no special difference in the field measurements between natural and triggered lightning.

Figure 9 shows field variations at the ten stations during the triggered lightning stroke A and also the discharge current at the end of the arc. One notices an unusual characteristic of the flash ; 400 milliseconds after the first return stroke a positive discharge occurred and the lightning current was reversed. This phenomena appears clearly on all ten field measurements.

For this triggered lightning, current measurements indicate that 32 return-strokes occurred. The effect of about twenty of these return-strokes is visible in the field variation signals at stations 3 and 6, which are the closest to the firing station.

2.5.3. Initial trials on localization of charges

As an example, we have drawn on figure 2, the localizations obtained for the negative and positive charges neutralized in the triggered lightning event, "A". Lightning current integration indicates that a minus 77 C charge was neutralized by the negative part of the discharge and a plus 19 C charge subsequently flowed to ground. Values obtained by calculation on the ten field measurements are minus 105 C and plus 23 C. This first correlation obtained for a single triggered lightning flash is encouraging. A more detailed analysis of the entire series of measurements is now being performed.

3. CONCLUSION

The electrostatic field sensor network, which is a part of the experimental installation at St-Privat d'Allier, has given, in 1978, significant measurements on 310 triggered or natural lightning flashes. The first attempt to localize and to calculate the value of the charges neutralized by a lightning stroke has shown satisfactory correlation. This treatment must now be extended and completed by analysis of the entire series of measurements.

ACKNOWLEDGEMENTS

ONERA wishes to thank the organizations which have participated in the St-Privat d'Allier Research Group for their contributions to the measurements described in this paper. The first chapter of this paper, describing the entire site, has been written with information furnished by Electricité de France (Direction des Etudes et Recherches).

The ONERA research program has been supported in part by DRET (Direction des Recherches et Etudes Techniques).

REFERENCES

1. Newman, M.M. et al. Journal of Geophysical Research, Vol. 72, pages 4761-4764, 1967.

2. Newman, M.M. Problems of Atmospheric and Space Electricity, pages 482-490, Elsevier, 1965.

3. Fieux, R., Gary, C., Hubert, P., "Artificial Triggering of Lightning above Ground", IEEE Conference on Lightning and Static Electricity, April 1965 Culham.

4. Hamelin, J., Meesters, A., "Mesure des Champs Electromagnétiques créés par des Décharges Orageuses", Colloque International sur la Mesure en Télécommunication - URSI, Lannion 3-4 October 1977.

5. Groupe de Recherches de Saint-Privat d'Allier (EDF, CEA, CNET, ONERA, IOPG) "Développement des recherches sur la foudre en France", 14ème Conférence International de Protection contre la Foudre, Gdansk 1978.

6. Golde, R.H., "Lightning - Vol. 1 : Physics of Lightning", Academic Press 1977.

7. Uman, M.A., "Lightning", Mc Graw-Hill Book Company, 1969.

8. Krehbiel, P., McCrory, R., Brook, M., "The determination of lightning charge location from multistation electrostatic field charge measurements", Conference on Cloud Physics, Tucson, Arizona October 1974.

9. Jacobson, E.A. and Krider E.P., "Electrostatic Field Charges Produced by Florida Lightning", Journal of Atmospheric Science, Vol. 33, January 1976.

EVALUATION OF THE RYAN STORMSCOPE AS A SEVERE WEATHER AVOIDANCE SYSTEM FOR AIRCRAFT - PRELIMINARY REPORT

Timothy J. Seymour
Program Manager

Lt. Robert K. Baum
Test Engineer

Atmospheric Electricity Hazards Group
Air Force Flight Dynamics Laboratory
Wright Patterson AFB, Ohio

BIOGRAPHY

Timothy J. Seymour received his B.S. in mechanical engineering technology from Purdue University in 1970. He has been with the Flight Dynamics Laboratory since that time and for the past four years has been involved in various research projects concerning aircraft vulnerability to lightning, including lightning transient analysis tests on the F111, YF16, A7(ALOFT) and AIM-9.

Lt. Robert K. Baum received his B.S. in electrical engineering from Utah State University in 1974. He has been assigned to the Flight Dynamics Laboratory for two years, with responsibility for programs involving in-flight temperature measurement on warhead fragments and methods for air borne measurement of lightning characteristics.

ABSTRACT

The Ryan Stormscope was evaluated for use as a severe weather avoidance system for aircraft. An instrumented T-39B aircraft was flown in the vicinity of thunderstorm activity while displays of the Stormscope and onboard weather radar were documented photographically. The coordinates of the Stormscope display points and their acquisition times were interfaced to an onboard computer system for post-flight data reduction and comparison with the ground-based LDAR system. Preliminary analysis of the data shows that Stormscope exhibits reasonably good correlation with weather radar precipitation contours. Stormscope does not exhibit the tight clustering of data points characteristic of the ground-based LDAR system, a result which is attributed to inaccuracies in the Stormscope ranging system.

BACKGROUND

In 1977 the Air Force Flight Dynamics Laboratory and the 4950th Test Wing conducted a joint test program to evaluate the Ryan Stormscope, a lightning detection and display system developed for use by general aviation aircraft to avoid thunderstorm activity. The results of this study, reported in Reference 1, were inconclusive due to transient noise problems encountered in the initial Stormscope ADF antenna installation. It was decided, however, that the results warranted further evaluation of the Stormscope system and funds for further testing were provided by the Federal Aviation Administration.

The program was again directed by the Flight Dynamics Laboratory while the 4950th Test Wing provided test engineering. The same T-39B aircraft used in the previous program was used as the test bed. Aircraft modification and equipment installation were performed at the 4950th Test Wing facilities at Wright-Patterson AFB, Ohio during April-June 1978. The flight test phase of the program took place at Patrick AFB, Florida from 5 July to 27 July 1978 and was planned to coincide with the Tunderstorm Research International Program-1978 (TRIP-78). This location was chosen for two reasons: 1)high level of isolated thunderstorm activity, and 2) availability of the Lightning Detection & Ranging System (LDAR). The LDAR system provided an accurate ground based mapping of the electrical activity occurring during the thunderstorm for comparison with Stormscope indications.

PRODUCTS/EXPECTED RESULTS

The Stormscope was evaluated for possible application as a research aid for lightning characterization studies and as a severe weather avoidance system for aircraft. This paper will discuss preliminary data and results as they apply to severe weather avoidance. The use of Stormscope in lightning characterization research will be reported in a future paper.

To evaluate Stormscope, an instrumented T-39B aircraft was flown in the vicinity of thunderstorm activity while displays of the Stormscope and onboard weather radar were documented photographically. The coordinates of the Storm-

scope display points and their acquisition times were interfaced to an onboard computer system for post-flight data reduction and comparison with the accurate ground-based LDAR system.

TECHNICAL APPROACH

General: Figure 1 illustrates the equipment locations on the aircraft. The Stormscope, weather radar and time code generator were installed in an equipment rack in the cargo/passenger compartment of the aircraft. A standard 33 mm intervalometer-controlled camera was mounted on the right side of the aircraft so as to provide a simultaneous photographic record of the Stormscope, weather radar and time code generator displays (Figure 2). The data acquisition and storage system for storing the raw Stormscope data used a PDP 11/05 computer which was installed on the left side of the aircraft as shown in Figure 3.

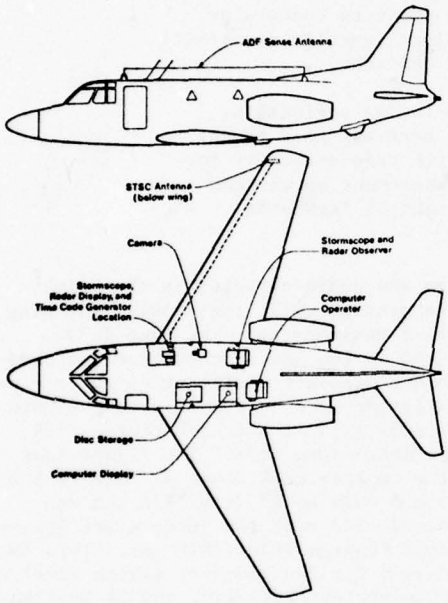

Figure 1. Location of the Test Equipment on T39B Aircraft

storage system for storing the raw Stormscope data used a PDP 11/05 computer which was installed on the left side of the aircraft as shown in Figure 3.

The automatic direction finding (ADF)-type antenna for the Stormscope was installed on the leading edge of the right wing tip. The sense antenna for the Stormscope was a 13 foot wire mounted on top of the fuselage. The antenna for the weather radar system was installed in the radome of the aircraft.

Equipment Description

a. Stormscope: The Ryan Stormscope (Figure 4) is a three-component, solid-state receiving system designed to detect the bearing and range of electrical disturbances in the 50 KHz region

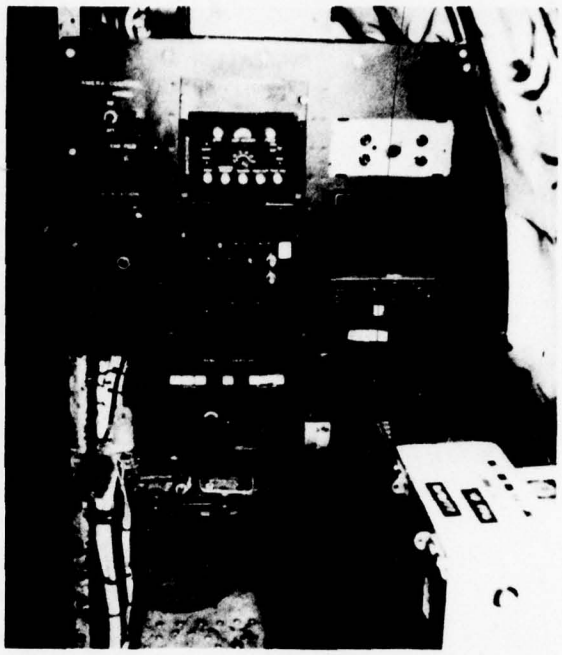

Figure 2. Stormscope, Weather Radar and Time Code Generator

Figure 3. Data Acquisition and Storage System

at up to 260 nautical miles from the aircraft over a 360° scan. Electromagnetic radiation from electrical disturbances is received via an automatic direction finding (ADF) antenna and fed into a central processing unit (CPU) which determines the bearing and range of the electrical disturbance. Each discharge is stored in one of the 128 available memory locations and is

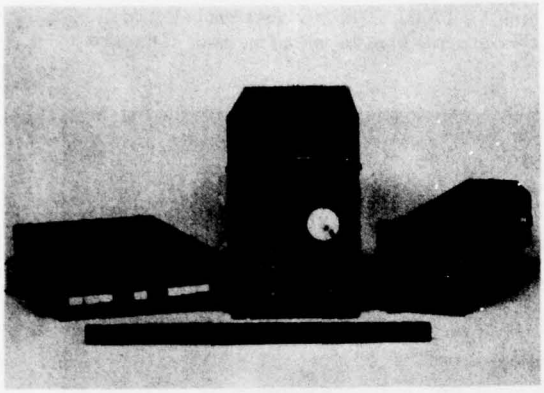

Figure 4. Stormscope Components

subsequently displayed on the CRT monitor. When the 129th discharge event occurs, the oldest event is erased from memory and the newest takes its place.

The CRT has an overlay consisting of a compass rose, two concentric range circles and a small plane outline in the center. The range can be varied by pushing a button on the unit so that the circles represent 20 and 40, 50 and 100 or 100 and 200 nautical miles, respectively. The CRT can be erased at any time by pushing the clear button, a process which requires four seconds and begins with the oldest events first. Partial erasure can be obtained by holding the button down for a shorter time. Since the location of each electrical discharge is displayed relative to the aircraft as stored in the memory, the CRT will continue to display the information in the same location in relation to the aircraft until the memory is erased or the 129th event occurs. Changes in heading of the aircraft will not affect those dots already displayed; consequently, frequent clearing is necessary to maintain an accurate presentation of the lightning activity with respect to the changing position of the aircraft in flight.

Azimuth of the lightning discharge is determined using a crossed-loop magnetic field antenna. Range is based on the assumption that, in the far-field region, the magnetic field intensity is essentially constant from discharge to discharge and is inversely proportional to distance from the discharge. The far-field magnetic component used in the ranging is derived from the crossed loop antenna. A long-wire antenna is used to provide electric field correlation with the magnetic field to enhance range accuracy. The long wire antenna is also used to eliminate azimuth ambiguity inherent in the crossed loop system. The crossed loop antenna is very sensitive to electrical noise generated by internal aircraft circuitry and it was necessary to relocate it from the lower fuselage to the right wingtip to reduce spurious response.

b. Onboard Data Acquisition System

b. Onboard Data Acquisition System

The diagram in Figure 5 illustrates the independent AFFDL system used to input, analyze and store the Stormscope data. The Stormscope used for the flight tests was modified by the manufacturer to output the X and Y coordinates of a given electrical discharge to a buffer for subsequent processing. An interface was constructed

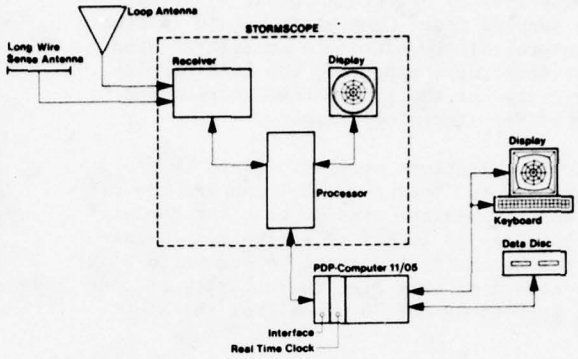

Figure 5. System Used to Input, Analyze and Store Stormscope Data

by AFFDL personnel to bring the coordinate data from the buffer register into the PDP 11/05 computer system where it was stored together with the signal acquisition time. Software was written to generate an updated visual display for preliminary inflight analysis. Data points and acquisition times were stored on flexible disc medium for post flight data reduction.

c. Weather Radar System: The onboard weather radar system used was a Bendix RDR-1300, 10 kilowatt, X-band unit. The three components of the system are a nose-mounted line-of-sight stabilizer antenna dish, a remote-mounted receiver-transmitter unit and a panel-mounted rectangular screen digital indicator. Digital techniques are used to display real time information and alphanumeric data on the radar screen. The readout indicates the mode of operation, range and range mark intervals (nautical miles). The system has a contour mode (Weather A) which is used to detect area of heavy precipitation. The total field of view for the system is 120° forward.

COMPARISON SYSTEMS

a. Lightning Detection and Ranging System (LDAR): The LDAR system determines range, azimuth and elevation of an electrical discharge using time of arrival of pulsed rf radiation emitted by the discharge. The LDAR system uses three physically separated antenna sites to determine discharge location. Three additional stations are used to check validity and accuracy of the primary antenna network. At a 40 nautical mile radius from the central LDAR site, range accuracy is ± 5% and azimuth accuracy is ± ½°. [1] Additional information on LDAR information may be found in Reference 2.

b. Ground Based Weather Radar: Ground based weather radar pictures were obtained from the weather station located at the Daytona Beach Regional Airport approximately 35 miles northwest of the LDAR site. These displays were available at five minute intervals and were used to give an overall indication of cloud formations and precipitation activity during the various flights.

Test Procedure: Personnel from the AFFDL attended daily weather briefings sponsored by TRIP 78 at the Kennedy Space Ctenter to obtain information on probable thunderstorm activity. When thunderstorms were expected, the LDAR display was activated at the KSC weather station and monitored for lightning activity.

Direct communications were maintained by the aircraft pilots, test personnel onboard the aircraft and the weather station to vector the aircraft to areas of lightning activity. In general, the aircraft flew straight leg vectors directly toward or away from the activity at distances between 20 and 70 miles from the storm center.

Initially, it was planned to obtain aircraft position from the aircraft's two TACAN receivers. However, it was found that the TACAN transponder interferred with operation of the test equipment. Therefore, their antennas were disconnected, and aircraft position was determined by recording headings and DME distances from the Orlando Vortac at regular intervals during each leg.

At the beginning of each flight, the onboard time code generator was synchronized to the LDAR time base. Prior to any data acquisition, the Stormscope was tested, set to the 100 nautical mile range and cleared. During the flight, the display was cleared after each heading change and at approximately two minute intervals. Pictures of the Stormscope, weather radar and time code generator were taken regularly during each run. X and Y coordinates of the Stormscope points in relation to the aircraft were recorded on disc together with the acquisition time.

Data Analysis: Data sources used in evaluating the Stormscope included: 1) in-flight photographs of the Stormscope, weather radar and time code generator displays, 2) ground radar photographs obtained from the weather station at Daytona Beach at specific times, and 3) 7 track magnetic tapes listing x and y coordinates of LDAR data points from the LDAR site with their respective acquisition times.

a. In-flight Photographs:

A visual comparison was made between a series of in-flight photographs of the Stormscope and weather radar displays. Particular attention was paid to the location of contour areas on the radar display to determine if these could be correlated with clustering formations (indicating a high degree of lightning activity) on the Stormscope display.

The first set of photographs (Figures 6 and 7) was taken during the second flight on 25 July at 17 13 37 and 17 17 07 EDT, respectively. In Figure 6 the Stormscope is showing two clusters

Figure 6. Stormscope and Weather Radar Comparison-25 July

over areas of approximately 340-360° at distances of 20-50 and 70-90 nautical miles, respectively. There is some indication of very light electrical activity northeast and northwest of the aircraft. Weather radar shows cloud formations ahead of the aircraft and to the northwest at 20 to 80 miles. The cloud formation at 350° and 70-80 miles shows contouring and corresponds well to the outermost Stormscope cluster. In Figure 7, taken about 4 minutes later, the weather radar shows the two

Figure 7. Stormscope and Weather Radar Comparison-25 July

storm cells have coalesced. The contour area at 55 to 70 miles on the radar (350°) also appears on the Stormscope. The Stormscope shows a high level of electrical activity in the 330 to 360° area.

Figures 8 and 9 were taken during a flight on 26 July at 15 58 29 and 16 17 38, respectively.

Figure 8 was taken with the Stormscope on the 100 nautical mile range and the weather radar on the

Figure 8. Stormscope and Weather Radar Comparison-26 July

80 nautical mile range. Again the Stormscope shows electrical activity in an area where storm cells are coming together. Stormscope shows a clear path to the northwest while weather radar indicates clouds; this is a case in which a pilot having one system or the other might respond in different ways. Later in the same flight, in Figure 9, a picture was taken with the Stormscope and weather radar both on the 40 mile ranges. A review of the sequence from which this picture was taken showed that Stormscope was populating

Figure 9. Stormscope and Weather Radar Comparison-26 July

very slowly over this time period-the level of activity within 40 miles of the aircraft is apparently now quite low. The line on the 030 radial probably illustrates the 'spoke' effect of the Stormscope. A stronger than normal stroke appears as a line of dots moving inward toward the nose of the aircraft along a particular radial.

As previously mentioned, only a preliminary analysis of the pictures has been performed. It is expected that many more comparisons of the above type will be included in the final report.

b. Comparison of Stormscope Data with LDAR and Ground-Based Radar Displays:

Before a comparison could be made between the various displays, it was first necessary to rotate and translate the Stormscope points from the aircraft coordinate system to a common coordinate system based at the central LDAR site. This transformation was accomplished on a point by point basis using the following equations:

$$R_x = S_x \cos \theta - S_y \sin \theta + P_x$$

$$R_y = S_y \cos \theta + S_x \sin \theta + P_y$$

where: S_x = Stormscope x coordinate relative to aircraft

S_y = Stormscope y coordinate relative to aircraft

P_x = Plane x coordinate relative to LDAR site

P_y = Plane y coordinate relative to LDAR site

θ = 360^o - aircraft heading

R_x = Translated x coordinate relative to LDAR

R_y = Translated y coordinate relative to LDAR

Software was developed to provide a graphic display of the translated data which could be compared with a similar display of the LDAR points acquired during the same time interval. The resulting program draws a scaled outline of the Florida coast, and provides reference markings indicating the location of the LDAR site, Patrick AFB, Daytona Beach radar site and the Orlando Vortac. The program then plots the translated Stormscope data and the cooresponding aircraft track positions during successive fifteen minute intervals.

Software was also developed to reformat the 7 track magnetic tape supplied by LDAR personnel to flexible disc suitable for use on the PDP 11/05 system. The software also was designed to eliminate LDAR data points which differed more than 1^o azimuth and 2 nautical miles in range between the independent receiving stations.

The ground radar photographs were also cropped and properly scaled to the LDAR and Stormscope displays to permit visual comparison of the three systems.

At the time of this writing, only LDAR data for the two flights on the afternoon of 25 July had been received and analyzed. Composites showing the Stormscope, LDAR and ground weather radar displays during different runs on 25 July were prepared to facilitate comparison of the data. Three of these composites are shown in Figures 10, 11 and 12, respectively.

In each composite, the central cross marks the location of the LDAR site at Kennedy Space Center. The range ring is at 80 nautical miles and the dotted line represents the plane track. The heading and beginning and ending times for the particular run are given in the upper right corner. Ldar data are depicted as solid circles, Stormscope data as open circles and weather radar data as shaded areas.

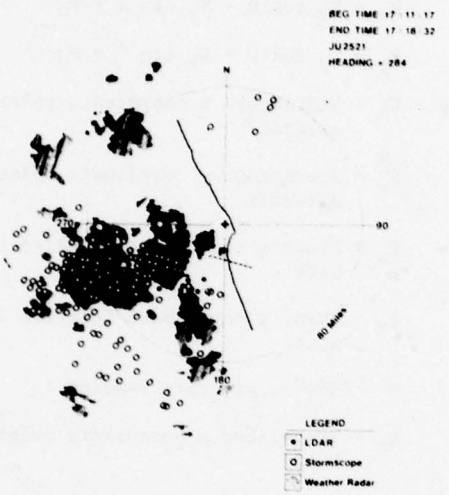

Figure 10. Stormscope, LDAR and Weather Radar Comparison - Flight 2, Run 1

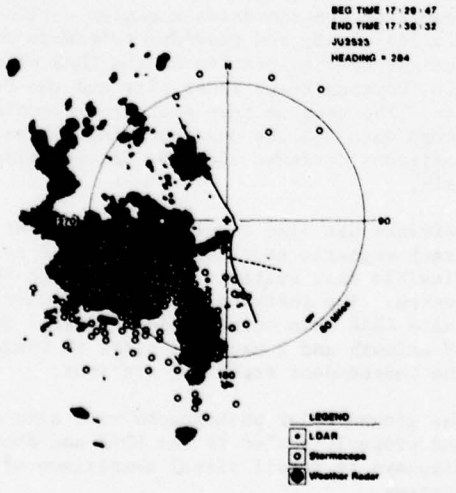

Figure 11. Stormscope, LDAR and Weather Radar Comparison, Flight 2, Run 3

SUMMARY

1. On the flights reviewed to date, Stormscope exhibits reasonably good correlation with weather radar precipitation contours. Some discrepancies were noted (and expected) since areas of

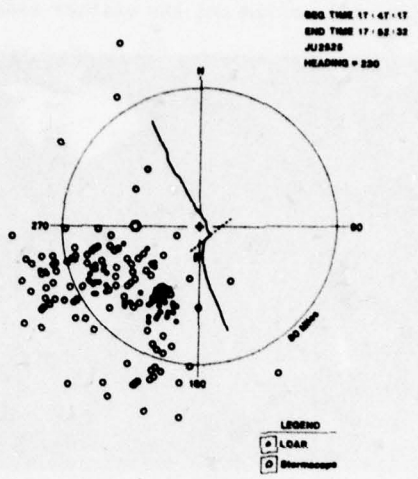

Figure 12. Stormscope, LDAR and Weather Radar Comparison - Flight 2, Run 5

high electrical activity do not necessarily occur in heavy precipitation areas.

2. On the runs reviewed to date, Stormscope does not exhibit the tight clustering of data points characteristic of the ground-based LDAR system. Point by point comparisons between LDAR and Stormscope for range and azimuth accuracy have not yet been accomplished. However, it is felt that inaccuracies in Stormscope ranging information are primarily responsible for the dispersion of the discharge locations. In certain respects this dispersion effect provides a margin of safety to the pilot avoiding severe weather since the electrical activity is displayed over a broader area.

3. Stormscope is highly sensitive to spurious electrical noise generated within the aircraft. The flat pack crossed loop antenna must be located in an electrically quiet region for successful operation.

4. On the flights reviewed to date there are several instances where Stormscope's 360° scan shows electrical activity behind and/or to the left or right of the aircraft in areas not visible on the weather radar. Activity is displayed regardless of altitude; no changes in antenna tilt such as may be required to interpret a weather radar display are necessary.

5. The Stormscope can be used on the ground in preflight planning to provide departure vectors that will avoid electrical activity. The 360° ground scan was used to verify planned departure vectors for the flight on 27 July when a thunderstorm passed over Patrick AFB prior to takeoff.

ACKNOWLEDGEMENTS:

The authors would like to thank Martin Risley, Technology/Scientific Services Inc. (T/SSI) for equipment design and construction, Jean Reazer, T/SSI, for assistance with computer operation,

data reduction and report preparation, and Carl Lennon, Kennedy Space Center, for providing LDAR data during the flight program itself and for subsequent analysis.

REFERENCES:

1. Mangold, V.L., Evaluation of Stormscope-Phase I, AFFDL/FES, January 1978.

2. An Accuracy Analysis of the LDAR System, Federal Electric Corporation (FEC-7146), Contract NAS 10-4967, 8 March 1977.

GROUND EVALUATION OF LIGHTNING MONITORING SYSTEM (STORMSCOPE)

JOHN G. SCHNEIDER, Test Engineer
Technology/Scientific Services, Inc.
Dayton, Ohio 45431

VERNON L. MANGOLD, Project Engineer
Air Force Flight Dynamics Laboratory
Wright-Patterson AFB, Ohio 45433

BIOGRAPHY

John G. Schneider is a test engineer for Technology/Scientific Services, Inc., Dayton, Ohio. He obtained his B.S. degree in electrical engineering from the University of Wisconsin in 1971. For the past four years he has been involved in various research projects concerning aircraft vulnerability to lightning, including lightning transient analysis tests on the F111, YF16 and A7 (ALOFT).

Vernon L. Mangold is a project physicist with the Air Force Flight Dynamics Laboratory with a B.S. in math and physics received in 1961. He was responsible for the establishment of the Air Force's Atmospheric Electricity Hazards research program and is a former chief of the Electromagneitc Hazards Group.

ABSTRACT

A ground-based lightning monitoring system was set up at the Kennedy Space Center (KSC) to evaluate its usefulness in locating and tracking lightning activity. Information from the ground-based system, a Ryan Stormscope, was compared to data obtained from the Lightning Detection and Ranging System (LDAR) and weather radar displays located at KSC. Correlation was obtained among the three systems. This paper reports on the data obtained during the program and evaluates and compares the three systems. The research was performed during the Thunderstorm Research International Program-1977 (TRIP-77).

BACKGROUND

During July and August, 1977 Technology/Scientific Services, Inc. provided contract support during an evaluation of a Ryan Stormscope by the Air Force Flight Dynamics Laboratory, Electromagnetic Hazards Group (AFFDL/FESL) at Kennedy Space Center (KSC), Florida. This location and time frame were chosen because of the high level of isolated thunderstorm activity and the availability of the Lightning Detection and Ranging system (LDAR) at KSC. The LDAR system provided an accurate mapping of the electrical activity occurring during a thunderstorm for comparison with Stormscope indications.

PRODUCTS/EXPECTED RESULTS

The Ryan Stormscope was developed for general aviation aircraft to locate electrical discharges and thus aid in thunderstorm avoidance. In a companion program in 1977 AFFDL/FESL equipped a T-39 aircraft with a Stormscope for inflight correlations of the Stormscope display with onboard weather radar and the ground-based LDAR system.[1]

Interest in the Stormscope centered on two objectives: its use as a severe weather avoidance system for general aviation aircraft and its use as a research aid for lightning characterization studies. This preliminary study showed that the Stormscope system gave sufficient general agreement with LDAR indications to justify further testing as planned by AFFDL/FESL.

TECHNICAL APPROACH

a. Ground Station Instrumentation

The Stormscope is designed to locate electrical discharges that have a 50 kHz component at a distance of up to 200 nautical miles. It consists of a receiver which detects, sorts and analyzes the incoming signals, a microprocessing (CPU) unit which performs the mathematical computations, and a cathode ray tube (CRT) which displays the 'dots' representing lightning storm activity. (See Figure 1.)

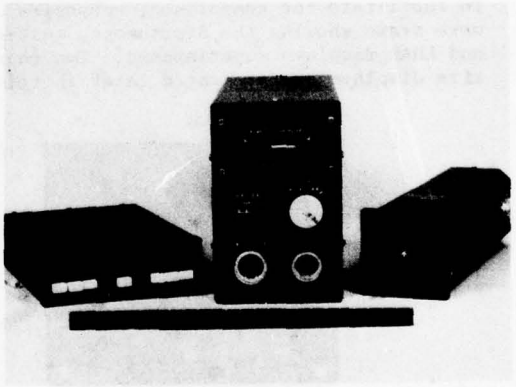

FIGURE 1. RYAN STORMSCOPE SYSTEM COMPONENTS

The Stormscope uses an automatic direction finding (ADF) antenna to receive electromagnetic radiation from lightning strikes. After the CPU determines the azimuth and pseudorange of the electrical disturbance, the discharge is represented as a dot on the CRT display. A sense antenna attached to the Stormscope detects the waveform of the disturbance. The CPU compares the waveform to a stored 'typical' lightning waveform; if the signal is only random noise, no dot appears on the CRT.

Up to 128 lightning discharges can be stored and displayed. The 129th discharge event causes the 'oldest' discharge event to be erased. Pushing a button clears the display, a process taking four seconds and beginning with the oldest dots. If only partial erasure is desired the button can be held down for a shorter time.

The display scope is a 3-inch CRT with an overlay containing a 12-point compass rose, an aircraft symbol and two concentric range circles. The scope provides a 360^{o} field of view. The range circles, which can be varied through 20-40, 50-100 and 100-200 nautical mile representations, provide a pseudo-range by assuming that all lightning strikes are essentially of the same intensity and generate the same electromagnetic field strength signal. The signal received is compared to a stored value and is processed in the CPU to represent distance from the aircraft for that lightning discharge event. A stroke of greater intensity than the standard or average intensity would therefore appear to be closer to the aircraft than it really was while a weaker one would appear to be farther away.

The Stormscope was set up at the ground station with a 15-inch long sense antenna and a standard two-loop ADF antenna. The CRT display was mounted on top of a time code generator set to Eastern Daylight Time ($\pm$ 1 second). The display and time were recorded with a 35mm camera. The Stormscope and time code generator are shown in Figure 2. These displays were then compared with LDAR and weather radar pictures.

To facilitate the comparison, composite overlays were drawn showing the Stormscope, weather radar and LDAR displays superimposed. Two representative displays are presented later in this report.

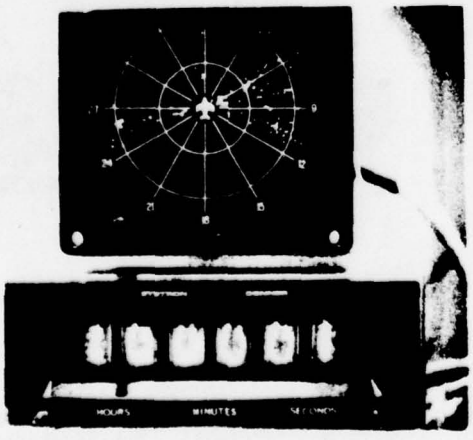

Figure 2. Stormscope and Time Code Generator

b. Comparison Systems

The LDAR system provided a space-time history of the lightning process by measuring the time of arrival of RF lightning pulses (30-50 MHz frequency) at different receiving stations. The lightning waveform data obtained were recorded, then processed by high-speed transient recorders to provide a 'dot'display showing the range, elevation and azimuth of the RF radiation source.

The LDAR system displays the location of lightning discharges within 40 kilometers with a high degree of accuracy.[2] During a typical activity period the display is allowed to collect one hundred dots before it updates. The initial and final acquisition times are printed on the display to allow determination of the rate at which electrical disturbances are occurring.

A typical LDAR display is shown in Figure 3. These displays were available at various intervals (depending on electrical activity levels) when thunderstorms were occurring within 40 kilometers of the site. The two concentric

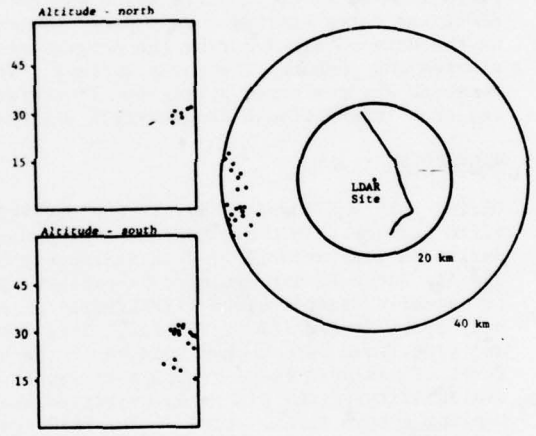

Figure 3. Typical LDAR Data Display

circles represent 20 and 40-mile ranges. The dark line shape in the middle of the inner circle represents the coastline of Cape Kennedy, with the single center dot representing the KSC LDAR site. The coastline and KSC representation is fixed to provide an overlay to the electrical data received and thus locate the azimuth and distance of the electrical disturbance. Each dot represents an electrical discharge having a component in the 30-50 MHz range as received by the LDAR system. The blocks to the left of the circles represent the altitude of the disturbance in the northern (top) and southern (bottom) directions.

A typical display from the Kennedy Space Center WSR72X radar and its accompanying time code is shown in Figure 4. The range in these displays

was limited to 38 nautical miles and the display shows cloud formations rather than electrical disturbances. Each circle on the display represents approximately 10 miles.

Since the time on the radar display is in GMT (1828), four hours must be added to the time shown on the time code generator when comparing the Stormscope displays to the weather radar data.

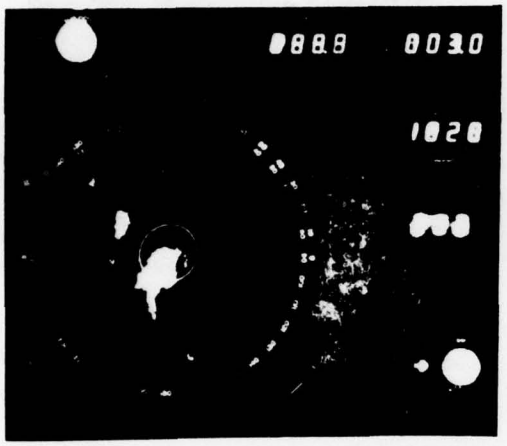

FIGURE 4. SAMPLE GROUND RADAR DISPLAY

c. Results

The Stormscope was set up with the reference airplane on the CRT headed north to facilitate comparisons with data from LDAR and weather radar. The central reference point for the LDAR system was located approximately 2 kilometers west-southwest of the Stormscope installation at the ground station. The proximity of these locations allowed accurate comparisons of data for storms at distances more than 20 miles from the two sites. At closer ranges the comparison is less accurate due to the different locations of the two systems.

Figures 5a, 5b and 5c show the Stormscope, LDAR and weather radar displays obtained on 22 July 1977. The LDAR and Stormscope data were recorded at 1815 GMT (2:15 EDT). The weather radar picture was taken five minutes later. Figure 5d is a composite representation in which data from the three displays are overlaid to facilitate comparison.

The Stormscope shows moderate to heavy electrical activity between 225° and 270° outward from about a five-mile range. Stormscope also shows high activity around 300° from about ten miles out. LDAR indicates moderate to heavy activity between 225° and 270° at a 15-mile range, light activity at 300° at a 10-mile range and scattered activity at 300° to 330° at 25 to 30 miles out.

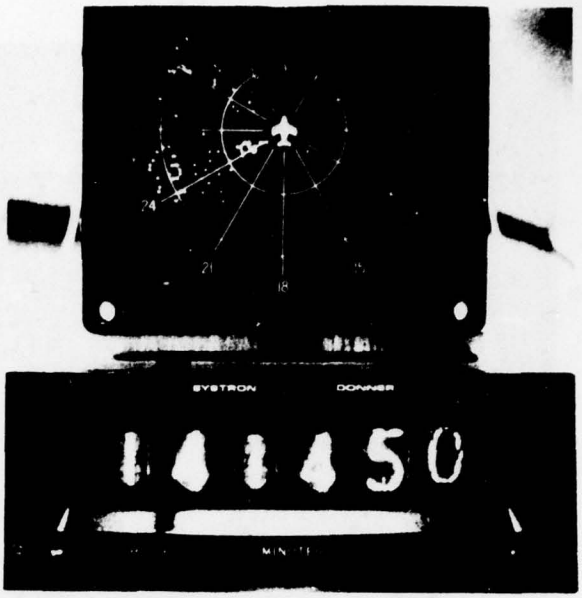

FIGURE 5a. STORMSCOPE-1815 GMT 22 JULY 77

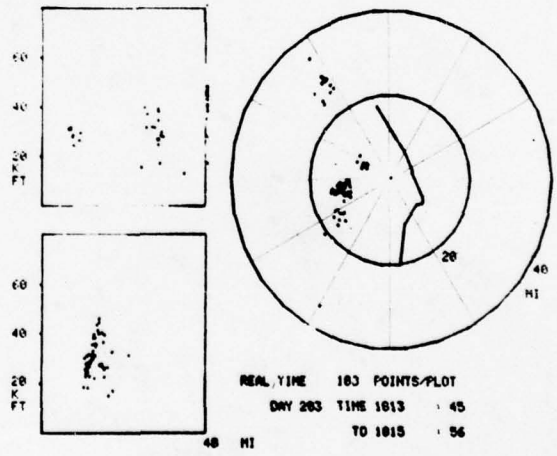

FIGURE 5b. LDAR-1815 GMT 22 JULY 77

The weather radar indicates cloud formations in these general areas, with some discrepancies due to the time lag and the fact that the radar antenna was located remotely from the control console, producing an angular displacement of 12° counterclockwise in the display. The heavier activity appears somewhat closer on Stormscope and more widespread because of its psuedo-range but the weaker activity at 300° has correlation between Stormscope and LDAR.

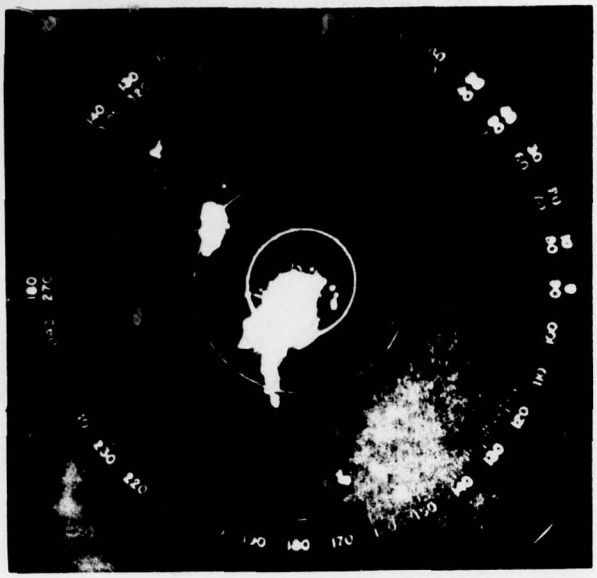

FIGURE 5c. WEATHER RADAR-1820 GMT 22 JULY 77

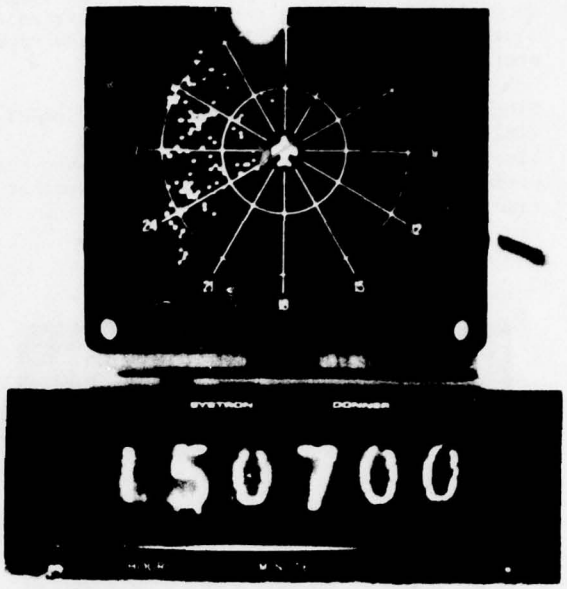

FIGURE 6a. STORMSCOPE 1907 GMT - 1 JULY 77

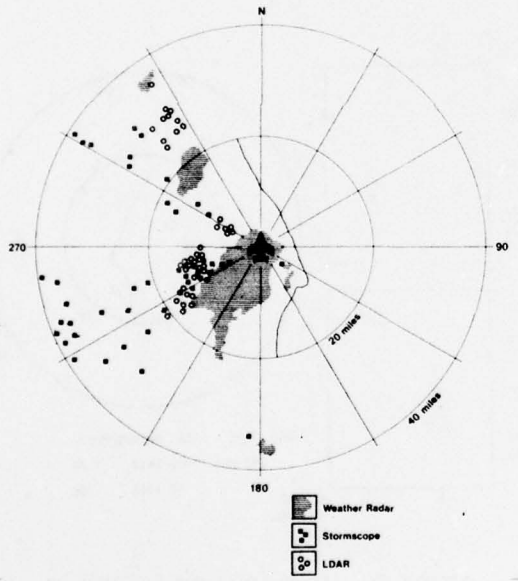

FIGURE 5d. OVERLAY OF STORMSCOPE, LDAR, AND WEATHER RADAR DATA 22 JULY 77

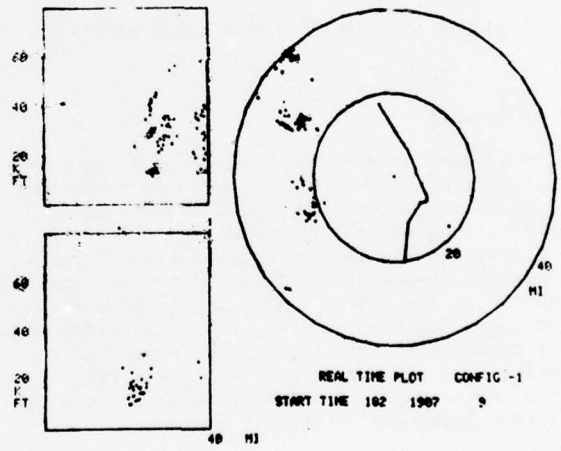

FIGURE 6b. LDAR 1907 GMT - 1 JULY 77

A second comparison is shown in Figures 6a, 6b, 6c and 6d. This information was recorded 1 July 1977 at 1907 GMT (3:07 EDT) and was from 20 to 40 miles from the ground station.

During this program no effort was made to compare the Stormscope data and LDAR data in real time. LDAR data was selected from available data printouts a number of days after the thunderstorm event and compared as closely as possible, in time, to the photographs taken of the Stormscope display. The Stormscope was not cleared; it was allowed to collect data over a definite time period and compared to similar time periods with the LDAR. There was an average of ±4 minutes between the time the Stormscope picture was taken and the time of the LDAR readout.

The azimuth and distance comparison between Stormscope and LDAR using the data available

shows a general agreement. This consists of indicating in what quadrant the lightning storm is located or developing and the general direction of the lightning storm movement.

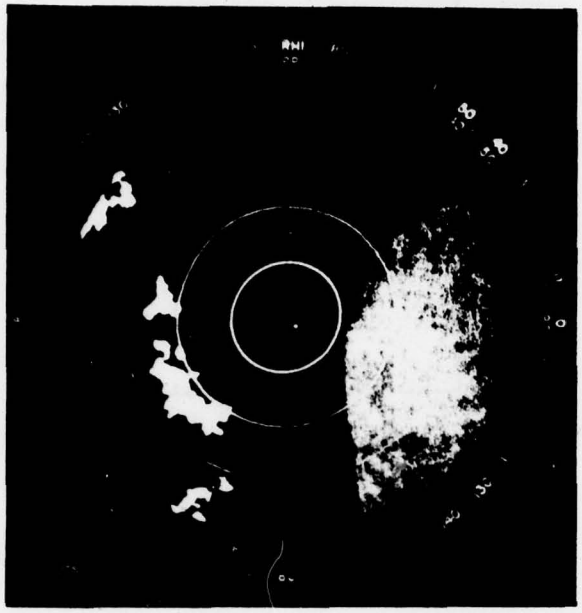

FIGURE 6c. WEATHER RADAR - 1908 GMT 1 JULY 77

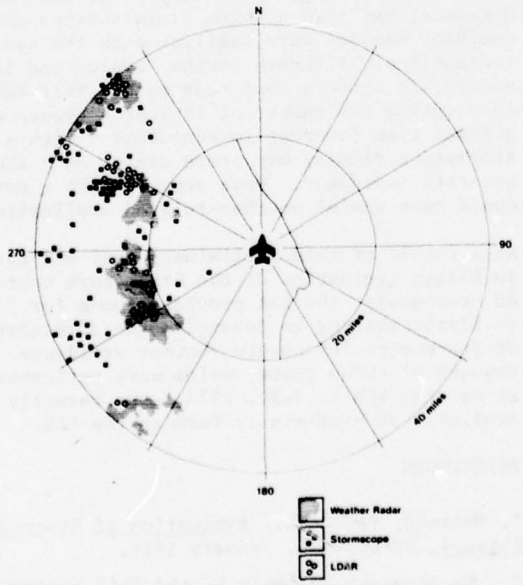

FIGURE 6d. OVERLAY OF STORMSCOPE, LDAR, AND WEATHER RADAR DATA - 1907 GMT 1 JULY 77

Tables 1 and 2 are general descriptions of lightning activity recorded by Stormscope and LDAR for the same storm.

	Average Location	Average Distance (n.m.)
Stormscope	278°	31.0 to 37.0
	250°	5.6 to 16.0
LDAR	243°	21.8 to 24.2
Stormscope	293°	26.6 to 38.8
	300°	14.6 to 19.2
	294°	40
LDAR	300°	22.4 to 27.8
Stormscope	278° to 286°	26.4 to 31.0
LDAR	295° to 304°	24.2 to 27.2
	290° to 293°	27.2 to 32.0

TABLE 1. GENERAL DESCRIPTION OF LIGHTNING ACTIVITY FOR STORM ON 22 JULY 77 (1815 GMT)

	Average Location	Average Distance (n.m.)
Stormscope	255°	6.1 to 15.2
LDAR	255°	9.6 to 15.0
Radar	Cloud	Cover
Stormscope	300°	10.6 to 17.5
LDAR	300°	6.0 to 9.6
Radar	290° to 310° Center on 300°	16.0 to 22.5
LDAR	325°	26.0 to 30.0
Stormscope	0	0
Radar	0	0
LDAR	0	0
Stormscope	240° to 270°	35.2 to 39.0
Radar	Past the	Range
LDAR	317° to 328°	24.0 to 31.0
Stormscope	300° to 315°	29.0 to 39.0
Radar	310° to 317°	34.0 to 37.0

TABLE 2. GENERAL DESCRIPTION OF LIGHTNING ACTIVITY FOR STORM ON 1 JULY 77 (1907 GMT)

Figure 7 illustrates the 'spoke' effect that can occur on a Stormscope display because of its pseudo-range. The storm at 60° is apparently a very severe one. Clusters of dots stretching from the storm area to the ground station ('plane') are shown as closer to the station than they actually are because of the high intensity of the strikes.

An attempt was made to determine if the number of events recorded by Stormscope over a fixed time interval could be correlated with the severity of the storm. A counter was connected to the sense antenna circuit on the Stormscope and monitored during storms on 1 August and

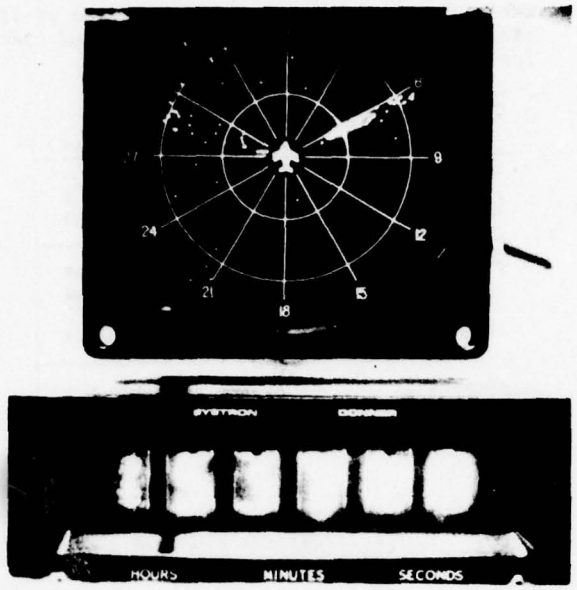

FIGURE 7. "SPOKE" EFFECT ON THE STORMSCOPE DISPLAY

3 August. Figures 8 and 9 show the number of events recorded for 10 second periods at intervals during the storm compared with LDAR data for the respective days, 1 August and 3 August.

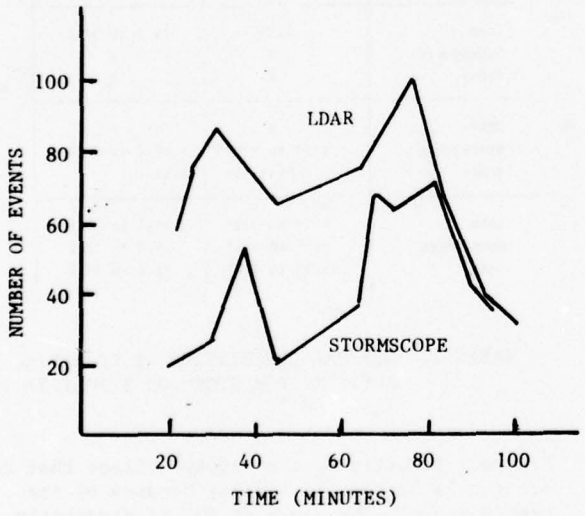

FIGURE 8. COMPARISON OF ELECTRICAL ACTIVITY LEVELS DETERMINED BY STORMSCOPE AND LDAR 8-1-77.

Results show that Stormscope data is in general agreement with LDAR data in regard to the severity of thunderstorm activity over a given area. Obviously, data from a counter alone cannot be used to indicate severity levels when more than one cell is building or decaying in the area but monitoring the display quickly indicates the activity level of individual cells.

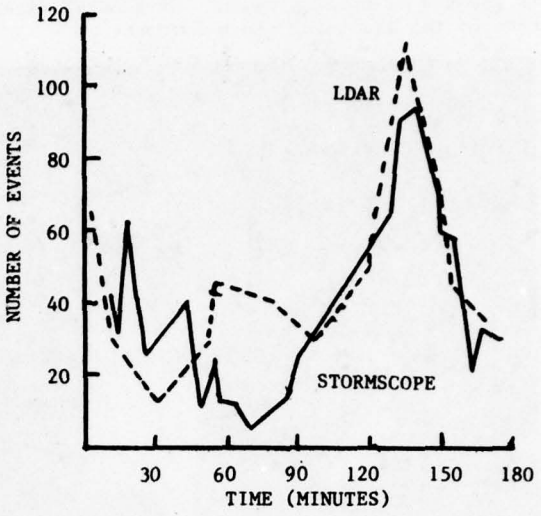

FIGURE 9. COMPARISON OF ELECTRICAL ACTIVITY LEVELS DETERMINED BY STORMSCOPE AND LDAR 8-3-77.

SUMMARY

The Stormscope gave promising results as an indicator of lightning activity. As an example of its accuracy, a NASA Lear Jet investigating lightning during in-flight tests as part of TRIP-77 was directed according to Stormscope's ground station indications and was able to locate lightning activity. Because of the pseudo-range there is some difficulty in estimating distance, but this problem diminishes as an operator becomes more familiar with the system indications. Although further evaluation is needed, it appears that some method that relies on counting the number of lightning events over a fixed time interval in conjunction with a Stormscope display may prove useful as a storm severity indicator. Once proven, such a method could have useful weather-related applications.

As a result of this preliminary test and the in-flight evaluation of the Stormscope mentioned previously, the FAA provided funds for further in-flight testing to determine the effectiveness of Stormscope for severe weather avoidance. The results of these tests, which were performed at Patrick AFB in July, 1978, were recently made available in preliminary form to the FAA.[3]

REFERENCES

1. Mangold, Vernon L., Evaluation of Stormscope-Phase I, AFFDL/FESL, January 1978.

2. An Accuracy Analysis of the LDAR System, Federal Electric Corporation (FEC-7146), Contract NAS. 10-4967,8 Mar. 1977.

3. Baum, Lt. R.K. and Seymour, T.J., Evaluation of the Ryan Stormscope as a Severe Weather Avoidance System for Aircraft, AFFDL/FESL, Dec. 1978.

TECHNIQUES FOR INCREASING THE LIGHTNING TOLERANCE OF THE NAVY/AIR FORCE AIR COMBAT MANEUVERING RANGE/INSTRUMENTATION SYSTEMS

J. E. NANEVICZ and E. F. VANCE
SRI International
333 Ravenswood Avenue
Menlo Park, California 94025

BIOGRAPHIES

J. E. Nanevicz is Assistant Director of the Electromagnetic Sciences Laboratory at SRI International, where he has been since 1954. He received BSEE and MSEE degrees from the University of Washington and a PhD from Stanford University. Dr. Nanevicz is an internationally recognized authority on lightning and static electricity and their effects on aerospace systems. He is the author of many papers and reports dealing with these subjects and is currently U.S. Editor for the Journal of Electrostatics.

E. F. Vance is a Senior Research Engineer at SRI International, where he has performed research on the Nuclear EMP and other interference and control techniques since 1959. Mr. Vance, who received a BS degree from UCLA and an MSEE degree from the University of Denver, has published numerous papers on electromagnetic interaction and is the author of a recently published book, Coupling to Shielded Cables.

ABSTRACT

This paper describes recommended lightning protection measures for the Tracking Instrumentation Subsystem (TIS) of the Navy Air Combat Maneuvering Range (ACMR) and Air Force Air Combat Maneuvering Instrumentation (ACMI). Physically, the TIS consists of an antenna tower, coaxial cables, and electronic instrumentation vans. Lightning strikes to the antenna tower have caused damage to sensitive components inside the van.

The design of the equipment and vans is such that excellent lightning tolerance could be readily incorporated into the design by applying the procedures recommended in the earlier paper, "Shielding and Grounding Topology for Interference Control," presented at the 1977 Workshop. The important features of the equipment are the all-metal van construction with more-or-less concentrated cable penetration areas, a "closed" ac power system (metal conduits and closed metal cabinets), metal cabinets and floor ducts for internal equipment, and a rational approach to grounding. These features are being developed into an effective two-level shield system without major redesign or reworking of the equipment. Incorporation of some of these shield improvements has already resulted in a major improvement in the system's lightning tolerance.

INTRODUCTION

The Navy/Air Force Air Combat Maneuvering Range/Instrumentation (ACMR/I) system is a sophisticated pilot-training aid consisting of remote tracking antennas and tracking instrumentation subsystem (TIS), and a control computing and recording facility located at a Navy or Air Force training range. Our concern here is primarily with the TIS, which consists of two all-metal vans, one containing electronic data processing and communication equipment. These vans are installed within communication range of the remote range tracking antennas, with which they communicate through tower-mounted VHF antennas. Within a few meters of the vans is thus a radio antenna tower that is typically about 156-m tall and is a frequent target for lightning.

A sketch of a typical TIS layout is shown in Figure 1. The equipment in the van is operated from commercial power, and local telephone service is provided to the vans. The power amplifiers for transmitting antennas and preamplifiers for receiving antennas are mounted on the tower base about 1 m above ground. Coaxial cables run from these amplifiers up the tower to the antennas and from the amplifiers into the equipment van and the RF amplifiers to supply the amplifier operating power. The all-metal equipment van is grounded externally by a large cable connected to a steel supporting beam on the underside of the van and to the tower footing about 10 m away. The ac power system is grounded 5 to 10 m from the van near the distribution transformers to one or more ground rods.

DIAGNOSIS OF PROBLEM

Discussion with on-site personnel regarding the effects of lightning strikes indicated that the principal damage occurred in the dc power supplies and in the line drivers and receivers at the ends of the interconnecting cables inside the van. The key components involved in these failures are sketched in Figure 2. Inside the van there are two interconnected equipment racks identified as XEROX COMP and RCVR XMTR in Figure 2. The dc power supplies in the XEROX COMP rack are connected to the outside power lines through the ac service entrance. If the power lines are struck by lightning, the power supplies may be subjected to transients entering on the ac power wiring. If the tower is struck, part of the stroke current

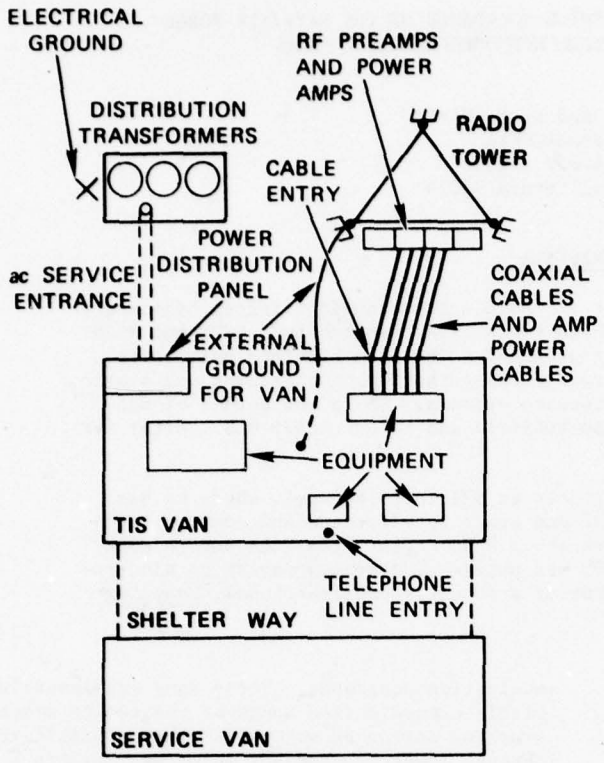

FIGURE 1 SKETCH OF A TIS INSTALLATION

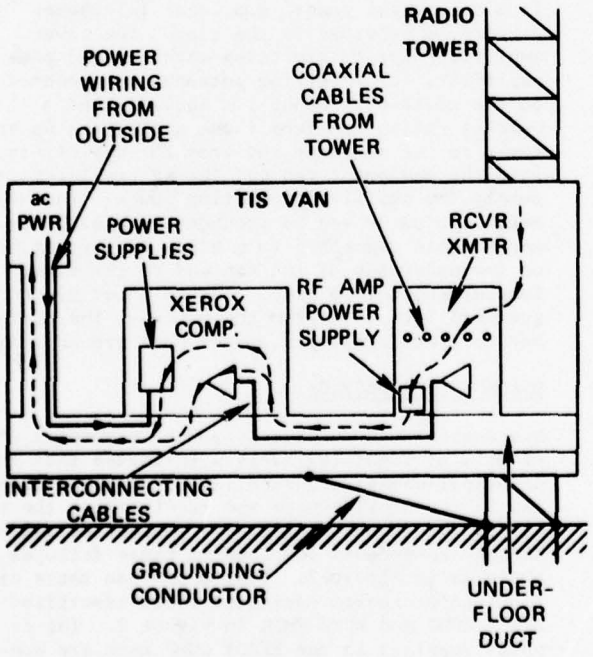

FIGURE 2 SKETCH OF COMPONENTS INVOLVED IN LIGHTNING DAMAGE

may enter the van on the coaxial cables and flow through the power supply and out on the ac power conductors (ground or neutral). Although some of the current on the coaxial cables may flow to ground through the outside grounding conductor, the van will be raised to a high potential by the Ri + Ldi/dt drop along this path, and this potential difference will appear in the power supplies between the case or chassis and the ac power wiring (which is externally grounded at the distribution transformers). In any event, the power supplies are subjected to large transients whether the power lines are the source of the transient or the exit path for tower currents.

When the coaxial cables from the tower are not connected to the van skin at the entry point, the shield currents are delivered to the RCVR XMTR rack. These very large currents can raise the potential of this rack with respect to the rest of the van (particularly if the rack is grounded to the van only through a long grounding conductor such as the power "green wire" ground). This potential may be divided between the RCVR rack and the interconnecting cables (see Figure 2) and between the interconnecting cables and the XEROX rack. The line drivers and receivers at the ends of the interconnecting cables will thus be highly stressed and subject to damage. A similar condition would prevail if the XEROX rack were driven by a large surge on the power conductors, although this mechanism appears to be less likely than the tower/coaxial cable excitation of the RCVR cabinet.

The observed failures were therefore compatible with the assessment that large surge currents may enter (or leave) the van on the power lines or on the coaxial cables from the radio tower. Therefore, damage to electronic components occurred because the integrity of shields such as the van skin was not preserved by diverting the current on penetrating conductors to the outside of the shield.

LIGHTNING PROTECTION

Properties of TIS Installations

In addition to diagnosing the probable cause of the damage produced by lightning, two installations were examined to identify features that might be useful in a hardening program. Although the two installations were similar in many respects, there were significant differences between the two insofar as their lightning protection is concerned. The TIS at Carrabelle, Florida (Tyndall AFB) was newer and displayed evidence of better lightning-protection practices than the TIS at Nag's Head, North Carolina (Oceana NAS). The installations had in common the following desirable features:

(1) The equipment vans were of all-metal construction such that they can be developed as primary shields.

(2) The vans were grounded to earth through a cable attached to the outside of the van (thereby preserving the integrity of the primary shield).

(3) All of the coaxial cables entered the van at one small region, making the use of a single entry panel feasible for these cables.

(4) Water and sewage pipes were plastic, so that these do not compromise the primary shield.

The installations also had in common the following undesirable features:

(1) The commercial ac power entering the van was not filtered; thus power-line transients could enter the van.

(2) Power for the RF preamplifiers and power amplifiers at the base of the tower was provided from supplies inside the van. Because these power leads were unprotected by shields or surge limiters, transients could enter the van and equipment cabinets along these power leads.

(3) The telephone lines were unprotected by shields or surge limiters, so that external transients could enter (or leave) the van on these leads.

(4) External conductors entered the van (primary shield) at three separate locations--near one end for the ac power, near the opposite end for the coaxial cables, and on the opposite side for the telephone lines.

The two installations were different in the following respects:

(1) At Carrabelle, the ac power conductors had secondary lightning arresters installed; at Nag's Head they had no protection.

(2) At Carrabelle, the coaxial cables from the radio tower entered the van through an entry panel that diverted the current on the shields to the outside of the van. At Nag's Head, the coaxial cables entered the van and the shields were connected to the equipment cabinet through the panel connectors; thus the external current on the cables was delivered to the equipment cabinet rather than diverted to the van.

(3) At Carrabelle, a coaxial cable used for local radio communications entered the van as an insulated conductor, thus violating the primary shield.

Primary Shield

Given the characteristics noted above, it therefore appeared that the TIS was ideally suited to an application of the shielding and grounding topology concepts described in Reference 1. In this approach, the all-metal van is developed as a primary shield and all lightning-produced current on power lines, coaxial cables, or other outside conductors is diverted to this shield as illustrated in Figure 3.

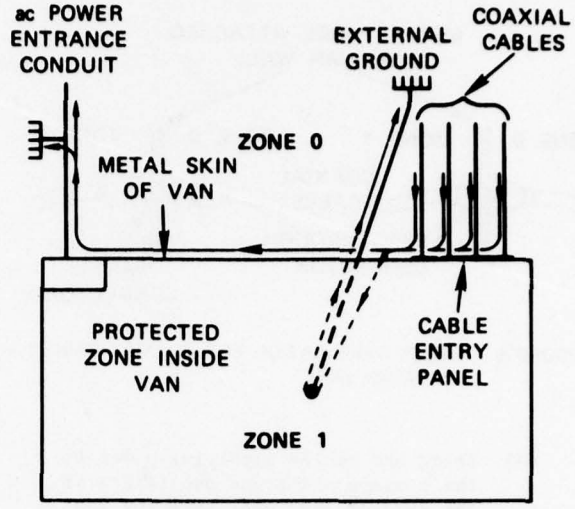

FIGURE 3 LIGHTNING PRODUCED CABLE CURRENTS DIVERTED TO VAN SKIN

Specific recommendations for the primary-shield treatments included:

(1) Install secondary lightning arresters and line filters on all ac power conductors entering the equipment van. (Secondary arresters were already installed at Carrabelle.)

(2) Ensure that the green-wire grounding conductor does not go outside the van, and that the outside electrical grounding conductor does not enter the van (see Figure 4).

(3) Make a metal entry panel for all coaxial cables entering the van (e.g., from the radio tower). Use feed-through or panel mounting connectors on the entry panel to connect the cable shield to the panel (see Figure 5). Bolt or rivet the entry panel to the skin of the van so that a very-low-impedance path between the cable shield and the van skin is formed. (Such a panel existed at Carrabelle.)

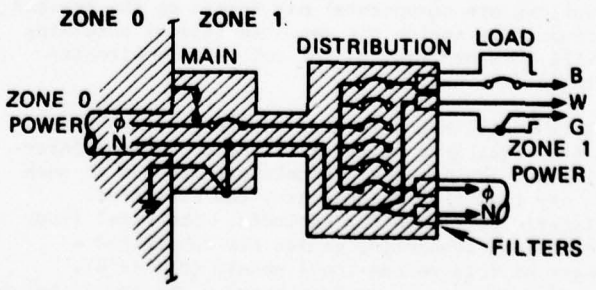

FIGURE 4 AC POWER PENETRATIONS AND GROUNDING CONDUCTORS

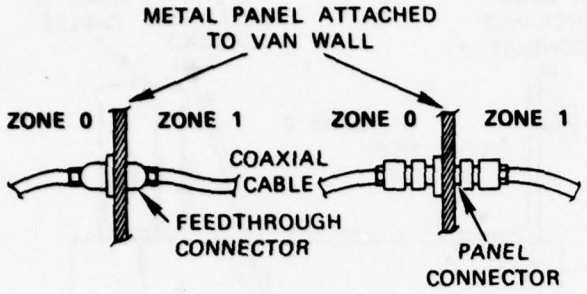

FIGURE 5 SHIELD TERMINATION FOR COAXIAL CABLES ENTERING VAN

(4) Bring the cables supplying power to the preamps and power amplifiers at the base of the tower into the van through treatment boxes on the entry panel. In the treatment boxes, surge arresters and tertiary limiters or filters should be installed on each conductor to prevent tower currents from being conducted into the van on these conductors.

(5) Bring telephone lines in through the entry panel (also through a treatment box, which may be provided by the utility). Treatment of the telephone lines should, at a minimum, include surge arresters.

(6) Treat any other cables or electrical conductors (such as local communication radio cables) that enter the van in the same way as the system cables discussed above.

Each of these recommendations is aimed at preventing large currents induced on outside conductors from entering the van; these currents must be diverted to the wall of the van where they cause no harm.

Second Level Shield

If the current on the outside conductors is of the order of kiloamperes, it is unreasonable to expect that the above treatments will make the interior of the van an interference-free region. Several amperes of current (enough to damage solid-state components) may remain on the treated conductors inside the van. Additional shielding will thus be required for solid-state circuits inside the van.

This additional shielding may be provided by the metal equipment cabinets if the conductors entering and leaving the cabinets are treated in such a way that they do not carry the room-level interference into the cabinets. The metal floor duct interconnecting cables are considered a part of this second-level shield (Figure 6). Therefore, one must first examine the connectivity between the racks and the floor ducts to ensure that the rack cabinets and ducts form a continuous closed shielding surface. All electronic equipment racks and cabinets should be firmly

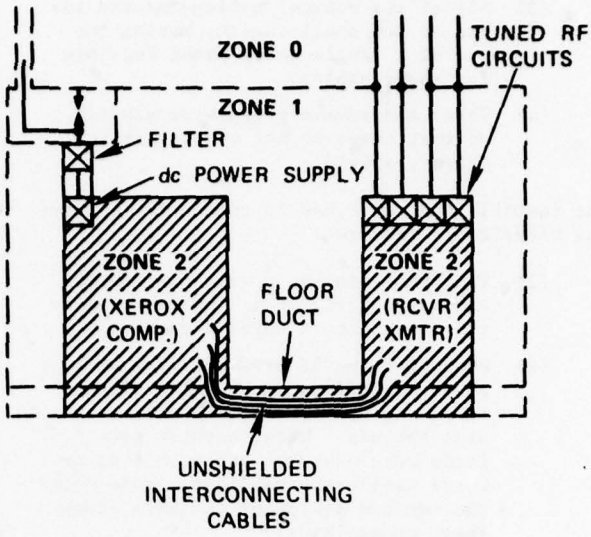

FIGURE 6 SECOND LEVEL SHIELD TOPOLOGY DEFINED BY CABINETS AND FLOOR DUCT

bolted to the floor duct structure in such a manner that electrical continuity is ensured. Similarly, all rack-mounted equipment should be bolted to the equipment racks so that electrical continuity between the rack and the equipment case is preserved. All cables interconnecting racks or cabinets within the van should (1) be routed through the floor ducts (inside the second shield), or (2) be shielded themselves (carry their own second-level shield). Any conductor that enters or leaves the second shield must be treated in some manner to make certain that it does not carry intolerable interference into the small-signal circuits.

Among the conductors that enter or leave the second-level shield are:

(1) ac power wiring--this goes primarily to the power supplies, which may serve as isolation devices for the power wiring interference.

(2) RF cables from tower--the shield terminates on the second-level shield, and the center conductor is usually filtered with a bandpass filter in the radio equipment.

(3) Power cables for external RF amplifiers--at present these are subjected to the raw outside environment. When the recommended primary-shield treatment is incorporated, line filters (or similar treatment) should be applied to the conductors carrying power to the internal circuits.

Present Status

Because these systems are operational, the recommended treatments are being implemented on a noninterference basis during inclement weather (when training flights are not possible). At

the Nag's Head installation, top priority was given to the entry panel and power service treatments, since these appear to be the most serious violations of the primary shield. Since these treatments were applied, the radio tower has been struck by lightning several times with only minor damage (one integrated circuit chip, one RF transistor), whereas previously several entire circuit boards were charred by similar strikes.

These results are encouraging, and it is anticipated that when all of the treatments have been applied, even these minor problems will be eliminated.

CONCLUSIONS

The concept of shielding and grounding topology introduced in Reference 1, has been applied to a medium-size facility to protect the electronic components against damage by lightning. Although all of the recommended changes have not yet been incorporated, substantial improvement in the lightning immunity of the system has been obtained with the high-priority first-level shield improvements.

It should also be remarked that the design of the equipment and vans was such that excellent lightning tolerance could readily be incorporated into the design. The important features of the equipment are the all-metal van construction with more-or-less concentrated cable penetration areas, a "closed" ac power system (metal conduits and closed metal cabinets), metal cabinets and floor ducts for internal equipment, and a rational approach to grounding. These features permitted the development of an effective two-level shield system without major redesign or reworking of the equipment. Thus, the cost of incorporation of the recommended improvements is probably less than the cost of one outage due to a lightning strike.

ACKNOWLEDGMENTS

The work described in this paper was supported by the U.S. Naval Air Systems Command under Contract N00019-78-C-0090.

REFERENCES

1. Vance, E. F., "Shielding and Grounding Topology for Interference Control," U.S. Department of Transportation, Federal Aviation Administration, Washington, D.C., Report No. FAA-RD-77-84, pp. 331-350, May 1977.

LIGHTNING CURRENT TRANSFER ALONG PERIODICALLY GROUNDED PIPELINES, FENCES, CABLE TRAYS AND BURIED CABLES

James R. Stahmann and Michael W. Brooks

PRC Systems Services Co.
Kennedy Space Center, FL 32899

BIOGRAPHIES

James R. Stahmann is manager of Technical Specialties on the Technical Staff of PRC. He received his M.S.E.E. from the University of Minnesota in 1952. Before joining PRC in 1974 he headed programs on the lightning protection of aircraft, natural lightning triggering and the generation of simulated lightning as Assoc. Director of Basic Research of the Lightning and Transients Research Institute. He joined LTRI in 1946. Currently he is working on the lightning susceptibility analyses of systems and the required protective measures.

Michael W. Brooks is an engineer on the Technical Staff of PRC specializing in computer circuit modeling and analysis of lightning problems and in susceptibility analyses. He joined PRC in 1974. He received his B.S.E.E. from the University of Florida and is a registered professional engineer in Florida.

ABSTRACT

Grounding cross-country pipelines, fences or cable trays every few hundred feet with ground rods sufficiently deep to give a one to five ohm resistance to earth "true ground" is generally believed to offer good lightning protection. Computer analysis, considering a model of the line as a LR network, shows that, while the high frequency direct and indirect current components are quickly attenuated, the low frequency direct stroke components travel long distances down the line. They are of long duration and peak long after the source current. Such components can produce lightning damage and effects by conducting currents several thousand feet along partially exposed well grounded fences, pipelines or cable trays into areas or buildings considered well shielded against lightning direct effects.

An actual stroke current, which traveled along a periodically grounded fence and then underground along a vinyl jacketed telephone line, periodically produced fused earth "fulgurites" each time current was ejected into the ground, to finally damage a guard shack, illustrates the problem. The building was shielded from direct lightning stroke contact by overhead lines.

INTRODUCTION

Lightning strikes the earth in a effort to reach "true ground", a region of very high conductivity and low current density somewhere under the surface of the earth. Good lightning protection requires providing means for the lightning current and energy to reach this region by impeding its progress as little as possible so that it will not damage sensitive equipment or structures. Too often we engage in wishful thinking when connecting a protection system to a ground rod that disappears from sight into the earth. Too readily we pronounce the system well grounded and therefore safe from lightning damage. We know that the rod does not make direct contact with "true ground" and we then measure the ground resistance of the rod. This resistance must be, we know, a function of the length and diameter of the rod and of the resistivity of the soil. Given a homogeneous soil, we can calculate the rod ground resistance using a formula such as:

$$R = (\rho/2\pi l)(\ln 4l/a - 1) \quad [1]$$

where ρ is the earth resistivity in ohm-m, l is rod length (m) and a is rod radius (m). However, we know that the soil is not homogeneous; that it at least tends to dry out near the surface resulting in a higher resistivity. We also know that there may be rocks, rock layers, buried cables or other metal and unknown things under the earth which could upset exact calculations. We, therefore, satisfy ourselves with an average measurement. Of course, some soils are better conductors than others, ranging from 10^4 ohm-m for bed rock and city industrial areas to about 10 ohm-m for wet organic soil.[2] We also know that the rod probably does not lose all its inductance just because it disappears from view.

At KSC the sandy soil resistivity is low due to the presence of salts in the soil water which comes very close to the surface. This resistivity averages less than 30 ohm-m so that a 3/4

inch diameter rod, 20 feet long, provides a ground of less than 5 ohms and a 40 foot rod provides a ground of less than 1 ohm. These must be classified as "good grounds".

As often happens, a lightning damage incident involving a strike to a fence grounded with ten foot rods raised questions about the effectiveness of grounding fences, pipelines, cable trays and buried cables. This incident and calculations on the effects of good grounds on lightning strike currents are discussed in this paper.

For calculation purposes the waveform shown in Figure 1 will be assumed. The Space Shuttle

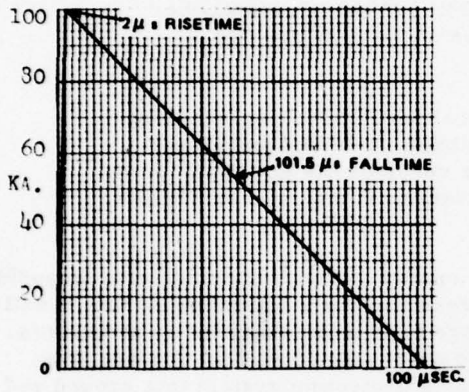

FIGURE 1. MODEL OF A SIMPLE LIGHTNING STROKE.

Lightning Protection Criteria Document, JSC-07636A,[3] uses a model waveform rising to 200 KA. in 2 microseconds and falling to 7 KA. in the next 98 microseconds where continuing currents are then added. The high initial rate of rise of current of 100 KA./microsecond insures maximum induction effects. We shall examine the effects of the long fall time which allows energy to be stored in the protective system and to be transmitted long distances. Because of the large peak power of lightning strokes, significant power may be transmitted. For example, a 100 KA. stroke into a 1 ohm ground is dissipating energy at a peak rate of 10 Gigawatts. Reducing the current by 1,000 times to 100 A. leaves a peak power of 10 Kilowatts. Such currents and the longer duration continuing currents can be conducted into areas considered safe from direct strokes via partially exposed fences, pipelines or even railroad tracks. The waveform shown in Figure 1 represents the current flowing in each direction when a 200 KA. strikes the middle of a pipeline. The current is assumed to go to zero at the rate of about 1 KA./microsecond.

STROKE TO FENCE

As shown in Figure 2, a lightning stroke hit a fence 192 feet from a point where a telephone line from an old guard shack to another guard shack crossed the fence. The shacks were about 160 feet apart. The telephone cable was armored with steel wire and covered with a vinyl jacket. Some of the lightning current entered the telephone cable. From the fence to the guard shack the cable was buried about 6 inches in the ground and the lightning current squirted periodically into the ground, every 12 to 18 inches, forming small fused earth "fulgurites" on the cable, Figure 3. These jacket punctures occur when the shield to soil voltage exceeds the dielectric strength of the jacket.[4] Part of the current followed the fence. Arcing occurred at the gate near the guard shack, Figure 4.

Where the lightning hit the fence damage was minor. Two of three barbed wires were severed, Figure 5. The relatively short cable from the fence to the old guard shack was about six feet above the ground supported on a fence post. It exploded due to the relatively high current which found a good ground at the terminal box on the outside of the old shack. The remains of the cable and the terminal box are shown in Figure 6. The long cable to the other shack was not destroyed since it experienced a lower current of longer duration. This current found a good ground at the power circuit inside the shack, exploding crossing telephone and communication lines in the process. The explosive force of the discharge blew out the north window, knocked the west window askew and split the door jam, Figure 7. No guard was on duty. Since guard shacks are usually located near fences, protective measures were indicated.

LIGHTNING CURRENT TRANSFER ALONG GROUNDED PIPELINES, FENCES AND CABLE TRAYS

A low frequency equivalent circuit of a pipeline, fence or cable tray is shown in Figure 8. Each section has a series inductance and shunting resistance. The resistance generally has a small inductance in series with the ground resistance. This is basically a LR filter network and its effects on the current waveforms are similar to those of a shield on current diffusing through it. For 5 ohm grounds, the current after 30 sections each 40 meters long (1,200 meters) peaks at 148 A., Figure 9, corresponding to a ground voltage rise of 740 volts. At this level the danger is primarily from sparking in areas sensitive to possible ignition. Induction is minimal because of the decreased rate of rise of current. As can be seen in Figure 9, the original waveform is attenuated and lengthened. Due to energy storage in the series inductance, the peaks of currents distant from the point of stroke contact occur long after the original

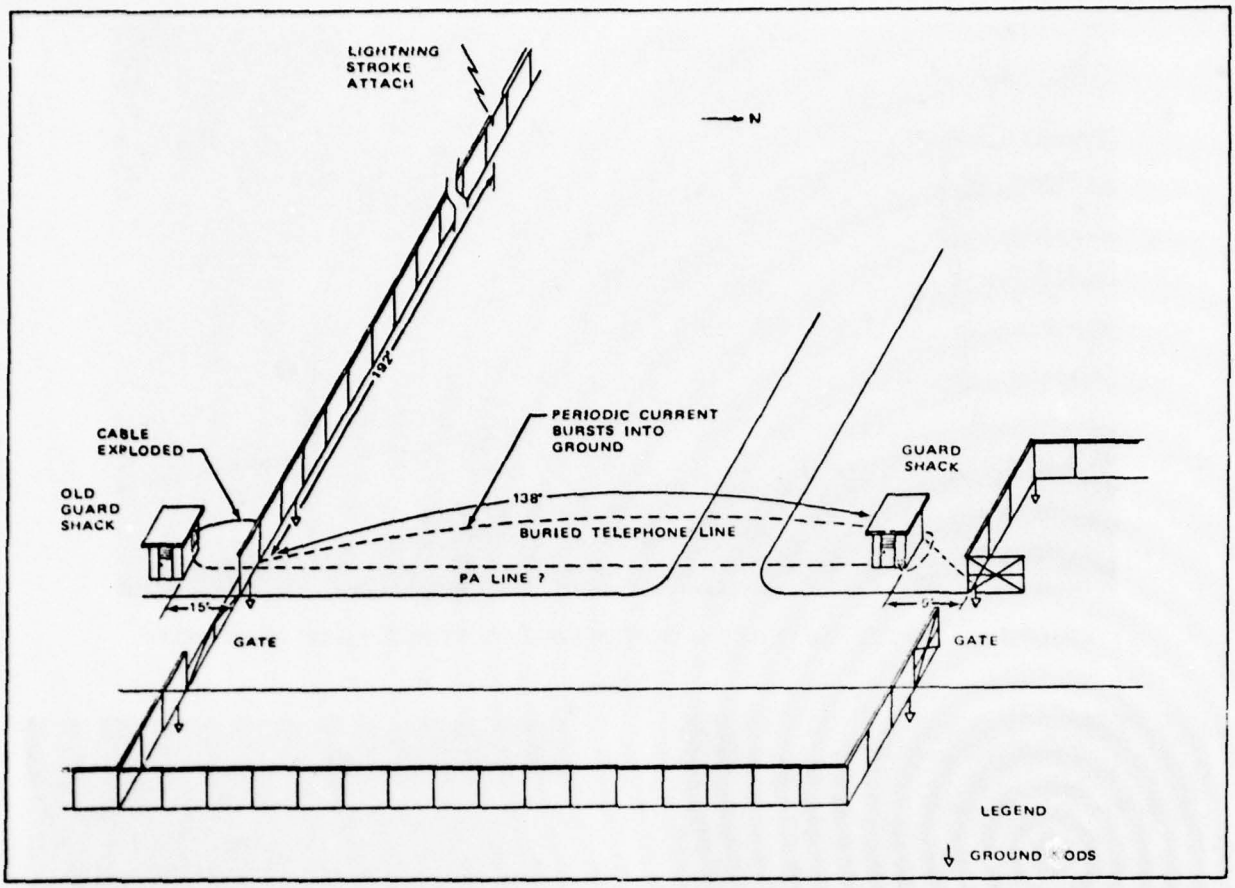

FIGURE 2. AN ACTUAL STROKE TO A FENCE HEAVILY DAMAGED A GUARD SHACK ABOUT 330 FEET AWAY.

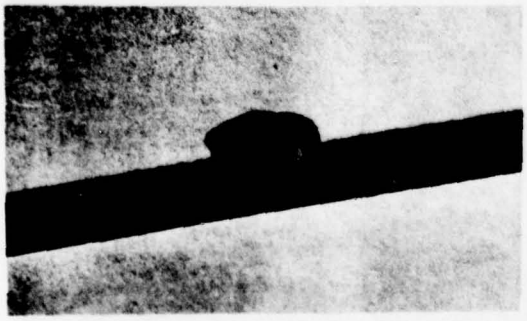

FIGURE 3. FUSED EARTH WHERE TELEPHONE CABLE JACKET WAS PUNCTURED BY THE LIGHTNING VOLTAGE.

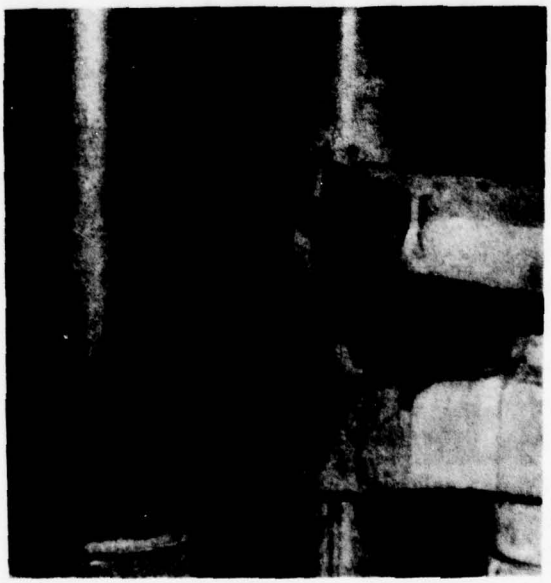

FIGURE 4. PITTING ON GATE POST NEAR THE GUARD SHACK.

FIGURE 5. STROKE SEVERED BARBED WIRE ON FENCE NEAR LEFT POST.

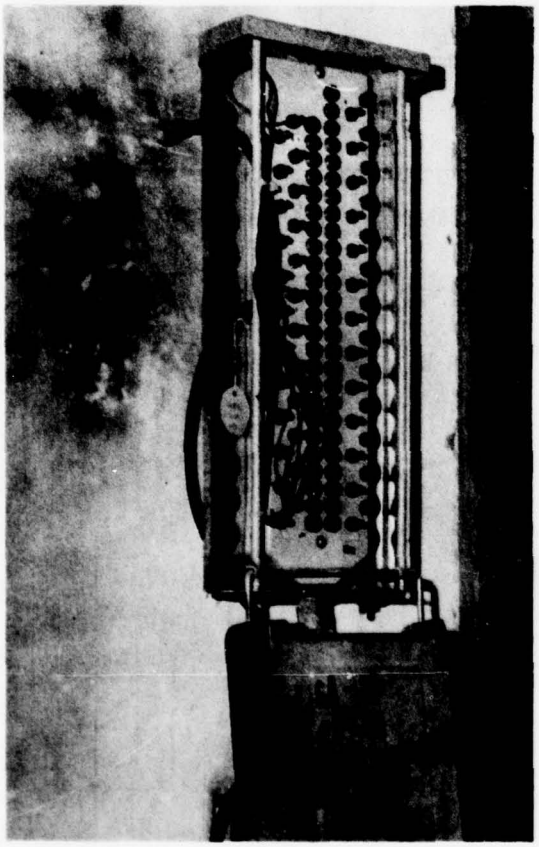

FIGURE 6. DAMAGE NEAR TERMINAL BOX OUTSIDE OLD GUARD SHACK.

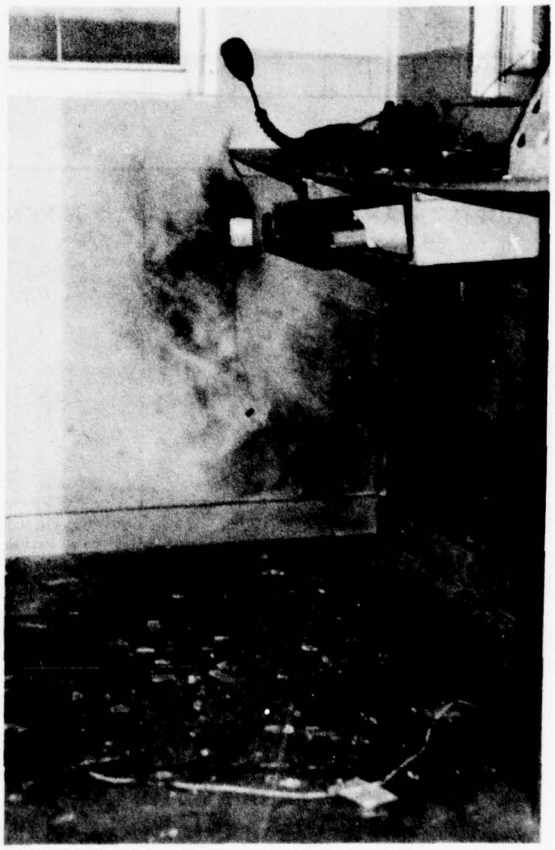

FIGURE 7. EXPLOSIVE DAMAGE IN GUARD SHACK.

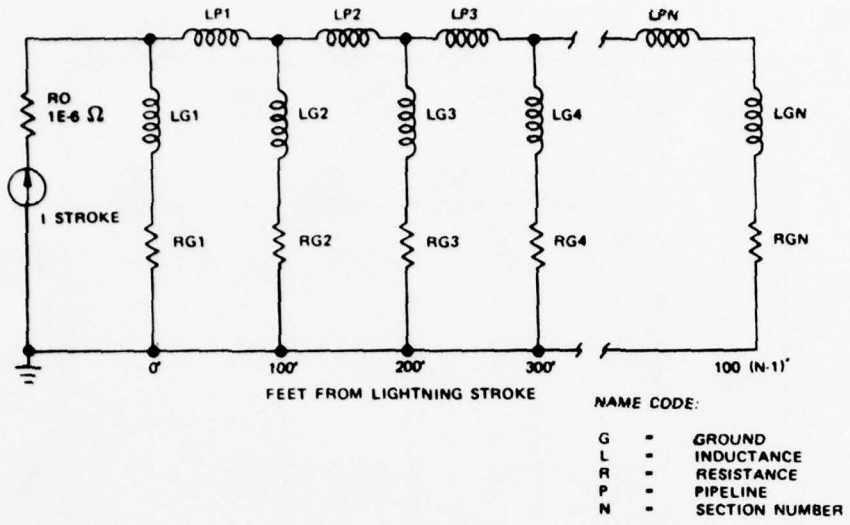

FIGURE 8. GENERALIZED EQUIVALENT CIRCUIT OF A PERIODICALLY GROUNDED PIPELINE, FENCE OR CABLE TRAY.

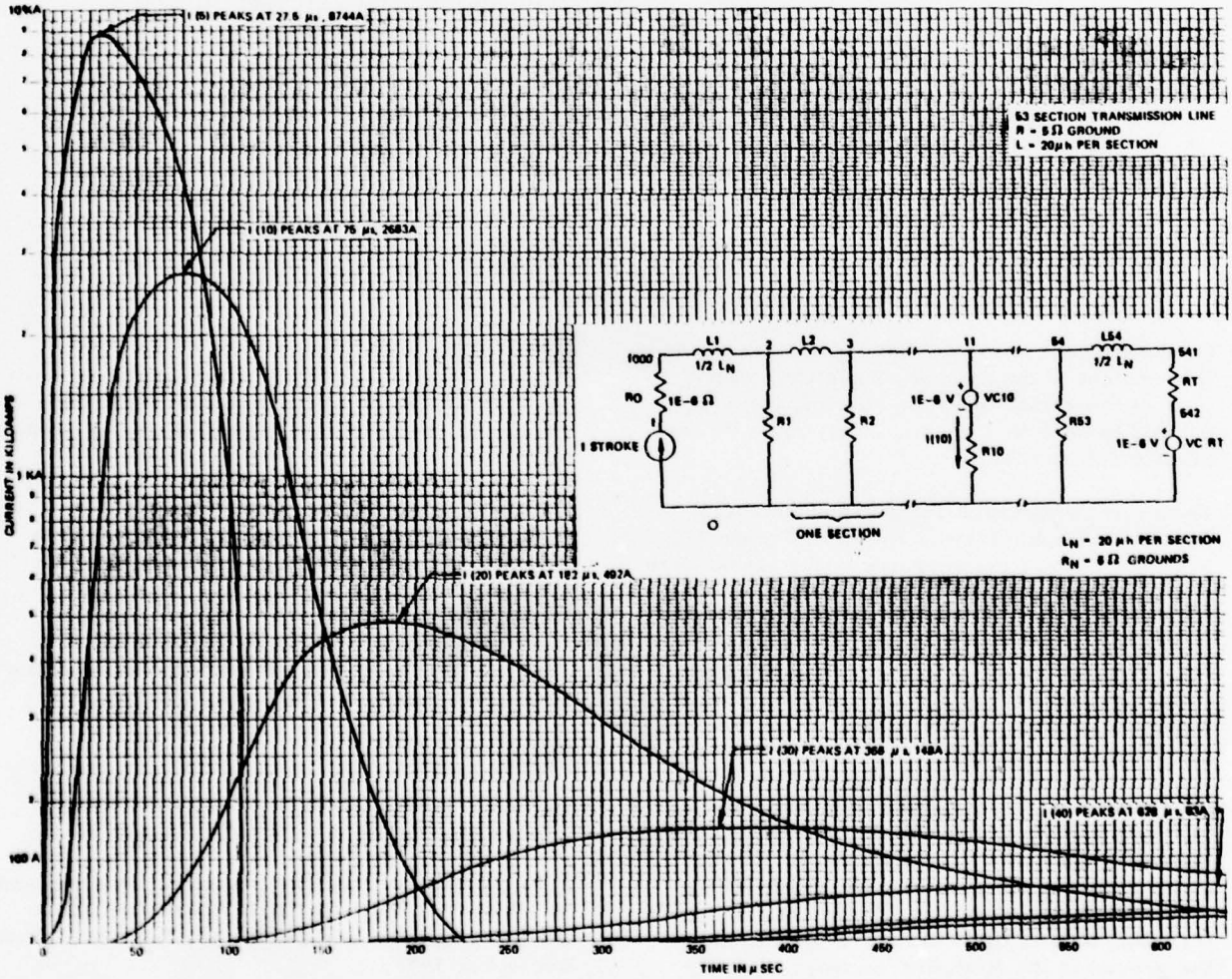

FIGURE 9. GROUND CURRENTS IN PIPELINE GROUND RODS, GROUNDED WITH A FIVE OHM GROUND RESISTANCE EVERY 40 METERS.

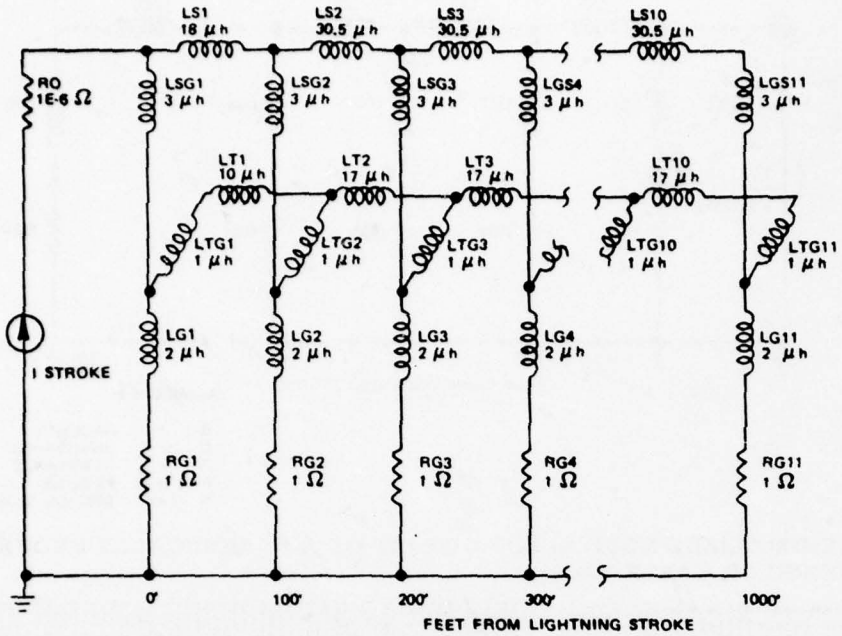

NAME CODE:

S	-	LIGHTNING SHIELD WIRE
T	-	CABLE TRAY
G	-	GROUND
SG	-	SHIELD TO GROUND
TG	-	TRAY TO GROUND
L	-	INDUCTANCE
R	-	RESISTANCE

FIGURE 10. COMPUTER EQUIVALENT CIRCUIT OF CABLE TRAY UNDER A LIGHTNING AIR SHIELD WIRE.

stroke current is over. Because the currents into and out of the ground connections do not peak at the same time, the current peaks do not add to zero at a node and they must be separately determined.

The equivalent circuit for a grounded shield wire over a cable tray is shown in Figure 10. Figure 11 shows the currents in the shield wire and cable tray. When the shield wire and cable tray are grounded to the same ground as shown in Figure 10, the cable tray carries more current than the shield wire because of the lower cable tray inductance and the common ground impedance. The cables located in the trays may have voltages induced in them proportional to the rate of rise of current and the transfer inductance.[5] Where the insulation punctures, a portion of the tray current will be conducted by the cable or cable shield. The ground rod currents for the air shield-cable tray system are shown in Figure 12. It is interesting to note that current is drawn out of the ground in the first five sections after the stroke source current has sufficiently decreased so that the current in the line inductance is greater than the source lightning current.

CONCLUSIONS

(1) Part of the energy of a distant lightning stroke may be conducted into susceptible areas by fences, pipelines or buried cables.

(2) The energy stored in the conductors or transmitted by them can cause damage where the progress of the current toward true earth ground is impeded.

(3) While good grounding is effective, it generally cannot be relied upon to eliminate all the dangerous energy of a lightning stroke.

REFERENCES

1. E.D. Sunde, Earth Conduction Effects in Transmission Systems, Van Nostrand, 1949.

2. H.W.Denny et. al., Grounding, Bonding and Shielding Practices and Procedures for Electronic Equipment and Facilities, Vol. 1, F.A.A. December 1975.

3. Space Shuttle Program Lightning Protection Criteria Document, JSC- 07636 A, Nov. 1975.

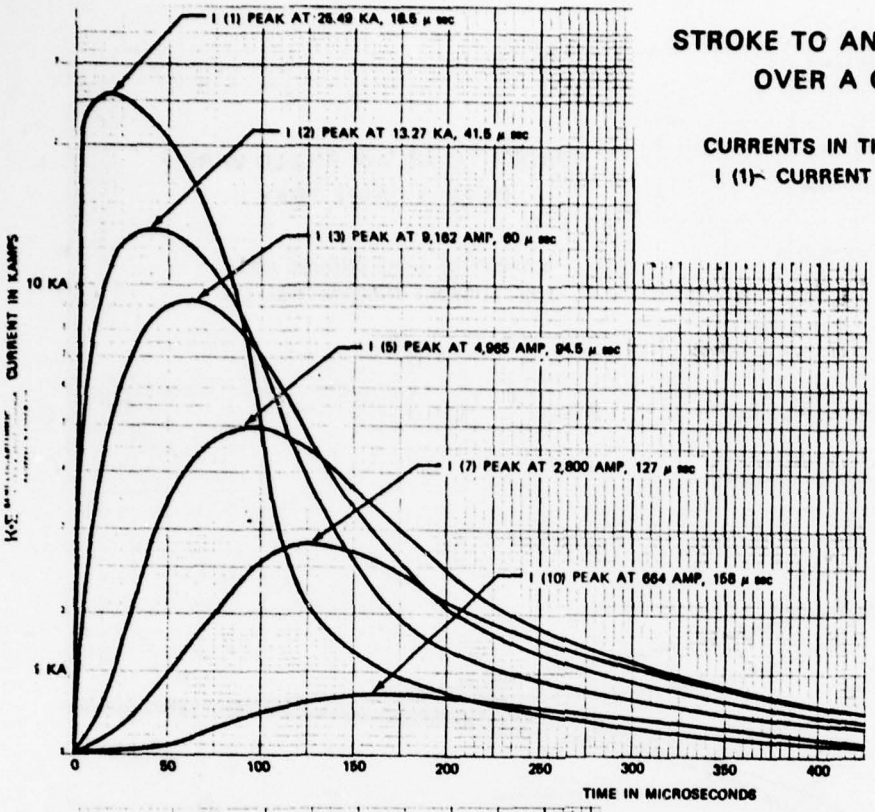

STROKE TO AN AIR SHIELD WIRE OVER A CABLE TRAY

CURRENTS IN THE AIR SHIELD WIRE
I (1)→ CURRENT THROUGH LS1, ETC.

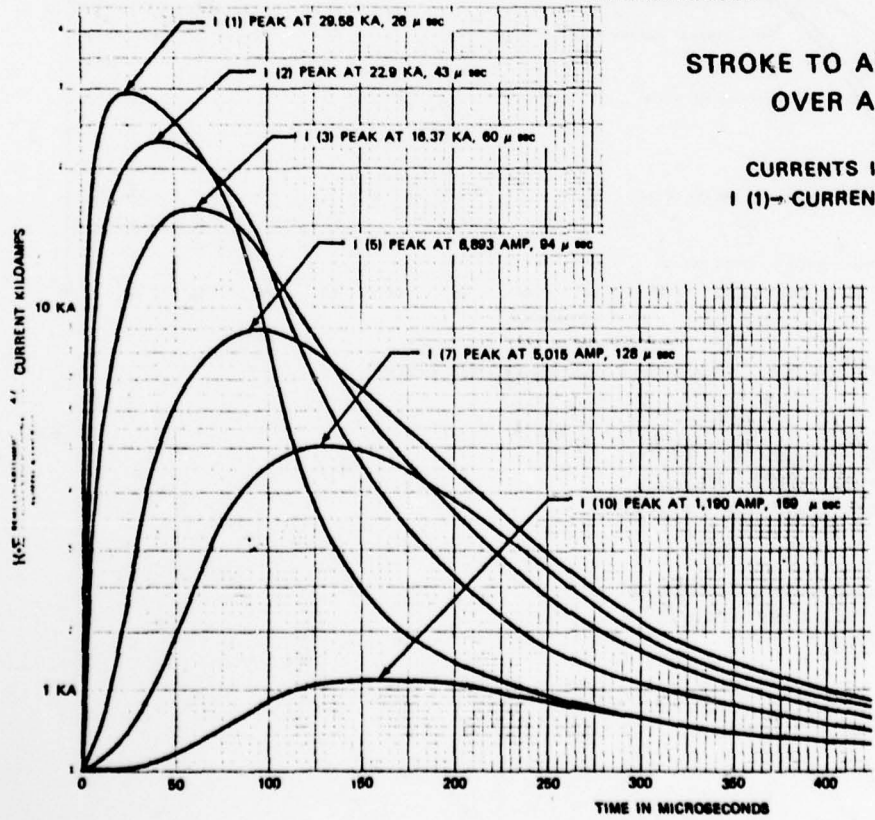

STROKE TO AN AIR SHIELD WIRE OVER A CABLE TRAY

CURRENTS IN THE CABLE TRAY
I (1)→ CURRENT THROUGH LT1, ETC.

FIGURE 11. CURRENTS IN SHIELD WIRE AND CABLE TRAY.

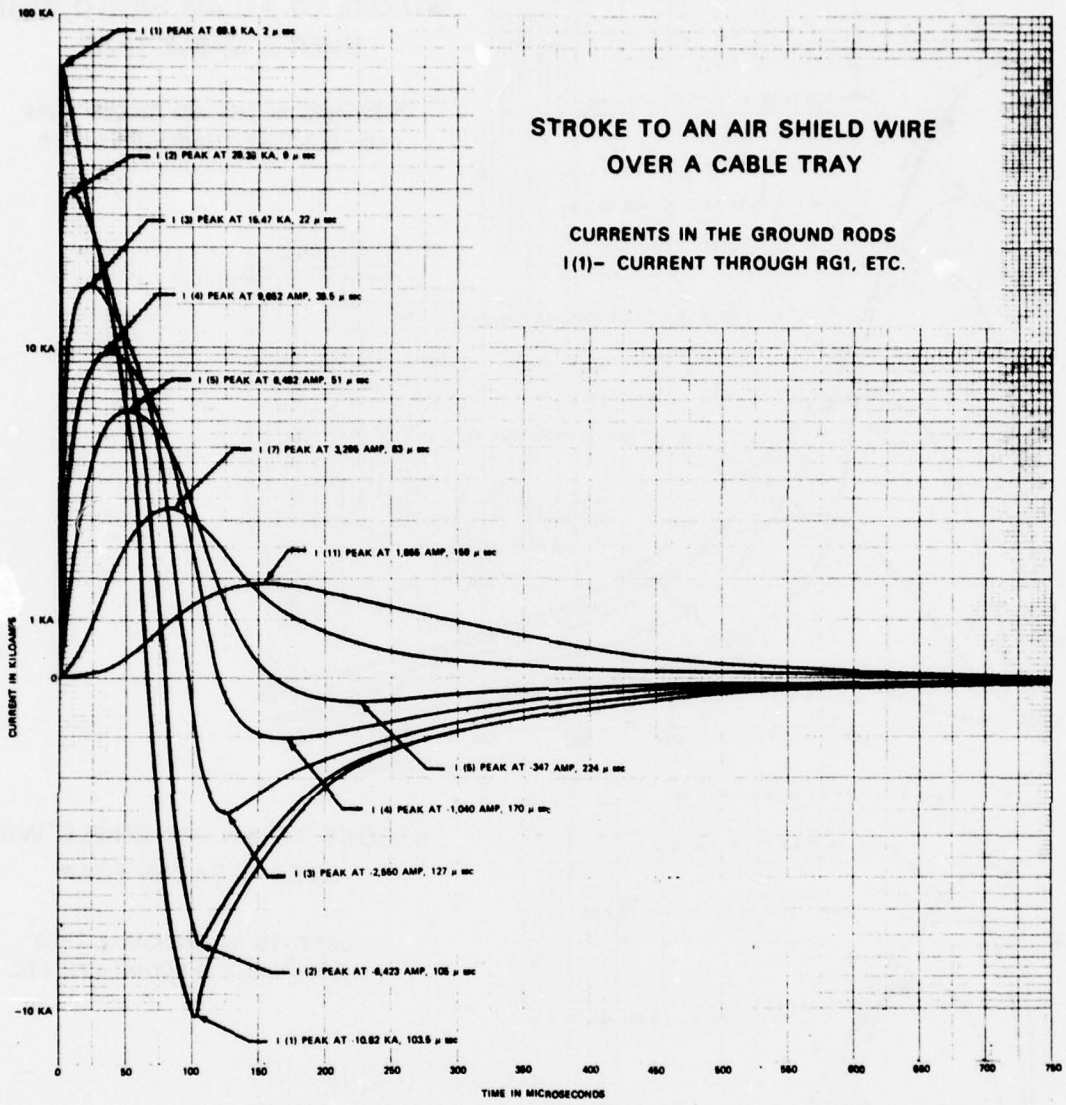

FIGURE 12. CURRENTS IN GROUND RODS.

4. K.E. Crouch, A Study of Lightning Transients in Telephone Cables, F.A.A.-G.I.T. Workshop on Grounding and Lightning Protection, May, 1978.

5. F.A. Fisher and J.A. Plumer, Lightning Protection of Aircraft, NASA Reference Publication 1008, October, 1977.

DESIGN OF ELECTRONIC SYSTEMS TOLERANT OF POOR GROUNDING

THOMAS H. HERRING
Research Engineer
Boeing Aerospace Company
Post Office Box 3999
Seattle, WA 98124

BIOGRAPHY

Thomas H. Herring has been engaged in electromagnetic interference work since 1951 and first joined Boeing in 1952 on the B-52 program. He has worked chiefly at the system level on cabling and grounding. He received an M. S. in physics from Cornell University in 1948 and is a registered electrical engineer in the State of Washington.

ABSTRACT

This paper presents an approach to the design of electronic systems lacking the benefit of wide, highly conductive, ground paths. The essential feature is a systematic treatment of low impedance loops.

INTRODUCTION

Image-Forming Ground and the Unbalanced Circuit

The kind of ground which is here assumed to be lacking will be called "image-forming." This is a sheet or coaxial cylinder which if connected in shunt with the return of an interconnecting circuit will produce a nearby image of the circuit net current. Ideally, the image is congruent with the circuit bundle; practically, it is within a few bundle diameters and, poorly done, it is remote or uncertain. This image-forming ground is a partial Lenz Law shield because it reduces the self and mutual inductances of the interconnecting circuit. An interconnect having this ground can be termed an "imaged" interconnect.

Unbalanced interconnects that are not at all imaged occur in two forms. The here called "strong tie" has a nominal return, a bus perhaps or a wire, in or near its bundle. The "sacrifice tie" has no return in or near its bundle. Fig. 1 illustrates.

Bundle Common Mode Impedance

All interconnect bundles except those optically isolated will in operation exhibit a net current I_c at some frequency, this current being the indication of a clamp-on ammeter (current probe). The associated common mode voltage Vc may be defined as the voltage measured between the end circuit references using voltmeter leads routed along the path of the bundle loop of interest that is being designed (see "Design"). Fig. 2 illustrates. The common mode impedance Zc of the bundle may be defined as Vc/Ic.

The common mode impedance of a bundle loop of interest is the sum of the component interconnect circuit Zc. An "isolated" interconnect circuit is one for which the Zc is much larger than that of any other bundle loop component circuit. A "balanced" interconnect has impedance symmetry to ground and may properly have Zc of any moderate value. A double grounded shield will reduce Zc to zero. Imaged and "strongly tied" interconnects have Zc so low as to be counted zero relative to the Zc of non-problem loops; loops formed by these interconnects constitute "shorted turns." Note that at different frequencies a given interconnect circuit might exhibit any or all three of the just noted behaviours.

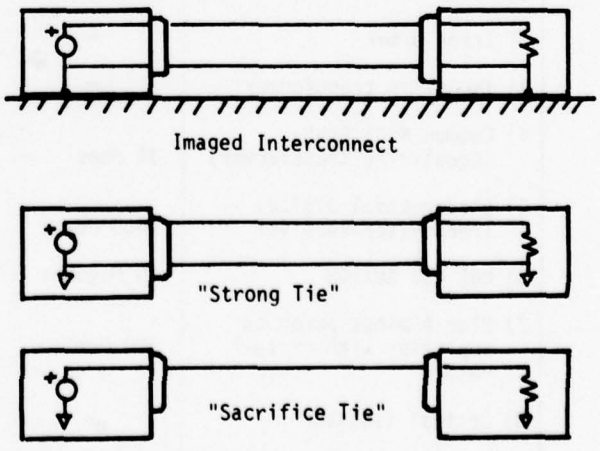

FIGURE 1. UNBALANCED INTERCONNECTS

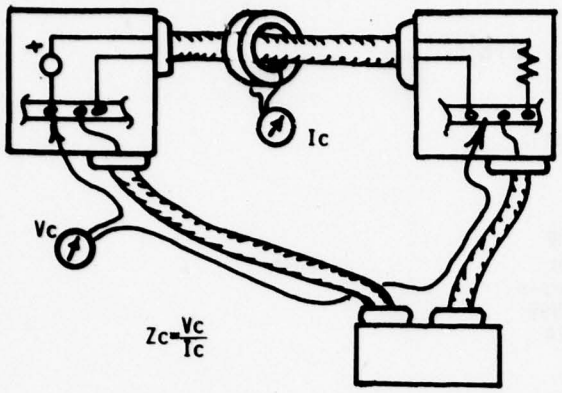

FIGURE 2. COMMON MODE IMPEDANCE

Measures of Interconnect Circuit Common Mode Pickup

The mechanisms by which interconnect circuits respond to grounding problems can be measured by the quantities common mode rejection, CMR, and here called "ground transfer impedance" Zgt. The former applies to balanced and isolated circuits and is determined using the particular common mode voltage noted above. The CMR of a device usually has sharp limits of linearity (and damage) and usually depends strongly upon frequency. Table 3 introduces balancers and isolators. Ground Transfer Impedance, Zgt, describes unbalanced circuits, being zero for a well-imaged interconnect and progressively worse for strong ties and sacrifice ties. It may be defined as received interconnect voltage divided by the common mode current of the bundle and nearby ground (if any) combination.

Effects of Ground Loss

Loss of imaging ground degrades unbalanced interconnect circuits, their filters and their shields, also affects the design of balanced circuits and does not affect isolated circuits at all.

For unbalanced interconnect circuits Zgt increases as the ground image goes farther away. Unbalanced circuit shields become ineffective if there is no imaging ground path (between shield pigtail and circuit reference) to which to ground. Common mode filtering is degraded to chokes only as shown in Figure 4.

The common mode impedance, Zc, of balanced interconnect circuits becomes an important design parameter in systems with poor ground; Zc determines how the members of a common mode loop share the problem.

The net effect of losing image-forming ground is degraded containment of high frequencies, especially EMI signals. Compensating steps are needed.

DEVICE DESCRIPTION	DC Zc	DC Balance	AC Zc	AC Balance	Vc max
1) Relay	10 Megohms	Yes	10 Megohms	No	600 volts
2) Transformer	∞	Yes	$(1000pF \times \omega)^{-1}$	Yes	600 volts
3) Isolation transformer	∞	Yes	$(10pF \times \omega)^{-1}$	Yes	600 volts
4) Common Mode Choke (Equalizing Transformer)	10 Ohms	No	$100mH \times \omega$	Yes	depends
5) Differential Digital Transmitter-Receiver	1000 Ohms	No	1000 Ohms	Yes	15 volts
6) MOS FET SWITCH	10 Megohms	Yes	10 Megohms	Yes	15 volts
7) Plus & minus power to amplifier with virtual return	100 Ohms	Yes	100 Ohms	Yes	5 volts*
8) Optical isolator	∞	Yes	∞	Yes	∞

*Termed "power supply rejection."

TABLE 3. BALANCING AND ISOLATING DEVICES TYPICAL PARAMETERS

Shields

Shields which image the charge of an interconnect bundle are called Faraday shields and are reasonably effective when grounded at one end only to the correct ground path. Shields which image the currents of an interconnect bundle are sometimes called Lenz Law shields and must be connected to circuit reference or chassis at both ends. Loss of image-forming ground outlaws Lenz Law shields and degrades Faraday shields.

Balanced circuit shields need no ground if balance is perfect and therefore are not very sensitive to poor ground: Ground the shield at the circuit low impedance end and terminate the other end with greater than Zc ohms. Shields must be discontinuous at isolators.

Overall, the designer must avoid unbalanced noisy interconnect circuits because these cannot be shielded above audio frequency in the poor ground system.

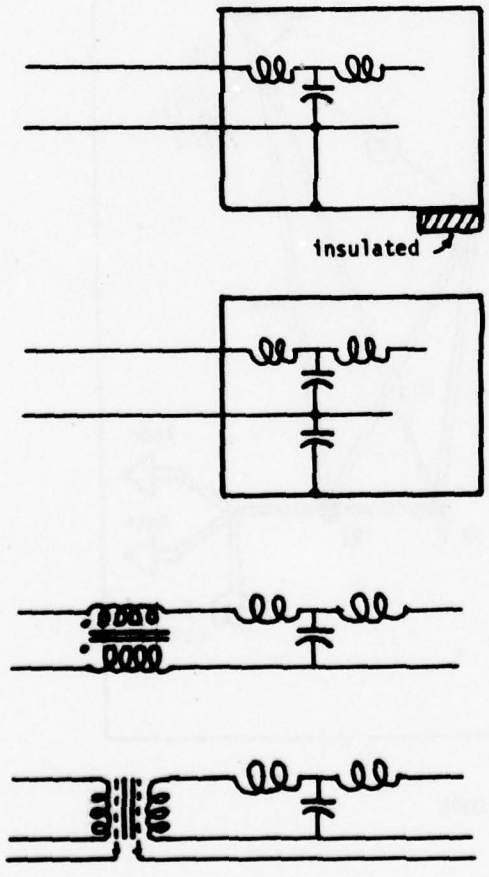

FIGURE 4. UNGROUNDED FILTERS

DESIGN

The most important compensation for poor ground is careful selection of components and modulations because more interference is coupled in a system with poor ground. Imagine that equipment under design must pass a MIL-STD-461 test performed on a wooden bench and the correct attitude toward detail will have been achieved.

Preliminary Design

During preliminary design for poor ground:

- Locate signal fanout near power fanout
- Select intrinsically compatible modulations
- Place noisy or ultrasensitive circuits in or on metal
- Plan twice as many connectors as the packagers recommend (for reducing loop areas)
- Identify for special care interconnect runs which may not get imaging ground paths.

Identification of loops is aided by the use of symbols such as those of Figure 5 and by the use of diagrams such as Figure 6.

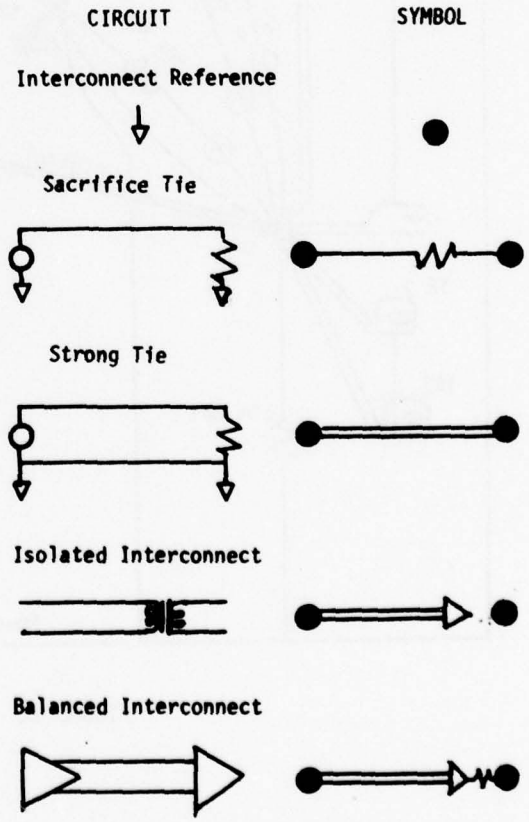

FIGURE 5. RETURN SYMBOLS

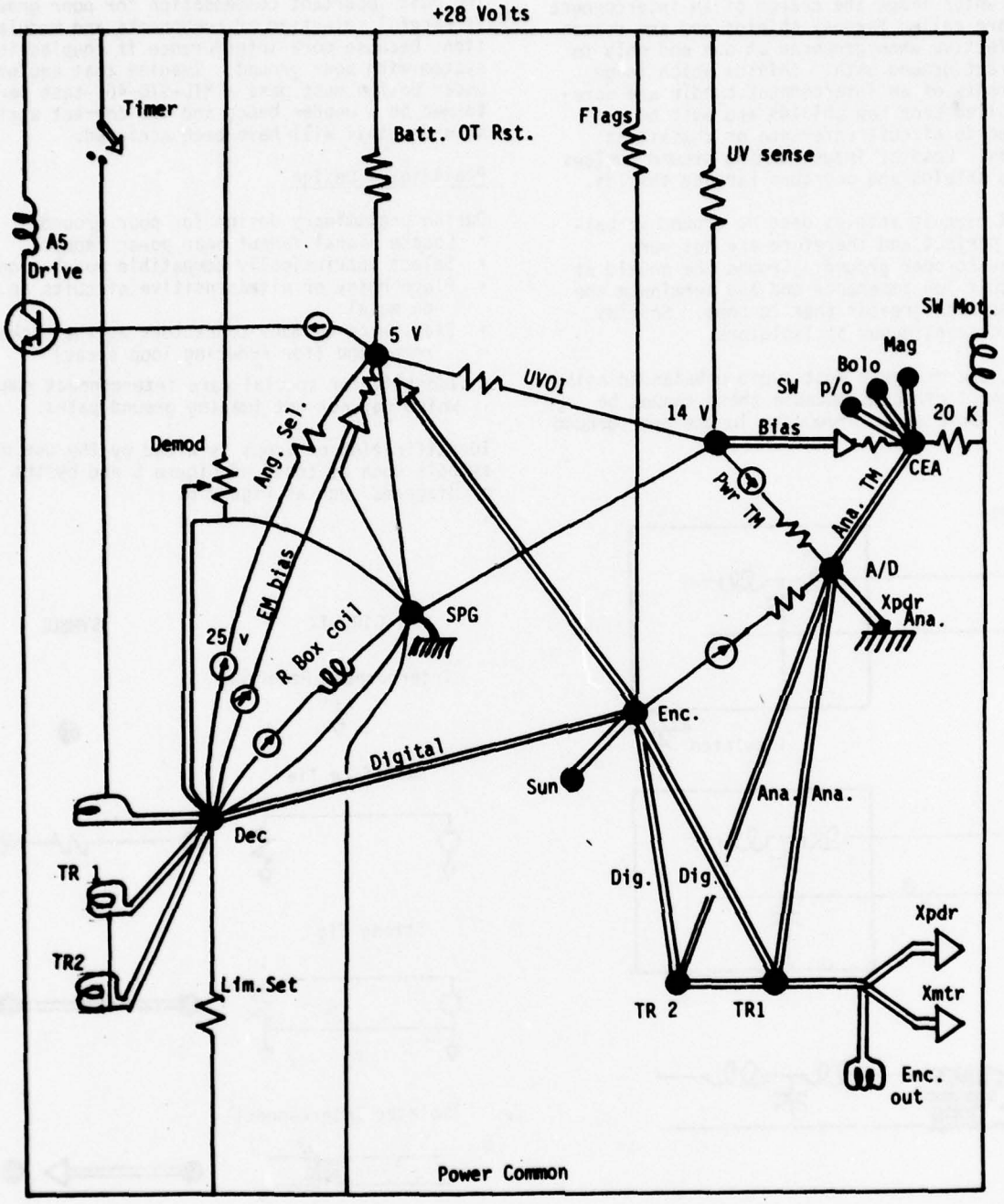

FIGURE 6. SPACECRAFT LOOPS

Common Mode Loop Design

Assuming that a legacy of preliminary design is a number of loops in interconnect circuit bundling, the compensation for poor ground is to adjust the design of loop members such that they become compatible. Loops whose members have image-forming ground paths do not necessarily need this attention.

Loop compatibility steps are:

a. Select Zc of member circuits to get moderate (50-50,000 ohm) value of loop Zc.

b. Select shielding.

c. Apply shorted turn rules.

d. Solve common mode circuit.

a. Select Zc. At least one loop member should be balanced or isolated (Table 3) in order to keep the loop Zc above 50 ohms. Very high Zc may permit electrostatic pickup which exceeds the CMR of loop devices, hence the suggested 50,000 ohm upper limit for the loop. In general, if a member Zc is high this tends to protect other members and if low protects itself.

b. Select Shielding. Shields, if any, must be grounded so as to not violate the Zc design. Full double grounding violates the 50 ohm floor and therefore is seldom advantageous. See "Shields" topic, and the following shorted turn rules.

c. Shorted Turn Rules. Shorted turns are good, innocuous or bad depending on geometry with respect to the circuit of interest, as shown in Figure 7 and below:

i) Shorted turn within circuit path is beneficial to that circuit.

ii) Shorted turn congruent with circuit path is optimum for that circuit.

iii) Shorted turn extending beyond a circuit's path is bad for that circuit (unless Zgt=0).

One important application of these rules is to the intrinsic conflict in a loop between the requirements of the members as to Zc: A shorted turn (shields or returns) that is congruent with a bundle loop always helps the common mode circuit and degrades the member circuits. For example, an isolator or balancer in a loop might suffer excessive common mode voltage; addition of a shorted turn will reduce that voltage at the possible expense of the other circuits.

d. Common Mode Circuit Solution. Quantitative solution of the common mode equivalent of the loop may be desired if conflict arises between member circuits. Estimate common mode current Ic as a fraction of circuit currents or as a fraction of circuit voltages divided by loop Zc. Evaluate coupling to member circuits as

Coupling = Ic x Zc x CMR
Coupling = Ic x Zgt

for balanced and unbalanced member circuits respectively.

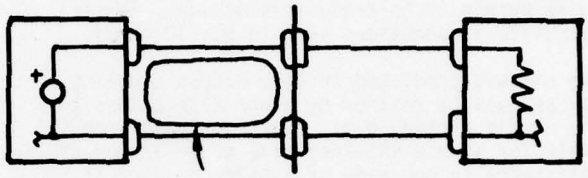

i) Shorted turn is beneficial

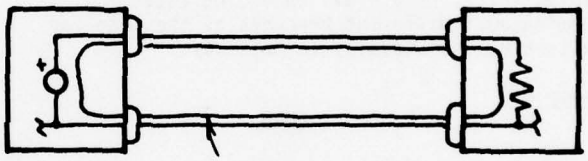

ii) Shorted turn is optimum

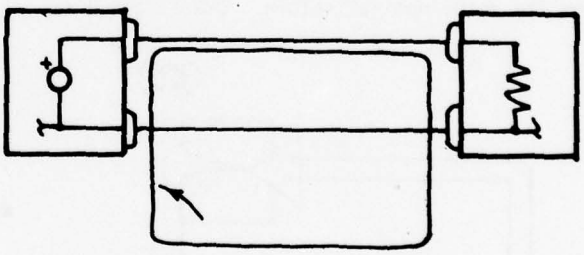

iii) Shorted turn is detrimental

FIGURE 7. SHORTED TURN RULE

Loop Fixes

It is assumed that circuit isolators and balancers have been considered and rejected (or that time precludes that much redesign). Options become:

- Increase loop Zc
- Improve Zgt or CMR
- Lenz Law shield

Increasing loop Zc to reduce Ic can be done at VHF and above by adding ferrite beads (toroidal cores) at any point in the loop. At lower frequencies the interconnect bundle may be wound 30 or so turns on a toroidal core (one turn = one bead). These measures failing, the ultimate Zc fix is sacrifice of one of the constituent circuits by opening its strong-tie return. Quite often one of the loop members has sufficient noise margin to tolerate this action. Partial sacrifice is sometimes seen (e.g., 10 ohms).

The circuit predicted to have excess coupling may perhaps be rescued by minor alterations to the bundle wiring, e.g., substitution of coaxial cable for single shielded wire or insertion of resistance in one side of a balanced circuit to improve balance.

Finally, one may install an imaging ground loop. This may be a heavy, shorted turn routed to minimize Zgt, or overall shielding carefully terminated. Different branches of the loop can be treated individually in this way.

Examples

In Figure 8, a differential digital link connects to a noisy reference, a stepper motor return. The link is balanced at signal frequencies and unbalanced at DC. Its Zc (1000 ohms) is high enough to not shunt motor waveforms away from the motor nominal return. CMR is adequate.

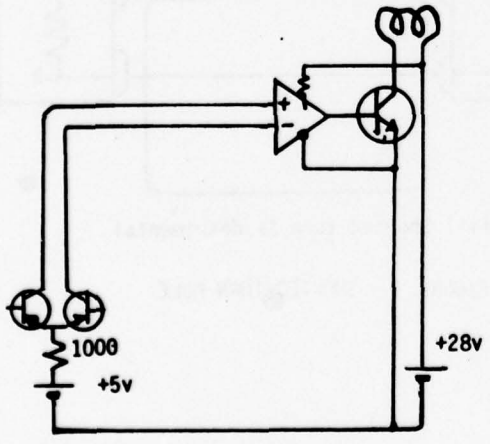

FIGURE 8. STEPPER MOTOR CONTROL

An example containing both a loop which did not function and one which did appears in Fig. 9. The power loop oscillated. When corrected by strapping together the 15 and 30 volt returns at the drawer, excessive ripple from the 30 volt circuit then appeared in the 5 volt circuit; this was filtered out. This illustrates inadequate common mode isolation between the two driver stages. The "LF Coax" loop has very low impedance, but the Zgt of the coaxial cable is low enough to ensure acceptable pickup.

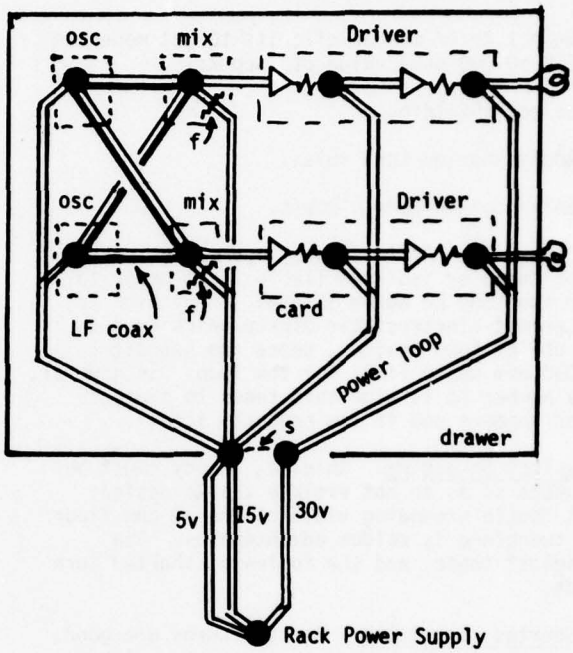

s= strap added

f= filter added

FIGURE 9. CONTROL SYSTEM

SUMMARY

A design approach developed over the years for various systems having no imaging ground paths has been described. The main feature is a discrimination between loops which are beneficial or innocuous and those which are detrimental. In spite of all care, it is stated that EMI coupling will increase with poor ground and that intrinsic compatibility should, in such situations, be stressed.

ANALYZING SURGE-PROTECTIVE DEVICES WITHIN A COMMON FRAMEWORK

BERNHARD I. WOLFF
Product Engineer for GE-MOV^R Varistors
Semiconductor Products Department
General Electric Company
Syracuse, N.Y. 13201

BIOGRAPHY

Bernhard I. Wolff is product engineer for design, characterization and rating of GE-MOV^R metal-oxide-varistors. He received a B.S. in Physics in 1961 from Syracuse University and has continued with graduate study in economics. He has been involved with the technology and application of surge-protective devices since 1973. His prior experience with GE and IBM includes a broad range of engineering in analog and digital circuit design, integrated circuits, computer application, and military radar systems.

ABSTRACT

The protective voltage level provided by suppressor devices of various technologies can be approximated as a function of current by a two-term equation. The parameters of this equation are related to figure-of-merit measures often used to compare nonlinear devices. The parameter values estimated for some examples give an indication of relative device effectiveness, but other application considerations also affect choice of an optimum component.

BACKGROUND

Surge-protective devices, also called suppressors, have been in use for many years to reduce the possibility of damage or malfunction in electrical and electronic equipment that may be caused by voltage transients originating in lightning strikes or other causes. Recently, the need for protection has increased as equipment incorporates an array of solid state devices of small, sensitive structure. New technology suppressors such as gas tube, transient suppression zener, metal oxide varistor, and hybrid devices are receiving widespread use alongside air gap, silicon carbide and other device types. To simplify use and comparison of manufacturer specifications industry standards are being prepared applicable to these types, and the IEEE test specification for gas tubes is the first to appear.[1]

Although standards are beneficial in developing understanding of different devices within a type they are of limited value in interpreting differences between types. It is the purpose of this paper to identify some measures of performance which are common to surge-protective applications, and to propose a common analytical framework for the analysis of the sundry suppressor types. These measures of performance expressed in defined parametric form will then be tested empirically on some suppressor examples.

This analysis is not intended to lead to conclusions on the relative merits of different suppressor types although it may indicate areas of similarity or difference in device type behavior. A complete evaluation of suppressor suitability for a particular application also requires consideration of many other electrical, mechanical, environmental, and cost factors. These are in the province of the suppressor device user.

APPLICATION PERFORMANCE ANALYSIS

At the core of the analysis problem is the difference in behavior between various types of suppressors. These fall into two generic classes. The discharge device class includes air gap, gas tube, and certain hybrid devices with "crowbar" action. These devices are typified by a V-I curve that includes a region in which voltage drops sharply after a threshold value is exceeded. Consequently, these devices also tend to draw follow current from the power source after the surge has passed. In the varistor device class the voltage varies monotonically and nonlinearly with current.[2] Devices operating on the reverse junction breakdown principle such as surge absorption zener diodes usually fall into this generic class along with devices named as varistors. What is needed then is a common framework in which the discharge and varistor class devices can be analyzed.

The elements of a common framework are straightforward. The specifications of suppressors are divided into two groups: ratings and characteristics. First, the ratings will give the levels of electrical stress the device has been designed and tested to withstand; such as continuous ac or dc voltage, peak transient current for a given surge waveform, and rated number of surge repetitions. Next, of principal interest in the device characteristics group is the specification giving the ability of the device to suppress the voltage excursion of the incident surge at a given peak current and waveform. This is usually termed discharge voltage for discharge type devices and clamping voltage for many other types of suppressors. The ensuing analysis will concentrate on this characteristic.

Since the purpose of surge protective devices is to control the level of transient voltage which appears across the protected equipment a transient control level, (TCL) philosophy provides the starting point for an analysis common to both classes of suppressors.[3] The key elements are:

a) Establish the concept of proof testing, rather than requiring ability to withstand unknown "actual" transients.
b) Define standard test waves.
c) Define surge source current capability.

Furthermore, the evaluation of the protection level provided by a suppressor is a two step process as illustrated in Figure 1. The combination of open circuit voltage, source impedance, and device clamping voltage determine the peak surge current. As will be seen the peak current can be important in determining the discharge voltage or clamping voltage of both classes of suppressors and must be carefully controlled to achieve standardized test conditions.

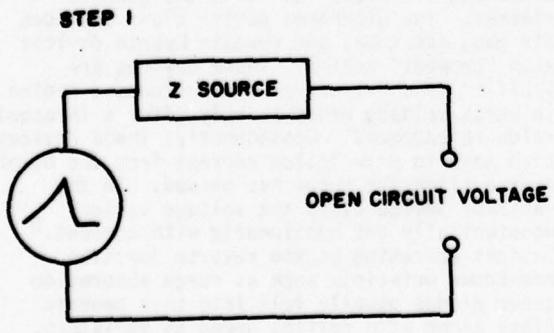

FIGURE 1. SUPPRESSOR EVALUATION STEPS

SUPPRESSOR VOLTAGE MODEL

The general shape of the V-I characteristic of discharge class devices is illustrated in Figure 2. Assuming that the device breaks down at a voltage independent of the peak value of surge current the discharge voltage is constant. However, except when used on systems with intrinsically limited source current a series resistive element is required to limit follow current until the device commutates off by ac line reversal or other means. A silicon carbide nonlinear resistance element has often been used in surge arrestors.[4] Thus, the V-I curve model for discharge devices is simple: a straight horizontal line breaking to an upward sloping line at high current when a series resistive element is used. These relationships are expressed by equations:

$V = B_v$ (1), discharge device alone

$V = kI^{\beta}$ (2), at higher currents with series element

where:

V is the suppressor discharge or clamping voltage

B_v is the discharge breakdown voltage

K is a device constant

β is the characteristic of nonlinearity, $0 < \beta < 1$

I is the peak surge current

It is worth noting that if β has the value unity then suppressor voltage has a linear resistive relationship to current. As β approaches zero the voltage becomes constant as in equation (1).

The expression for clamping voltage of a varistor class device is analogous to the above. The terminal voltage varies slowly with current over a wide range, but at high current density the relationship tends toward linear as the effect of variable resistance approaches saturation. This mechanism is represented by the equivalent circuit model of Figure 3 where R is the device bulk resistance, and R_v is the instantaneous variable resistance component.

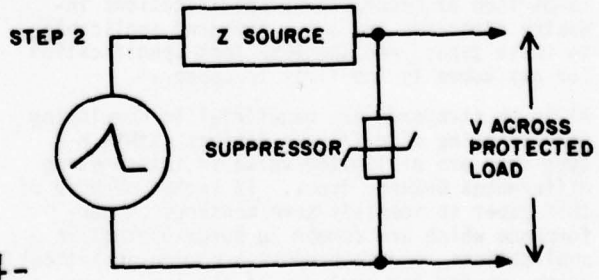

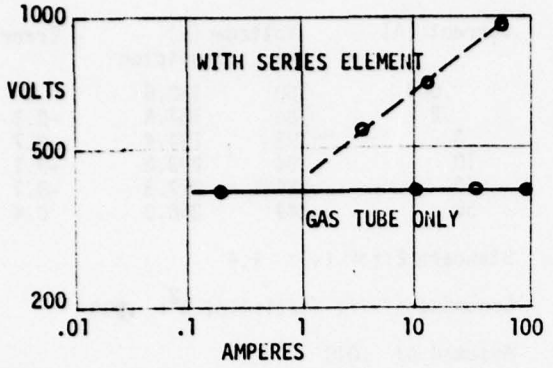

FIGURE 2. DISCHARGE DEVICE V-I CURVE

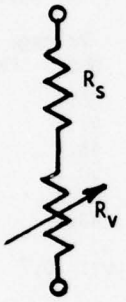

FIGURE 3. VARISTOR EQUIVALENT CIRCUIT

The terminal voltage-current relationship for Figure 3 can be expressed as

$$V = KI^{\beta} + R_S I \qquad (3)$$

Evidently, for devices of the same value of constant K the clamping voltage will depend on values of β and R, where β is relatively more important at low currents and R_S may be more significant at medium and high currents. Of course, real devices may not behave in a manner as simple as posited by the ideal model and its equation, but the adequacy of them as explanatory and predictive tools must be judged on empirical grounds. The next section reports the results of parameter estimates obtained from testing of examples of several device types.

EMPIRICAL ESTIMATES OF PARAMETER VALUES

The estimate of parameters on three specimens of varistor class devices will be considered first. One specimen is metal-oxide-varistor of 130 Vac continuous rating (about 210V nominal varistor voltage) 14mm nominal diameter, commercial type V130LA10A. The other two specimens are transient suppression zeners corresponding to JEDEC Types 1N5649, 47V nominal breakdown voltage, and 1N5664, 180V nominal breakdown voltage. All three specimens were selected randomly from commercial sources and are assumed to be representative of device generic behavior. Device voltages at 1mA test current were measured first. Then measurements of clamping voltage were obtained at selected points within the range of rated transient peak current. These measurements were performed on a Key Tek System 1000 Surge generator/monitor instrument. An 8x20 μs pulse current test waveform as considered representative of lightning was used, and typical device response is shown in Figure 4.

The V-I curves measured for the three specimens are shown in Figure 5. Linear regression analysis techniques which originated in the biological and social sciences are used to estimate the parameter values of equation (3) which best fit the V-I curves.[5] The multiple regression procedure yields estimates of constant K and resistance R_S directly. But, estimates of β must be determined apriori and observation values of I^{β} for the first independent variable in equation (3) must be calculated accordingly. Through iterative regressions the estimate of β can be refined by a trial-and-error process using a goodness-of-fit criterion. However, on an F statistic, Chow test comparison basis the estimated coefficients of the regression will not vary significantly over some range of assumed values of β. Hence, although a solution for β may be approximate a statistically satisfactory estimate of R_S can be obtained.

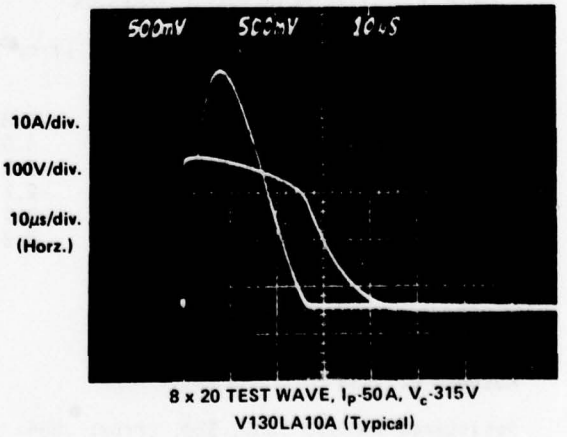

FIGURE 4. VARISTOR TEST WAVEFORMS

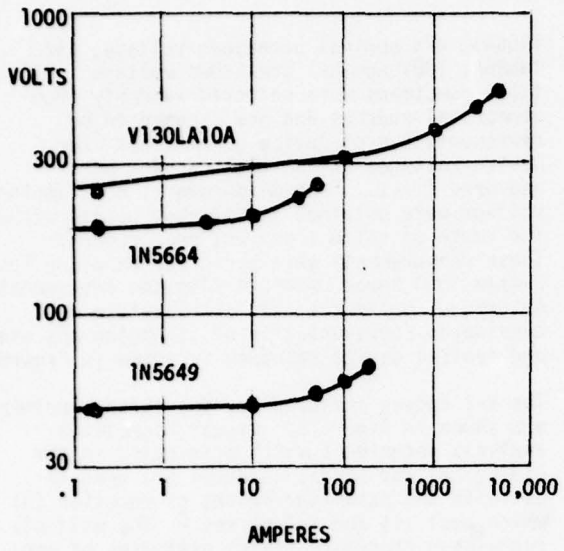

FIGURE 5. TEST SPECIMEN V-I CURVES

The regression analysis was run using the STAREG program available in the statistical library of General Electric Mark III timesharing computer service. The results are presented in Tables 1, 2 and 3 where the fits of the model to the specimen data are summarized. As can be seen the two term equation (3) describes V-I characteristics with remarkable accuracy over current ranges that span up to nearly 7 decades and includes observations at or exceeding device ratings. These results have been obtained on devices of different technology and voltages. Series resistance of the metal-oxide varistor specimen is very low relative to device voltage, but an excellent fit is obtained.

TABLE 1 FIT TO METAL-OXIDE VARISTOR

Current (A)	Voltage (v)		Error %
	Obs.	Predicted	
.001	223	215	-3.8
.2	254	265	4.0
100	332	339	2.0
1000	409	400	-2.2
2800	481	477	-0.9
4800	549	553	0.8

Standard Error (v): 10.7

Goodness-of-fit Statistic, R^2: .996

Assumed β: .033

Resistance (ohms): .035, Std. Error: .004

TABLE 2 FIT TO 180BV DIODE

Current (A)	Voltage (v)		Error %
	Obs.	Predicted	
.001	180	180.0	0
.2	188	187.5	-0.3
3	193	194.4	0.7
10	204	203.8	-0.1
30	229	227.3	-0.7
50	249	250.0	0.4

Standard Error (v): 1.4

Goodness-of-fit Statistic, R^2: .998

Assumed β: .010

Resistance (ohms): 1.09; Std. Error: .04

TABLE 3 FIT TO 47 BV DIODE

Current (A)	Voltage		Error %
	Obs.	Predicted	
.001	46.9	47.2	0.6
.2	47.4	47.0	-0.8
10	48.4	47.7	-1.5
51	50.3	50.8	1.1
101	54.2	54.8	1.1
206	63.6	63.2	-0.7

Standard Error (v): 0.7

Goodness-of-fit Statistic, R^2: .992

Assumed β: .004

Resistance (ohms): .080; Std. Error: .006

The analysis can now reconsider discharge class devices. The V-I curve measured on a gas tube specimen typical of the type used in telecommunication applications was illustrated in Figure 2. A 1.2x50 μs voltage waveform (8x20 current waveform) was used for the tests, and the surge source impedance was changed to vary short circuit current. The observed suppressor breakdown voltage was virtually constant at about 390V.

If the gas tube is interpreted in terms of equation (3) the value of β can be considered zero. Therefore, the first term is a constant as in equation (1). The suppressor voltage at high current depends on whether a series current limiting element is used. Assuming that the arc voltage of the discharge device in breakdown is sufficiently low to ignore, then the high current V-I characteristic of the suppressor is determined solely by the limiting element. With a nonlinear element equation (2) becomes applicable at high currents. However, for elements with a typical value of about 0.2 for β it is clear that suppressor voltage will rise relatively rapidly at high currents.

OTHER MEASURES OF NONLINEARITY

Another approach for representing the relative effectiveness of suppressor devices is based on device instantaneous resistance, and this concept has received some use in the industry in the past. For a nonlinear device the instantaneous resistance is a variable as shown previously in the equivalent circuit of Figure 3. Assuming that the fixed component R_S is relatively very small then the variable resistance component R_V at any operating point is by definition:

$$R_V = \frac{V}{I} \qquad (4)$$

For a perfectly nonlinear device the voltage v is constant, and the plot of R_V versus I on a symmetrical log-log graph would be a straight line with a negative slope factor of unity. The characteristic of a typical metal-oxide-varistor is illustrated by Figure 6. A defect of this characteristic for suppressor analysis is that it is a relatively insensitive measure of comparative performance. Also, since transient voltage protection is the purpose of suppressors the voltage determining parameters are more directly to the point.

A more sensitive resistance type measure of nonlinear performance is small signal dynamic impedance which is defined as the rate of change of device voltage with current at a given operating point:

$$Z_V = \frac{dV}{dI} \qquad (5)$$

This characteristic is commonly specified for zener diodes used in voltage reference or stabilization applications. The characteristic of a typical metal-oxide-varistor suppressor is illustrated by Figure 7. Its value tends to decrease as operating point I increases in value depending on the relative nonlinearity of the device. The exact nature of this relationship can be determined by noting that equation (5) is the derivative of equation (2) with respect to I. By performing the calculus operations it can be shown that:

$$Z_V = \frac{dV}{dI} = \beta K I^{\beta-1}$$

$$Z_V = \beta K I^{\beta} I^{-1}$$

$$Z_V = \beta \frac{V}{I} \qquad (6)$$

By substitution of (4) into (6) it is apparent that the nonlinear exponent β provides the simple relation between instantaneous resistance and dynamic impedance:

$$Z_V = \beta R_V \qquad (7)$$

If interpreted in terms of the equivalent circuit, Figure 3, exponent β generally describes the nonlinearity of element R_V. However, from a terminal-to-terminal view the element R_S dominates at high currents and β approaches the value unity. In the limit Z_V cannot be less than R_S.

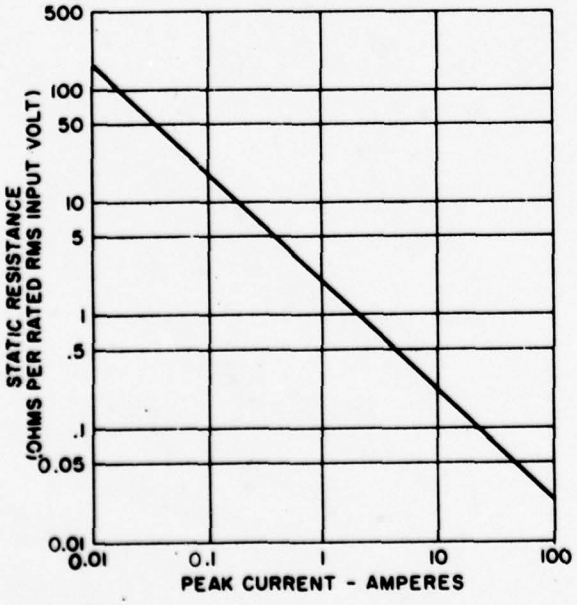

FIGURE 5. TYPICAL VARIABLE RESISTANCE R_V

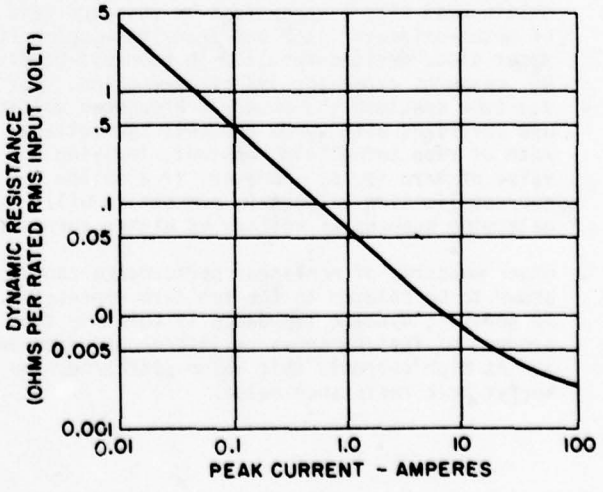

FIGURE 6. TYPICAL DYNAMIC IMPEDANCE Z_V

In passing it also should be noted that nonlinearity of varistor class devices is often given using the exponent α by the expression:

$$I = K V^{\alpha} \qquad (8)$$

This is the same as the relationship given by equation (2) except that the independent and dependent variables are reversed. It can be shown that

$$\alpha = 1/\beta \qquad (9)$$

Therefore, equations (2) and (8) are complementary descriptions where the exponents are reciprocally related. Although equation (2) is the form of most interest since suppressor voltage is the dependent variable it sometimes may be useful to transform exponent values as per equation (9). This results in exponents with high values for a high degree of nonlinearity which may be simpler as an intuitive relationship.

CONCLUSIONS

For analysis purposes suppressor devices can be divided into discharge class and varistor class devices according to generic behavior. The voltage suppression performance is modeled as a function of peak surge current by a two term expression. The first term is the familiar power law relationship between voltage and peak current in which the exponent β describes the degree of voltage nonlinearity. The second term is linear in current and the coefficient is the series bulk resistance or "on" resistance when the device is in a conduction saturated state.

Empirical estimates of the parameters of specimen suppressor devices can be obtained by multiple linear regression analysis methods. Values for exponent β are assumed apriori and selected to obtain best fit. Regressions on observed data of metal-oxide-varistor and transient suppression zener diode devices resulted in goodness-of-fit, R^2, measures exceeding 99% of perfection. For a gas tube specimen the observed breakdown voltage was invariant with surge current, the voltage rate of rise being held constant, implying a value of zero for β. However, if a follow current limiting element is present it will determine suppressor voltage at higher currents.

Other measures of nonlinear performance can be shown to be related to the two term expression. In general, dynamic impedance is equal to the product of instantaneous resistance and exponent β. At high currents this value approaches the series bulk resistance value.

The results of suppressor voltage parameter analysis can help to identify areas of sameness or dissimilarity in behavior between devices. However, the user must also make a complete analysis of all requirements of an application including other electrical, mechanical, environmental and cost factors.

REFERENCES

1. Cohen, E.J., "A Universal Gas Tube Specification", Telephone Engineer and Management Magazine, April 1, 1977.

2. IEEE Std 100-1977, IEEE Standard Dictionary of Electrical and Electronics Terms, Second Edition, New York, 1977.

3. Martzloff, F.D. and Fisher, F.A., "Transient Control Level Philosophy and Implementation - The Reasoning Behind the Philosophy", IEEE 77CH1224-5EMC, Proceedings of the 2nd Symposium on EMC, Montreux (Jan. 1977).

4. Walsh, G.W., "A New-Technology Station Class Arrester For Industrial and Commercial Power Systems." Conference Record of the IEEE Industry Application Society, Eleventh Annual Meeting, October 11, 1977, Chicago, Illinois, pp 30-35.

5. Johnston, J., Econometric Methods, McGraw-Hill, Inc., New York, 1972.

EFFECT OF LEAD WIRE LENGTHS ON PROTECTOR CLAMPING VOLTAGES

O. Melville Clark
Programs Manager
and
Joseph J. Pizzicaroli
Applications Engineer
General Semiconductor Industries, Inc.
Tempe, Arizona 85281

Biography

O. Melville Clark has responsibilities for diode and suppressor applications, modular assembly designs and development contract programs. He received his BA and MA degrees from Arizona State University. He has 22 years of experience in semiconductors, concentrating on transient suppression since joining General Semiconductor Industries in 1971. Many articles have been contributed on the subject of transient voltage suppression and three patents are held in high voltage and transient suppression technologies.

Joseph J. Pizzicaroli has been involved in both development and applications engineering at General Semiconductor Industries for more than two years. He is a retired Air Force career officer, having experience at educational, staff and command levels. He is a graduate of DeVry Institute.

ABSTRACT

Under high current pulse conditions, excessive lead lengths on suppressor components can be responsible for destruction of the protected circuit. This is caused by voltage build-up across the small but finite amount of inductance in the interconnecting leads of the protector. Some suppressor devices have been tested and observed to have more than twice the specified clamping voltage which was subsequently shown to be caused by inductive effects. Problems and corrective measures are illustrated and discussed in this paper.

SEMICONDUCTOR FAILURE THRESHOLDS

MOS and small area geometry semiconductors are particularly vulnerable to the effects of transient voltages. Unfortunately there has been very little information published on this subject. The work reported by Van Keuren[1] illustrates how fragile CMOS and TTL devices can be. Minimum failure pulse voltage thresholds are shown in Table I.

Electrostatic Discharge (ESD) failures of MOS microcircuits have been measured by Gallace and Pujol[2]. Comparisons among several suppliers indicate that failure levels can be a function of manufacturing technique. Repeated step stressing of a sample of 25 CD4011AF type devices shows that at a given stress level devices would eventually fail, as shown in figure 1.

TABLE I
Minimum Failure Thresholds of CMOS and TTL

Device Type	Pulse Width					
	20μsec	2μsec	1μsec	0.2μsec	.1μsec	.025μsec
55107	22V	16V		22V		
55109	36V	38V		60V		
5404			30V		50V	120V
54L30			20V		50V	90V

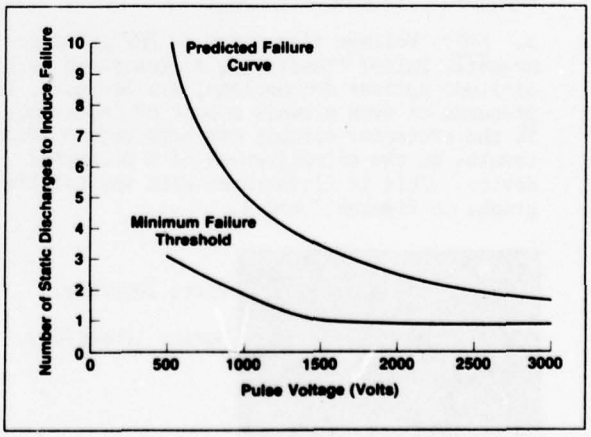

FIGURE 1: STRESS FAILURE OF CD4011AF

EQUIVALENT CIRCUIT OF PROTECTOR

The equivalent circuit of a Silicon Transient Suppressor, such as the TransZorb® which is manufactured by General Semiconductor Industries, is shown in figure 2. All parameter values are fixed by manufacturing processes and device construction except L_1, the inductance resulting from the lead wires connecting the protector across the circuit for which protection is intended. Normal wiring practice results in lead lengths of the order of centimeters. In some power installations this has been observed to be of the order of feet.

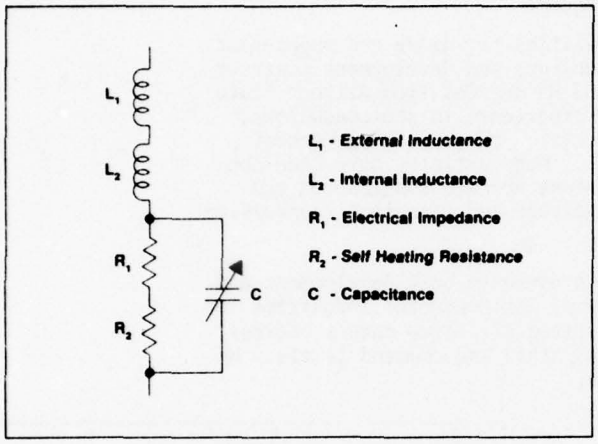

FIGURE 2: EQUIVALENT CIRCUIT OF PROTECTOR

The inductance within an axial leaded part, as represented by L_2, is of the order of 10^{-8} henrys while the inductance within a modular assembly can be one to two orders of magnitude greater, depending on the design and the number of subcomponents. The capacitance of a silicon avalanche suppressor can vary over an order of magnitude, depending on the degree of reverse biasing.

TRANSIENT VOLTAGE RISE-TIMES

a. EMP: Voltage rise-times of EMP (Electromagnetic Pulse) transients, as generated by high altitude nuclear detonations, are 5kV/nsec. The presence of even a small amount of inductance in the protector circuit can have very profound results on the effectiveness of a protector device. This is illustrated with the oscillographs in figures 3 and 4.

Vert: 200V/div.

Horiz: 10nsec/div.

FIGURE 3: 7.5 CM LEAD WIRES

TransZorb® Registered Trademark of General Semiconductor Industries, Inc.

Vert: 200V/div.

Horiz: 10nsec/div.

FIGURE 4: ZERO LENGTH LEAD WIRES

In figure 3, a 30V TransZorb® in the DO-13 package was pulsed with a 100A 4kV/nsec rise-time transient. With 7.5 cm leads on each end, at which current was injected and voltage measured, the overshoot voltage is slightly greater than 800V. The energy under this curve is calculated to be 70µjoules, sufficient energy to destroy most types of MOS and some TTL devices. By reducing the lead length to zero and repeating the pulsing, the overshoot voltage is reduced to about 200V. The energy under this curve is less than 1µjoule, below the destruct threshold of MOS and TTL devices.

b. LIGHTNING AND INDUCTIVE SWITCHING: From measurements made on 120V ac power systems, Martzloff[3] has proposed a waveform which rises to peak in 500nsec, and then subsequently decaying in a sinusoidal waveform with a frequency of 100kH. The lightning stroke, which is usually reported with current rise-times ranging from 1 to 3µsec, has been more recently measured by Llewllen[4] to be as low as 500nsec. Transients on shipboard ac power systems have been defined by MIL-STD-1399 as having transient rise-times of 1.5µsec.

Normal wiring practices are usually considered adequate for protection of electronic circuitry. "Normal" and "adequate" are relative terms and usually prevail under conditions in which equipment performance is acceptable. What is normal and adequate protection for vacuum tubes is not the same for power semiconductor devices. Protection for microcircuits is also quite different from power semiconductors. With increased usage of microprocessors and other small area geometry semiconductors, equipment is becoming more vulnerable to transient voltages, under both single pulse and repetitive pulse conditions.

INDUCTIVE EFFECTS IN COMPONENT LEADS

a. CALCULATION: The inductance in a straight wire appears, at first glance, to be very small and insignificant. Assuming a value of 1µH/m for a straight wire, most lead wires have inductance values in the nanohenry region. The voltage drop developed across an inductor under pulse conditions is expressed as:

$$V(t)=\frac{di}{dt}$$

where L is inductance in henries

$\frac{di}{dt}$ is time rate change of current

For the fast rise-times of EMP as shown above, the associated problems are obvious; however, for the slower rise-time of switching and induced lightning the degree of exposure and protection required can be defined only after carefully studying all boundary conditions.

b. CASE STUDY: In the following application, a silicon transient suppressor is being used to both regulate the voltage to power a telecommunications repeater and also provide transient suppression. The schematic is shown in figure 5. This is one of two repeaters powered and protected by the same component.

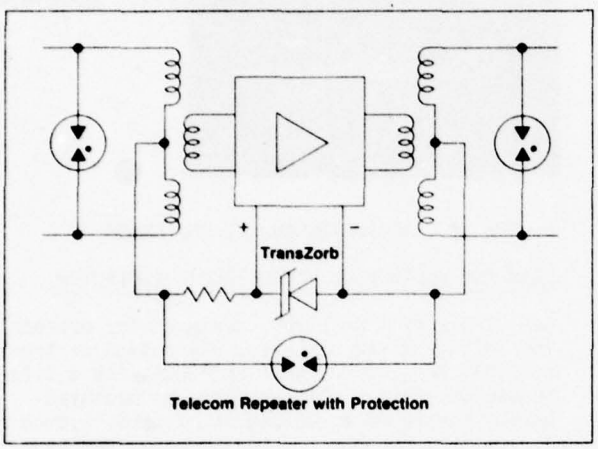

FIGURE 5: TELECOM REPEATER WITH PROTECTION

The microcircuitry used in this equipment has some well defined failure levels; 20V in the positive direction and 6.5V in the negative direction. The suppressor has a well defined clamping voltage in the avalanche direction under a specified rise-time. The forward polarity measurements are specified at 100A with an 8.4 msec, ½ sine wave pulse. To determine higher current capability, pulse tests were made with a 1.2x50μsec waveform. During the process of taking data, small differences in lead length in the protection circuit were observed to have profound effects on the suppression capability of the device. Measurements extended over the range from 100A to 500A with lead lengths from the body of the device of zero, 1.0 cm and 2.0 cm. Tests were made on a molded 1.5kW TransZorb®. The peak clamping voltage was plotted against pulse current as shown in figure 6.

After tests were made with zero, 1.0 cm and 2.0 cm lead lengths, the plastic body was carefully cut away leaving only the cell containing the junction and the leads. Voltage measurements were then made across the cell, virtually eliminating inductance within the package. A lead length of 2 cm has a peak clamping voltage of 4V at 100A and 13.5V at 500A. By contrast, the cell only has a peak clamping voltage of 1.3V at 100A and 3V at 500A. Voltage probe placement for taking measurements is shown in figure 7.

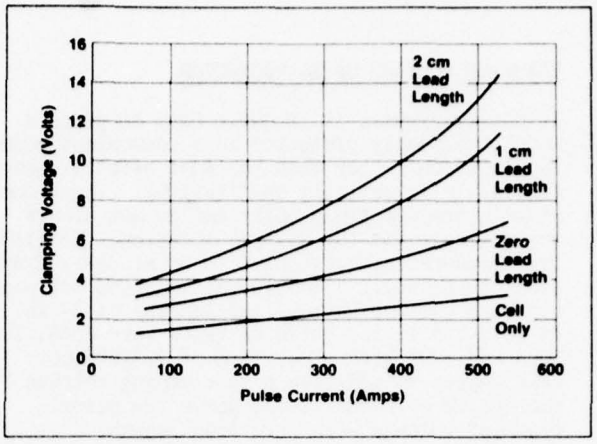

FIGURE 6: CLAMPING VOLTAGE VS. PULSE CURRENT

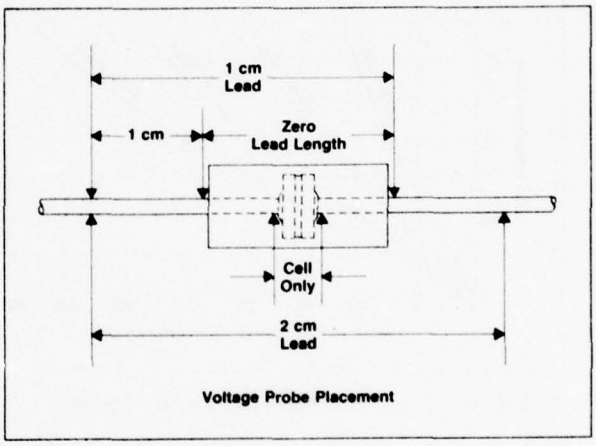

FIGURE 7: VOLTAGE PROBE PLACEMENT

Voltage drops across the lead wires contributing to peak clamping voltage can be attributed to both resistive and inductive components. Calculations were made for both resistive and inductive voltage drops for a 1.0 cm .040 in. dia. copper wire at pulse current levels from 100A to 500A. Rise-time is 1.2μsec. This data is shown in Table II.

TABLE II
Pulse Current Level and Voltage Drop

Pulse Current (Amps)	Measured Voltage Drop (Volts)	Calculated Resistive Voltage Drop (Volts)	Calculated Inductive Voltage Drop (Volts)
100	.75	.019	0.83
200	1.3	.038	1.66
350	2.3	.066	2.91
500	3.3	.095	4.16

Note that the calculated inductive voltage drop compares favorably with the measured voltage drop while the resistive component contributes less than 10% of the total.

CLAMPING VOLTAGE OF AC PROTECTOR

In power systems, it is quite easy to place a modular assembly protector in a convenient mounting location rather than the most effective one, especially in retrofit applications. These components are sometimes bulky and do not always conveniently fit the desired location. To illustrate reduced effectiveness in an ac power transient suppressor, a module was measured for peak clamping voltage having lead lengths of 24 in., 48 in., and 72 in. Pulse currents were 100A, 200A 300A and 400A with a waveform of 1.2x50μsec. Lead length vs additive peak clamping voltage plotted here is that value above the normal clamping voltage with zero lead length.

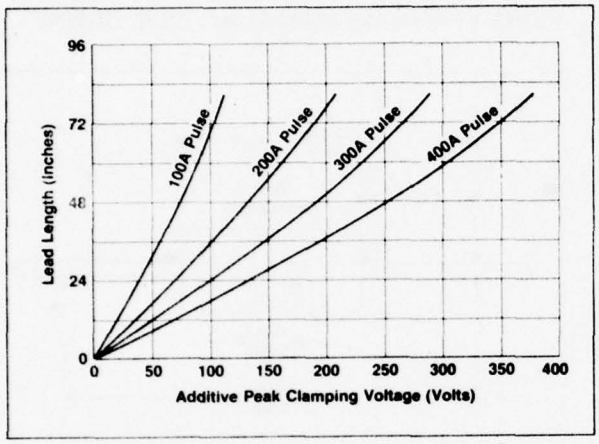

FIGURE 8: LEAD LENGTH VS. CLAMPING VOLTAGE

Note that the additive clamping voltage can be down in the range of 35V at 100A for 24 in. leads extending up to 350V at 400A for 72 in. leads. An oscillograph depicting optimum protection at 100A and 400A is shown in figure 9. The 100A pulse is being clamped at about 215V and the 400A pulse at 265V. The peak clamping voltage is substantially increased by the inductive effects of 72 in. leads as shown in figure 10. In this oscillograph, the 100A pulse produced a peak of about 320V and the 400A pulse produced a peak of about 615V. The inductive overshoot illustrated in figure 10 is quite profound by comparison with figure 9.

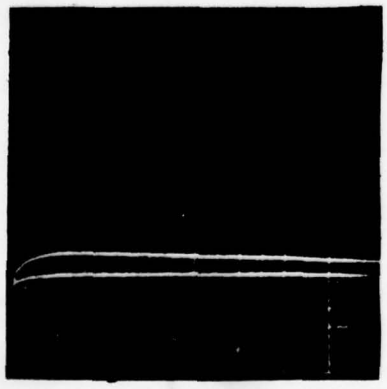

Vert: 100V/div.

Horiz: 2μsec/ div.

FIGURE 9: AC PROTECTOR, OPTIMUM PROTECTION

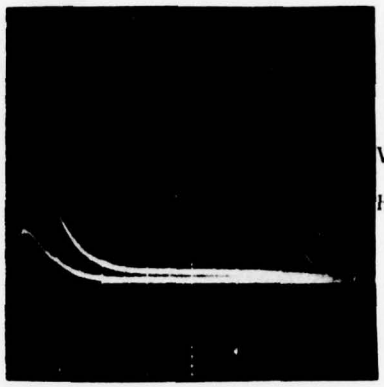

Vert: 100V/div.

Horiz: 2μsec/div.

FIGURE 10: AC PROTECTOR, 72 IN. LEADS

CLAMPING VOLTAGE OF MICROCIRCUIT PROTECTOR

An ICT-5 type TransZorb®, designed for protecting low voltage logic circuits, was pulsed at levels of 100A, 200A, 300A, 400A and 500A with a 1.2x 50μsec waveform. Voltage drop was measured across the leads at distances of zero, 1.0 cm and 2.0 cm from the body of the package, adding a total of 4.0 cm .030 dia. straight wire contributing to inductance and subsequently adding to the peak clamping voltage. A graph plotting total lead length vs. peak clamping voltage is shown in figure 11.

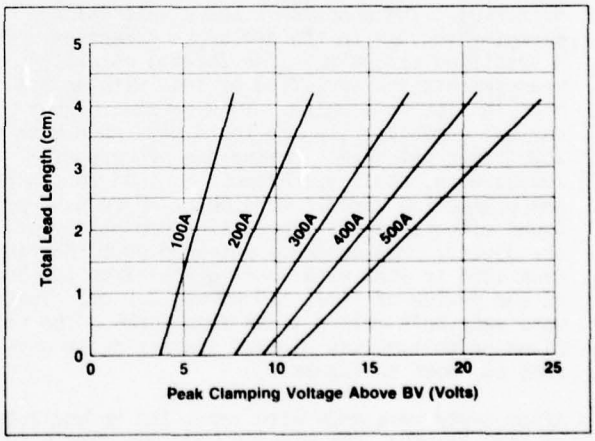

FIGURE 11: LEAD LENGTH VS. PEAK CLAMPING VOLTAGE

These curves are plotted as additive above the breakdown voltage (BV) at 1mA, which was 6.3V for the device tested. The clamping voltages increase with pulse current using zero lead length due both to the electrical impedance and thermal self-heating effect on the silicon pn junction. Observe that the clamping voltage covers a very broad range, from 3.6V above BV to 24V above BV depending on peak current and insertion method.

REDUCING INDUCTIVE EFFECTS

The most obvious method of reducing inductive effects and thus optimizing protector capability is to reduce lead wire lengths in the protector circuit. If it is not possible to reduce the conductor length, other options are available. Inductance in a given length of conductor can be reduced by replacing a small diameter wire with a wide strip conductor. On circuit boards, a ground plane on one or both sides of the board has been used by the author as a method for optimizing protector clamping.

Since voltage drop across the lead length is a function of the transient rise-time, it may be feasible to add series inductance between the transient source and the protector to reduce the rise-time and subsequently the peak clamping voltage. A TransZorb® used for 5V logic protection was tested with a 300A pulse having a 1.2x 50μsec waveform with voltage measurements made at 2.0 cm from each end of the body of the device. This is shown in figure 12, peaking at 24V. Placing a 12μH choke ahead of the suppressor to reduce the rise-time, reduced the peak to 19V and using 24μH reduced the peak to 17V. These curves are also shown in figure 12.

Vert: 5V/div.

Horiz: 500nsec/div.

FIGURE 12: COMPARATIVE CLAMPING VOLTAGES

CONCLUSION

Inductive effects can be, and often are, a source of abnormally high peak clamping voltages compared to the inherent capability of a transient voltage suppressor. These high clamping voltages can cause failure of vulnerable electronic components; thus a suppressor capable of providing adequate protection can be rendered useless due to poor insertion methods. So it behooves the design engineers working on both mechanical layout and circuit design to be acutely aware of inductive effects and the problems which they can cause along with corrective measures in order to optimize transient voltage protector components.

REFERENCES

1. E. Van Keuren, "Effects of EMP Induced Transients on Integrated Circuits", IEEE Electromagnetic Compatibility Symposium Record, October, 1975.

2. L. Gallace & H. J. Pujol, "The Evaluation of CMOS Static-Charge Protection Networks and Failure Mechanisms Associated With Overstress Conditions as Related to Device Life", presented at the 1977 Reliability Physics Symposium. April, 1977.

3. F. D. Martzloff, "A Guidance on Transient Overvoltages in Low-Voltage AC Power Circuits". GE Report No. 77CRD221, September, 1977.

4. Sigrid K. Llewllyn, "Broadband Magnetic Field Waveforms Radiated from Lightning", Masters Thesis, Florida Institute of Technology, 1977.

The Application of Nuclear EMP Protection Technology to Lightning Protection Problems

Thomas J. Lange
The Boeing Company
P.O. Box 3999
Seattle, Washington 98124

BIOGRAPHY

Thomas J. Lange is a senior specialist engineer in the Electromagnetic Technology Staff organization, currently supporting the Ballistic Missile Division. He received his B.A. in mathematics in 1957 from Northwestern University. For the last ten years he has worked missile ground electronics EMP analysis tasks in the area of critical circuit identification, and the testing and modeling of circuits. His previous experience was in the areas of missile system engineering and system performance evaluation.

ABSTRACT

The hardening of aircraft and electronic systems to the Nuclear Electromagnetic Pulse (NEMP) has resulted in the development of analysis and test techniques for circuit damage threshold characterization and terminal protection device selection and characterization. This paper discusses these techniques and their application to lightning problems.

INTRODUCTION

NEMP and lightning provide similar threats to aircraft and electronic systems. The increasing use of digital flight control systems and integrated circuits is increasing the threat to these systems. For example, a typical discrete audio transistor failure level to a 1μs rectangular pulse is in the range of 100 watts to 1 kilowatt. A typical integrated circuit failure level ranges from 5 watts to 100 watts. As the integration scale gets larger and circuit speeds increase the susceptibility is expected to get worse. The increased use of composite structures on aircraft also tends to increase the severity of the problem. A systematic methodology and analytic tools have been developed to assess the effect of NEMP induced pulses at electronic equipment. Corbin[1] has shown how this system analysis methodology can be applied to lightning problems. This overall methodology is shown in Figure 1 (from Corbin[1]).

Starting with a description of the environment applied to an aircraft coupling model[2] the transient signals coupled to the circuits are determined. The transient signals are then applied to models of the circuits to evaluate their damage thresholds. Where necessary terminal protection is applied to the circuits to prevent lightning induced damage. Note, however, that hardening of an aircraft need not be totally accomplished at the circuit level. Hardening can also be accomplished at the aircraft external structure. In some cases a combination of hardening approaches may be required to achieve adequate safety margins.

The NEMP technology as applied to the coupling analysis of aircraft in a lightning environment has been previously presented[2]. This paper discusses the circuit aspects of the analysis, including the evaluation of circuit thresholds and the selection of terminal protection devices. Specifically, the tasks are: 1) measuring the damage parameters of the circuit; 2) modeling the circuit; 3) using the model to establish the safety margin; 4) selecting the terminal protection candidates and 5) iterating the tasks 1-3 including the model of the terminal protection device to demonstrate adequate safety margin. This general approach to circuit threshold evaluation and hardening is shown in Figure 2. The strategy used to characterize semiconductors and terminal protection devices is to develop models where:

1. The necessary model data can be obtained from test measurements at the device terminals,
2. Details of the semiconductor manufacturing process (geometries, doping, etc.) are not required,
3. Can be readily implemented on standard computer aided design programs.

All the models to be discussed in this paper meet these requirements.

The following sections of this paper discuss parts testing, the damage modeling of semiconductor circuits, and the selection and characterization of terminal protection devices.

PARTS TESTING

Two purposes are achieved by the parts testing. The damage threshold test results can be manually compared to the predicted transients to initially prioritize the safety margins. This is usually accomplished by estimating a rectangular pulse equivalent for the predicted

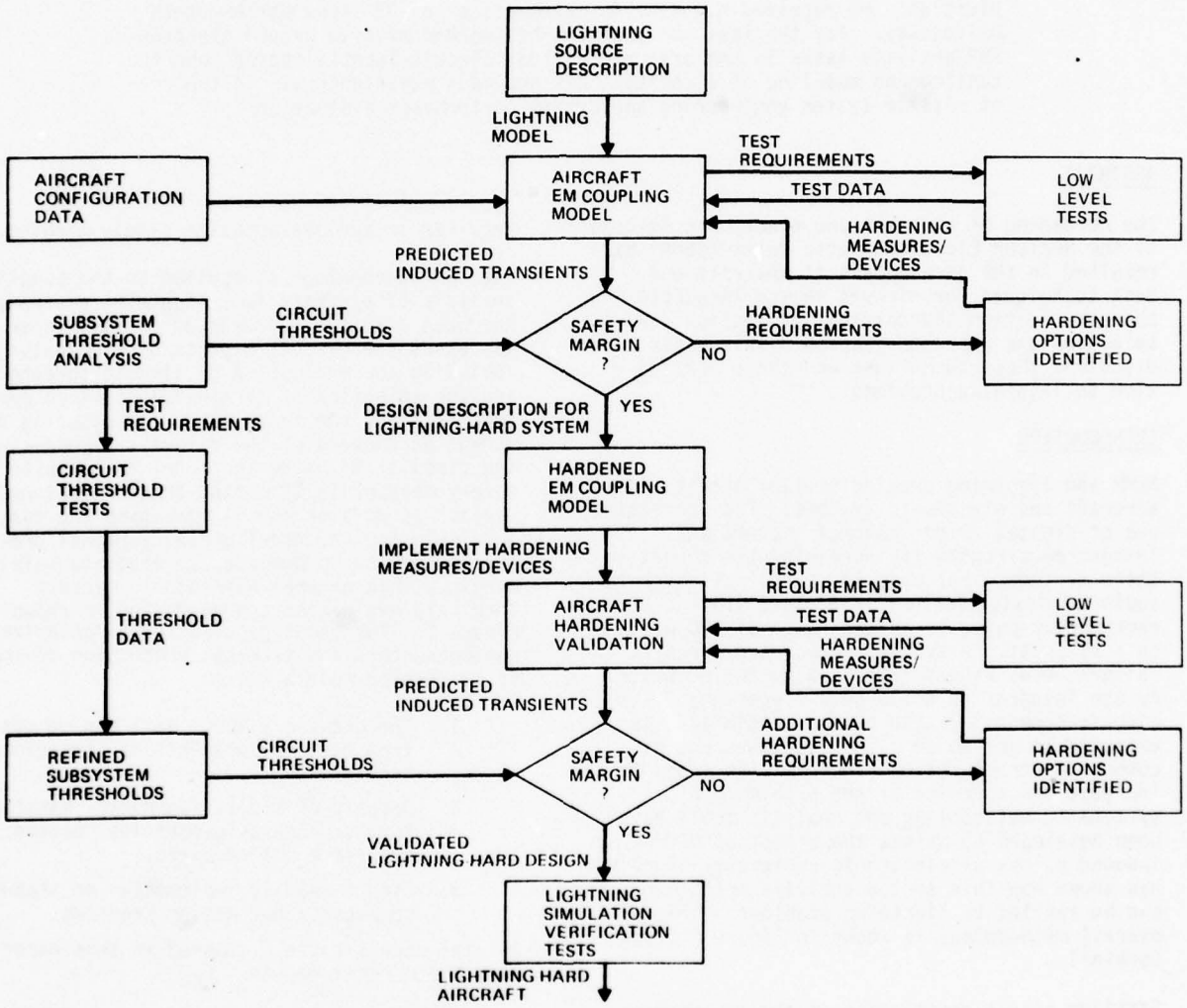

FIGURE 1. GENERAL APPROACH TO VALIDATED LIGHTNING-HARD AIRCRAFT

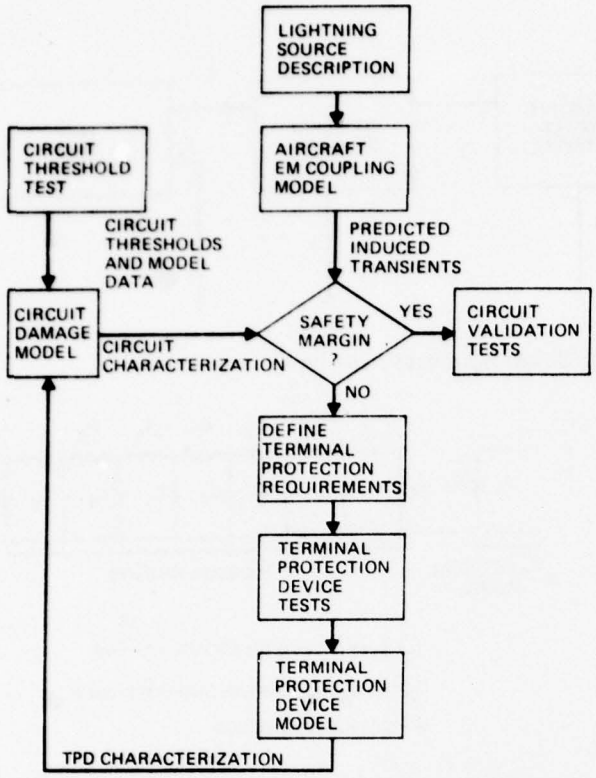

FIGURE 2. GENERAL APPROACH TO CIRCUIT THRESHOLD EVALUATION AND CIRCUIT HARDENING

transient. Also the testing provides the data required to model the circuit. The typical parts test set up is shown in Figure 3. The testing is conducted by step stressing the test part with rectangular pulses and evaluating for damage after each applied pulse. This evaluation, for discrete semiconductors, consists of observing their i-v characteristics on a curve tracer. Integrated circuit damage is usually evaluated using a switching setup and observing the device input-output response. All the necessary data required for modeling a semiconductor part (discrete or integrated circuit) is obtained from measuring the current and voltage at the test part for each pulse. The necessary data is:

1. The Breakdown Voltage (V_{BD}).
2. The i-v relationship above V_{BD}.
3. The power dissipated at damage.

The data is obtained for both positive and negative polarity pulse drives.

An additional consideration is that integrated circuits should have power applied during the testing. A comparison of power on versus power off has shown that the application of power makes little difference in the damage power threshold. However, the breakdown voltage and the i-v relationship after breakdown can be greatly different in the two situations. An example is shown in Table 1 where the term "bulk resistance" is the device impedance after breakdown.

Parameter	Power Off	Power On
Damage Power$^+$ (1μs)	23W	17W
Damage Power$^-$ (1μs)	65W	31W
Breakdown Voltage$^+$	0.8V	8.8V
Breakdown Voltage$^-$	0.8V	0.7V
Bulk Resistance$^+$	7.8Ω	2.0Ω
Bulk Resistance$^-$	8.7Ω	11.6Ω

TABLE 1. INTEGRATED CIRCUIT DAMAGE PARAMETERS POWER OFF VERSUS POWER ON.

In addition, some integrated circuits will "latch up" when pulsed and then destroy themselves due to excessive power supply current. Power off testing would not discover latch-up conditions.

For discrete semiconductors power off testing is adequate.

Typical damage results for an integrated circuit (National DM7098 Line Receiver) are given in Figures 5 and 6.

SEMICONDUCTOR DAMAGE MODELING

Heating of a semiconductor due to a high amplitude transient is the damage mechanism. Tasca[3] has shown that the energy in a rectangular pulse revised to fail a semiconductor is given by:

$$E_F = \left(\frac{4}{3}\pi a^3 \rho C_p + 4\pi a^2\sqrt{\rho C_p K_p t} + \frac{8}{3} a\pi K_p t\right) (\Delta T)$$

where a is the radius of spherical defect region, ρ is the material density, C_p is the material specific heat, K_p is the material thermal conductivity, t_p is the pulse width, ΔT is the temperature rise above ambient, and E_F is the energy required to produce the temperature rise ΔT.

The result is typically implemented with empirical data in the form

$$P_F = At^{-1} + Bt^{-1/2} + C$$

or

$$P_F = Kt^{-1/2}$$

where the constants A, B, C and K are obtained by curve fits to experimental data and P_F is the failure power and t is the pulse width. These models work well where the transients can be related to rectangular pulses.

A Thermal Damage Model (TDM) usable with Computer Aided Design (CAD) programs such as CIRCUS-2 and SCEPTRE, capable of determining the thermal response of semiconductor to arbitrary waveforms

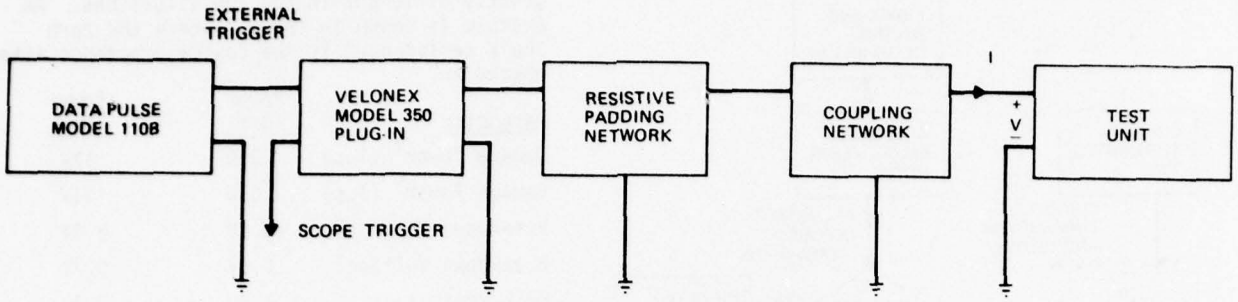

FIGURE 3. TYPICAL PARTS TEST EQUIPMENT SET-UP

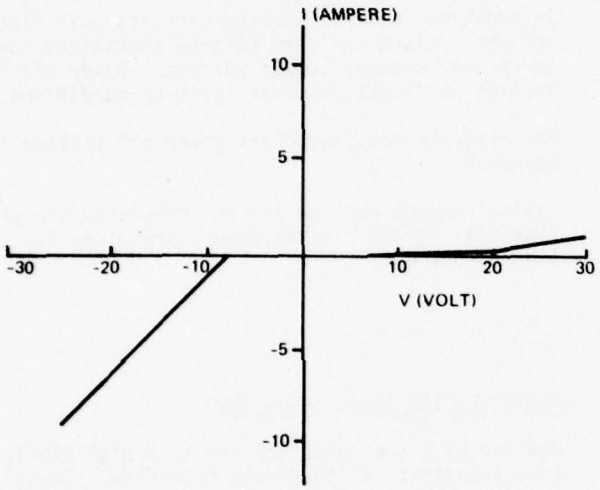

FIGURE 5. I-V CURVE FOR DM7098 LINE RECEIVER

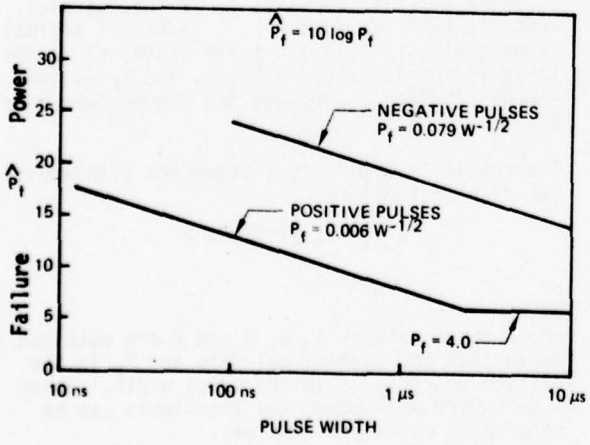

FIGURE 6. DAMAGE CURVE FOR DM7098

has been developed [4,5]. Schematically the model is given in Figure 4.

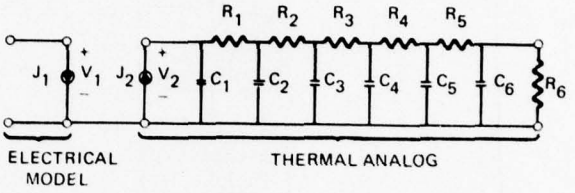

$J_1 = f_1(V_1)$ DERIVED FROM V-I CURVE

$J_2 = K \cdot V_1 \cdot J_1$ = INSTANTANEOUS POWER · K

K = DEVICE PARAMETER

FIGURE 4. THERMAL DAMAGE MODEL

The TDM has been shown to provide good agreement with experiment for a variety of waveforms[4] and with good failure prediction accuracy to very high frequency transients[5].

The DM7098 data presented previously will be used as an example of the use of the damage model. The data in Figure 5 and 6 results in the DM7098 model of Figure 7, where the parameter WF is the pulse width at which the failure power, PF occurs. The parameter FFF relates the forward bias failure level and the reverse bias failure level.

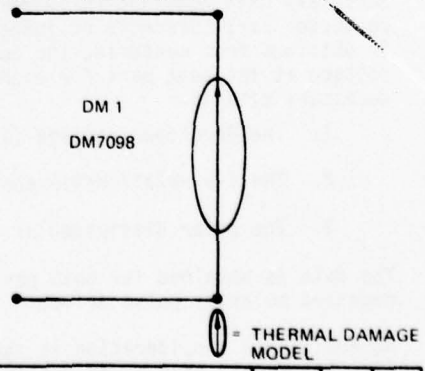

Device	V-I table	WF	PF	FFF
DM1	J(-1000.0, -7.6, 0.0, 7.0, 20.0, 1000.0), (-496.0, -7.6E-4, 0.0, 7.E-4, 0.26, 97.0)	10.E-6	25.0	0.2

FIGURE 7. MODEL DM7098 LINE RECEIVER INTEGRATED CIRCUIT DAMAGE MODEL

Lightning induced waveforms at interface circuitry will vary from damped sinusoids to primarily exponential signatures[6]. The form depends upon the coupling and the source and load impedance of the circuit of interest. The waveforms from a study of both direct attached and indirect lightning to a Learjet aircraft[6] will be used as an example with the DM7098 damage model. The frequency range of damped sinusoids varied from about 3 MHz to 12 MHz. For this example the sinusoid will be taken as a 3 MHz damped sine

$$V(t) = V_p e^{-\alpha t} \sin(2\pi f t)$$

where $\alpha = .345 \times 10^6$

$f = 3.0 \times 10^6$

V_p = Peak Voltage

The exponential will have the characteristics of the lightning stroke used in the analysis

$$V(t) = V_p (e^{-t/t_f} - e^{-t/t_r})$$

where V_p = Peak Voltage

$t_f = 59\mu s$

$t_r = 0.27\ \mu s$

The damage threshold of the DM7098, using the model of Figure 7, to the damped sine is 20 watts. The failure threshold to the exponential waveform is 1.8 watts. Note, the variation on the threshold, as a function of the waveform, with the thresholds differing by more than a factor of ten.

TERMINAL PROTECTION

Protection is required for those circuits where damage is predicted by the circuit analysis. The form of the protection will vary from passive devices such as resistors and filters to active limiting devices. The technique used to choose the means of protection is based upon the magnitude of the transient and the signal requirements of the circuit requiring protection. The protection device model is added to the circuit model and the problem run again to establish that adequate safety margin exists.

Current limiting resistors or filters are often required by design requirements other than the transient protection. Filters may be required for electromagnetic interference reasons, for example. These elements can be utilized for transient protection and if the transient levels are low enough they could be totally sufficient. At higher transient levels an active terminal protection device will be additionally required to protect the circuit. Terminal protection devices (TPD's) can be grouped into two classes: surge arrestors and limiters. The surge arrestors are characterized by a high turn on voltage and a low voltage in the on state. Limiters will turn on at a lower voltage compared to ESA's, and will remain at approximately the limiting voltage during the on state.

ACTIVE TERMINAL PROTECTION DEVICE MODELS AND CHARACTERISTICS

Electrical surge arrestors are protection devices containing a spark gap. When the breakdown voltage of the gap is achieved an arc is established in the gap. The gap thus approximates a short circuit and limits the impressed transient. These devices are widely used as lightning arrestors on power lines.

The significant characteristics of electrical surge arrestors (ESA) are:

1. High impedance until the breakdown voltage is reached.
2. Low impedance, low voltage (compared to the breakdown voltage) in the on state.
3. The breakdown voltage is a function of the rate-of-rise of the applied signal.

The i-v relationship for a surge arrestor is given in Figure 8. Available devices have a d.c. breakdown voltage varying from a few hundred volts to a few thousand volts.

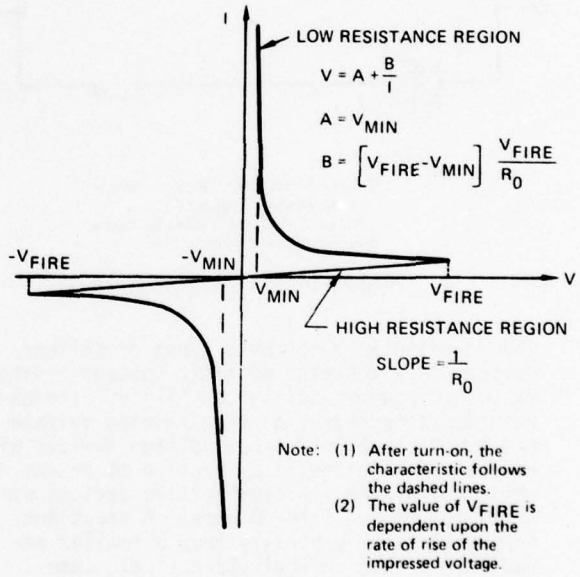

FIGURE 8. ESA I-V CHARACTERISTICS

Analytically an ESA is modeled as in Figure 9. The treatment of the non-linear resistance has taken different forms, depending upon the investigator. Andersen[6,7] treats the gap as a non-linear resistor whose value depends on the gap voltage, with an equivalent inductance to account for gap inertia. Kleiner, et al[8] treat the gap as a non-linear resistor whose value is dependent upon the energy in the gap. Details of the models and the experiments required to obtain the model parameters will be found in the references.

Limiters are grouped into two classes based upon the material from which they are manufactured. The first class is the silicon diode limiters which includes zener diodes and transient suppressors. The second is the varistors which are typically manufactured from silicon carbide or a metal oxide. The silicon diodes are characterized by a sharp knee in their i-v curve while the varistors have a much softer knee characteristic.

The important parameters, of limiters are their voltage, on resistance, capacitance, switching speed and power handling capability. Both zener diodes and transient suppressors are available in breakdown voltages from a few volts to a few hundred volts. The upper limit of available transient suppressors is about 200 V while zener diodes are available with limiting voltages greater than 300 V.

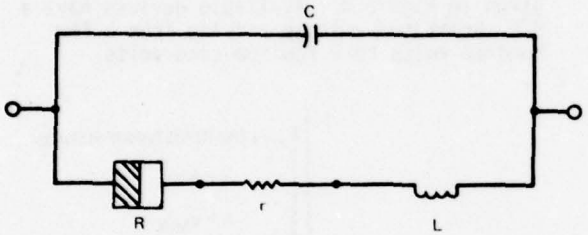

where:

C = Dynamic capacitance of the gap
r = Discharge resistance
L = Lead inductance plus gap inertia
R = Nonlinear gap resistance

FIGURE 9. ESA GAP MODEL

The on-resistance of both types of silicon devices is a function of their voltage limiting value and power handling capability. The on-resistance increases as the limiting voltage and power capability. Low voltage devices will have on-resistances of a fraction of an ohm while the higher limiting voltage devices will be in the range of 10-20 ohms. A transient suppressor will generally have a smaller on-resistance than an equivalent (i.e., same breakdown voltage) zener diode.

The capacitance relationship for these devices is related directly to the junction area (i.e., power dissipation capability) and inversely to the junction voltage. A high voltage device will typically exhibit a capacitance of a few 10's of pF while a low voltage device will have a few hundred pF's for the same power dissipation device.

The switching speed of the limiting devices is quite variable. Zener diodes typically are much slower than the transient suppressors. The usable frequency of zeners is typically a few megahertz. Transient suppressors are quoted as having switching speeds of less than 1 ps.

The silicon limiter diodes are modeled in exactly the same manner as the semiconductor circuits discussed earlier. For example, the model of a 1N6113 transient suppressor (a nominal 20V bipolar device) is given in Figure 10.

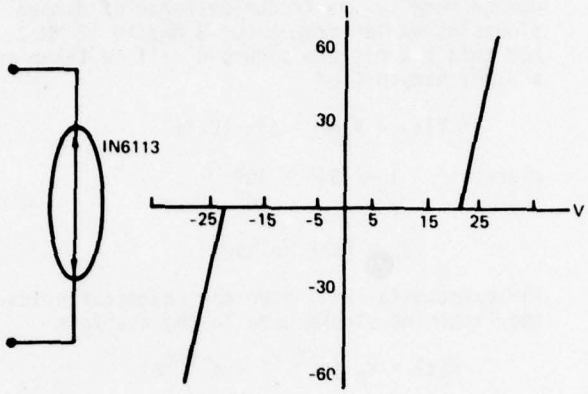

V-I table	WF	PF	FFF
J (-1,000.0, -22.0, 0.0, 22.0, 1,000.0), (-10,000.0, -2.2E-4, 0.0, 2.2E-4, 10,000.0)	1.0E-6	10.E3	1.0

FIGURE 10. IN6113 TRANSIENT SUPPRESSOR DAMAGE MODEL

Varistor damage is an area that has not been widely addressed theoretically. However, the manufacturers typically provide maximum operating curves such as in Figure 11, which presents the maximum allowable current as a function of pulse width. This curve can be modeled using a similar strategy as for the semiconductors discussed earlier. The model is given in Figure 12. When the voltage V_2 reaches 1.0 the maximum current has been reached.

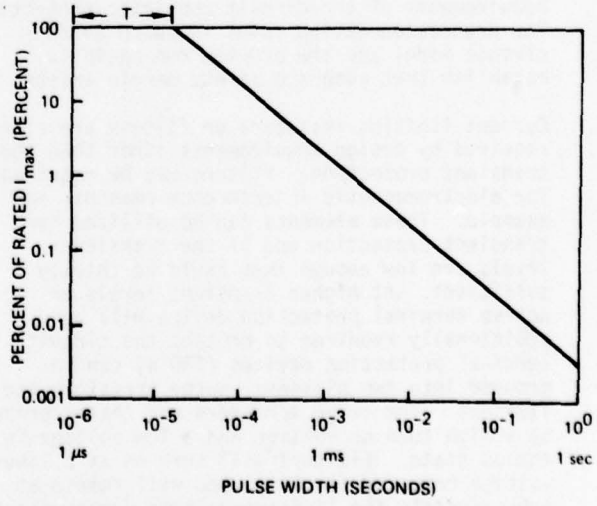

FIGURE 11. TYPICAL DAMAGE CHARACTERISTIC FOR VARISTOR

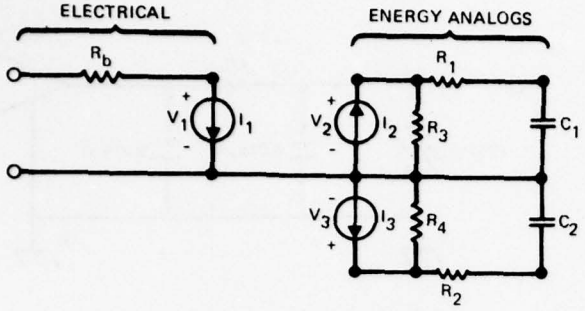

$R_b = 1 - 10\Omega$

$R_1 = R_2 = \frac{1}{I_{max}}$

$I_1 = \frac{V_1}{V_1} \; K \left|V_1\right|^{\alpha}$

$C_1 = C_2 = I_{max} \times T$

$$I_2 = \begin{cases} I_1 \text{ if } V_1 \geq 0 \\ 0 \text{ if } V_1 < 0 \end{cases} \qquad R_3 = \begin{cases} 10^6 \text{ if } V_1 \geq 0 \\ 0.1R_1 \text{ if } V_1 < 0 \end{cases}$$

$$I_3 = \begin{cases} 0 \text{ if } V_1 \geq 0 \\ I_1 \text{ if } V_1 < 0 \end{cases} \qquad R_4 = \begin{cases} 0.1R_2 \text{ if } V_1 \geq 0 \\ 10^6 \text{ if } V_1 < 0 \end{cases}$$

FIGURE 12. VARISTOR DAMAGE MODEL

The choice of ESA's, limiting diodes or varistors is dependent upon the magnitude of the transient to be protected against and the threshold of the circuit to be protected. The failure level of a silicon diode limiter is typically a fraction of a joule while a varistor will fail at more than 40 joules. A typical surge arrestor will withstand several kilojoules. These devices can also be used in combination with each other, and with current limiting resistors and filters to provide terminal protection[10]. Extensive tables of candidate terminal protection devices will be found in references 11, 12, and 13. A comparison of the important characteristics of terminal protection devices is given in Table 2.

Parameters	Spark Gaps	Varistor Devices	Transient Suppressors
Typical Surge Capability (AMPS)	10,000	1,000	200
Failure Level (Joules)	>1,000	40	5.0
Capacitance (fd)	10^{-11}	10^{-9}	10^{-10}
Voltage Range (volts)	90 and higher	40-700	2-300
Insulation Resistance	High	Medium	Medium
Bipolar Operation	Yes	Yes	Yes
Failure Mode	Short*	Short	Short
Activated State	Short Circuit	Clamped	Clamped

*Gap failures are usually short circuits - some surge arrestors are limited by the lead wires which fail open.

TABLE 2. TERMINAL PROTECTION DEVICE COMPARISON

SUMMARY

The circuit analysis and models used to evaluate circuit damage and terminal protection device performance have been presented. Given the transient at the circuit the safety margin and terminal protection requirements can be determined. The safety margin after the incorporation of terminal protection can be demonstrated.

The circuit of Figure 13 will be used as an example. The circuit had to withstand a current pulse having a damped sine waveform similar to that discussed earlier. The failure level of the line driver without terminal protection is approximately 4.0 amperes which was below the 10 amperes required hardness level. The terminal protection device-filter combination was designed for both electromagnetic interference and transient protection. The 1N6113 transient suppressor discussed earlier was used for the limiting device. The failure level after incorporation of transient protection is 100 amperes providing a margin of 20 dB.

These techniques are readily implemented on any time domain computer program allowing user defined models and provide an accurate means for evaluating circuit thresholds to either predicted or test waveforms.

REFERENCES

1. John C. Corbin, Jr., "Vulnerability and Assessment of Aircraft Systems to Indirect Lightning Effects", Certification of Aircraft For Lightning and Atmospheric Electricity Hazards Conference, Paris, France, September 1978.

2. J. C. Corbin, Jr., and Dr. D. F. Strawe, "Electromagnetic Coupling Analysis of a Learjet Aircraft in a Lightning Environment", Proceedings of the IEEE 1978 National Aerospace and Electronics Conference, Vol. 2, 78CH1336-7.

3. Dante, M. Tasca, "Pulse Power Failure Modes in Semiconductors", IEEE Transactions on Nuclear Science, Vol. NS-17, No. 6, Dec. 1970.

4. G. A. Hjellen and T. J. Lange, "A Thermal Damage Model for Bipolar Semiconductors", Conference Record, 1977 IEEE International Symposium on Electromagnetic Compatibility, IEEE Publication 77CH1231-0 EMC, August 1977.

5. T. J. Lange and G. A. Hjellen, "A Comparison of Test and Model Predicted RF Pulse Susceptibilities of UHF Transistors", IEEE Transactions on Electromagnetic Compatibility, Vol. EMC-20, No. 4, November 1978.

6. Dr. D. F. Strawe, M. O'Byrne, S. Sandberg, "Electromagnetic Coupling Analysis of A Learjet Aircraft, June 1978, Boeing Document D180-24256-1, Final Report.

7. J. Andersen, "Modeling Techniques of Electrical Surge Arrestors For EMP Simulations", IEEE Transaction on Nuclear Science, Vol. NS-24, No. 3, June 1977.

8. J. Andersen, "Gap Inductance Evaluations of Surge Arrestor Models", Proceedings of the IEEE Power Engineering Society Winter Meeting, 1977.

9. C. T. Kleiner, E. D. Johnson, L. R. McMurray, and F. T. Suzuki, "An Electrical Surge Arrestor (ESA) Model For Electromagnetic Pulse Analysis", IEEE Transactions on Nuclear Science, Vol. NS-24, No. 6, December 1977.

10. John C. Corbin, Jr., "Protection/Hardening of Aircraft Electronic Systems Against the Indirect Effects of Lightning", Certification of Aircraft For Lightning and Atmospheric Electricity Hazards Conference, Paris, France, September 1978.

11. T. J. Sheppard, "Interface Circuit Protection in Satellite Applications", Nuclear EMP Protection Engineering and Management Note PEM-40, July 1975.

12. L. W. Ricketts, J. E. Bridges and J. Miletta, "EMP Radiation and Protective Techniques, John Wiley and Sons, 1976.

13. William C. Hart and Daniel F. Higgens, "A Guide to the Use of Spark Gaps for Electromagnetic Pulse (EMP) Protection", Joslyn Electronics Systems, 1973.

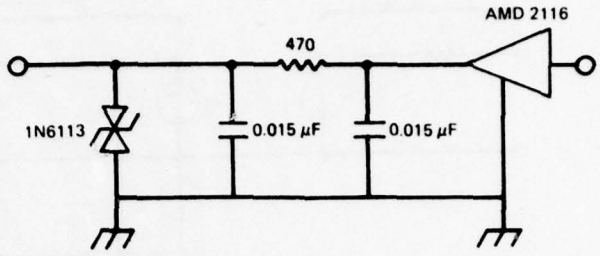

FIGURE 13. TERMINAL PROTECTION EXAMPLE

SPACE SHUTTLE LIGHTNING PROTECTION

D. L. SUITER, R. D. GADBOIS, AND R. L. BLOUNT
National Aeronautics and Space Administration
Lyndon B. Johnson Space Center
Houston, Texas 77058

BIOGRAPHY

D. L. Suiter is an aerospace engineer, flight systems, in the Engineering Evaluation and Analysis Office of the Program Operations Office at the NASA Lyndon B. Johnson Space Center (JSC). He received his B.A. in mathematics and physics from Texas Christian University in 1960. Before joining NASA in 1963, he worked for 3 years in electrical design with General Dynamics in Fort Worth, Texas, and 3 years as an electronic design project engineer with Brown Engineering and the Hayes International Corporation.

R. D. Gadbois is also an aerospace engineer, flight systems, in the Engineering Evaluation and Analysis Office of the Program Operations Office at the NASA JSC. He received his B.S.E.E. in 1957 from Illinois Institute of Technology and his J.D. in 1974 from South Texas College of Law. Before joining NASA in 1962, he worked for 5 years as a circuit designer at General Dynamics-Astronautics in San Diego, California.

Robert L. Blount is the manager of the Engineering Evaluation and Analysis Office at the NASA JSC. He received his B.S.E.E. from the Missouri School of Mines and Metallurgy in 1957. Before joining NASA in 1964, he worked 7 years in electronic design with General Motors and Emerson Electric.

ABSTRACT

The technology for lightning protection of even the most advanced spacecraft is available and can be applied through cost-effective hardware designs and design-verification techniques. In this paper, the evolution of the Space Shuttle Lightning Protection Program is discussed, including the general types of protection, testing, and analyses being performed to assess the lightning-transient-damage susceptibility of solid-state electronics.

INTRODUCTION

In keeping with a national commitment to provide a low-cost space transportation system, the Space Shuttle vehicle (Fig. 1) must accommodate numerous launch and landing operations in an adverse weather environment each year. The advanced solid-state electronics and the unique thermal protection system required for atmospheric entry create particular lightning protection problems.

From past experiences with lightning, the most notable of which was the Apollo 12 lightning strike incident[1] and the resulting Apollo-Soyuz Test Project Overall Simulated Lightning Test[2], NASA Lyndon B. Johnson Space Center engineers recognized that protection for the Space Shuttle would require the application of state-of-the-art technologies. To be cost-effective, protective design measures had to be incorporated into the initial hardware designs.

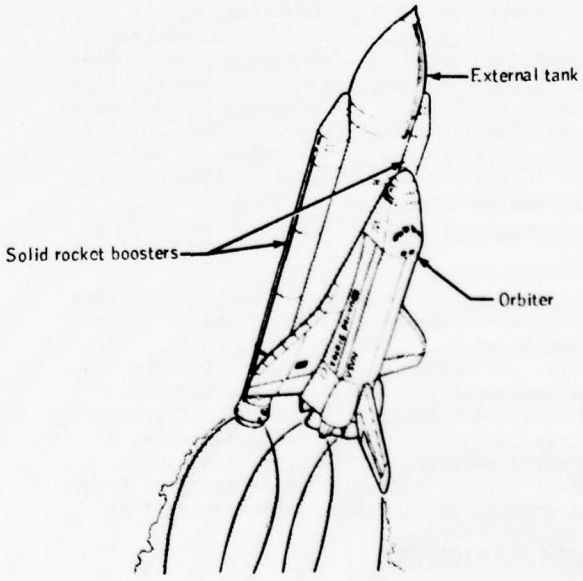

FIGURE 1. SPACE SHUTTLE SYSTEM.

LIGHTNING COMMITTEE

The management approach was to assemble a group of specialists who would provide an early definition of the lightning environment (design model) and who would develop the design requirements. The Space Shuttle Lightning Committee

thus formed consisted of representatives from the Shuttle element contractors, the integrating contractor, the U.S. Air Force, the three NASA centers actively involved with the Space Shuttle Program, and four consultants from the engineering and scientific community.

The product of this committee was the Space Shuttle Lightning Protection Criteria Document[3], a document that is being used in the Shuttle hardware design. The committee continues to function to help resolve particular lightning protection design problems as they arise.

DESIGN REQUIREMENTS

The formulation of the design requirements centered around two basic questions. To what degree or depth should protective measures be applied? What design limits should be imposed?

From a practical approach, circuit upsets would be acceptable, if adverse actions were unlikely to occur. Some damage would be acceptable only if such damage did not result in loss of the vehicle. Several factors, such as vehicle safety, weight, simplicity, cost, and existing technology for protective designs influenced the design requirements. The Shuttle specification thus imposed specific protection requirements in some areas while criteria and guidelines for protection were provided in other areas.

The design requirements were divided into two categories - direct lightning effects and indirect lightning effects. The direct effects were defined as burning, blasting, direct coupling of voltages and currents, and structural deformation caused by lightning-arc attachment. Also included in this definition were the high-pressure shock waves and magnetic forces caused by the high lightning currents. The indirect effects were defined as the damage or malfunctions (circuit upsets) caused by induced currents and voltages that are produced by the electromagnetic fields that occur with lightning.

Lightning protection measures are divided into four groups: the control of lightning paths, isolation of sensitive circuits, unique circuit design, and design verification. These measures fundamentally entail the application of low-resistance electrical bonding and grounding, circuit isolation, aperture closeouts, wire and cable shielding, filtering, and special circuit designs to negate the effects of lightning-induced voltage and current transients.

DESIGN VERIFICATION

The capability of the hardware to withstand both the direct and indirect effects of lightning can be verified through analysis or test; but, in some cases, a combination of both is required. For the Space Shuttle, a full-threat-level direct effects test has been specified for antennas, pitot tubes, thermal protection coverings, vents, doors, and other external hardware that must be located in main current paths or arc-attachment zones.

To determine the arc-attachment zones, a test was conducted on a 0.03-scale model of the Space Shuttle vehicle (Fig. 2). The results of this test are contained in Reference 4. Of particular concern to the designers was the extent of damage to the Orbiter thermal protection coverings. Hence, two further tests were conducted. The purpose of the first test was to perform a preliminary evaluation to determine the vulnerability of the various protective materials to lightning and to determine the feasibility of incorporating lightning diverter strips. The results[5] led to the conclusion that diverter strips that could withstand entry heating were too heavy. Therefore, the second test was conducted to establish the extent of damage caused by a full-threat swept-stroke lightning strike. An analysis of the results[6] showed that the area of damage produced in the latter test was thermally acceptable with no special protection required.

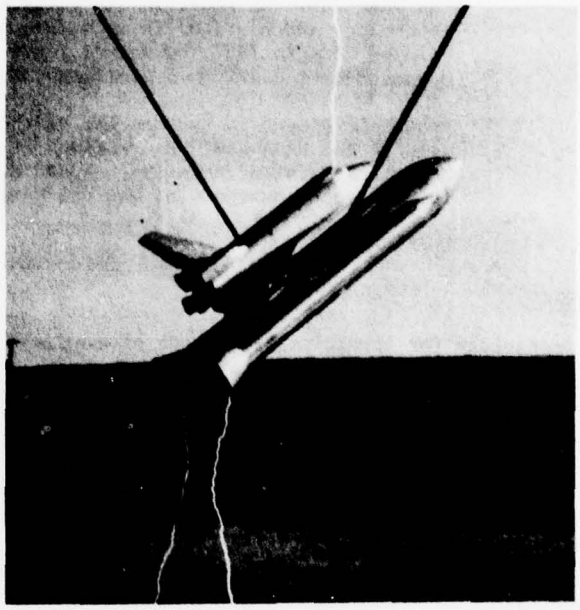

FIGURE 2. LIGHTNING ARC-ATTACHMENT TEST.

Another area of primary concern was the pyrotechnics, which could be ignited or damaged with direct lightning arc attachment. Two worst-case candidates, the Orbiter outer panel severance system (for crew inflight escape) and the solid rocket booster frustrum separation system, were tested. The results of these tests are given in References 7 and 8, respectively. The tests indicated that both ordnance systems could withstand a full-threat (200 000 A) lightning strike without any adverse effects.

Many other direct effects tests were conducted on Shuttle hardware. For the interested reader, results of the more important tests may be obtained from References 9 to 21.

Various indirect effects tests were also conducted, and of special note was the testing on the solid rocket booster nozzle severance (ordnance) system cable that is detailed in Reference 22. In this test, a 40 000-A lightning current was driven through the ordnance cable outer shield (triple shielded) without firing or dudding the explosives. In addition, the pyrotechnic initiator controller that provides the electrical signal to fire the ordnance was not adversely affected.

A method for terminating cable shields using diodes was tested for possible Shuttle application and the results are discussed in Reference 23. This scheme can be used when a conflict exists in electromagnetic interference and lightning-shielding requirements.

Verification that hardware is immune to the indirect effects of lightning, however, proved to be more difficult than originally envisioned.

ANALYSIS VERSUS TEST

The original plan to assess the indirect effects of lightning on Shuttle hardware was twofold. First, the electromagnetic field levels inside the vehicle were calculated based on a full-threat-level (200 000-A design model) lightning strike to the vehicle. (The details of the analytical procedure used will be discussed in another paper presented at this conference.) Various unshielded circuit runs, using worst-case loop areas routed through these magnetic fields, were postulated and analyzed. From these analyses, open-circuit voltages and short-circuit currents were calculated. The results were then discussed with the Lightning Committee. Based on experience with indirect lightning effects on similar types of equipment, the committee concluded that the off-the-shelf avionics equipment being proposed for the Shuttle should withstand a 50-V and 10-A (2-μsec) lightning transient without damage. Thus, this requirement was imposed on all flight-critical electrical and electronic hardware. The electromagnetic environment inside the vehicle would be controlled, with at least a 6-dB margin, to levels below the equipment design levels. This lightning design control would be exercised through the use of shielding, aperture closeouts, judicious equipment location, and other design techniques.

Secondly, the calculated electromagnetic field environment would be verified by actual measurement in an overall vehicle (Orbiter only) simulated lightning test. Prediction of the electromagnetic fields inside symmetrical vehicles, such as the solid rocket booster and the external tank, is well established from first principles of physics; therefore, testing at the vehicle level to verify internal fields was not planned. Avionics and other critical electrical equipment would be verified at the unit, subsystem, and vehicle levels using transient analysis tests similar to those described in Chapter 17 of Reference 24.

Lightning transient testing at the unit and subsystem levels was a new experience for most equipment vendors. Costs quoted for such testing were prohibitive and serious weight penalties (up to 600 lb) for shielding were necessary to maintain the induced-voltage levels below design limits. Also, during the Apollo-Soyuz lightning test, induced voltages as high as 350 V were measured with no resulting component damage. In addition, studies performed for the U.S. Air Force[25] indicated that component pulse failure powers could vary by 1 or 2 orders of magnitude among components with the same part number. Thus, qualification testing to determine failure levels for electrical and electronic hardware proved to be impractical. At this point, the lightning protection program for the Shuttle vehicle was redirected.

Space Shuttle critical avionics systems have been designed to be failure tolerant; that is, sufficient redundancy has been used so that the vehicle can still perform a mission after one failure in a critical system. A second failure in that system, at worst, will still allow a successful return of the Orbiter. The vehicle is, therefore, designed to be fail-operational/fail-safe. Lightning-induced failures in critical avionics equipment can be tolerated, as long as the fail-safe design requirement is not violated.

LIGHTNING TRANSIENT DAMAGE ANALYSIS

The lightning transient survivability of electrical components and equipment can be determined by analysis. Theoretical and experimental work by D. C. Wunsch and R. R. Bell[26] has shown that the power level required to damage a semiconductor junction is proportional to the minus one-half power of the pulse width of the applied power for pulse widths between 0.1 and 100 μsec.

$$P_F = Kt^{-1/2}$$

where P_F = failure power, K = proportionality constant, and t = pulse width.

The proportionality constant has been named the "Wunsch" or "damage" constant. In general, the pulse widths of lightning-induced voltage fall within the cited range, and the Wunsch damage equation can be used directly to predict whether avionics semiconductors will survive lightning-induced voltages. Based on the Apollo-Soyuz Test Project lightning test, a 5-μsec pulse width was chosen for Shuttle systems analysis. Damage constants of semiconductor devices were calculated using the junction capacitances C_j and breakdown voltages V_{bd}, and the thermal impedances from junction-to-ambient θ_{ja} or from junction-to-case θ_{jc}, using the equations given in Reference 27. The damage constants can also be determined by testing, but a statistically significant number of components (six to nine) must be tested to failure. A wide dispersion (plus or minus 1 to 2 orders of magnitude) exists in damage constants for like components

with the same part number. The significance of this fact cannot be overlooked when contemplating lightning transient damage susceptibility testing at the unit or subsystem level. Damage levels can, however, be calculated to within plus or minus 1 to 2 orders of magnitude; and, through the use of derating techniques, a damage constant can be calculated to ensure that at least 95 percent of the components will actually have a higher damage constant. This fact, along with the multiple redundancies used in critical systems, allows an analytic approach to be taken to assure that, from a component damage standpoint, the vehicle will be able to return safely after being struck by lightning. The analytic techniques described in this paper are quite similar to those that are currently in use for electromagnetic pulse survivability analysis.

Damage constants have been determined for more than 18 000 components by the U.S. Air Force. These data, stored in a computer program called SUPERSAP, were made available for the Shuttle analysis effort. References 25, 27, and 28 have been used for Shuttle analysis.

The analytic approach used by the Space Shuttle Program is divided into three steps, the first two of which are performed in parallel. First, for each criticality I (failure of which causes loss of life or vehicle) black box or component, the internal circuits that are connected in flight were identified and detailed to the external connector and pin numbers. Using electromagnetic pulse analysis techniques, the damage levels, failure voltage, and failure current are established for each connector contact. In the analysis, all damage constants are derated by a factor of 0.1, unless other data indicate that the damage constant corresponds to the lower 95-percentile failure level. A pulse width of 5 μsec is used for all circuits except those that cross the Orbiter/external tank, solid rocket booster/external tank, or the Shuttle vehicle/ground checkout interfaces. For those interface circuits, a pulse width of 50 to 100 μsec is used because lightning currents can flow directly in the overall shields of the interconnecting cables. Simplifying assumptions are used whenever possible to shorten the analysis. Such assumptions, however, are always selected to provide a more conservative answer.

Second, the induced open-circuit voltage and short-circuit current for each interconnecting wire are calculated using the method established in Appendix F of Reference 3. If the calculated induced-voltage and short-circuit current exceed the calculated failure voltage and current, step 3 is undertaken.

Third, the analysis is expanded to include total end-to-end circuit impedances, and the simplifying assumptions are removed. An analysis of the total circuit then yields the voltage that appears at each end of the circuit and a current that is limited by the total circuit impedance. If these values exceed the failure voltage and current, corrective action is taken. This action consists of adding shields to wires, relocating equipment and wiring to areas of lower magnetic field intensity, adding transient suppression devices, or redesigning the affected equipment. A sensitive circuit is shown in Figure 3. The equivalent circuit and sample analysis are shown in Figures 4 and 5. It is interesting to note that the most susceptible components in the circuit shown in Figure 3 are zener diodes that were added to protect the rest of the circuit from transients. If the diodes are removed, the circuit failure

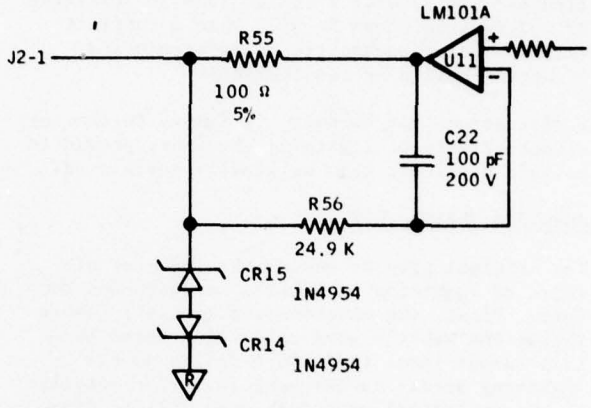

FIGURE 3. TYPICAL CIRCUIT FOR LIGHTNING TRANSIENT ANALYSIS.

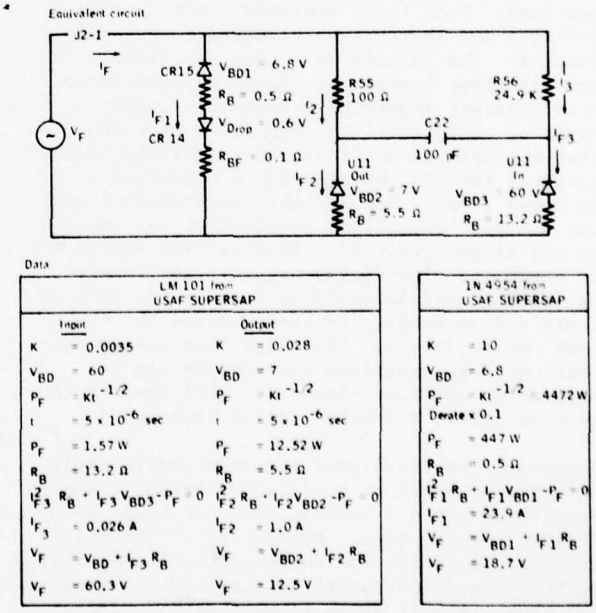

Data

LM 101 from USAF SUPERSAP	
Input	Output
K = 0.0035	K = 0.028
V_{BD} = 60	V_{BD} = 7
$P_F = Kt^{-1/2}$	$P_F = Kt^{-1/2}$
$t = 5 \times 10^{-6}$ sec	$t = 5 \times 10^{-6}$ sec
P_F = 1.57 W	P_F = 12.52 W
R_B = 13.2 Ω	R_B = 5.5 Ω
$I_{F3}^2 R_B + I_{F3} V_{BD3} - P_F = 0$	$I_{F2}^2 R_B + I_{F2} V_{BD2} - P_F = 0$
I_{F3} = 0.026 A	I_{F2} = 1.0 A
$V_F = V_{BD} + I_{F3} R_B$	$V_F = V_{BD2} + I_{F2} R_B$
V_F = 60.3 V	V_F = 12.5 V

1N 4954 from USAF SUPERSAP
K = 10
V_{BD} = 6.8
$P_F = Kt^{-1/2}$ = 4472 W
Derate x 0.1
P_F = 447 W
R_B = 0.5 Ω
$I_{F1}^2 R_B + I_{F1} V_{BD1} - P_F = 0$
I_{F1} = 23.9 A
$V_F = V_{BD1} + I_{F1} R_B$
V_F = 18.7 V

Notes:

1. R_B taken from Table 2 of Reference 25.
2. LM101 failure powers are not derated because Figure 32 of Reference 25 gives 2.5 W and Figure 33 gives 27 W as lower 95-percentile failure powers for linear integrated circuit input and output, respectively.

FIGURE 4. SAMPLE EQUIVALENT CIRCUIT AND FAILURE DATA.

For CR15, $I_{F1} = 23.9$ A

$V_F = V_{BD1} + I_{F1}(R_B + R_{BF}) + V_{Drop} = 21.74$ V

For U11 Out, $I_{F2} = 1.0$ A

$V_F = I_{F2}(R_{55} + R_B) + V_{BD2}$

$V_F = 118.7$ V

For U11 In, $I_{F3} = 0.026$ A

$R_{55}C_{22} = 0.01\ \mu$sec

$0.01\ \mu\text{sec} \ll 5\ \mu\text{sec}$

Therefore, C_{22} can be considered open

$V_F = I_{F3}R_{56} + V_{BD3} = 707$ V

V_F for CR15 is less than V_F for U11 input and output; therefore, CR15 is the most susceptible component, and

$V_F = 21.7$ V

$I_F = I_{F1} + I_2 + I_3$, $I_3 = 0$ because U11 input $V_{BD} < V_F$

$$I_F = I_{F1} + \frac{V_F - V_{BD2}}{R_{55} + R_B}$$

$I_F = 24$ A

Legend

V_F = Failure voltage

I_F = Failure current

R_B = Reverse bulk resistance

R_{BF} = Forward bulk resistance

V_{BD} = Reverse breakdown voltage

FIGURE 5. SAMPLE CALCULATIONS.

voltage would increase from 22 V to 119 V, a greater than fivefold increase. However, the failure current would decrease from 24 A to 1 A. The diode suppression, therefore, would be adequate only if impedance in series with the induction generator (at the other end of the wire run) is high enough to limit the short-circuit current to less than 24 A.

ORBITER SIMULATED LIGHTNING TEST

The present plan is to conduct a simulated lightning test on the Shuttle Orbiter vehicle. The primary objectives will be to identify the critical circuit upsets (i.e., those that could cause loss of the vehicle) and to verify the predicted lightning-induced magnetic fields within the vehicle. It should be noted that, although upset levels can be analytically determined, the analysis would be extremely complicated. Also, upset levels should not vary significantly from vehicle to vehicle, so results obtained from testing one vehicle should apply to all vehicles. For the first phase, the Orbiter will be isolated from ground, powered up, and systems configured for flight operations below 50 000 ft. The output of a high-voltage generator, fed through a pulse-forming network, will be connected to the vehicle and a series of voltage waveforms (Fig. 6) will be applied to excite the vehicle as an open-ended transmission line. Figure 7 shows a rudimentary test configuration. The systems will be monitored

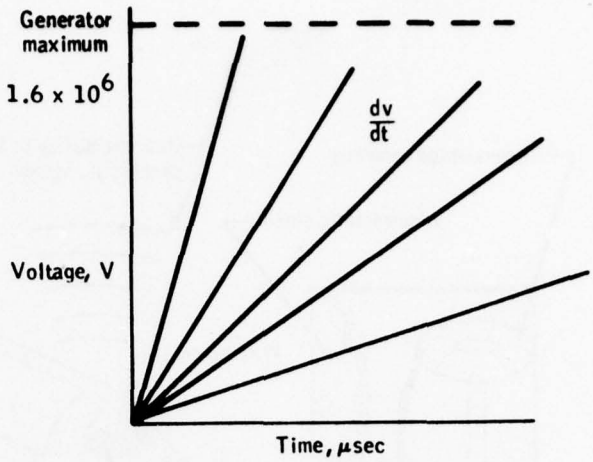

FIGURE 6. PHASE I TEST VOLTAGE WAVEFORMS.

through the existing radiofrequency link to the launch processing system and by onboard visual observation (manned). A number of circuits, particularly sensitive to lightning-induced effects, will be monitored by a special fiber optics system.

For the second phase, the vehicle systems and test configuration will be the same as for the first phase except that a test current (Fig. 8) will be passed through the vehicle and returned through a number of wires placed symmetrically around the vehicle.

The results of these tests and the results of the aforementioned analyses will then be used to evaluate the lightning protection designs of the vehicle.

CONCLUDING REMARKS

Adequate lightning protection can be provided efficiently and effectually in a spacecraft by incorporating well established and relatively simple practices into system designs. Proper analyses are required to determine where and how to apply these practices in the design.

The costs (i.e., weight and effects on systems) to implement a lightning protection program must be closely balanced against the gains in the utility of the vehicle to perform its mission.

The indirect effects analyses and the planned vehicle level lightning test are perhaps "breaking new ground"; however, they are practical and economical ways to ensure that the design will protect critical circuits.

The damage analyses for all critical circuits are expected to be completed before the vehicle-level test of Orbiter vehicle 102, which should occur in early 1980. For this test, the goal will be to identify critical circuit upsets and

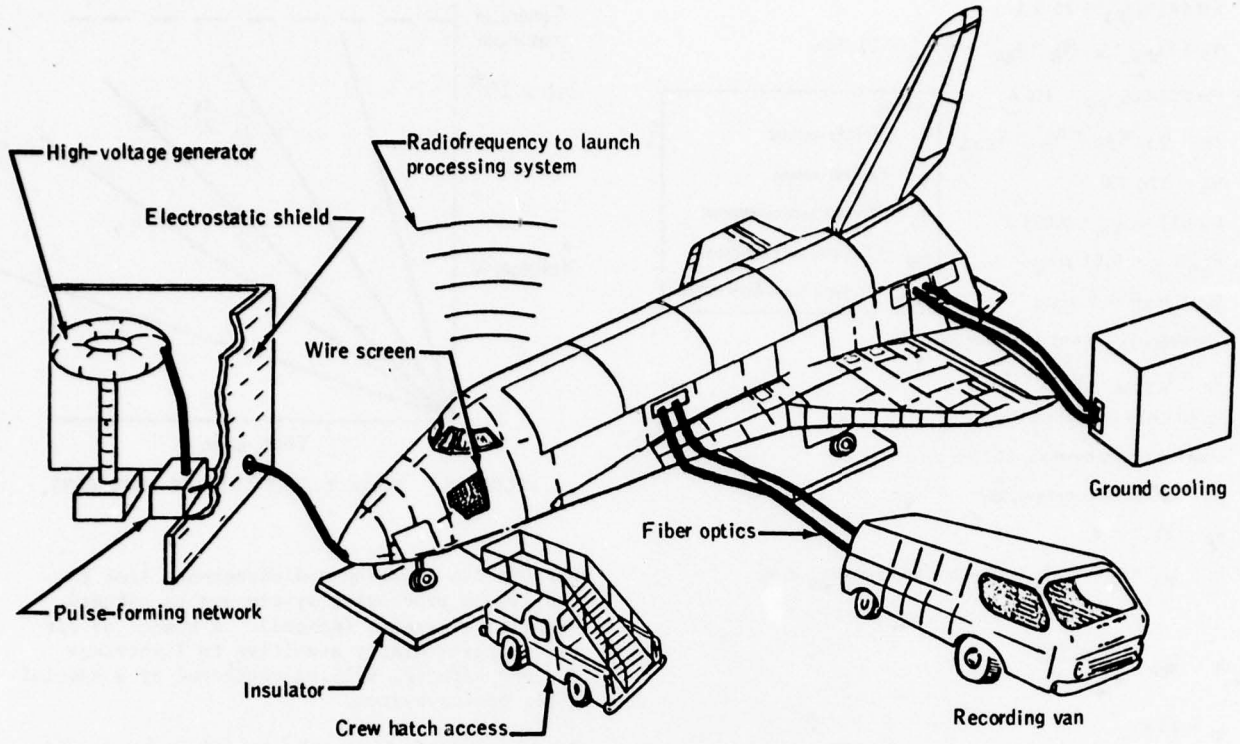

FIGURE 7. PHASE I TEST CONFIGURATION.

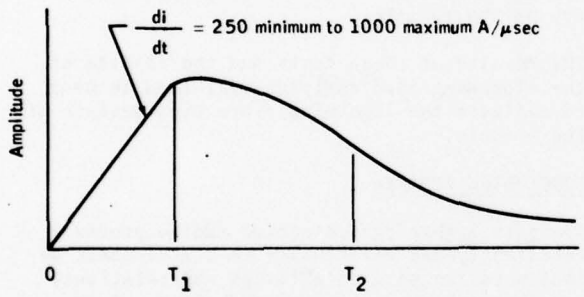

T_1 (time to peak value) = 2 μsec

T_2 (time to half value) = 50 μsec

FIGURE 8. PHASE II TEST WAVEFORM.

to verify the induced-voltage predictions with the least possible risk of damaging equipment and with the least effect on program schedules. The voltage test waveforms that will be applied to the vehicle as an open-ended transmission line need further understanding in terms of their similarity to the actual voltage rise experienced by a vehicle when struck by lightning in flight. Perhaps additional data are presently available or will become available before the testing is performed. Your knowledge in this area is solicited.

ACKNOWLEDGMENTS

The NASA Lyndon B. Johnson Space Center is indebted to F. A. Fisher of General Electric, John Robb of Lightning and Transients, Dr. Martin Uman of the University of Florida, and the late Dr. E. T. Pierce of Stanford Research Institute, for their guidance and technical expertise rendered as members of the Space Shuttle Lightning Committee.

REFERENCES

1. Analysis of Apollo 12 Lightning Incident, NASA Report No. MSC-01540, Feb. 1970.

2. ASTP Simulated Lightning Test Report, NASA Report No. JSC-09221, Nov. 1974.

3. Space Shuttle Lightning Protection Criteria Document, NASA Report No. JSC-07636, Nov. 4, 1975.

4. Simulated Lightning Test Shuttle .03 Scale Model, McDonnell Douglas Report No. MDC A3155, Dec. 1974.

5. Preliminary Evaluation of Space Shuttle Thermal Protection System (TPS) Response to Lightning Strikes, McDonnell Douglas Report, May 1973.

6. Swept Stroke Simulated Lightning Tests Space Shuttle Thermal Protection System, Lightning and Transients (L&T) Report No. 595, Dec. 1974.

7. Lightning Test of Space Shuttle Orbiter Outer Panel Severance System Phase I, McDonnell Douglas Report No. MDC E1568, Sept. 1976.

8. Lightning Tests of Space Shuttle Pyrotechnics Phase II Rocket Booster Frustrum Separation Ring, McDonnell Douglas Report No. MDC A4864, June 1977.

9. Lightning Current Effects on the Space Shuttle External Tank Thermal Protection Systems, Martin Marietta Report No. 826-2058, Sept. 1974 (L&T Report No. 591).

10. Artificial Lightning Tests of Space Shuttle External Tank Gaseous Oxygen Line, Martin Marietta Report No. 826-2097, March 1975 (L&T Report No. 597).

11. High Current Lightning Test of Space Shuttle External Tank Lightning Protection System, Martin Marietta Report No. 826-2019, Feb. 1976.

12. TPS Covered GO_2 Line Lightning Test (External Tank), Martin Marietta Report No. 826-2163, Aug. 1976 (McDonnell Douglas Report No. A4308).

13. External Tank Gaseous Oxygen Line Simulated Lightning Tests, NASA TM X-73322, 1972.

14. Simulated Lightning Discharge Current Effects on Space Shuttle Exhaust Nozzle Coolant Tubing, L&T Report No. 563, May 1973.

15. Lightning Current Distribution Tests on a Scale Model, Space Shuttle Rocket Engine, General Electric Report No. SRD-73-117, Sept. 1973.

16. Space Shuttle SRB/ET Forward Attach Point Lightning Test, George C. Marshall Space Flight Center, Nov. 1977.

17. Lightning Tests of the Shuttle SRB Nozzle Severance System, L&T Report No. 629, Feb. 1977.

18. Direct Effects Tests Space Shuttle SRB Thermal Protection System (TPS), L&T Report No. 652, Dec. 1977.

19. Static Charge Measurement and Lightning Tests of Shuttle ET Skin Welds, TPS, and Lightning Protection System, Martin Marietta Report No. 826-2171, Sept. 1977.

20. An Experimental Study of Electromagnetic Coupling Into the Shuttle SRB Cable Tray From Lightning Passage Through the Shuttle Vehicle, prepared for Mission Research Corporation by LTRI, Aug. 1975.

21. Shielding Effectiveness of a Cable Tray to be Used on the Space Shuttle External Fuel Tank, prepared by General Electric for Martin Marietta Report No. 826-2099.

22. Lightning Tests on the Shuttle SRB Nozzle Severance System Cable, L&T Report No. 629, Feb. 1977.

23. Lightning Activated Electrical Cable Shield Ground, presented by K. D. Castle of NASA at the AIAA Second Annual Technical Mini-Symposium at the Johnson Space Center, Houston, Texas, March 1977.

24. Fisher, F. A., and Plumer, J. Anderson. Lightning Protection of Aircraft. NASA Reference Publication 1008, Oct. 1977.

25. EMP Susceptibility of Semiconductor Components, Defense Department Report No. D224-13042-1, Sept. 1974.

26. Wunsch, D. C., and Bell, R. R. Determination of Threshold Failure Levels of Semiconductor Diodes, and Transistors Due to Pulse Voltages. IEEE Transactions on Nuclear Science, Vol. NS-15, No. 6, Dec. 1968.

27. EMP Electronic Analysis Handbook, Defense Department Report No. D224-10022-1, May 1973.

28. EMP Electronic Design Handbook, Defense Department Report No. D224-10019-1, April 1973.

An RF Compatible Lightning Diverter Strip

John Robb, LTRI
Jay Cline, Dayton-Granger Aviation, Inc.
John Raney, Dayton-Granger Aviation, Inc.
Capt. J. Dunn, USAF, Eglin AFB

ABSTRACT

Airborne and Ground Radome Lightning protection with superior RF characteristics is the subject of this paper. Dayton-Granger "STRIKEGUARD" is examined along with a presentation of laboratory test data. Additional material is presented describing major thunderstorm penetrations by USAF.

INTRODUCTION

The "STRIKEGUARD" concept was developed by Dayton-Granger to improve the lightning performance of its static dischargers. Aircraft skin protection of a radius around the discharger was the objective. The success of "STRIKEGUARD" in this application and its ability to guide repeated 200 KA strokes led to protection of Radome and other plastic or composite areas. Of particular interest was "STRIKEGUARD" minimum reflectance characteristics when exposed to strong RF fields. It was determined by tests in the Dayton-Granger Laboratories and later verified by field testing by the Norton Co.,Brunswick and Air Force that "STRIKEGUARD" was literally invisible to RF from low frequency through 17 GH. Its reflectance approaching the epoxy level. Flight test of "STRIKEGUARD" in the lightning environment have been made by the Air Force on the RF4C, T39 and F111, General Aviation aircraft include helicopters and the Sabreliner.
The RF4C Flights were made by Eglin AFB in conjunction with the National Severe Storm Laboratory. Eight flights were made from Tinker AFB by Capt. James Dunn resulting in sixty penetrations of major thunderstorms. The aircraft flew at 300 knots indicated at levels of 15 to 20 thousand feet. Six major lightning strikes were observed with numerous lessor strikes. The aircraft suffered damage to several metal areas. "STRIKEGUARD" was used on the radome, over the pilots canopy and on plastic antenna housings on the vertical stabilizer. No lightning penetration of plastic areas was observed. Capt. Dunn will discuss the flight tests and answer questions. The following tests of "STRIKEGUARD" were carried out by Lightning and Transients Research Institute and will be described by Mr. John Robb.

L & T REPORT NO. 679 SEPTEMBER 1978
LIGHTNING TESTS OF AN ALUMINUM PARTICLE LIGHTNING DIVERTER STRIP
(Dayton-Granger "STRIKEGUARD")
FOR AIRCRAFT RADOMES

LTRI Industry Cooperative
Period: Program Lightning & Static
Fall 78 Electrification Reduction

FORWARD

This report L & T No. 679 describes tests of a new type of lightning diverter strip. The L & T technical personnel taking part in the test included J. D. Robb, Dr. T. Chen and G. Baxter. J. Cline of Dayton-Granger, representing the manufacturer, witnessed and participated in the tests.

ABSTRACT

Lightning tests have been carried out on a new lightning protection strip for aircraft radomes identified as the Dayton-Granger "STRIKEGUARD" high current damage tests and long arc diversion tests were carried out on protection strips which were mounted on flat panels ranging up ten feet in length and also on a small aircraft radome. Tests were made with the strips covered with a thin coat of polyurethane paint (.004 inch) and also unpainted. When painted over,

they carried one high current 200 KA discharge with some deterioration and a puncture did occur. Unpainted, they carried multiple high current discharges (200 kiloamperes), provided diverting action over ten foot lengths and no punctures occurred in tests of an actual small radome. As for all lightning diverter systems, lightning tests are recommended for each actual installation.

1.0 INTRODUCTION

Tests have been conducted on a new aluminum particle type of diverter strip for radome protection from lightning. Both high current damage tests (200 kiloamperes) and long arc diversion tests (one megavolt discharges) were carried out on the test strips.

2.0 IDENTIFICATION OF PROTECTION STRIP

The test strip is identified as the Dayton-Granger "STRIKEGUARD" and consisted of fine aluminum particles deposited on a flexible substrate 1/2 inch wide. The strip measured open circuit with D. C. potentials.

3.0 HIGH CURRENT TESTS

3.1 Calibration

A calibration test discharge was fired to a 15 inch long metal strip. The test arrangement and current oscillogram are shown in Figure 1a and b. The current magnitude was calculated from the measurement of the period and decrement of one cycle of the oscillatory wave form and from a computor computation using the exact linear circuit equations. The results were compared with the measured value of crest current shown on the oscillogram.

3.2 High Current Test

The first test diverter was 15 inches long and mounted on a 0.031 inch fiberglas flat panel and painted over with 0.007 urethane paint. With 50 kilovolts on the current generator, the test sample did not spark over. It was replaced with a second test sample which was covered with a layer of paint only 0.004 inch thick. This sample did spark over. The discharge current was 198 kiloamperes current crest. The urethane paint and a majority of the strip was badly damaged in the test. The strip did demonstrate that it could carry a single high current discharge; it provided one shot protection. The test discharge photographs, the oscillogram and the damaged strip are shown in Fig. 2a, b, and c.

A second unpainted test sample 20.5 ins. in length was tested. The test sample did sparkover at 50 kilovolts with a resultant current of 185,000 amperes. There was little damage done to the strip. A photograph of the test along with an oscillogram and photograph of the diverter strip after test are shown in Fig. 3a, b, and c.

4.0 ATTACHMENT POINT TESTS

4.1 Test Waveform

The fast rate of rise waveform (2 microseconds to crest) was used in the tests. This waveform is most conservative in the tests of dielectric puncture.

4.2 Radome Tests

A Gates Learjet Radome was used for the attachment point tests. Four diverter strips were mounted on the radome as shown in Fig. 4. The radome and the strips were painted over with a 0.007 inch thickness of urethane paint. A metal disc simulating the radar dish was mounted under the radome as shown in Fig. 5.

The test electrode was positioned 1-1/2 meters from the radome and aimed mid way between the #1 and #2 diverter strips. The radome was equipped with a rain erosion boot and the diverter tape ended approximately 1/4 inch under the rain erosion boot. The radome punctured approximately mid way down and slightly to the left of painted diverter strip #1. The paint and small portions of the diverter strip were damaged during the tests. A photograph of the test and of the strip after the test are shown in Figures 6a

and b.

Next, the painted strips were replaced with unpainted diverter strips. Tests were run with the test electrode positioned directly over the radome, and at positions of 0 and 45 to each side. The electrode spacing was 1-1/2 meters over the radome, as shown in Fig. 7a. The test discharges attached to diverter strip #2 and #4. There was little sign of damage to the diverter strip and no punctures of the radome occurred. The test discharges are shown in Figure 7b, c, and d. The unpainted diverter strips thus demonstrated protection of the radome.

4.3 Attachment Point Tests - 10 Foot Diverter

Next, attachment tests were carried out on a 10 foot length of diverter strip. The test sample was affixed to a ten foot length of wood, a 2" x 4". The diverter strip was grounded at one end and test electrode was located at an angle of approximately 45 to the ungrounded end of the diverter strip at a spacing of 1-1/2 meters as shown in Fig. 8. Two test discharges were fired to the strip, and in each case the discharge traveled down the diverter strip rather than over the short air gap of 10 inches or less to the test floor below the strip. Thus the diverter strip demonstrated diverting effectiveness for a full ten foot length.

5.0 CONCLUSION

Tests of the aluminum particle lightning diverter strips have shown that unpainted, they can divert long arc discharges over a ten foot length, and that they are capable of carrying multiple high current restrikes as demonstrated in tests of a small radome. When painted over the diverter effectiveness is much reduced. For all lightning diverter strips, even for solid aluminum bars, it is recommended that tests be made of any actual radome installation.

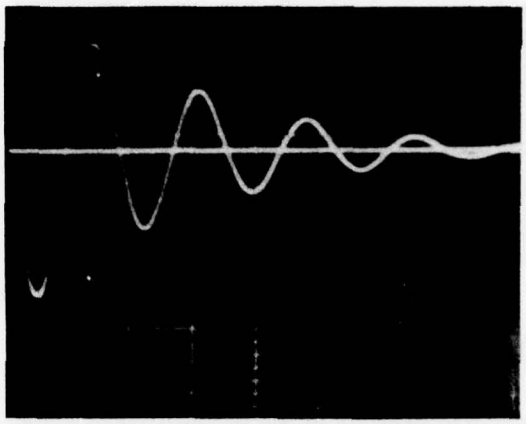

1a. 50 us/cm, 10 KV, 40 KA Calibration Shot

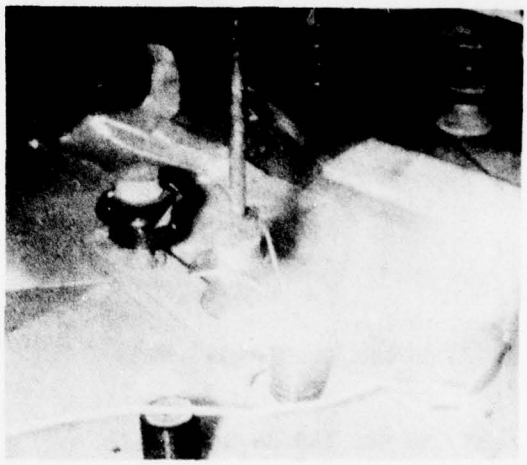

2a. 50 KV, 198 KA Strike

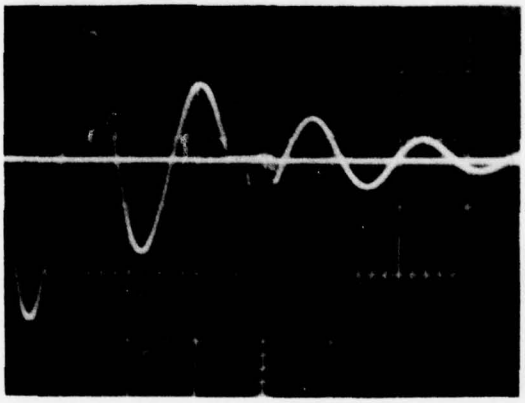

2b. 50 KV, 198 KA Waveform

Figure 2. Photograph and Oscillogram of Test on Painted Over Diverter Strip

Figure 2c. Diverter Strip with .0004" Urethane Paint after 198 KA Strike.

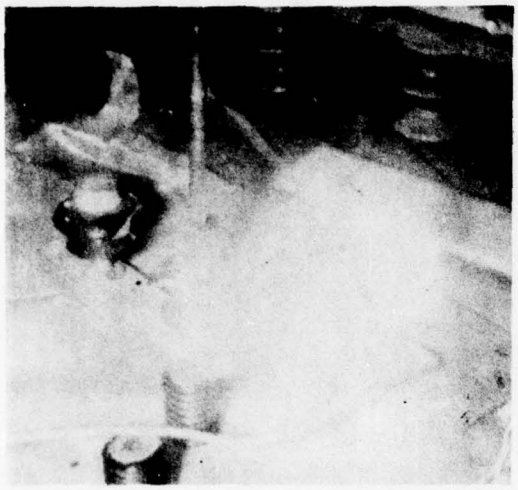

50 KV, 185 KA Strike

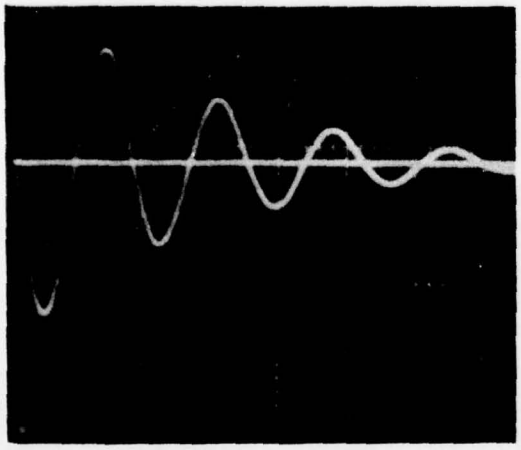

50 KV, 185 KA Waveform

Figure 3a. Test Photograph and Oscillogram for Unpainted Diverter Strip.

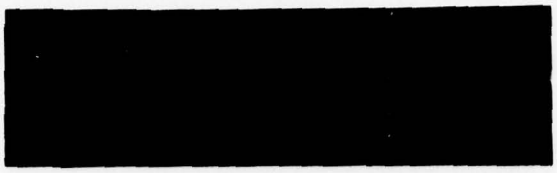

Figure 3c. Unpainted Strip shows Little Signs of 185 Kiloampere Test Discharge.

$1x10^6$ and 10 KA Lightning Strike *to Radome with* Painted Diverter Strips

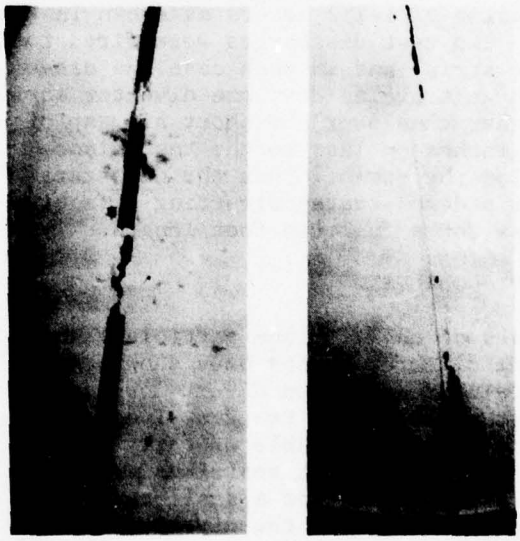

Painted Strip #1 After Strike

Painted Strip #3 After Strike

Figure 6. Test Discharge to Painted Strips above #1 and #3 Diverter Strips after the Discharge Shown Below.

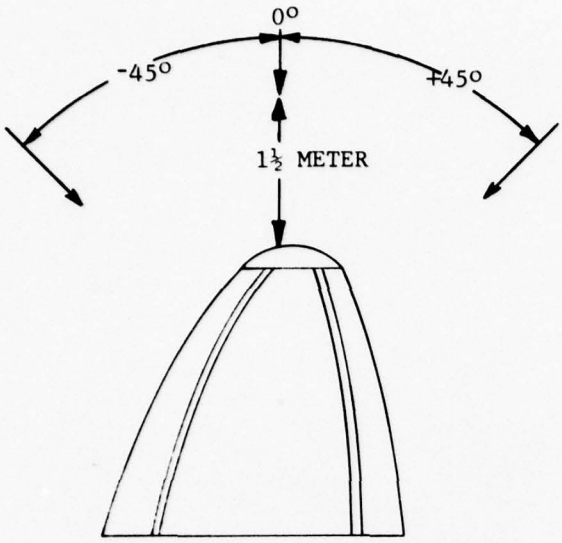

Position of the probe for testing with unpainted diverter strips.
Fig. #8

Figure 7a. Position of the Probe for Testing with Unpainted Diverter Strips.

Figure 7b. 0° Lightning Strike to Diverter Strip #2.

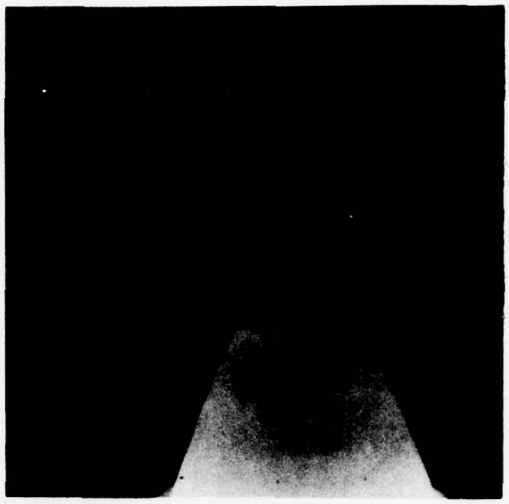

+45° Lightning Strike to Diverter Strip #4

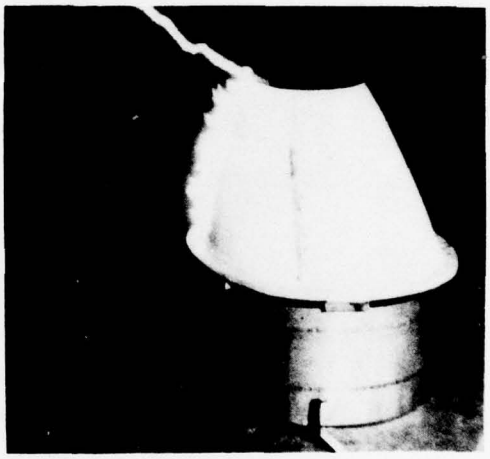

-45° Lightning Strike to Diverter Strip #2. Fig. 7c. Additional Tests of Unpainted Diverter Strips on Learjet Radome.

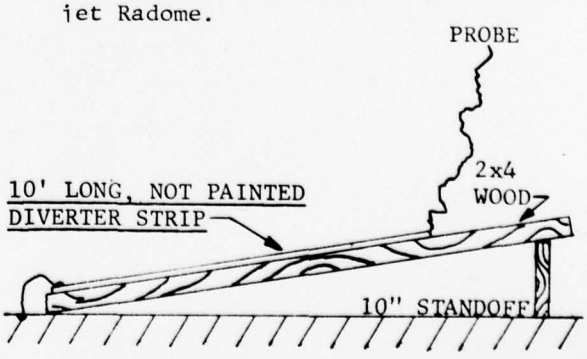

Attachment Point tests of 10 foot long diverter strip
Fig. #12

Figure 8. Attachment Point Tests of 10 Foot Long Diverter Strip.

PROTECTION/HARDENING OF AIRCRAFT ELECTRONIC SYSTEMS AGAINST THE INDIRECT EFFECTS OF LIGHTNING

JOHN C. CORBIN, JR.
Atmospheric Electricity Hazards Group
Air Force Flight Dynamics Laboratory
Wright-Patterson AFB, Ohio 45433

BIOGRAPHY

Dr. Corbin is a senior electrical engineer in the Atmospheric Electricity Hazards Group of the Air Force Flight Dynamics Laboratory (AFFDL). He received the Bachelor of Electrical Engineering degree from Cornell University in 1950 and the M.S. and Ph.D. degrees in electrical engineering from Ohio State University in 1963 and 1974, respectively. Prior to his AFFDL assignment, he served on the staff for the Assistant for Operations, Air Force Wright Aeronautical Laboratories (AFWAL) for one year. During the period from 1964-1975, he was Deputy Director of the Plasma Physics Laboratory of the Aerospace Research Laboratories. He has authored articles and reports in the areas of skin effect, plasma wave instabilities and control, nonlinear optics, multiwave parametric processes, and assessment of atmospheric electricity hazards to aircraft.

ABSTRACT

A number of different approaches which can be be applied to protect or harden aircraft and their electronic systems against the indirect effects of lightning are discussed in this paper. The basic approaches include (1) hardening the external structure to prevent or greatly reduce the penetration of rf energy into the aircraft, (2) shielding equipment and cables, (3) hardening electronic circuits, and (4) combinations of all three. The use of filters, limiters, circuit design, and functional hardening are described as techniques which can be applied for protecting electronic circuits. A systems approach is recommended for achieving an optimum hardened configuration.

INTRODUCTION

Lightning is a dual hazard to aircraft because of both its damaging direct, or physical, effects as well as its induced or indirect electromagnetic effects. The most obvious direct effects are physical damage and burnout of the aircraft structure caused by extreme heat loading as a result of high current lightning pulses. Resultant pitting/puncture points indicate the location of lightning entry/exit points on the aircraft. The most frequent direct effect damage occurs at radomes, pitot booms, canopies, external antennas, and wing tips. Unless protective devices and designs are used, damaging currents can penetrate directly into the interior of the aircraft.

Indirect or induced effects due to lightning may cause temporary disruption (upset) or permanent damage to internal electrical/electronic systems. Lightning currents on the skin of the aircraft (which result from a direct strike or a nearby strike) can couple energy into the aircraft interior to produce voltage and current surges on sensitive electrical circuits. The coupled energy flow path is shown in Figure 1 (Ref. 1). Important lightning parameters include rise time of the current and voltage pulses, peak current, total charge transferred, peak electric and magnetic fields, and the frequency spectrum of radiated fields.

Because earlier vacuum tube electronics were relatively immune to transients or surges induced in aircraft electrical circuits by lightning, induced effects were of little concern. However, during the past decade, electronics technology has progressed to discrete solid state electronics and more recently to integrated circuit electronics. The next step, which is now underway, is the application of microcircuitry in new commercial and military aircraft and in new missile systems. These components are inherently more susceptible to voltage and current surges because of their low operating voltage, current, and power handling capabilities. Moreover, they are being used in critical electronic subsystems which may be essential for the integrity of safe and controlled flight. Even use of circuit and component "redundancy" may not prevent interruption or failure of a critical subsystem caused by simultaneous lightning-induced transients. Evidence of impact or damage to avionic/electrical systems without direct lightning attachment to electrical components has recently appeared in airline lightning strike reports (Ref. 2).

Another factor that is contributing to awareness of the hazard of induced effects is the increasing trend for the greater use of advanced composite materials in aircraft structures. These composite materials (e.g., graphite epoxy) have inherently reduced electromagnetic shielding properties over the frequency spectrum generated by lightning. Hence, sensitive electronic flight controls and avionics may be exposed to considerably higher levels of induced electromagnetic

energy if proper protective design and installation techniques are not employed.

VULNERABILITY ASSESSMENT FOR INDUCED EFFECTS

Vulnerability assessments of aircraft systems to a lightning environment can be made by using analysis, test, or a combination of both. Maximum confidence in the assessment is obtained by the coordinated use of both analysis and test (Ref. 3). In following the suggested approach as outlined in Ref. 3, if safety margins are found to be negative or inadequate as a result of the vulnerability assessment, then hardening measures are required. This paper identifies hardening measures or options that are available and can be implemented to achieve a hardened system - one that is adequately protected against the induced electromagnetic effects of lightning.

HARDENING APPROACHES

Four basic approaches can be used to harden aircraft and their electronic systems against lightning electromagnetic pulse (LEMP) effects. The suggested approaches are:

(1) Harden the external structure to prevent or greatly reduce the penetration of rf energy into the aircraft.

(2) Shield equipment and cables to prevent or greatly reduce the penetration of rf energy through the shielded enclosure.

(3) Harden electronic circuits to withstand the signals that do penetrate.

(4) Combine (1),(2), and/or (3) above.

HARDENING THE EXTERNAL STRUCTURE

Approach (1) has been applied to a number of aircraft to reduce induced electromagnetic transients. In hardening these aircraft, it was determined that it would be most cost-effective to begin by closing the points-of-entry (POEs) where fields or currents enter from the outside. Energy which is conducted inside on cables or which propagates through the holes or apertures in the structure can result in other currents being induced on cables inside. These currents can further propagate along the cables to critical or sensitive electronic systems where permanent damage or transient upset can result. Fast digital circuits are the most susceptible to upset.

To determine POEs, different tests were run on the aircraft. The first test involved a visual inspection and an rf "sniff test" in which an rf source was placed inside the aircraft and a detector was used outside the aircraft to detect points of leakage. Additional tests involved injecting currents onto the exterior of the fuselage and measuring cable currents inside as the various POEs were closed.

Important POEs that were found included cockpit windows, cables in various locations (e.g., wings, empennage, radome, nose wheel well), various doors (e.g., engine nacelle, personnel access, avionics bay, cargo loading), power return via structure, coaxial cable shield bonding, deicing lines, and mechanical shafts and control lines.

After important sources of rf coupling were found, various techniques were developed to close the POEs. Some of these were (Ref. 4):

(1) The use of fine wire mesh in cockpit and other windows.
(2) The use of rf gaskets and special corrosion protection techniques around doors and access covers.
(3) The use of filters on cables that go outside the fuselage.
(4) the use of improved bonding on coax shields, waveguide, hydraulic lines, pneumatic lines and some mechanical shafts.
(5) The use of ferrite cores around control lines and some mechanical shafts to absorb and reflect transients.
(6) The use of a separate wire return for the neutral on power lines rather than using the structure.
(7) The use of shielding on some exposed cables in the wings, wheel wells, empennage and under the nose radome.

Using various simulated closure techniques, the average transient current on all cables inside the fuselage was reduced about 20 dB below the unhardened condition.

Approach (1) is advantageous in that it uses the existing structure to protect a large number of electronic packages that would be expensive to modify to withstand large lightning-induced transients. If needed, filters, surge protection devices, coupling transformers and other hardening devices can be made smaller, lighter, and less expensive. However, closing the POEs adds some weight, particularly in the filter packages for cabling coming into the fuselage from the wings and empennage. Also, reliability and maintainability of hardening techniques have yet to be determined over the extended life of the aircraft.

Recently, studies of the degradation of some of these hardening techniques (e.g., filtering, cable shields and conductive gaskets) were reported (Ref. 5). The shielding effectiveness of double shielded cables was measured both before and after the cables were subjected to a series of bending, twisting, and stretching tests (500 bends, 500 rotations). The shielding effectiveness was found to degrade from an expected 60 dB to about 30 dB in some cases. Measurements on filter packs in systems subject to field environments showed that filters which had been expected to provide 50 dB of attenuation provided as little as 22 dB due principally to improper grounding or installation. Conductive gaskets were measured under varying pressures to predict EM degradation with age since they are known to take a set when compressed for a long period of time.

SHIELDING EQUIPMENT AND CABLES

Approach (2) was employed in shielding electronic system elements, known as Line Replaceable Units (LRUs), in the B-1 aircraft against the nuclear electromagnetic pulse (Ref. 6). As far as practicable, LRUs were grouped in a relatively few avionics bays which were designed and constructed to give 70 dB attenuation against the external NEMP environment over a specified frequency range. Within the bays, further shielding was not necessary. In the design and construction of the bays, special attention was given to joint fabrication, door seals, and to intrusion control. Electrical interconnections between bays were made principally by high permeability conduits. In high vibration areas, and for ease of manufacture, braided-shield cables were used extensively. Special care was exercised in shielding and terminating the cables. The remainder of the aircraft was protected by the basic structure of the aircraft which was conservatively considered to be 20 dB.

The following guidelines have been recommended when shielding all the cables and electronic packages within the aircraft (Ref. 7):

(1) Use a one-point circuitry ground.
(2) Separate all power leads.
(3) Balance power leads on all cable runs.
(4) Use the shielded twisted pair wiring concept on all lines except power lines.
(5) Build all power leads in separate bulk shielded cables.
(6) Build all other leads in bulk shielded cables.
(7) Use metallic enclosures for all electrical and electronic packages.
(8) Filter all leads entering or leaving high noise level packages. This includes motors, choppers, inverters, power relays, high power transistor switching circuits, etc.
(9) Filter all leads entering or leaving a transmitter package except the transmitter output coax.
(10) Use a filter/arc suppressor on all deliberate receiving antennas and on low power transmitters using semiconductor output devices. Filtering will be limited by pass band requirements, but the combined filter/arc suppression will, in general, handle the problem.

HARDENING ELECTRONIC CIRCUITS

Techniques which can be employed in Approach (3) to harden electronic circuits to withstand transients that penetrate the external structure and shielded equipment bays and cable runs include filtering, limiting, circuit design, and functional hardening. Each of these techniques is discussed below.

a. Filtering

A filter provides a reduction in power to a load of undesired signals while permitting desired signals to pass with little or no attenuation. The filter accomplishes this by discriminating against the frequency content of the undesired signals. However, if the interfering signal has high content in the desired (pass) band, the filter effectiveness is reduced.

A filter must meet some or all of the following requirements to be effective:

(1) Have extremely high or low input impedance relative to the source in the frequency rejection (stop) band.
(2) Have high loss to frequencies in the stop band.
(3) Have high dc current carrying capability without changing stop band characteristics.
(4) Prevent cross coupling.
(5) Prevent arcing across its elements.
(6) Have low dc resistance (primarily power line consideration).
(7) Have high reliability.

A wide range of filter types are available for lightning electromagnetic pulse (LEMP) hardening. These include:

(1) Discrete R, L, C filters
(2) Ferrite filters
(3) Filter pin connectors
(4) Coaxial filters
(5) Electromechanical filters
(6) Active filters

Passive discrete filters use combinations of discrete R, L, and C components. They permit implementation of any of the functional filter characteristics (i.e., high pass, low pass, bandpass, and band reject). With careful attention to component selection, they can be designed for use at frequencies up to 100 MHz.

The ferrite filter is a special category of discrete passive filters. This filter achieves a frequency dependent resistive insertion loss by using a dissipative filter at the high frequencies in the stop band while avoiding the low frequency (pass band) dissipation associated with the other discrete passive dissipative filter, the RC filter.

Filter pin connectors are passive and use the coaxial shell of cable connectors as a capacitor plate along with added series inductance to obtain a network filter. They are low pass filters and provide cut off frequencies above 10 kHz.

Coaxial filters are distributive passive filters that utilize short sections of high impedance or low impedance transmission line to simulate series inductance and shunt capacitance, respectively.

Monolithic crystal and ceramic filters and mechanical filters are categorized as electromechanical filters. Crystal and ceramic filters use the piezoelectric effect to transform electrical energy to mechanical energy and then use the mechanical resonance properties of the crystal or ceramic to achieve frequency selectivity. Mechanical filters use a mechanical resonator with electromechanical transducers at the input and output to achieve electrical filter proper-

AD-A065 410 FEDERAL AVIATION ADMINISTRATION WASHINGTON D C SYSTE--ETC F/G 4/1
FEDERAL AVIATION ADMINISTRATION - FLORIDA INSTITUTE OF TECHNOLO--ETC(U)
MAR 79

UNCLASSIFIED FAA-RD-79-6 NL

2 OF 2
AD
A065410

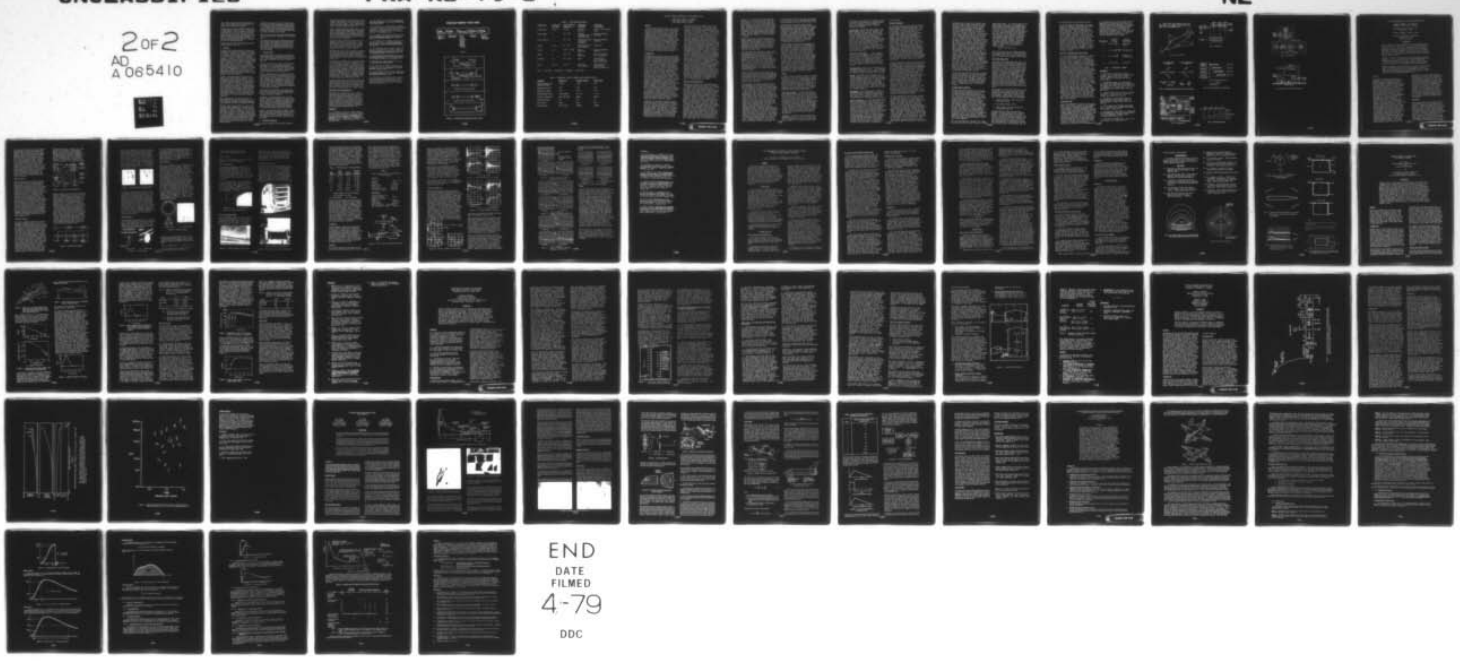

END
DATE
FILMED
4-79
DDC

ties. These filters are basically bandpass circuits, but low and high pass functions can be achieved by adding passive elements.

Active filters, while not generally applicable to LEMP protection, may be useful in some specific applications. Active filters are hybrid devices that use one of four basically different active circuits or devices in conjunction with passive frequency discrimination elements. The four circuits include the negative impedance converter, the operational amplifier, the gyrator, and the phase-locked loop.

Filter types and their characteristics are summarized in Table 1 (Ref. 8).

b. Limiting

Limiting is an effective method to reduce coupled energy from getting into sensitive electronic circuits. Limiting (or clamping) is achieved by using special suppression devices which are of two basic types - "crowbar" and "constant voltage." "Crowbar" devices are those which, on sensing an overvoltage, switch to a low impedance state and thus cause the impressed voltage across them to collapse to a low value. "Constant voltage" devices are those which, on sensing an overvoltage, tend by virtue of their nonlinear current-voltage relation to maintain their voltage at a predetermined level and do not collapse the voltage. Examples of the first type are spark gaps and gas filled surge arrestors. Examples of the second type are Zeners and silicon avalance diodes and varistors.

Crowbar or switching devices inherently offer greater surge power handling capability than do the Zener or varistor type of devices. The instantaneous power dissipated in a suppressor device is a product of the surge current through the device and the voltage across the device. For a constant surge current, a switching device like a spark gap which has low voltage across it when conducting will dissipate less power than a device such as a Zener diode which retains a high voltage across it. Thus, a spark gap will be physically smaller than a Zener diode or varistor device for a given surge power handling capability.

Major disadvantages of switching devices are their inability to clamp surge voltages to a low level and their tendency to continue conduction once started on dc lines of significant voltage.

The metal oxide varistor (MOV) is a "soft" limiter whose shunt resistance is inversely proportional to the applied voltage. No critical voltage level of surge is required to activate this protection device as it is always in the circuit as a path to ground. As the surge voltage rises, the varistor lowers its resistance thus providing a low shunt impedance in parallel with the device being protected. A major disadvantage of this type of device on some circuits is its loading effect on the circuit during periods of steady state operation.

Semiconductor devices such as the Zener diode and silicon junction suppressor have the ability to provide protection on voltage limiting down to low voltage levels necessary to protect integrated circuits and other semiconductor devices. Their major drawback is their limited capability to handle significant surge energy.

Table 2 lists several of the basic surge protection devices and their advantages and limitations (Ref. 9).

Hybrid protection using both spark gaps and silicon avalanche suppressors have been developed for optimizing the capabilities of both of the device types. The spark gap contributes the high current surge capability while the silicon component responds to the fast rise time wave front components.

c. Circuit Design

An important means of controlling lightning-related interference is through proper circuit design. Basic considerations about circuit design and signal transmission are shown in Figure 2 (Ref. 2).

As shown in Figure 2(a), signal circuits should avoid the use of the aircraft structure as a return path. If the structure is used as a return path, resistively and inductively generated voltage drops will be included in the path between transmitting and receiving devices.

Signal transmission over a twisted pair circuit as shown in Figure 2(b) with signal grounds isolated from the aircraft structure tends to couple lower voltages in the signal path. However, the use of twisted pair transmission lines does not eliminate the common mode voltage to which electronic systems may be subjected. Common mode voltages applied to the unbalanced transmission path can lead to line-to-line voltages comparable to the common mode voltage.

For differential transmission and reception devices shown in Figure 2(c), a many-fold improvement can be achieved in rejecting common mode voltages produced by lightning.

In general, it is good practice not to interconnect two different pieces of electronic equipment at semiconductor junctions as shown in Figure 2(a) and 2(c). Resistance inserted between the junction and the interconnecting wires as shown in Figure 2(d) can dissipate transient energy and effectively protect semiconductors from lightning induced voltages and currents.

Finally, interconnection through balanced transmission lines and transformers as shown in Figure 2(e) in conjunction with input protection for semiconductors probably provides maximum protection against unwanted transients induced on signal wiring.

d. Functional Hardening

Functional hardening is particularly important

in protecting digital circuits which have broad bandpass characteristics and which are most susceptible to system upset. From a system standpoint, functional hardening can be pursued using several different approaches (Ref. 10).

Use of a higher operating voltage level for digital circuits probably obtains more protection than is possible by any other means. If digital data are transmitted over a cabling system at 10 volts, for example, a 60 dB advantage results from a protection standpoint than if a 10 millivolt drive level were chosen.

Coding and signal processing techniques can be employed to minimize the possibility of operational upset. Some of the techniques include error detection and correction codes, repeated data, parity checks, closed loop information transfer, and detection reject circuits.

Hard memories can be used as temporary storage in critical applications where long computational processes are required to generate needed data. This technique can obviate complete recycling of computer programs should some form of operational upset occur.

Circumvention techniques can be used when hardening requirements are physically difficult to apply. For a specific threat, circumvention involves detecting the event and using this information to blank or reset a computational process. For non-specific threats, a duty cycle technique is used whereby information is accepted only during small increments of time so that the probability of a lightning event, for example, happening during this time period is negligible or extremely small. Event sensors can also be used to reset systems or initiate master resets.

The use of fiber optics in signal circuits offers the possibility of practically eliminating electromagnetic interference and transient pulse effects. However, fiber optics is presently limited to signal circuits and will not affect the problem of transients induced via power circuits.

CONCLUSIONS AND RECOMMENDATIONS

This paper has touched briefly upon a number of approaches and techniques that have proved effective in protecting aircraft electronic circuits from induced electromagnetic transients. To be most effective, a systems approach is required to insure that no one system is either overly hardened or underprotected. With proper analysis and testing, a balance of hardening options can be chosen and applied to achieve an optimum hardened configuration (Ref. 11).

REFERENCES

1. J.C. Corbin, Jr. and D.F. Strawe, "Electromagnetic Coupling Analysis of a Learjet Aircraft in a Lightning Environment," Proceedings of the IEEE 1978 National Aerospace and Electronics Conference, Vol. 2, 78CH1336-7; Air Force Flight Dynamics Laboratory Technical Report 78-121, September 1978.

2. J.A. Fisher and J.A. Plumer, Lightning Protection of Aircraft, NASA Reference Publication 1008, October 1977.

3. J.C. Corbin, Jr., "Vulnerability Assessment of Aircraft Systems to Indirect Lightning Effects," Conference on Certification of Aircraft for Lightning and Atmospheric Electricity Hazards, Paper No. 21, September 1978.

4. G.E. Morgan, "EMP Aircraft Hardening," 1975 IEEE Electromagnetic Compatibility Symposium Record, IEEE 75CH1002-5 EMC.

5. G.L. Maxam and J.E. Solberg, "Degradation of EMP Hardening Devices," DNA EMP Environments and Protection Implementation Seminar Abstract, October 1977.

6. J.M. Oberholtzer and N. Thomas, "EMP Shielding and Zoning Practices on the B-1 Aircraft," DNA EMP Environments and Protection Implementation Seminar Abstract, October 1977.

7. Electromagnetic Pulse Handbook for Missiles and Aircraft in Flight, Air Force Weapons Laboratory Technical Report 73-68, September 1972.

8. EMP Electronic Design Handbook, Air Force Weapons Laboratory, April 1973.

9. W.C. Hart and E.W. Malone, "Lightning and Lightning Protection," Interference Technology Engineers' Master (ITEM), 1976.

10. R.J. Haislmaier and T.A. Martin, EMP Protection Engineering Study, Final Report, Naval Surface Weapons Center, July 1977.

11. D.L. Suiter, R.D. Gadbois, and R.L. Blount, "Space Shuttle Lightning Protection," Federal Aviation Administration/Florida Institute of Technology Workshop on Grounding and Lightning Technology, March 1979.

COUPLED ENERGY FLOW PATH

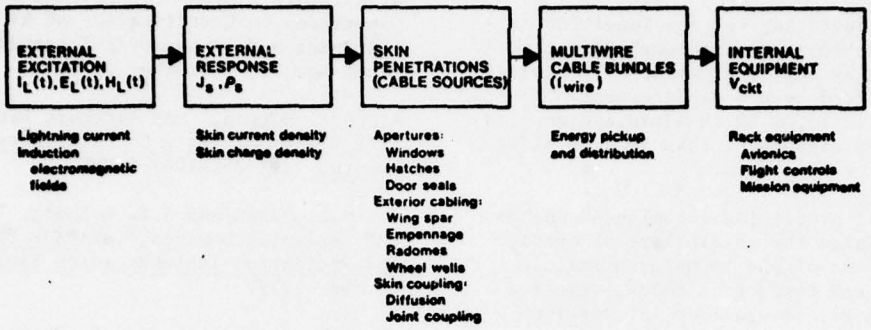

FIGURE 1

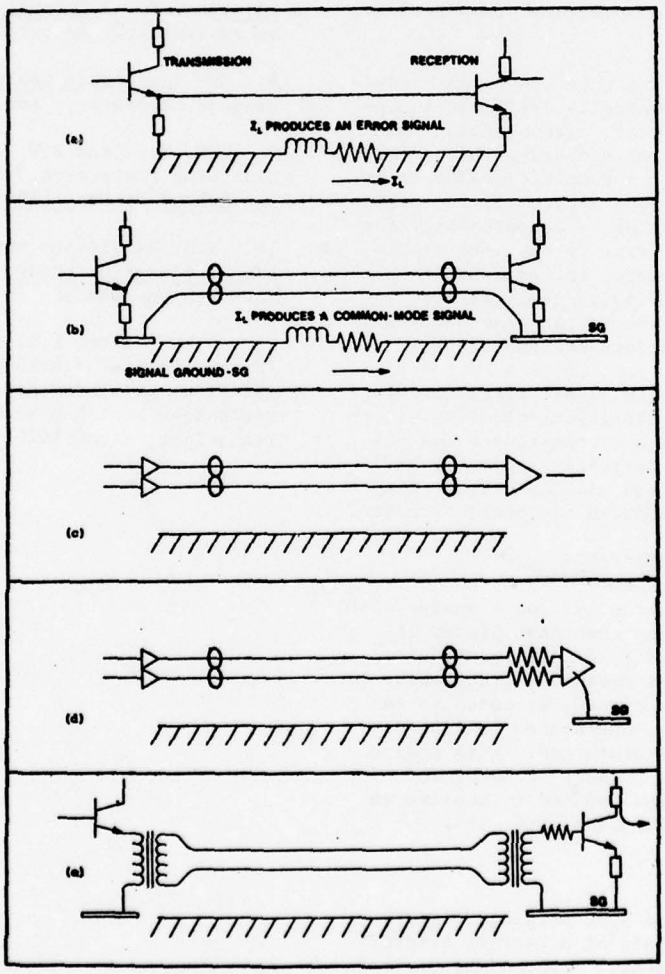

FIGURE 2 - CONSIDERATIONS REGARDING CIRCUIT DESIGN

TABLE 1 - FILTER COMPARISON MATRIX

FILTER CLASS	FILTER TYPE (See Code)	USEFUL FREQUENCY RANGE (Hz)	SIGNIFICANT ADVANTAGES	SIGNIFICANT DISADVANTAGES
Discrete R,L,C	1,2,3,4	To 10^8	Versatile Low cost	Large for low frequency Low Q
Ferrite Beads	1	10^6 - 10^8	Versatile Dissipative with low pass band loss	Spurious resonances Saturation
Filter Connector	1	10^4 - 10^9	Design integration simplicity Dissipative	Spurious resonances Saturation
Coaxial	1,2,3,4	10^7 - 10^9	High frequency use Low Parasitics	Large size
Crystal	3,4	$5x10^6$ - $1.5x10^8$	High Q Small size	Spurious resonances High cost
Ceramic	3	10^5 - 10^7	High Q Small size	Spurious resonances Not IC compatible
Mechanical	3,4	10^3 - $2x10^4$	High Q	Limited range Not IC compatible High insertion loss
Active	1,2,3,4	To 10^5	Small size Gain provision	Power requirement Limited range Damage susceptibility

Code: 1 - low pass; 2 - high pass; 3 - bandpass; 4 - band reject

TABLE 2 - COMPARATIVE VALUES OF SEVERAL SURGE PROTECTION DEVICES

PARAMETER	SPARK GAPS	VARISTOR DEVICES	ZENER DIODES
Typical surge current capability (Amps)	10,000	1,000	500
Response time (sec)	10^{-8}	10^{-8}	10^{-9}
Capacitance (farad)	10^{-12}	10^{-10}	10^{-10}
Voltage range (volts)	90 and higher	40 - 700	2 - 300
Insulation resistance	High (10^9 ohms)	Medium	Medium
Bipolar operation	Yes	Yes	No
Failure mode	Short	Short	Short
Activated state	Short circuit	Clamped	Clamped

INFLIGHT LIGHTNING CHARACTERISTICS MEASUREMENT SYSTEM

F.L. Pitts, M.E. Thomas, R.E. Campbell,
R.M. Thomas, and K.P. Zaepfel
NASA Langley Research Center

ABSTRACT

A research data-gathering system being developed for inflight measurement of direct and nearby lightning strike characteristics is described. Wideband analog recorders used to record the lightning scenario are supplemented with high-sample-rate digital transient recorders with augmented memory capacity for increased time resolution of specific times of interest. The endless-loop data storage technique employed by the transient recorders circumvents problems associated with oscilloscopic techniques and allows unattended operation. System integrity and immunity from induced effects is accomplished by fiber-optics signal-transmission links, shielded system enclosures, and the use of a dynamotor for power system isolation.

INTRODUCTION

The NASA Langley Research Center is undertaking development of experimental equipment and techniques for inflight measurement of the lightning-generated electromagnetic environment affecting aircraft. The motivation for this development activity is based on inadequate lightning-hazard definition as related to the projected use of digital avionic systems and composite structures in future aircraft. These two technology applications compound lightning related problems in that, on the one hand, digital avionic systems can be "upset" by electrical transients, while on the other hand, composite structures may not provide the Faraday shield and protection provided by metal aircraft. The notion of "upset," as applied to digital systems, concerns the potentiality for a digital system process to be perturbed (without permanent damage) by an electrical transient, and thus not correctly perform the intended function until reset, reloaded, or re-initiated. This malfunction differentiates digital-system susceptibility from analog-system susceptibility wherein an electrical transient may only be manifest as a momentary "glitch" in system function. Advanced digital systems will employ various approaches to system redundancy to achieve protection against classical random failure modes; lightning induced transients, however, could conceivably "upset" the entire system.

Fundamental to the design of advanced digital system architectures (and protection schemes) for flight critical applications is the requirement for a comprehensive definition of the lightning hazard. Two programs[1, 2] have been conducted to obtain inflight data on lightning characteristics. These activities have been hampered by instrumentation problems germane to oscilloscope technology. These problems are characterized by the nature of oscilloscope triggering which can result in loss of data occurring prior to the trigger, and in time resolution limitations of 1/100 of the sweep time for systems employing conventional oscilloscopes[1] and 1/500 for systems employing state-of-the-art scan converter tubes[2]. A full lightning scenario consists of a number of events such as leader activities, multiple strikes, etc., lasting over several seconds, and does not lend itself to characterization using the aforementioned technique. The intent of the instrumentation system development described herein is to employ state-of-the-art digital and analog data-acquisition technologies to obtain inflight data on the full lightning-hazard scenario. The wide bandwidth and transient nature of lightning phenomena, coupled with the resulting harsh electromagnetic environment, create a formidable instrumentation problem. A number of factors provide a framework for synthesis of an instrumentation system design for inflight measurement of direct and nearby lightning-strike characteristics. Published lightning data indicates that frequencies of lightning electromagnetic phenomena range from near 0 to several gigahertz. The state-of-the-art for instrumentation is not such as to allow continuous time-domain recording of data over the total bandwidth; it is known, however, that there is an inverse dependence of amplitude with frequency[3] which weights the frequency response importance (as concerns the hazard problem) toward the lower portion of the spectrum. It is anticipated that correlation of the flight data obtained over the system design bandwidth of 100 MHz with the existing statistically significant body of ground-based data will provide information of fundamental importance to lightning protection needs[4].

GENERAL SYSTEM DESCRIPTION

Among the key elements which characterize the instrumentation system described are utilization of "endless loop" digital transient data recorders and state-of-the-art wideband analog tape recorders. The "endless loop" digital transient data recording concept involves a fast, parallel analog-to-digital converter along with an interleaved solid-state memory to accomplish high-speed data storage in a memory that is continually refreshed. Upon occurence of an event to be permanently stored, a trigger is generated, the memory is "frozen," and the data are read into a slower recording medium. Trigger criteria for the digital transient recorders are significant considerations. The trigger scheme to be employed will most likely be based on peak values; other approaches such as output from AM receivers operating at various frequencies have been considered, but the exact scheme will of necessity evolve during flight tests. Off-the-shelf transient recorders are available with up to 500-MHz sample rates (100-MHz input analog bandwidth), six-bit resolution, and 1 024 word memories. At the fastest sample rate, a time domain recording

of about 2 μs can be made with these off-the-shelf units. In order to provide a much wider data window, the transient recorder memory is being expanded in an in-house development effort to 131 072 data words, which will allow a time domain recording of 262 μs at the fastest sample rate. The sample rate can be varied in fixed increments so that much longer data windows may be obtained with correspondingly lower sample rates. The data readout to the slower recorder (50 000 bits per second) will require around 10 seconds.

Wideband analog tape recorders with data frequency response from near 0 to 15-Mhz and data record time for two channels of 24 minutes are available. These recorders will be used to record the full lightning scenario and will be augmented by the digital transient recorders for increased time resolution of portions of the total lightning event.

With the exception of the static electric field measurements, sensors selected for the lightning measurement tasks are passive analog devices which were designed for use by the Nuclear EMP community.[5] The sensors were designed to have a simple relationship between sensitivity and geometry over a broad frequency band. Table 1 lists the measurement requirements and sensors selected for the primary lightning measurements. The amplitude ranges are based on electric field change of 10^6 V/m (near breakdown) in 0.1 μs and on a peak stroke current of 20 kA.

Figure 1 shows the sensor locations for the airborne lightning measurement system employing four D-dot ($\dot{D}$) sensors near aircraft extremities, eight B-dot ($\dot{B}$) sensors arranged in symmetrical pairings about the aircraft fuselage and wings, one I-dot ($\dot{I}$) sensor and three orthogonal $\dot{B}$ sensors on the nose boom.

Electromagnetic interaction with the aircraft was considered for incident radiation with a half-wavelength on the order of fuselage length. For this condition, currents flow on the surface of the aircraft in a manner which is described as the "first symmetric mode"[6] and the "first antisymmetric mode," as shown in Figure 2. An examination of the scattered fields (magnetic fields resulting from the current distributions) shows that the field is minimum along the centerline of the aircraft. This is due to the symmetry of the field around the fuselage and cancellation of the opposite fields about the wings for the symmetric mode. Vertical components of the scattered field are present, however, along the centerline for the antisymmetric mode. Therefore, measurements of undisturbed incident fields are made with sensors located on a nose boom aligned with the aircraft centerline and sensitive axes in the longitudinal and lateral directions only. For incident radiation of shorter wavelengths, current modes can be excited in the vertical tail which will disturb the measurements made in the lateral axis. Therefore, alignment of the sensitive axis of the sensor with the longitudinal axis of the aircraft is the optimum sensor orientation to minimize disturbance to the measurement caused by electromagnetic interaction with the aircraft.

Instrumentation-system isolation to protect against spurious responses (responses other than those generated by calibrated inputs) is obtained by employing fiber-optic data links for signal transmission and a dynamotor for power-system isolation. Sensor data are transmitted to the shielded instrumentation-system enclosure using battery-powered optical transmitters operating into fiber-optic transmission lines. In this manner, only modulated optical signals and mechanical power is input to the shielded instrumentation system enclosure.

A block diagram of the overall instrumentation system is shown in Figure 3. Most elements of the system have been previously discussed; the data flow is as follows: All sensor signals are input to the shielded system enclosure via fiber-optic data links. Each signal is then routed to a peak detector which continually monitors the signal and stores the peak values on a magnetic tape recorder. The sensor signals are also routed to the wideband analog recorder, to the transient recorders, and to the trigger control system. The output of the transient recorders are recorded in digital form on the magnetic tape recorder for permanent data storage. The television and film cameras (with wide-angle lenses) will provide information on the details of lightning attachment to aid in data analysis. Specific details of fundamental subsystem components are described below.

SENSORS

The sensors have been chosen to permit a thorough description of the lightning phenomena as experienced by an aircraft. Electromagnetic sensors measure the fields and currents caused by direct or nearby lightning strikes over a wide frequency range, while a group of secondary sensors help in locating the lightning channel with respect to, or on, the aircraft. The following paragraphs give brief descriptions and applications of these sensors in the system.

Flush Plate Antenna. The flush plate antennas, also known as D-dot sensors, will be mounted at the extremities of the aircraft, such as on the bottom of the nose, on the tops of the wing tips, and on the bottom of the tail, to obtain electric field data from direct and nearby strikes. Although they have a very wide frequency response, D-dot sensors respond to time rate of change of the electric flux density and not to the static field. Therefore, the data must be integrated to obtain the electric field intensity. However, if these sensors are in corona, they will also measure the normal conduction current density caused by the corona in addition to electric flux density.

Field Mill. Because the D-dot sensors do not respond to the static E-field, four field mills will be mounted on the aircraft to measure the three components of the ambient electric field,

the charge on the aircraft, and the total change in the static field caused by a lightning event. They will be located so that the effects of corona and precipitation static discharge currents are minimized.

Loop Antenna. The multigap loop antennas, also known as B-dot sensors, will be mounted on the wings, fuselage, and nose boom. Those on the wings and the fuselage will measure the circumferential fields about these sections of the aircraft resulting from direct and nearby strikes. The loop antenna on the nose boom with sensitive axis in the longitudinal direction will measure the fields from nearby strikes without being greatly disturbed by the aircraft. Although they have a wide frequency range, the loop antennas are designed to respond to time rate of change of the magnetic flux density, and the data must be integrated to obtain the magnetic field intensity.

Inductive Current Probe. This inductive sensor (I) will be mounted on the nose boom so that the total attachment current to the boom can be measured. The sensor is a hollow conductive ring, with a gap around the inside perimeter, which fits around the outside of the boom. The output is measured across the gap. The sensor output must be integrated to obtain current.

Resistive Shunt. This total current sensor is a complement to the above sensor. Its advantage is frequency response to 0; the output is a voltage generated across an internal resistive shunt.

Cameras. Both video and film cameras, with a variety of lenses to visually cover the aircraft and surrounding airspace, will be used to analyze lightning phenomena and to aid in locating lightning on, or near, the aircraft. Video tape systems with more lines per frame and higher frame rates than standard television are available for better resolution. Photographic cameras will be single-frame, 35-mm types with motorized film advance mechanisms.

Microphones. Visual observations of lightning from aircraft have often produced inaccurate distance estimates. Therefore, thunder (shockwave) data will be recorded to determine the distance between the lightning and the aircraft.

Sensor Calibration. The field measurement sensors will be calibrated apart from the aircraft in a laboratory environment. Then in order to calibrate out field distorting effects of the aircraft, the sensors will be check-calibrated while mounted in the aircraft. For a dc calibration of the field mills, a close-proximity plate charged by a high-voltage generator will be placed over the field mill rotor. The total current sensor will be calibrated by using a high current generator, such as an impulse generator or a Marx generator, applying a known waveform directly into the nose boom of the aircraft. Internal wire sensors will be calibrated by replacing them in each measuring channel with current or voltage sources, as appropriate to each channel.

TRANSIENT RECORDERS

The transient recorders to be used are modified Biomation Model 6500 Waveform Recorders. The Biomation 6500 is a fast analog-to-digital converter (ADC) with internal storage for 1 024 six-bit words. At the fastest rate, the Biomation 6500 samples an analog signal every 2 ns and has an input analog bandwidth of 100 MHz. The recorders are operated in an "endless loop" mode, wherein the recorder continuously samples and stores data until a trigger event occurs which causes the record phase to end. The recorded data is then output to an analog recorder at a slower rate for storage. Once the memory has been read out, it returns to the record phase to await the next trigger event. The data-record time window can be adjusted relative to the occurrence of the trigger event by delaying the cessation of the recording. This feature allows an adjustable data window from just before the trigger event up to 10 000 sample times after the trigger event via front panel switches (e.g., at a 2-ns sample interval time, the data window can be delayed up to 2 μs).

The memory modification was undertaken to provide a significantly longer data record at the maximum sampling rate. In particular, an expansion from 1 024 samples to better than 100 000 samples was desired without compromising the capability for 500 million samples per second. A review of available memory integrated circuits (IC's) resulted in selection of the INTEL 2147-3. It is an N-channel silicon-gate MOS technology random access memory (RAM) organized as 4096 x 1 bit with a write cycle time of 55-ns. As a comparison the standard memory utilizes an emitter coupled logic (ECL) RAM organized as 128 x 1 bit with a write cycle time of 10-ns. The major characteristics of the modified recorder are storage for 131 072 samples as compared to 1 024; increase of memory IC's from 48 to 192; and provision for delaying the trigger by up to 100 000 interval times. The modified recorder can capture a 262-μs "snapshot" at the maximum sample rate compared to a 2-μs snapshot for the standard recorder.

The major components of the transient recorder are indicated in Figure 4. The signal to be recorded is presented to the input attenuators and amplifier, digitized, and then stored in the memory. The trigger and control circuitry controls and selects the data period to be retained. Once a snapshot has been obtained, it is output for recording on the analog recorder. The Biomation 6500 recorder achieves its high sampling rate by employing a parallel ADC technique. The output of the ADC is converted to a six-bit gray code. At the maximum sampling rate, a new data sample is taken every 2 ns. In order to provide more time for the storage of the data, the ADC output is double buffered into two six-bit registers on an alternating basis. Thus, each of these registers has new data every 4 ns. The output of these two registers is presented to

the memory board on two six-bit parallel buses. Through the use of memory interleaving, the effective speed of a memory can be increased. The memory is divided into sections and the write cycles are overlapped. For example, consider a memory divided into four sections, each section having a write-cycle time of 4 time units, as shown in Figure 5. A time period 4 time units long is equally divided into four parts. Memory section 1 begins a write cycle at time 0. Memory section 2 begins a write cycle at time 1, etc. All write operations are performed in this sequence. Each memory section has 4 time units to complete a write cycle, but the effective write cycle of the four-section memory is equivalent to 1 time unit. The storage is organized as an eight-way interleaved memory in the standard Biomation 6500; the modified memory is organized as a 32-way interleaved memory. The data is routed to the 32-section memory via three stages of temporary storage. The two registers that sample the ADC output change data at a 4-ns rate and each of these registers then feed four more registers sequentially. These registers are updated at a 16-ns rate. Finally, each of these registers then feeds four more registers, which are updated at a 64-ns rate. The 64-ns data period provides sufficient margin for the 55-ns write cycle memory IC's to allow for delays in the circuits. Each of the memory sections is organized as 4 096 six-bit samples; thus 6 of the 2147-3 IC's are required for each memory section.

The addressing and control section of the memory consists of two parts. One part selects memory sections and the other part generates 12-bit addresses (12-bits are required to address the 4 096 word sections). The memory section selection is accomplished by decoding a high-speed parallel counter and the 12-bit address generation is accomplished using a 12-bit binary counter.

WIDEBAND ANALOG RECORDING

Wideband analog data recording will be accomplished using an instrumentation tape recorder that employs video recording techniques originally developed for television broadcast use. Using rotary magnetic heads with a head-to-tape speed of 3 120 inches per second (twice standard television), wideband FM signal-processing electronics, and improved magnetic-head efficiency, the recorder will provide simultaneous recording or playback of two wideband (15-MHz) channels and two auxiliary (audio and digital) channels for a total time of 24 minutes. Development is currently underway to extend this record time to approximately 30 minutes by using newer, more efficient heads and magnetic tapes. The initial instrumentation system will use a similar recorder, the RCA ADVISER-62 (airborne dual-channel variable-input severe environment recorder/reproducer), which has a 6 MHz bandwidth.

The video instrumentation recorder has a signal-to-noise (S/N) ratio of about 30 dB and a limited input dynamic range. It is anticipated that the dynamic range of the data to be recorded will exceed 60 dB, necessitating logarithmic dynamic range compression in the signal-conditioning circuitry. Since the compressed signals must serve both the wideband analog tape recorder and the fast transient recorders, the logarithmic amplifiers must have a bandwidth of 100 MHz. This bandwidth, coupled with the large dynamic range needed, requires the use of a pseudo-logarithmic amplifier[7] having a nearly, but not true, logarithmic response. The pseudo-logarithmic response can be realized by summing cascaded linear-limiting amplifier stages, as shown in the block diagram of Figure 6, where

$$e_{out} \simeq k_1 \log \left(k_2 \ e_{in} \right)$$

The initial system will use integrated-circuit psuedo-logarithmic amplifiers (Texas Instruments Part Number TL 441) that have a maximum bandwidth of 40 MHz and input dynamic range of 80 dB.

FIBER-OPTIC DATA LINKS

The purpose of the fiber-optic data links is to obtain noise-free transmission of wideband data signals from the various remote sensors to the data-recording system. The link consists of a transmitter, a fiber-optic cable, and a receiver. The transmitter converts the electrical sensor signals to an optical signal by modulating the output of a light-emitting diode (LED). The receiver, consisting of a photodiode, a trans-impedance amplifier, and an amplifier/buffer, converts the light signal to an appropriate electrical signal for data recording. The optical fiber consists of a core of transparent dielectric material surrounded by a cladding material of lower refractive index. An optical cable may contain many such optical fibers to improve the optical coupling from the LED to the cable.

The advantages of fiber-optic data links in this application are the total electrical isolation and superior EMI resistance provided by the optical cable. Along with the usual aircraft environmental considerations, the fiber-optic data link must meet the following requirements:

- Frequency Response: near 0 to 100 MHZ (rise time ≤ 3.5 ns)
- Input Dynamic Range: >60 dB
- Output Signal: 0.2V peak-to-peak min. to 2V peak-to-peak max.

Wideband fiber-optic data links have been designed[8] and one of them operates at 160 MHz. However, its data bandwidth is only 20 MHz. Moreover, the state-of-the-art in optical fiber links is such that for a 100-MHz bandwidth, the attainable signal-to-noise ratio is less than the expected 60-dB data signal dynamic range. Other considerations in the design of this data link are the LED type, the photodiode type, the

the optical couplers, and the optical cable.

To solve the dynamic range problem, the signal compression circuitry (logarithmic amplifiers) required for the analog tape-recording process will be incorporated into the fiber-optic transmitter. LED's and photodiodes are available with rise times on the order of 2 ns and the length of the optical cable (≤20 m) simplifies fiber selection. The primary problems are design of the LED drive circuitry and the receiver circuitry so that they meet the bandwidth requirement, provide the required stability, and maintain the electrical isolation between the fiber-optic transmitters and the rest of the data system. The latter will be accomplished using plug-in rechargeable battery packs for the transmitter assemblies. A block diagram of the complete fiber-optic data link is shown in Figure 7.

SHIELDING, ISOLATION, AND POWER SYSTEM

The lightning measurement equipment must operate in a harsh electromagnetic environment, and because of the low-level circuits employed in the data system, it is subject to interference caused by the electromagnetic environment (EMI). Therefore, system integrity is accomplished by protection with shielding which is more effective than that provided by a metallic aircraft, and by electrical isolation from EMI sources. A system constraint resulting from the EMI protection design requires that the measurement system (excluding sensors) be enclosed by a Faraday shield. The shield is a double-walled enclosure with the outer wall grounded to the aircraft structure in several places and the inner wall electrically insulated from the outer, allowing a one-point ground as shown schematically in Figure 8. The outer wall is capable of conducting the currents which will flow in the aircraft structure as a result of a direct strike. Fiber-optic data links are used to transmit sensor signals into the enclosure, thus eliminating electrical conduction paths which might carry interference signals to the data system. System power will be coupled into the enclosure either mechanically or hydraulically. The apertures in the Faraday shield for the fiber-optics and the mechanical power system can be kept very small, thus maintaining the shielding effectiveness of the enclosure.

STATUS AND PLANS

An initial developmental flight activity using a NASA F-106 aircraft is planned for the summer of 1979 to prove and demonstrate the measurement system concept. The sensor complement will utilize existing nuclear EMP designs which adequately meet lightning measurement requirements. The augmented memory design for the transient recorder is complete and testing is at the breadboard stage; circuit techniques to allow operation at the 500-MHz sample rate have been demonstrated. Laboratory operation of the logarithmic amplifiers and fiber optic data link has been demonstrated up to 40-MHz and development is continuing to achieve the full 100-MHz bandwidth. It is planned that the initial flight test will employ two of the transient recorders and one wideband (6-MHz) analog recorder. Future plans include acquisition of 15-MHz analog recorders and investigation of wider bandwidth analog recording technologies. Also planned are completion of development, and flight tests over instrumented lightning ranges, of a system capable of simultaneous acquisition of eight 100-MHz transient recorder channels.

Measurement	Amplitude Range	Sensor Description
$\dot{D}$	0.01 to 10 $\frac{A}{m^2}$	Flush Plate Dipole
$\dot{B}$	10 to 10 000 $\frac{tesla}{s}$	Multigap Loop
$\dot{I}$	0.1 to 100 $\frac{kA}{\mu s}$	Inductive Current Probe
E	10^2 to 10^6 $\frac{V}{m}$	Field Mill

TABLE 1. MEASUREMENTS SUMMARY

REFERENCES

1. Measurements of Lightning Strikes to Aircraft. B.J. Peterson and W.R. Wood, Sandia Laboratory Report SC-M-67-549, (DS-68-1). Sandia Laboratory, Albuquerque, New Mexico. January 1968.

2. Airborne Measurement of Electromagnetic Environment Near Thunderstorm Cells (TRIP-76). SRI Project 5536 (under NASA Contract NAS9-15101). J.E. Nanevicz, R.C. Adamo, and R.T. Bly, Jr., Stanford Research Institute, Menlo Park, CA; March 1977.

3. A Ground Lightning Environment for Engineering Usage. N. Cianos and E.T. Pierce, SRI Project 1834, August 1972, Page 103.

4. Proceedings: Second Annual Workshop on Meteorological and Environmental Inputs to Aviation Systems. NASA CP-2057, March 1978, Page 211.

5. IEEE Transactions on Antennas and Propagation. C.E. Baum, et al, January 1978, Volume AP-26, Number 1, Pages 22-35.

6. EMP Interaction Note Number 63, "Interaction of Electromagnetic Fields With an Object Which has an Electromagnetic Symmetry Plane". C.E. Baum, AWFL, March 3, 1971.

7. Logarithmic Video Amplifiers. R.S. Hughes, Artech House, Inc., Dedham, MA, 1971.

8. Flight Operational Wideband Fiber Optic Data Links. L.L. Stewart, Spectronics, Inc., AFAL-TR-77-54, November 1977.

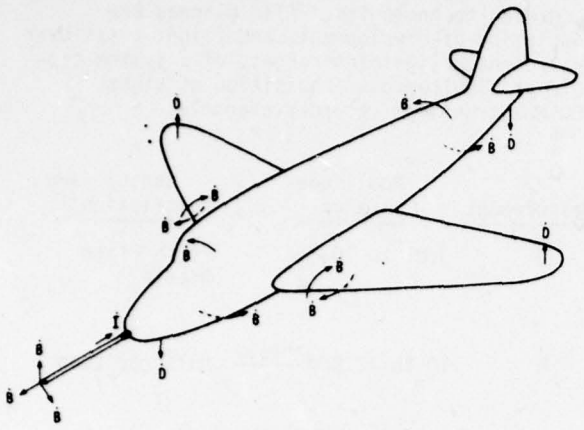

Figure 1. - Primary sensor locations.

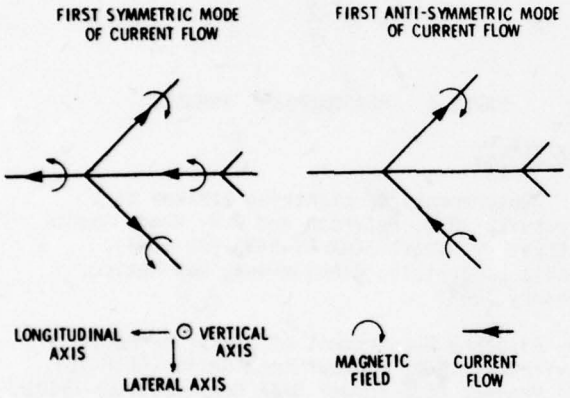

Figure 2. - Scattered magnetic fields resulting from modal current distributions.

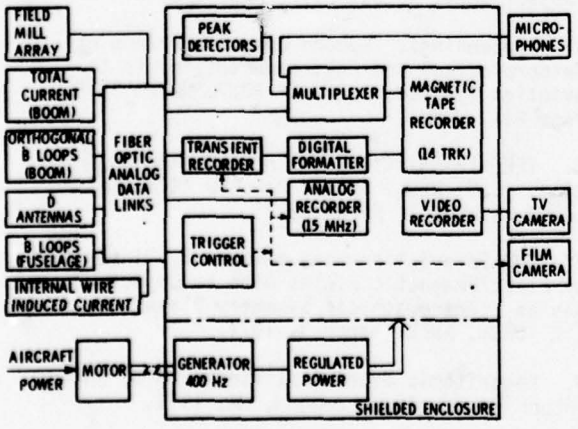

Figure 3. - Instrumentation system.

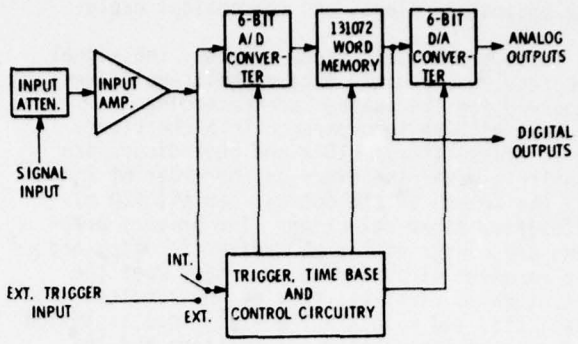

Figure 4. - Transient recorder.

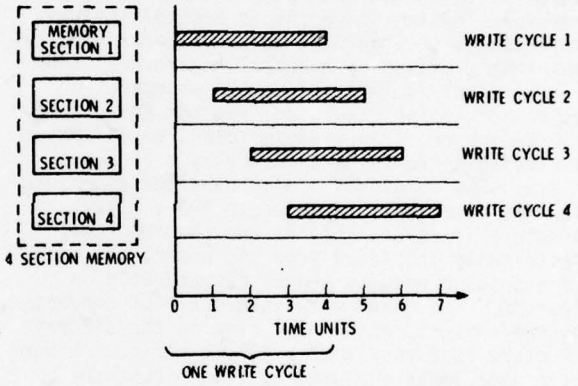

Figure 5. - Write cycle overlapping for a four-section memory.

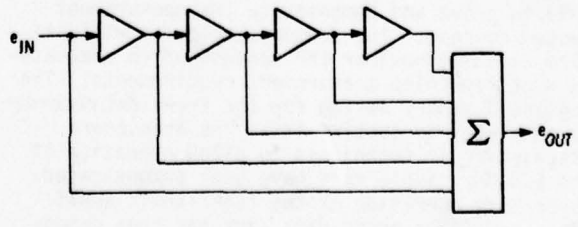

Figure 6. - Pseudo logarithmic amplifier.

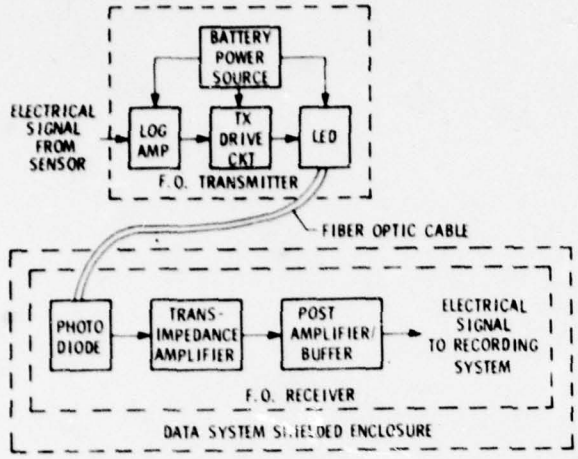

Figure 7. - Fiber optic data link.

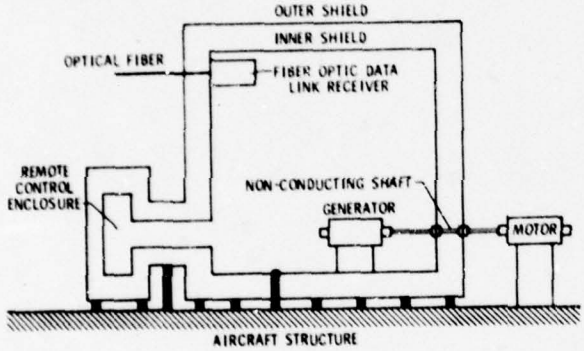

Figure 8. - Shielded enclosure for the lightning measurement system.

IN FLIGHT MEASUREMENTS OF LIGHTNING CHARACTERISTICS

KEITH J. MAXWELL, Senior Engineer
LAWRENCE C. WALKO, Senior Engineer

Technology/Scientific Services, Inc.
Dayton, Ohio 45431

VERNON L. MANGOLD, Project Physicist

Air Force Flight Dynamics Laboratory
Wright-Patterson AFB
Dayton, Ohio 45433

BIOGRAPHIES

Keith J. Maxwell is a senior engineer with Technology/Scientific Services, Inc. He received a B.S. in physics from Oklahoma State University in 1967. While at the McDonnell-Douglas Corporation Lightning Simulation Laboratory, he developed their multi-megavolt generators and worked on lightning protection for such systems as the F-15, B-1 and Space Shuttle. Before joining T/SSI in 1976 he spent 3 years as a staff physicist with General Electric Corporate Research and Development.

Lawrence C. Walko is a senior engineer with Technology/Scientific Services, Inc. He received a B.S. in Electrical Engineering from Pennsylvania State University in 1966. Before joining T/SSI in 1975, Mr. Walko was a staff engineer with the General Electric High Voltage Laboratory and Corporate Research and Development.

Vernon L. Mangold is a project physicist with the Air Force Flight Dynamics Laboratory with a B.S. in math and physics received in 1961. He was responsible for the establishment of the Air Force's Atmospheric Electricity hazards research program and is a former chief of the Electromagnetics Hazards Group.

ABSTRACT

A program was conducted to develop and demonstrate an instrumentation system for time-synchronized in-flight measurement of the electromagnetic characteristics and effects of nearby lightning. A four-channel instrumentation system was developed using capacitive top-loaded E-field sensors, Moebius loop H-field sensors, slot antenna skin current sensors, four transient digitizers, a PDP-11/05 minicomputer, and specialized data acquisition, processing and analysis software. The instrumentation, which had a DC to 30 MHz bandwidth, was developed, calibrated, installed on a Pilatus Porter aircraft, and flown during the 1978 (June to October) thunderstorm season. The design parameters of sensitivity, bandwidth and dynamic range were chosen based on previous experience and verified during ground tests and the flight program. The orthogonal configuration of the E and H field sensors, the time synchronization of all inputs, and specially developed software based on sophisticated analytical models permit the derivation of range and azimuth of nearby lightning strokes, their spectral energy content, and significant coupling parameters based on calculated energy transfer functions. The system was successfully flown during eight thunderstorms and several hundred lightning waveforms were obtained, thus demonstrating its capability as a state-of-the-art in-flight lightning research tool. As a result of data acquired during the program it was confirmed that near-miss lightning strikes do not pose a hazard to conventionally constructed all-aluminum aircraft without sophisticated electronic flight control systems. It is recommended that future lightning research programs use systems employing the concepts described herein and that a flight program whose intent is to get "struck" be conducted using the system and methods of analysis developed during this program.

BACKGROUND

Ground based lightning test systems and computer models exist for predicting aircraft response to lightning strokes.[1,2] There is, however, a dearth of actual in-flight measurements with which to compare these forecasts. Accordingly, the Air Force Flight Dynamics Laboratory (AFFDL) E.M. Hazards Group, through its on-site contractor Technology/Scientific Services, Inc. (T/SSI) began a series of flight programs in 1976 to quantify the airborne threat.[3] The objectives of the flight test program reported herein were to (1) develop sensor and instrumentation techniques

with the proper sensitivity, dynamic range, and bandwidth, (2) fly these sensors and evaluate their performance, and (3) simultaneously measure the relationship between magnetic (H) field and electric (E) field, H-field and skin current response and E-field and skin current response for nearby (0.5-5 mile) lightning strokes. Simultaneous measurements permit the calculation of the system transfer functions. These are necessary to accurately predict the response of aircraft avionics systems to the airborne lightning threat. While a statistical analysis was not part of this program, limited sampling of lightning frequency content and amplitude was obtained. The flight test portion of the program took place during the 1978 thunderstorm season (June to October).

EXPECTED RESULTS

Based on the methods of analysis available for the interpretation of electromagnetic measurements, it was anticipated that an instrumentation system that measured a few parameters simultaneously (i.e. time-synchronized) would yield considerably more useful information than the more complex systems normally used and which depend on statistical samples and analyses. Although the data collected are still being processed and analyzed, the preliminary indications are that the quantity and quality of data resulting from the instrumentation and methods described will significantly improve computer model predictions of aircraft avionics response to lightning-like threats. The data will also provide some benefit to the interpretation and application of ground-based lightning simulation test (LST) measurements. This is considered to be the first flight program to successfully obtain simultaneous wideband, high-resolution transient measurements of the lightning threat and the aircraft response to it.

TECHNICAL APPROACH

In order to completely identify the threat, one would, ideally, measure three vector components of magnetic field, electric field and skin currents and monitor induced voltage on a variety of on-board avionics circuits. This implies at least ten simultaneous measurements with a comparable number of sensors, plus data acquisition units. Practically, the same information is obtainable from sets of fewer measurements. Accordingly, a four sensor data acquisition system was developed, installed in a Pilatus Porter aircraft and flown during the program. The four sensors consisted of E and H field sensors, a skin current sensor and a long wire (trigger) antenna, and their respective signal conditioning circuits. The data acquisition system was comprised of a transient digitizer system and interface electronics. All the sensors were constructed and calibrated at the E.M. Hazards Group Laboratory facilities. Figure 1 is a block diagram of the complete instrumentation system. The four sensors and processing methods were chosen to yield a maximum of information while limiting the complexity of the instrumentation and data acquisition system. The magnitudes of two orthogonal H-field or E-field vectors permit the calculation of azimuth to the lightning stroke.

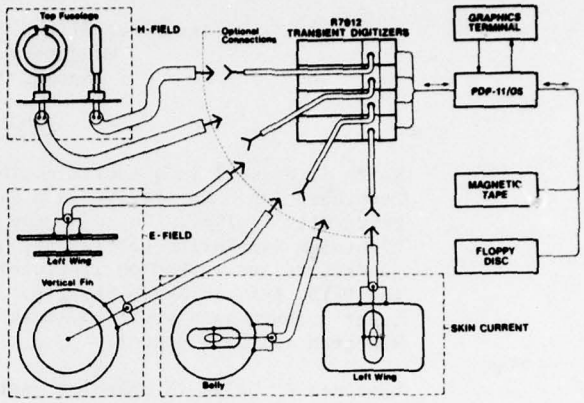

Figure 1. Diagram of Instrumentation

Range information may be derived by computing the ratio of magnetic field to electric field (H/E) at a given frequency according to the method proposed by Rhunke.[4] The spectral energy content of the lightning strokes can be determined by computing the Fourier components, while the significant coupling parameters can be identified by calculating energy transfer functions. Data acquisition in-flight and processing post-flight with the instrumentation system described was the result of specially developed software as illustrated in the Figure 2 logical flow diagram. The aircraft was flown in close proximity to well developed cells at altitudes between 5000 and 10,000 feet and in VFR conditions. Some isolated, slow moving, dissipating systems were circled; however, the aircraft was generally flown in the northwest quadrant and always away from any roll clouds and their overhang or anvil.

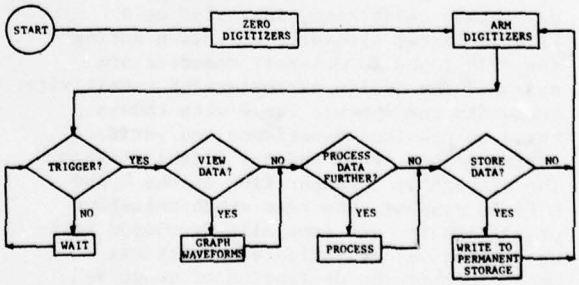

Figure 2. Logical Flow Diagram

Weather radar depictions of the storm systems were obtained from National Weather Service installations at Detroit (DTW) and Pittsburgh (PIT). These films were studied to provide data on the location, size, intensity and direction and rate of movement of the storm systems. Figure 3 compares the displays for a storm on 18 September 78 as recorded at Detroit (left) and Pittsburgh (right) at 1703 GMT on the 250 nautical mile range. The system under study is located in the ENE area of the DTW display and the NNW corner of the PIT display.

Figure 3. Storm Displayed by Weather Radar

Its southern extension, which shows contour levels indicating heavy precipitation, is over the greater Cleveland area at this time. The entire system extends northward for approximately 125 miles over Lake Erie and into Canada and is about 50 miles wide. Comparison with a picture taken 30 minutes later showed the storm 25 miles to the east, indicating a rate of movement of 50 knots. Data for this particular system were taken with the aircraft west of the storm at a distance of approximately 5 nautical miles. Consistent triggering of the data acquisition equipment showed a high level of electrical activity, an indication which could be confirmed by pilot and test operator observations.

E-Field Sensors

From previous flight experience it was decided that a transient electric field sensor responding to field intensities in the range 1 v/m through 1.0 kv/meter was required. The selected antenna was a capacitively top-loaded monopole as illustrated in Figure 4.

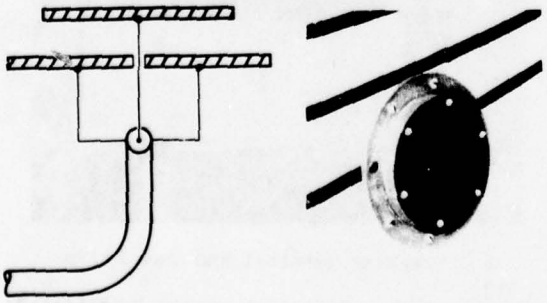

a. Construction b. Installation

Figure 4. E-Field Sensor

This high impedance antenna was connected to a unity gain buffer amplifier which drove the 50Ω impedance input to a Tektronix R7912A transient digitizer. The capacitive load was approximately 8×10^{-12} farad. The 3 dB frequency response of this antenna/amplifier system was from d.c. to 30 MHz. Two of these were mounted on the aircraft.

H-Field Sensors

Detection of magnetic flux is usually performed using some form of loop sensor. Previous attempts by others to use either shielded air core or ferrite core multi-turn loops have suffered from the, predictable, loss in frequency response. The Moebius loop sensor has been used extensively by the EMP community and has received much attention.[5] For loops whose diameter is small compared to the highest wavelength of interest one obtains comparable sensitivity to multi-turn loops without the attendant loss in frequency response.[6] For this program two 8 inch diameter Moebius loops employing balanced 50Ω coaxial cable surrounded circumferentially by a copper tube were used.[7] Experience again dictated that the loop signal be amplified 100 times then carried by a balanced twin-axial 100Ω cable to a differential input at the R7912A transient digitizers. Overall loop/amplifier frequency response was calculated to be 2KHz ≤ f ≤ 26MHz and measured to be 10kHz ≤ f ≤ 40MHz Figure 5 shows the Moebius loop sensor and its electrical equivalent circuit.

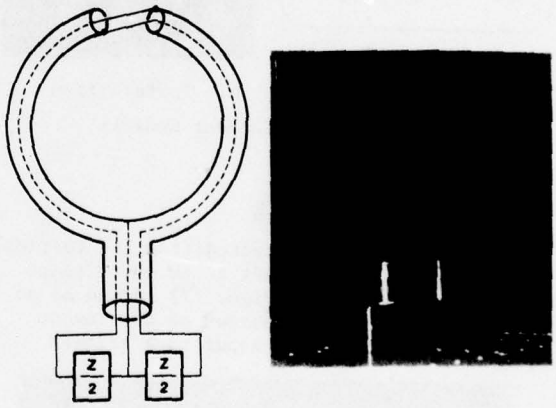

a. Construction b. Installation

Figure 5. H-Field Sensors

The output voltage generated in the loop was recorded and stored on magnetic tape. Later these signals were integrated using the PDP-11 computer to obtain the magnetic field intensity from:

$$B(t) = 15.4 \int_0^t V(t)dt + 3.2 \times 10^{-7} V(t) \quad (1)$$

where the constants are dependant upon loop size and thickness of copper shield.

V(t) is the measured loop voltage
B(t) is the computed magnetic field

thus

$$H(t) = B(t)/\mu_o \qquad (2)$$

Moebius loop sensitivity ranged from 3×10^{-2} amp/meter to 1.6×10^{3} amp/meter.

Skin Current Sensor

A shorted slot antenna was constructed in replaceable aluminum panels on the aircraft. The slot antenna consists of a long slot cut perpendicular to the current flow path. A shorting wire is placed across the slot and a current monitoring probe measures the current flowing in this short. The output of the probe is proportional to the local current in the fuselage.

Figure 6 illustrates the slot antenna design used during this program. The slot antenna frequency response ranges from 800kHz $\leq f \leq$ first slot resonance (> 100MHz). The output of the current probe was amplified by a factor of 10 and the slot/amplifier frequency response was 800kHz $\leq f \leq$ 30MHz.

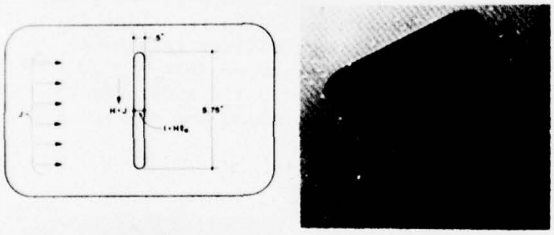

a. Construction b. Installation

Figure 6. Skin Current Sensors

Long Wire Trigger Antenna

A long wire antenna connected from the vertical stabilizer of the aircraft to an entry point just behind the wings (Figure 7) served as an "event" detector. The output of this event detector was used as an input to a trigger unit which drove a "daisy chain" of trigger cables interconnected between transient digitizers. Maximum trigger delay between any two digitizers was ≤1nsec which was essentially the propagation delay along different coax cable lengths. This method assured "simultaneous" triggering.

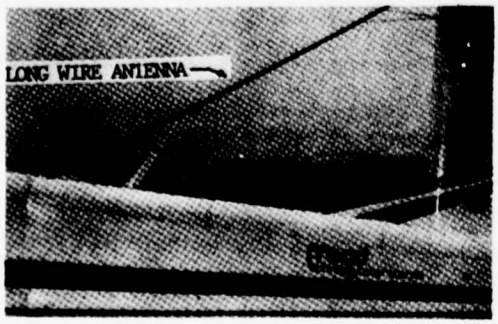

Figure 7. Long Wire Antenna Installation

Data Acquisition System

A Tektronix WP2221 Waveform Digitizing system was used as the heart of the data acquisition system to process and record all high-resolution transient measurements. This system is pictured in Figure 8 as installed in the aircraft, and consists of four Tektronix R7912 Transient Digitizers, PDP-11/05 mini-computer, magnetic tape drive, graphics terminal, and a dual floppy disc. The data acquisition system was installed in a specially constructed equipment rack.

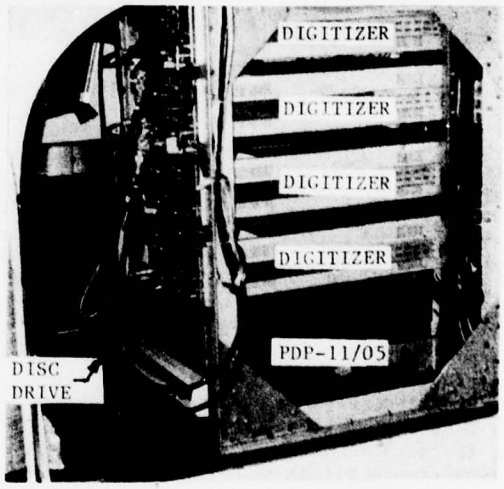

a. Digitizers, Computer and Disc Drive

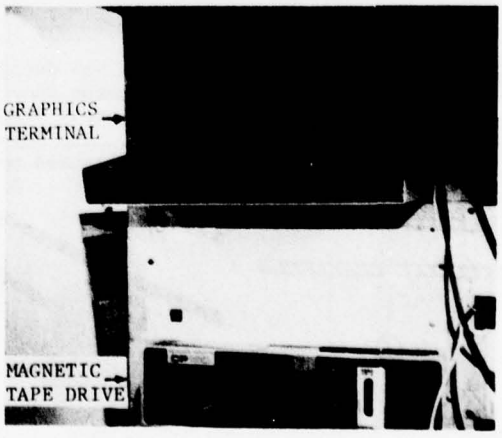

b. Graphics Terminal and Tape Drive

Figure 8. Data Acquisition System Installation

The R7912 Transient Digitizer is essentially a high-speed analog-to-digital converter which can sample at rates of up to 1GHz. Operation is similar to that of an oscilloscope, except that the raw data is converted to a numeric array of 512 elements or samples. Transient waveforms are subsequently processed and stored in this form by the computer. The effective system bandwidth is dependent on the sample rate and on the R7912 sweep speed. Table 1 shows the effective system bandwidths based on sample period, sweep speed, and Nyquist interval (time window width).

Table 1 - R7912 Effective System Bandwidth

SWEEP SPEED*	TIME WINDOW WIDTH	SAMPLE PERIOD**	EFFECTIVE SYSTEM BANDWIDTH
50 nS	500 nS	1 nS	500 MHz
100 nS	1 µS	2 nS	250 MHz
500 nS	5 µS	10 nS	50 MHz
1 µ	10 µS	20 nS	25 MHz
2 µ	20 µS	40 nS	12.5 MHz
5 µ	50 µS	100 nS	5 MHz
10 µ	100 µS	196 nS	2.5 MHz

* Sweep speeds used in this program

** 51 samples per division

µS = microseconds nS = nanoseconds

The PDP-11/05 minicomputer performs data processing and control functions under software operator control. Real-time operator communication with the system is accomplished with the 4010-1 graphics terminal. The CP100 dual cassette drive provides a means of storage and retrieval of programs, data files, and waveform files using magnetic tape cassettes. The operating system was loaded from the disc unit. The digitizers were connected to the various transient sensors, and the resulting transient waveforms were stored on magnetic tape by the computer. The stored information was later retrieved for processing (e.g. Fourier transformations) and analysis.

Stormscope

A Ryan Stormscope system was also installed on the aircraft. Normally the Stormscope is used as an avoidance device; however, in this instance, it was used as a homing device. Pre-flight weather briefings with Wright Patterson meteorologists and viewings of the Wright-Patterson weather radar provided information on thunderstorm activity and tops out to 150 miles or so. Once a "GO" decision was made, Stormscope was used to home-in on the desired electrical activity.

Aircraft

The aircraft selected as the flight test bed was a Swiss Pilatus Flugzeugwerke AG Porter PC-6 single-engined aircraft manufactured, under license, by Fairchild Industries in the U.S. This aircraft has short take-off and landing (STOL) characteristics and is a versatile aircraft that can be rapidly converted to a variety of configurations such as from pure freighter to passenger transport. It was easily adapted for the flight program instrumentation. It is a braced high wing monoplane with an all metal semi-monocoque fuselage structure, cantilever all metal tail structure, and non-retractable landing gear with a steerable tail wheel. Table 2 lists the pertinent physical and performance characteristics of the aircraft.

Table 2

Porter Aircraft Physical and Performance Characteristics

Physical

Wing Span	49 ft. 10 in.
Length	36 ft.
Wing Area	310 sq.ft.
Empty Weight	2,415 lbs.
Useful Load	3,381 lbs.
Available Test Load	2,000 lbs.
Max. Load for Takeoff	5,796 lbs.

Performance

Takeoff Ground Roll at Max. Gross Weight	330 ft.
Landing Roll at Max. Weight	110 ft.
Stall Speed	33 knots
Cruise Speed	140 knots
Service Ceiling	over 28,000 ft.
Max. Speed (never exceed)	270 knots

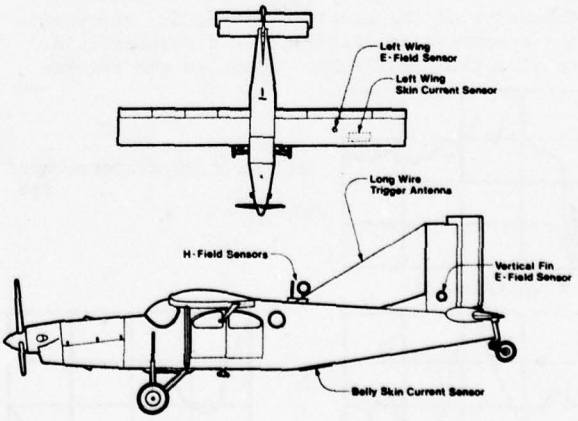

Figure 9. Porter Aircraft and Sensor Locations

Figure 9 illustrates the basic Porter airframe and the location of the lightning detection probes as installed for the flight program. Double shielded RG58 coaxial cables were routed through the leading edge of the wings or through the fuselage and connected to the amplifiers installed at the probe. The installation of the amplifier at the probe maximized the signal to noise ratio by amplifying sensor signals prior to cabling the signal back to the digitizers.

Power for the total system was supplied by three 28VDC to 117 VC (60Hz) inverters. Two 750 watt inverters were located forward of the front right seat (co-pilot side) while a 1 kilowatt system was mounted on special tracks aft of the crew compartment. The two 750 watt circuits or the single 1 KW circuit were adequate to power the entire system.

The crew consisted of a pilot, an equipment operator and a data logger. The payload consumed a total of 1000 pounds out of the maximum 2000 pound useful load.

RESULTS AND ANALYSIS

Data was collected under three conditions: first, natural lightning parameters were measured while the aircraft was parked on the ramp and thunderstorms passed nearby. Second, data was collected for simulated lightning strokes (2 x 20 μsec waveform) generated by an impulse generator while the aircraft was parked on the ramp. Third, the aircraft was flown in close proximity of thunderstorms. Figures 10, 11, and 12 show typical measurements of dH/dt and electric field for these three conditions, respectively. In each figure dH/dt‖ represents the magnetic field measured by the loop whose axis is parallel to the direction of flight; dH/dt ⊥ represents magnetic field measured by the loop whose axes are perpendicular to the direction of flight. E_{vert} is the vertical component of the electric field; E⊥ represents the component of electric field perpendicular to direction of flight. Also, in the figures

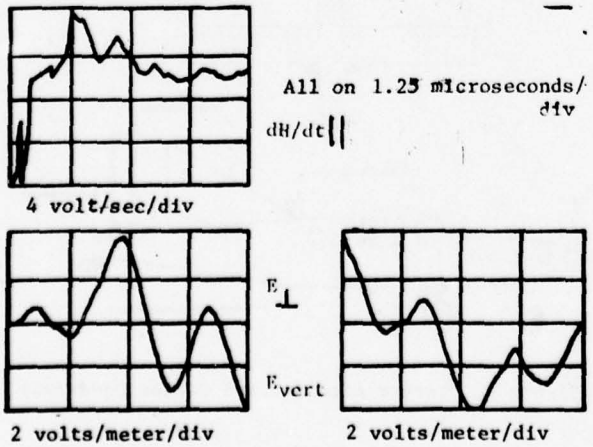

Figure 10. Natural Lightning on the Ground

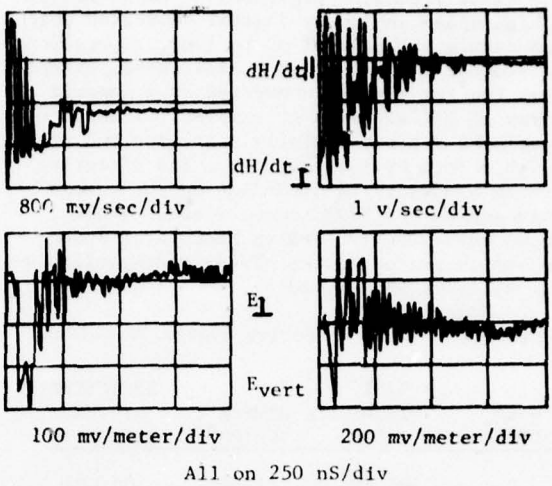

Figure 11. Natural Lightning on the Ground

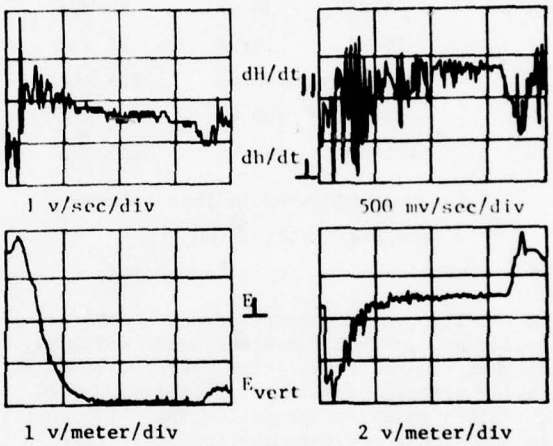

Figure 12. Natural Lightning In-Flight

J_{wing} and J_{fus} represent the wing and fuselage skin current density, respectively.

Data reduction is currently in process so that statistical evaluation of risetimes and dominant frequencies is not yet available. However, figures 13, 14, and 15 are typical Fourier Transforms of the previously illustrated data. Because the amplitude of some spectral components was so low, the data plotted are actually shown as $\log_{10} |Fm(f(t))|$ where f(t) is the time domain H-field, E-field or skin current density and Fm is the magnitude of its Fourier Transform in polar coordinates.

Figure 16 illustrates the Fourier Transform of the skin current density waveform for ground based simulated lightning and airborne natural lightning excitation modes. The similarity between these two waveforms is attributable to the fact that in both cases the stimulus was spectrally rich and that the characteristic lengths of the aircraft determine what frequencies are dominant in the skin current response. Ideally, one would compute the transfer

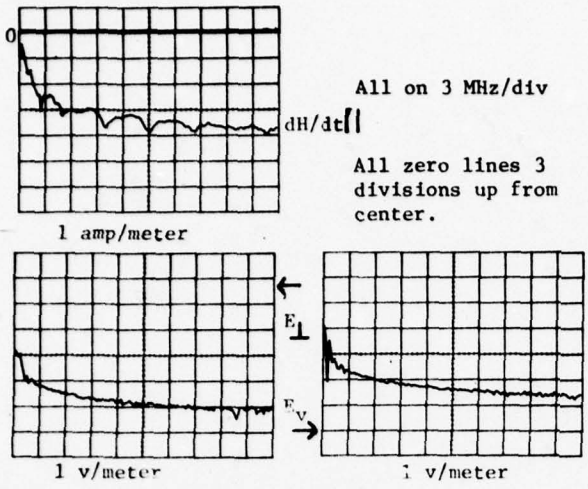

Figure 13. Fourier Transform of Natural Lightning on the Ground

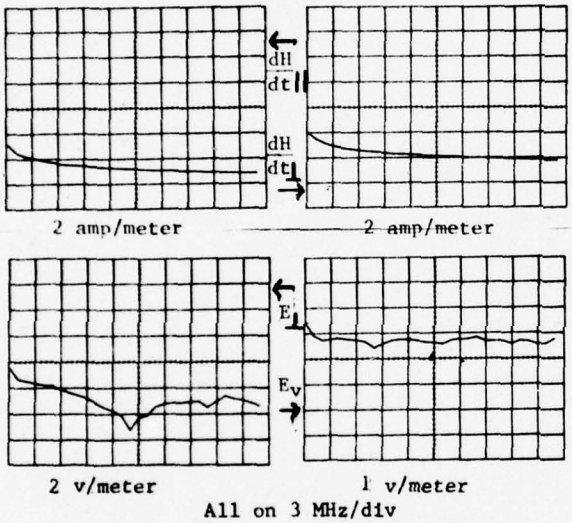

Figure 14. Fourier Transform of Simulated Lightning on the Ground

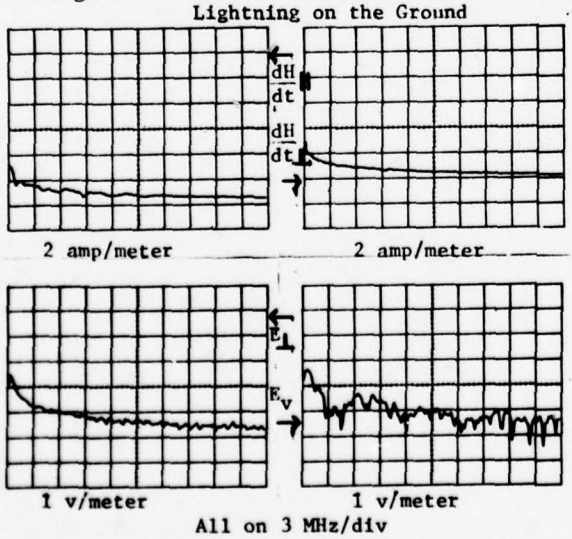

Figure 15. Fourier Transform of Natural Lightning on the Ground

function for the input/output pairs. This is another data reduction task awaiting completion.

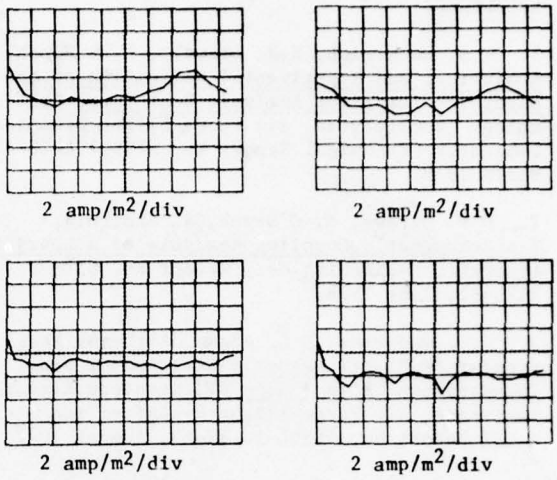

a. Simulated on the Ground b. Natural Lightning in Flight

Figure 16. FFT of Skin Current Density

SUMMARY

To date, lightning protection of aircraft has been based upon only a partial knowledge of the threat. Aircraft skin current response has been postulated as that of crossed dipoles whose lengths are that of the wings and fuselage. From this flight program, sensors and methods have been demonstrated which can define the airborne threat. This definition must result from simultaneous wideband measurement of several parameters. From the measurement of electric field and magnetic field one may obtain the total energy and spectral content of the threat. From the induced skin currents one may compute that the aircraft geometrical configuration produces a different resonance/antiresonance structure than that computed by using classical assumptions. This knowledge is required as input to computer models for predicting lightning induced voltages in aircraft avionics systems. In addition, the data can be used to refine ground based test systems. With the establishment of this capability, full threat definition must be completed through a flight program whose intent is to get the aircraft struck using the types of systems and principles proven in this program.

The authors wish to acknowledge the assistance of Ms. Jean Reazer for operation of the computer during thunderstorm flights; of Mr. Ralph Lusk of Mead Technologies Inc. whose skills as pilot made measurements possible and of the financial and moral support of Mr. John Birken of NAVAIR.

REFERENCES

1. W.S. McCormick, K.J. Maxwell, R.B. Finch, Analytical and Experimental Validation of the Lightning Transient Analysis Technique, Technology Incorporated, Air Force Flight Dynamics Laboratory Technical Report No. AFFDL-TR-78-47, March 1978.

2. D.F. Strawe, M. O'Bryne, S. Sandberg, Electromagnetic Coupling Analysis of a Learjet Aircraft, The Boeing Co., Report No. D180-24256-1, June 1978.

3. J.E. Nanevicz, R.C. Adams, Airborne Measurement of Electromagnetic Environment Near Thunderstorm Cells (TRIP-76), Stanford Research Institute, Air Force Flight Dynamics Technical Report No. AFFDL-TR-77-62, August 1977.

4. Lothar H. Ruhnke, Determining Distance to Lightning Strokes from a Single Station, U.S. Department of Commerce National Oceanic and Atmospheric Administration (NOAA) Technical Report Number NOAA TR ERL 195-APCL 16, January 1971.

5. Paul H. Duncan, Jr., Analysis of the Moebius Loop Magnetic Field Sensor, Air Force Weapons Laboratory Electromagnetic Pulse Sensor and Simulation Notes, Note 183, September 1973.

6. Carl E. Baum, Characteristics of the Moebius Strip Loop, Air Force Weapons Laboratory Electromagnetic Pulse Sensor and Simulation Notes, Note 7, December 1964.

7. Keith J. Maxwell, Development of a Magnetic Field Sensor for In-Flight Lightning Research, Technology/Scientific Services, Inc., Air Force Flight Dynamics Laboratory Technical Memorandum No. AFFDL-TM-78-__, January 1979.

TEST TECHNIQUES FOR SIMULATING LIGHTNING STRIKES TO CARBON (GRAPHITE) FIBRE COMPOSITE STRUCTURES

P F Little, A W Hanson and B J C Burrows
Culham Laboratory, United Kingdon Atomic Energy Authority

SUMMARY

The paper considers the differences in physical properties between graphite epoxy composite and aluminium alloys, and discusses how this affects the lightning testing techniques to be applied. Damage mechanisms and hazards arising from both direct and indirect effects are discussed and compared with those of metal alloys. Appropriate diagnostic techniques are suggested for tests on both small and large structures. Special problem areas resulting from the properties of the material and the manufacturing techniques employed are identified.

INTRODUCTION

Test techniques for lightning effects on conventional aircraft comprising a metal skinned airframe, plastic canopies, fibre glass radomes etc., are now fairly well established internationally[1,2,3]. These test methods were standardised before graphite fibre epoxy laminates (GR/EP) had been developed to the point where they could be used to cover significant areas of an aircraft fuselage. New designs in GR/EP will require engineering tests to assist in development and in the study of their impact on aircraft systems, and qualification (certification) tests to demonstrate safety.

The features of GR/EP composites which merit special attention in testing are their non-homogeneous structure and their relatively high resistance (approximately 10^3 greater than aluminium alloys). These differences affect the current distribution in a graphite or metal/graphite structure and require a scientific appraisal of the test techniques.

The problems associated with testing GR/EP composites are discussed below, both in reference to indirect and direct effects of lightning.

INDIRECT EFFECTS

Basic Theoretical Considerations

This section discusses the impact on indirect effects testing, that is, testing for induced voltage and currents in both wiring and important metal sub-structures such as fuel pipes.

Conventional metal aircraft are well-shielded against the indirect effects of lightning current. The normal thickness of aluminium skinning - usually $\geq$ .080" (2 mm) - keeps the current to the external skin of the fuselage, wings, tail plane, fin etc., because the pulse is too short to allow magnetic flux to diffuse through the skin. Resistive (IR) voltages and induced voltages from electromagnetic induction are therefore in general negligibly small. This accounts for the very low incidence of aircraft damage from fuel tank fires and explosions caused by current flow in the wing, since the massive box section of the wing, often with metal skinning much greater than 2 mm, keeps the current out of the fuel tank inner surfaces.

Induced voltage problems in metal aircraft are therefore largely due to apertures in the metal which act as points-of-entry for magnetic flux. Such apertures are the cockpit, radomes, fibre glass skinning, antenna installations, poorly bonded equipment bay covers, and open undercarriage bays, flap bays etc. The removal of induced effects consists of examining these several points-of-entry and taking the appropriate precautions. Generally the effect of each aperture can be treated separately owing to the presence of metal bulkheads between them.

Compared to aluminium, GR/EP panels exhibit little or no apparent skin effect since the resistivity ρ is increased and skin depth δ is proportional to $\sqrt{\rho}$. Thus within a few nanosecs current diffuses through to the inside surface of most GR/EP panels used in aircraft and lightning current pulses penetrate with negligible attenuation.

Thus in an aircraft skinned with GR/EP, every GR/EP panel becomes a point-of-entry for magnetic flux, generating large resistive voltages and allowing diffusion flux to penetrate and combine with the aperture flux from the cockpit or some other point-of-entry. Another difference arises because the current flow pattern in a metal aircraft is determined essentially by inductive sharing (at least for the lightning parameters of interest in indirect effects work) whereas, in a graphite or metal/graphite aircraft in which the resistance is several orders of magnitude higher, both inductive and resistive sharing will occur in times of interest to indirect effects. This is because the redistribution time constant τ is reduced inversely as the resistivity is increased.

The effects on test techniques of these and other considerations are now briefly described.

The Current Flow Pattern in the Aircraft

The airframe, or part airframe, under test should be installed with simulated lightning current return conductors so that the current flow pattern for both fast-changing and slow pulses is the same as it would be in a natural inflight strike. This requires that the return conductors are positioned such that their presence has a negligible effect on the magnetic field at the airframe structure under test.

To achieve this, the field pattern produced by the aircraft in flight (when it is an isolated body with no return conductors near) must be simulated by some arrangement of nearby conductors. Such a system has been described previously for testing both metal[4,5] and metal/graphite structures[6]. The field distortion due to an incorrectly placed return conductor can be seen by comparing Figures 1(a) and 1(b). The structures in Figure 1(a) will exhibit current crowding on the fuselage lower surface during the inductive sharing regime, and therefore generate excessively high aperture and diffusion flux voltages on the lower panels in the lower bays, and also give lower voltages across the top. The inflight strike gives a field shape as in Figure 1(b) and this is simulated exactly by a suitably spaced fully-coaxial system, or approximately by the Culham Quasi Coaxial (CQC) system as in Figure 2. This gives a good simulation of the field around the whole fuselage and therefore a balanced ratio of voltages in top, bottom and side panels. The three conductor system is ideal for fuselage testing, but a four conductor CQC system is ideal for wing tests as in Figure 3. Three conductors would not be suitable for a structure with wing type symmetry. Careless use of return conductors for a wing test will often over-emphasise the current in the mid-chord position, therefore return conductors must be placed well to the for and aft as shown in Figure 3.

The close spaced fully-coaxial and CQC systems have a considerably potential advantage for whole aircraft tests owing to the low inductance ($\sim 1\mu H$) of the load assembly, comprising the aircraft and return conductors. A small inductance both simplifies and reduces the cost of a full threat test, which may become necessary for both direct and indirect effects tests.

The flux patterns change very quickly in a graphite and metal/graphite structure, and the above discussion largely concerns the first few microseconds of a pulse. As referred to previously the current redistribution time, τ, is about 0.5 to 10μs. The fast-changing and high amplitude components of lightning typically have this order of pulse length and therefore induced voltages in the initial inductively shared period and transitional time are important. Conversely in an all metal aircraft (excluding special stainless steel or titanium alloy aircraft) the induced voltages occur exclusively in the inductive sharing regime, because the redistribution time τ is of the order of milliseconds.

Individual Panel Testing

Individual panel testing for induced voltage effects is not very satisfactory owing to the different current redistribution when a panel is not in its intended airframe environment. Therefore testing on a full-size airframe is recommended; a Hawker Hunter fuselage is used as a test rig at Culham.

Where individual panel testing is necessary the details of the frame into which it fits, and the fasteners, must be correct: the amplitude of the diffusion flux depends on the panel resistance plus the joint resistance. (See Ref. 6 page 134). The effect of a metal frame on the flux penetration will only be observed fully if the correct frame is used with all fasteners both transverse and longitudinal. Fewer fasteners (i.e. higher joint resistance) tends to reduce the current in the panel somewhat and to increase the observed induced voltage. Measurements on a panel in a metal frame show that for a fast pulse the current across the centre of a GR/EP panel flows in a reverse direction (compared to bulk current flow) while the current is falling but positive as shown in Figure 4. The explanation for this phenomenon is that flux which entered the panel during the time of the initial current rise must leave as the current reduces, so generating 'back emf' and so a reverse current flow. This unexpected result has been observed and confirmed in several different geometries.

Diagnostics

Diagnostics on GR/EP tests will in general follow the techniques used on metal structure tests, but more care in choice of diagnostic measuring positions and all cable routes will have to be taken.

For example, care will be needed to avoid errors due to the use of one connection point simultaneously for current entry and voltage sensing. Small sample tests in particular need separate current entry and potential sensing (the "4-wire" method) if reliable resistivity measurements are to be taken, either for pulse testing of d.c. tests.

The routing of diagnostic connections and wiring is also important if dependable measurements are to be made. For example, when potential drops along a panel are measured during pulse tests it is vital that the wire to the further test point runs straight back along the panel to the second test point, and then the two wires twisted together are taken back to the measuring system (e.g. on oscilloscope with differential input facility). The sensing wire measures the voltage along its route, including the effects of aperture and diffusion flux coupling to the loop formed by the wire and the test panel. Therefore only when the wire runs back hard against the panel (so making the area

of the loop negligibly small), will the voltage be correct[6,7]. Figure 5 illustrates the effect of wire routes. A measures the IR drop along the panel, B measures the sum of the two joint voltages only, and C measures the total joint plus panel IR voltage. Measurement A is useful for determining the panel current if its electrical characteristics are known; the panel acts as its own current shunt.

Figure 6 demonstrates how the induced voltage principle of equivalence between resistive (IR) and diffusion ($d\phi/dt$) voltages [6,7] may be applied to diagnostics where it is inconvenient or forbidden to drill holes or make attachments to the graphite. The loop shown measures the panel IR drop along the line of the wire, although it does not contact the panel electrically.

Voltages will, of course, be very large in long thin graphite panels, up to several thousand volts per metre length at full threat lightning current. Therefore diagnostic wires which run some length of an aircraft fuselage must allow for the large common mode voltage occurring between, say, an aft reference point and the position of measurement. Diagnostic routes should be chosen to make best use of longitudinal metal components in the fuselage by running wires within, or hard against them. Similar routes may have to be used in aircraft design to mitigate the problems created by the introduction of GR/EP panels.

One useful diagnostic technique is to use a fibre optic communication system, for example the FOL 100 by Electro Optic Developments Limited of England. This system has a 150 MHz bandwidth for analogue signals, with input attenuators of 0-30dB and a calibration signal, both remotely switchable. Viewed in the frequency domain, a GR/EP panel acts as a low pass filter with a cut off frequency normally in the range of 10 to 20 MHz. The cut off frequency is given approximately by

$$f_o = \frac{1.17\rho}{h^2} \text{ MHz}$$

where h is the panel thickness in metres, and ρ is the resistivity in Ω-m. Thus the measuring bandwidth should extend to 2 f_o or 3 f_o to ensure that the full spectrum of transients is recorded, and the FOL 100 instrument is satisfactory in this regard.

DIRECT EFFECTS

Basic Theoretical Considerations

Carbon fibre structures are subject to direct effects (damage by ohmic heating, magnetic forces and arc root heating) in the same way as metal structures. The difference in the physical properties of GR/EP compared to aluminium alloy however leads to significant differences in the nature and magnitude of the resultant damage. This in turn can affect the testing techniques that need to be applied.

Differences of particular interest to the lightning technologist lie in the non-homogeneous nature of the material; the resistivity (which is anisotropic in the individual fibres and in the bulk material); the higher arc burning voltage; and the low thermal conductivity.

It has been shown previously that significant arc damage to metal panels is mainly restricted to burn through at the arc root, which for any given thickness of any specific metal requires a calculable minimum current, and a calculable minimum time to effect[8]. Other current parameters are of no consequence and negligible damage occurs in the surrounding area due to ohmic heating. Thus there is no longer need for arc root tests on metal skins for zones where both current and time requirements are not satisfied, or where small holes are acceptable.

With GR/EP the arc burning voltage is approximately ten times that of aluminium, and consequently ten times the heating energy is available in the arc root per coulomb of charge transfered. In the surrounding area the much higher bulk resistivity (up to 1000 times greater than aluminium) can give rise to severe ohmic heating damage with pulses of high action integral. This often takes the form of delamination.

The dissipation of the heat generated is also affected by the lower thermal conductivity. Thus the damage in and around the arc root region is dependent not only on the pulse current level and duration as in metal panels, but also on the charge transfered and the pulse action integral.

Consider now the current flow in the bulk material. Although some composites are produced using woven carbon fibres most GR/EP is made in the form of multi-ply lay ups. Each ply consists of unidirectional fibres, but successive plies are laid at differing angles of fibre orientation depending upon the structural requirements of the component. The resistance within a ply to current flowing across the fibre lay can be some orders of magnitude greater than the resistance to current flowing along the fibre lay, and thus the current distribution between plies will depend upon the direction of the current flow, and the orientation of the fibre lay in each particular ply. The contact resistance between adjacent fibres in the vertical and horizontal directions and between plies, will vary with the lay up pattern and the manufacturing techniques used. The effective resistance to current flow and therefore the total ohmic heating and the distribution of that heating, will depend upon the lay up of the composite, and the current path in it. The direction of the test current is therefore very important, and the tests must be carefully designed so that the current flows in the appropriate path during the test.

Direct measurements on GR/EP panels[9,10] have shown that Ohm's Law is obeyed both for low

d.c. currents and high current pulses of short duration with low action integrals, where the temperature rise is small. This is true over a very wide range of current densities. Resistance of the bulk material becomes non linear above 110°C(11) whilst the temperature co-efficient of resistance of the fibres becomes negative above 65°C(11).

Direct Effects Testing

For zones 1 and 2, the differences in the arc root damage mechanisms imply that a reappraisal of the test waveforms suitable for arc root testing on GR/EP may be desirable.

For zone 3 testing a similar reappraisal may be required. Recent unpublished work at Culham has shown that the damage resulting from current pulses of a fixed action integral into identical panels varies with the waveshape of the pulse. Both the character and the magnitude of the damage are affected. The reason for this is not yet understood, but it is suspected to be caused by an uneven current distribution enhanced by the negative temperature coefficient of resistance of carbon (graphite) fibres above 65°C and the low thermal conductivity of the composite as a whole. Work is still proceeding on this. A more precise specification of waveshape and initial di/dt, in addition to peak current and action integral, may be needed for zone 3 direct effects tests on GR/EP.

The discussion in the section 'The Current Flow Pattern in the Aircraft' applies with equal force to direct effects testing. The current distribution within the airframe must be properly reproduced.

Interfaces and Special Constructions

Current crossing interfaces within the composite or at metal/composite joints is often forced to take a disadvantageous path through the GR/EP e.g. crossing interlaminate boundaries. There is therefore a far greater potential hazard at such interfaces than exists at a metal/metal interface. The test programme must include a realistic investigation of all such interfaces.

Particular care must be taken at glued interfaces where there is a possibility of current crossing the glue line. In such cases current will tend to concentrate in voids in the glue causing explosive expansion of the air in the void, and subsequent failure of the glue line.

In a similar manner aluminium honeycomb in GR/EP sandwich panels can give rise to explosive delamination of the panel when current in the honeycomb crosses the honeycomb interfoil glue lines. Aluminium honeycombs are very sensitive to this type of failure and very precise simulation of the true environment is important in these tests.

Other systems worthy of particular attention in the testing programme include hybrid systems of mixed glass and carbon fibre reinforcing, as high currents restricted to a few carbon fibres can result in the explosive fusing of the carbon fibres.

Diagnostics

Various techniques for measuring current sharing and redistribution between CFRP components have been described in the section on diagnostics for Indirect Effects. These are applicable to direct effects tests also. Some means of measuring the peak temperatures, and temperature gradients are also required. Sophisticated infra red cameras and detectors have been used, but for most tests the simple application of temperature sensitive paints will suffice.

TESTING EQUIPMENT

Generators

For tests on indirect effects the initial value of di/dt is often the most important parameter, and this not much affected by the higher resistance of GR/EP composites. For tests on direct effects the value of the action integral $\int i^2 dt$ is clearly more important in GR/EP than in aluminium alloys. In generators using initial capacitive storage, $\int i^2 dt = \frac{CV^2}{2R}$ where R is the total circuit resistance. The higher resistivity of GR/EP therefore requires a higher value of C or V than would be required for the same test in aluminium alloys. There is always some inductance in the circuit so $\hat{I} = VK_1 \sqrt{\frac{C}{L}}$ (K_1 is a complex function of R, C and L) so changes in either V or C affect $\hat{I}$. For circuits using a critically damped capacitive discharge, there is a further restriction on the choice of circuit constants as $\frac{4L}{R^2C}$ must be unity. It has been seen that the rise time and total pulse duration may also be important parameters of the test current, and it is often difficult to choose circuits constants that give the cirrect rise time, duration, peak current and action integral. Greater flexibility can be achieved whilst still maintaining the unidirectional pulse waveform by the use of clamped circuits, i.e. by first discharging the capacitors into the inductor, and commutating the current into the test piece when the required value of $\hat{I}$ has been reached. This technique is however much more difficult: it is described in detail by Hanson(12).

Test Circuits and Equipment

In Zone 3 hard contact tests, the effects of the magnetic field of the return conductors is more important for mixed GR/EP and aluminium structures than it would be for aluminium structures.

Previous Culham Publications(12,13) have indicated the importance of electrode spacing, and the effects of electrode jets. In GR/EP panel tests it is important to use a jet diverting electrode, and an adequate gap between panel and electrode to eliminate punch through

from arc explosion over pressure.

ACKNOWLEDGEMENTS

The authors acknowledge the support given by the Procurement Executive of the UK Ministry of Defence for the basic research conducted at the Culham Lightning Studies Unit.

REFERENCES

(1) Lightning Test Waveforms and Techniques for Aerospace Vehicles and Hardware. SAE Committee AE4L.

(2) Draft Stanag 3659AE NATO. Standardisation Agreement Lightning Qualification Test Techniques for Aircraft and Hardware.

(3) J Phillpott. Recommended Practice for Lightning Simulation and Testing Techniques for Aircraft. Culham Laboratory Report No. CLM-R163.

(4) B J C Burrows, C Luther and P Pownal. Induced Voltages in Full Size Aircraft at 10^{11}A/s. IEEE Conference Seattle 1977.

(5) ASTP Simulated Lightning Test Report. National Aeronautics and Space Administration Report. JSC-09221.

(6) Composite Forward Fuselage Systems Integration. Volume II. AFFDL Technical Report (In Draft, to be issued shortly).

(7) B J C Burrows, C Luther. Culham Lightning Studies Unit Memo 69.

(8) P F Little, A W Hanson and J Dobbing. Arcs on Metal Sheets in Simulated Lightning Discharges. IEEE Conference Seattle 1977.

(9) B J C Burrows, C Luther and P Pownal. Culham Lightning Studies Unit Memo 56.

(10) C Banks. Culham Lightning Studies Unit Memo 65.

(11) L A Scruggs, W J Gajola. University of Notre Dame, Indiana 46556. Low Frequency Conductivity of Unidirectional Graphite/ Epoxy. IEEE Conference Seattle 1977.

(12) A W Hanson. Recent Developments in High Current Testing Techniques for Lightning Simulation. IEEE Conference Seattle 1977.

(13) J Phillpott. Factors Affecting Puncture of Aluminium Alloys by Simulated Lightning. L and SE Conference 1972.

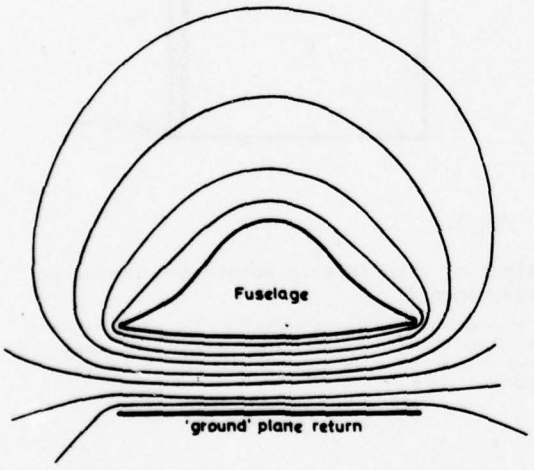

Fig. 1a Field distortion (giving rise to current distribution error) due to close spaced single return conductor.

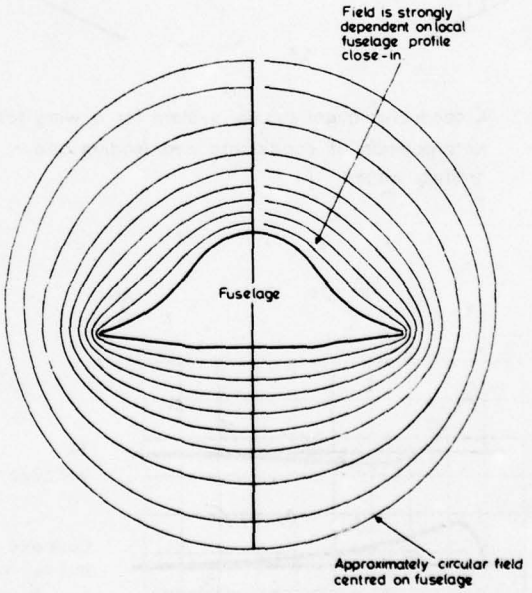

Fig 1b Free Space Field Configuration.

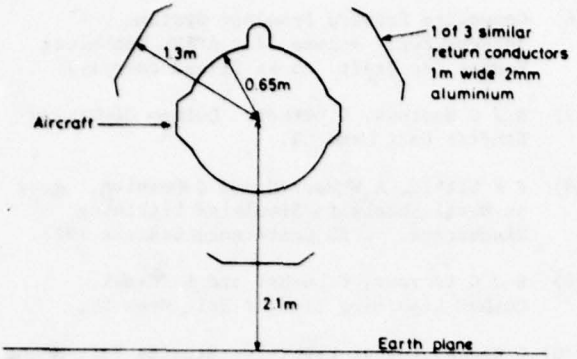

Fig. 2 3 conductor quasi coaxial system around fusilage.

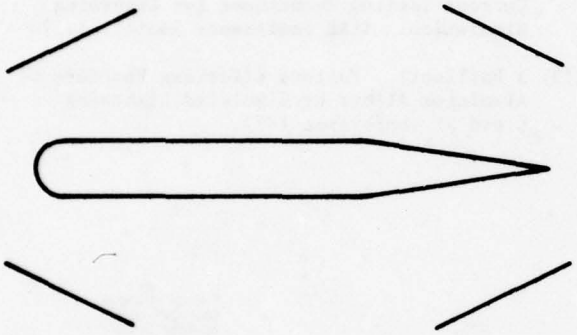

Fig. 3. 4 conductor quasi coaxial system for a wing test. Note position of conductors near leading and trailing edges

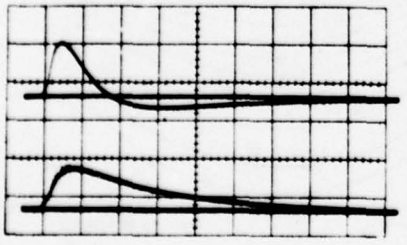

Fig 4 IR voltage measured as in Fig 5A showing current reversal. This occurs when the GR/EP is shunted by metal structure.

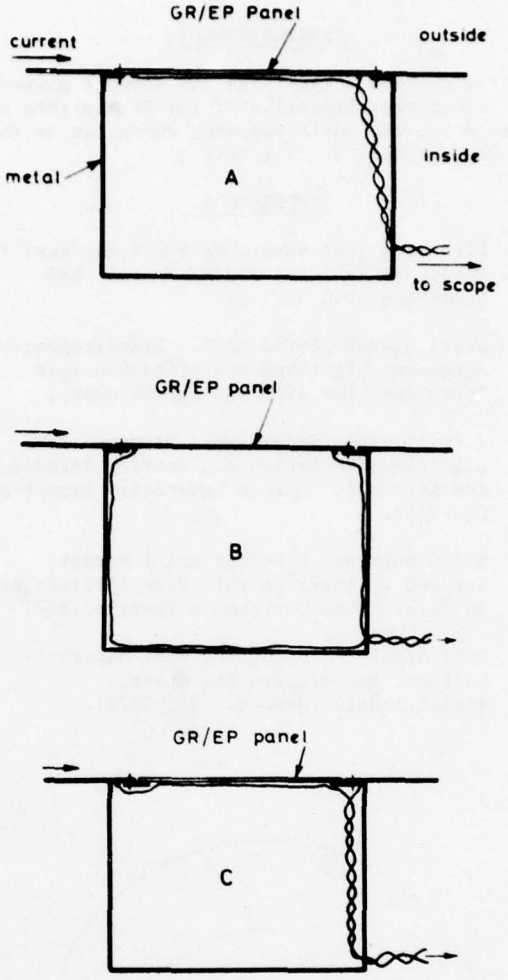

Fig 5.

Effect of wire contact points and routes on measurements.

Cross section of skin and metal walled equipment bay with GR/EP panel. In all cases diagnostics wires shown must be hard against the adjacent metal or GR/EP surface.

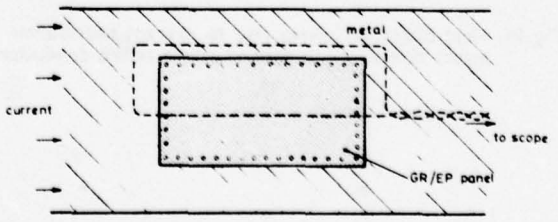

Fig. 6 View of fuselage skin or test rig, showing GR/EP panel. Wire loop (shown dashed) is tight against the inside surface of the panel and metal surround.

INDUCED EFFECTS OF LIGHTNING ON AN ALL COMPOSITE AIRCRAFT*

R. A. Perala
Electro Magnetic Applications, Inc.
P.O. Box 8
Golden, Colorado 80401

and

K. Lee, Hughes Aircraft Corporation
Fullerton, California 92634
R. Cook, Electro Magnetic Applications, Inc.

BIOGRAPHIES

Rodney A. Perala is the manager of the Colorado office of EMA, and is responsible for programs involving nuclear EMP and lightning. He received his Ph.D. in Electrical Engineering from the University of Denver in 1971. He then taught for two years and then joined Mission Research Corporation where he spent 5 years on the technical staff, doing work in nuclear EMP and lightning. Mr. Cook is on the technical staff of EMA doing research in NEMP and lightning and received his M.S. in Electrical Engineering from the University of New Mexico in 1977. Kuan Min Lee received the B.S. degree in electrical engineering from Taiwan University in 1969, the M.S. in 1971, and the Ph.D. degree in 1976 in applied physics from Harvard University. He was a research fellow at Gordon McKay Laboratory at Harvard University, before joining Mission Research Corporation. He is currently with Hughes Aircraft Company in Fullerton, California where he is doing research in electromagnetic theory.

ABSTRACT

Results are presented for lightining induced cable currents and voltages on typical cable runs inside an all composite aircraft. Both a direct stroke and a nearby stroke are considered. Results are also given for the case in which the aircraft is coated with 6-mil aluminum flame spray. It is shown that, as expected, the direct stroke induces the largest voltages, but the effects of the nearby strike are not negligible.

INTRODUCTION

Because of their high strength to weight ratios, graphite epoxy composite materials are finding increased usage as structural elements in modern and future aircraft. In addition, modern aircraft are relying more heavily on more sensitive logic in avionics and weapon circuitry, and fly-by-wire technology is already being used. Because of the composite's relatively low electrical conductivity, it does not shield the sensitive circuitry as much as would a conventional airplane. Because of these considerations, the induced effects of lightning on such an aircraft are assuming more importance.

*Work sponsored by the AFFDL, Wright Patterson Air Force Base, under Contract F33615-77-C-5169 to Grumman Aerospace Corporation, when all the authors were with Mission Research Corporation.

The objective of the study reported here is to compute voltage and current levels induced on cables internal to an all composite aircraft, which is referred to as an Advanced Design Composite Aircraft (ADCA), a conceptual aircraft of the 1980's. Nuclear EMP coupling results to this same aircraft were presented at the IEEE meeting in Atlanta in 1978[1]. The study concerns only the indirect effects, which includes the threat to an aircraft from a stroke attaching directly to it as well as the lightning induced electromagnetic pulse (LEMP) from a near miss.

The numerical solutions are obtained by the same methods used for the NEMP computations[1]. The surface current densities are obtained from the three-dimensional finite difference code THREDE[2] and the computation of the internal cable responses is obtained by a finite difference multiconductor transmission line code[3]. The ADCA structural outline overlayed by the THREDE finite difference model outline, and location of the cable runs is given in Figure 1. The fuselage is approximately 18m long. Skin thicknesses on the ADCA vary between .152 cm and 1.52 cm, with a nominal average value of .254 cm.

RESULTS FOR A DIRECT STROKE

The threat current waveform used for a direct stroke attaching to the aircraft is the return stroke model commonly used for system studies[4]

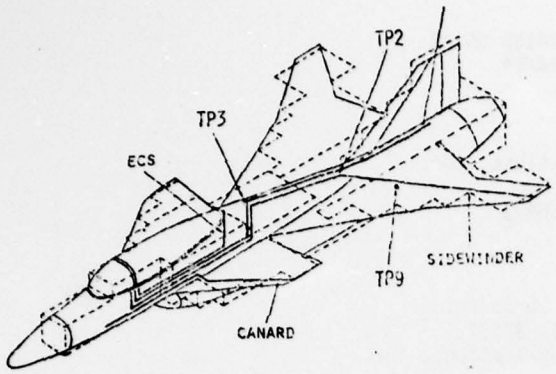

FIGURE 1. OVERLAY OF THE THREDE MATHEMATICAL MODEL AND STRUCTURAL OUTLINE OF THE ADCA, AND CABLES SUBJECTED TO INTERNAL COUPLING ANALYSIS.

and is shown in Figure 2. It is noted that the spectral content falls off rapidly and is down more than 80 dB in the vicinity of principal aircraft resonances (6-7 MHz). Thus, the solution to the direct stroke problem involves principally the static solution.

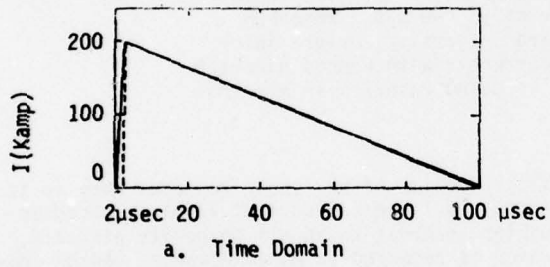

a. Time Domain

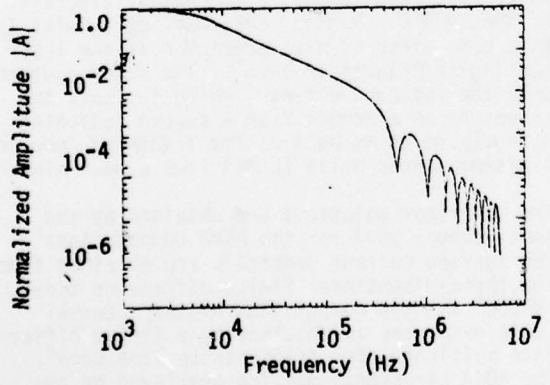

b. Spectral Amplitude

FIGURE 2. LIGHTNING RETURN STROKE CURRENT USED IN THE DIRECT STROKE ANALYSIS.

The solution is obtained by modifying THREDE to handle current injection and applying it to the configuration of Figure 3[5]. Because the maximum time step used in THREDEs finite difference algorithm is limited by the cell size, THREDE cannot be used to compute the response much beyond one microsecond because of computational cost. Because the threat lasts 100 µsec, a new approach is desired.

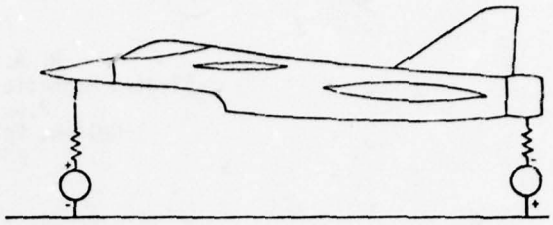

FIGURE 3. ADCA THREDE MODEL USED FOR LIGHTNING DIRECT STROKE ANALYSIS.

The approach takes advantage of the low frequency content of the threat.

A current is injected into the ADCA that is short enough so that THREDE can compute a sufficiently complete transient response. The injected current waveform is shown in Figure 4, which shows a 200 kA nearly triangular waveform, whose total time duration is 500 ns. The source of this injected current is an isosceles triangular voltage source of 500 ns duration. The resistances in Figure 3 are 900 ohms in the front wire and 800 ohms in the rear wire. These values are chosen to represent the high values of the source impedance for the lightning channel as discussed in Reference 6, which states that this is in the vicinity of 1000 to 3000 ohms. The importance of this impedance for this problem is that the aircraft resonances will be most greatly excited when the end impedances are much higher than the characteristic impedance of the transmission line formed by the aircraft, with respect to the ground plane. This value is nominally 156 ohms, so an 800-ohm load implies a large reflection coefficient (~0.7). The choice of resistances at the lower end of the range was dictated by code limitations on how much resistance can be readily modeled. The resistance must be limited to 100 Ω or less per cell as larger values lead to instability and only a finite number of cells are available for modeling the resistance of the lightning channels.

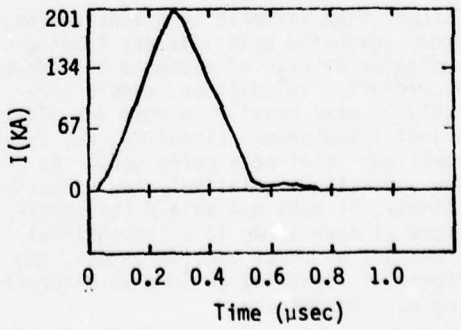

FIGURE 4. CURRENT INJECTED AT THE NOSE.

Figure 5 shows a sample current density response computed on the fuselage skin for the injected current of Figure 4. Apart from some rather small excitation of ADCA resonances, the waveforms are of the same triangular shape as the input. The same observation is true for skin currents elsewhere. It is therefore concluded that the waveshape of the response is approximately independent of location on the aircraft, which implies a static solution. If this is true for the current waveform of Figure 4, it will be even more true for the threat current (Figure 2) whose spectral content is at lower frequencies.

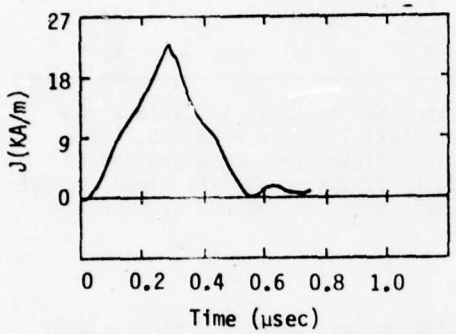

FIGURE 5. SAMPLE CURRENT DENSITY WAVEFORMS AT THE FUSELAGE BOTTOM, REAR CENTER (TP5) FOR THE INJECTED CURRENT OF FIGURE 4.

Therefore, the current density at various locations on the ADCA is assumed to be of the same shape as the threat, but the relative amplitudes are given from the THREDE solution to the triangular problem with smaller pulse width. These current densities multiplied by the skin transfer impedances then provide the electric field source terms which drive the cables internal to the ADCA.

It should be pointed out that the presence of the ground plane (which is a necessary artifice for THREDE computations) in Figure 3 affects the circumferential variation of the currents. For example, the current density on the fuselage bottom is nearly twice that on top. This problem is corrected by using the average of the top and bottom values to get the true amplitude of the current density.

Table 1 is a summary of the worst case open circuit voltages and short circuit currents for several cables. The open circuit voltage waveshape follows that of the incident current and the short circuit current is the integral of it.

Because of the possible deleterious effects of these voltages and currents, the effectiveness of using an aluminum flame spray coating on the composite skin was investigated. Calculations were done for a 6-mil thick aluminum flame spray, which is assumed to have a conductivity of 10^6 mho/m[7]. The effect of the flame spray is to reduce the internal voltages and currents by about 14dB, which is only a factor of 5. Thus, it does not appear that such a fix will provide absolute protection, but it will statistically reduce the threat.

Table 1. Summary of Peak Open Circuit Voltage and Short Circuit Current Computations for σ = 15,000 mhos/m (for Direct Stroke)

Cables	V_{oc}(V)	I_{sc}(Amp)
Side Winder	4.5×10^3	2.1×10^3
Fly-by-Wire	4.7×10^3	2.0×10^3
ECS	4.3×10^3	5.8×10^3

The quantities V_{oc}, I_{sc}, are defined as follows:

V_{oc} = The open circuit voltage on the back end of the cable with the forward end short circuited.

I_{sc} = The short circuit current on the back end of the cable with both ends short circuited.

RESULTS FOR LEMP

The main problem in computing the LEMP hazard is the lack of knowledge of the LEMP threat. The LEMP waveshape and amplitude are not well known because of the lack of experimental data at aircraft altitudes. In recent years, programs have begun in which instrumented aircraft were to fly near thunderstorms and record electromagnetic fields and induced cable currents. This has not yet been very successful, because of an abnormal lack of thunderstorm activity in the test region[8,9].

In investigating the LEMP problem, LEMP from both stepped leaders and return strokes were considered. It was found that the stepped leader LEMP response resulted in less than 10V induced on internal cables, which is much less than that caused by the direct stroke or a nearby return stroke. Therefore, the return stroke LEMP will only be considered further.

The LEMP field waveforms for a return stroke are computed using the model of Uman[10]. This model was used to compute the LEMP electric fields from a severe lightning stroke at various ranges and altitudes. The return stroke current was assumed to be the 200 KA SRI model[11] which differs from Figure 2 in that it is a double exponential instead of a triangle. It is assumed to be traveling upwards at a velocity of 2.4×10^8 m/sec, which is the fastest recorded velocity[12]. The lightning channel between cloud and ground is assumed to be vertical and 4 kilometers long. The earth is assumed to be a perfect conductor. The radial and vertical electric fields were computed at many altitudes and ranges. In all cases it was found that the horizontal electric field was the larger threat.

One problem is to determine how close the stroke can be to the aircraft without actually attaching to it. This distance is determined mainly by ascertaining the distance from the aircraft at which the aircraft does not perturb the static fields significantly. This distance is estimated to be on the order of one aircraft dimension, or 18.3 meters[13]. This, then will be used for the purposes of specifying the distance at which the aircraft can be from the stroke without sustaining a direct strike. Although this distance may be subject to some controversy, it should provide a good worst case for protection purposes. The horizontal electric field at this range and a height of 500 meters, as well as other heights, is shown in Figure 6, and is used as the LEMP threat for this study.

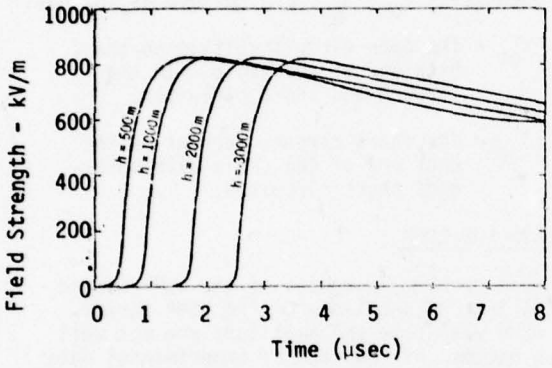

FIGURE 6. HORIZONTAL ELECTRIC FIELD AT 18.3 METERS WITH HEIGHT AS A PARAMETER.

Figure 7 illustrates the axial current density at the top of the fuselage for incidence from the top. It is noted that the response consists of the superposition of a large term proportional to the geometrical optics term ($2\hat{n}x\vec{H}_{inc}$ for a cylinder, $\hat{n}$ is outward normal) plus the smaller dipole mode response which involves the high frequency oscillations. Responses on the side of the aircraft (the shadow boundary) involve only the dipole mode because there $2nxH_{inc} = 0$.

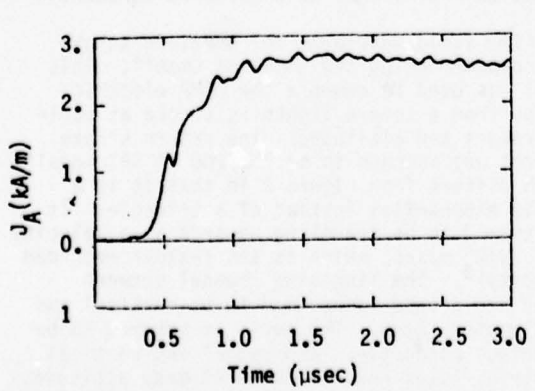

FIGURE 7. AXIAL CURRENT DENSITY AT TP3 FOR RETURN STROKE FIELD.

Table 2 is a summary of the worst case peak open circuit voltages and short circuit currents for sample cables for σ = 15,000 mho/m. The peak amplitude of the incident pulse is roughly 820 kV/m. The cable voltages and currents have the same waveshape as discussed for the direct stroke.

Table 2. Summary of Peak Open Circuit Voltage and Short Circuit Current Computations for σ = 15,000 mho/m for LEMP.

Cables	V_{oc}(V)	I_{sc}(Amp)
Side Winder	210	51
Fly-by-Wire	1000	177
ECS	40	19

It is noted that the response in Table 2 is sufficient to possibly cause a hazard. If 6 mils of aluminum flame spray were applied to the aircraft, as discussed for the direct stroke case, the levels would be reduced by approximately 14dB.

CONCLUSIONS

Several conclusions are offered. First, it is observed that the direct strike is the worst case, as one would expect, but the levels from a near miss are also significant. However, because an aircraft is illumined by lightning induced fields more than it undergoes a direct strike, it is difficult to say which is a more significant threat. The effect of the flame spray is to significantly reduce the threat to a level that is still high if one considers the worst case, but statistically the threat should be small.

Another important observation is the significance of the high frequency threat. Most lightning data gathered so far relates to the low frequency regime because this is the regime responsible for the direct effects (damage). However, there is not as much data available on the high frequency threat of lightning. It is these frequencies which excite the aircraft and cable resonances, and would be most responsible for the upset or damage done to internal black boxes. It is noted that the threats used for this paper are primarily the low frequency components, because of lack of definition of the high frequency components.

Finally, it should be pointed out that the results presented were for a skin conductivity of 15,000 mhos/m. Because of the low frequency of threat used in this analysis, the results would scale linearly with conductivity, because skin thicknesses are much smaller than the skin depths.

REFERENCES

1. Perala, R. A., K. M. Lee, and R. B. Cook, "EMP Coupling to a Composite Aircraft," Proceedings of the 1978 IEEE International Symposium on Electromagnetic Compatibility, Atlanta, Georgia, 20-22 June 1978.

2. Holland, R., "THREDE: A Free Field EMP Coupling and Scattering Code," Mission Research Corporation, AMRC-R-85, September 1976.

3. Trybus, P. R., and D. E. Merewether, "A Time Domain Solution of Multiconductor Transmission Line Coupling Problems," Mission Research Corporation, AMRC-R-21, January 1974.

4. "Space Shuttle Lightning Protection Criteria Document," NASA, Lyndon B. Johnson Space Center, Houston, Texas, JSC07636, September 1973.

5. Kunz, K. S., B. W. Torres, and R. A. Perala, "Surface Current Injection Techniques: A Theoretical Investigation," presented at the 1978 IEEE Conference on Nuclear and Space Radiation Effects, Albuquerque, New Mexico, July 1978.

6. Wagner, C. F., and A. R. Hileman, "Surge Impedance and its Application to the Lightning Stroke," IEEE Trans., February 1962.

7. Golam, G., "Protection Optimization for Advanced Composite Structurs," Grumman Aerospace Corporation Eighth Monthly Progress Report, April 1978.

8. Corbin, J. C. Jr., and D. F. Strawe, "Electromagnetic Coupling Analysis of a Learjet Aircraft in a Lightning Environment," presented at the 1978 NEM Convention held at the University of New Mexico, Albuquerque, New Mexico.

9. Clifford, D. W., "The Impact of the Total Lightning Environment on Aircraft Flight Control Systems," presented at the 1978 IEEE International Symposium on Electromagnetic Compatibility held in Atlanta, Georgia, 20-22 June.

10. Uman, M. A., et al, "Electric Field Intensity of the Lighting Return Stroke," Jo. Geo. Research, Vol. 78, No. 18, June 1973.

11. Cianos, N., and E. T. Pierce, A Ground Lightning Environment for Engineering Usage, Stanford Research Institute, Technical Report No. 1, Project 1837, August 1972.

12. Uman, M. A., et al, "Currents in Florida Lightning Return Strokes," Jo. Geo. Research, Vol. 78, No. 18, June 1973.

13. Robb, J. D., Lightning and Transients Research Institute, St. Paul, Minnesota Personal Communication.

PROTECTING FACILITIES AND EQUIPMENT FROM INDUCED LIGHTNING AND VOLTAGE SURGES ON THE A.C. POWER LINE

RICHARD ODENBERG
Senior Staff Engineer
at Transtector Systems a
Division of Konic International Corporation
Monterey Park, California 91754

BIOGRAPHY

Richard Odenberg received his B.S. degree in applied physics in 1960. He is presently a Senior Staff Engineer at Transtector Systems and has been since 1968. During the last twelve years, he has been designing, developing, and applying solid-state, voltage protection systems. He holds several circuit patents in the area of solid-state voltage surge suppressors. He is a member of two IEEE Working Groups on Voltage Protection Devices for the A.C. power line. Prior to 1968, he worked in the aerospace industries at Space Technology Labs (TRW Systems). His work involved design and test of space power, instrumentation, and control systems.

ABSTRACT

A.C. line protection (secondary arrestor) has become the most difficult problem in interfacing electrical energy with the electronic equipment it powers. Although a number of filtering systems are a regular part of most electronic equipment, none have provided adequate protection against lightning and A.C. line transients.

1. A general discussion of components, circuits, and systems protectors, and how they apply to the A.C. power line.

2. Six major considerations for electronic equipment and facility protection.

3. A description of what IEEE/SPD Working Groups are doing about standardization of A.C. power line suppressors and a guideline on surge voltage in the A.C. power circuits.

4. Details in selecting and placement (at the entrance or inside the facility) of protecting equipment based on sensitivity of equipment to be protected and energy levels in the lightning transients or power line surges.

INTRODUCTION

A computer mysteriously dumps logic; a circuit board fails; a telecommunication microprocessor fails or acts erratically; a power supply burns up. What causes these occurrences? High-speed, overvoltage transients are one of the least understood, yet most troublesome of problems which plague the electrical/electronic engineer and service technician. Actually, the problem has existed ever since electrical power has been transmitted from one place to another, but the recognition of the problem and its seriousness has only come about since the development of solid-state microelectronics.

As their function has become more sophisticated, faster, and precise, components have become smaller and more prone to disruption, destruction, and erratic behavior. Any major deviation in power can disrupt or destroy a chip. To this problem we suggest that a solution must be very fast at keeping the excess energy to a minimum (clipping), and it must do what it does (suppress) at a level which prevents any excessive energy from being strong enough to destroy or disrupt. In the computer, this condition can create mislogic because some of the excess energy can disrupt logic circuits as well as destroy or disrupt memory programs. In either case, computer malfunction or breakdown, spikes and surges cost money and time.

Solid-state components generally are

engineered to function efficiently for a long lifetime of service. If voltages are constant and there is no variation, they may last forever (theoretically). In theory, there are only three causes for solid-state component failure: heat, vibration, and high-speed, overvoltage transients. Most systems are engineered to be either air-conditioned or ventilated sufficiently to eliminate heat failure. Most systems are vibration isolated, but few systems have been engineered to adequately handle high-speed, overvoltage transients.

What happens to solid-state, microelectronic components when they are attacked by overvoltage spikes? You might try and think of a wall as a form of solid-state device. The wall is basically solid. The wall is there to separate one space area from another. Try to think of an overvoltage spike as a demolition worker with a sledgehammer, chisel, and crowbar. Also, try to think of energy as B.B.'s, golf balls, tennis balls, or basketballs. Some forms of energy such as tennis balls or basketballs will simply bounce off the wall. Some such as golf balls or B.B.'s may make dents. This is the case with lower-intensity overvoltage variations (these can sometimes traumatize an electronic logic system). But, when the demolition worker begins pounding away with the sledgehammer, chisel, and crowbar, there is permanent damage wrought by his efforts. The gradual deterioration or erosive effect on solid-state components is just as destructive as this but takes place at a sub-microscopic level, maybe one ten-thousandth the diameter of a human hair.

When the demolition worker has pounded away on that wall enough, he breaks through and the wall collapses. After being chipped away at enough by high-speed, overvoltage spikes, solid-state components, like the wall, break down. Of course, if the demolition worker really wanted to be efficient, he would use dynamite and, as quick as a flash of lightning, would break down the wall. Such is the case with very intense overvoltage spikes, lightning surges, inductive motor and SCR switching surges.

In analyzing the problem, there are three basic conditions of solid-state components after being attacked by high-speed, overvoltage spikes: TRAUMA, EROSION, and BREAKDOWN. In the case of breakdown, the analysis is simple. The component no longer is working. In the case of erosion, eventually the component will test as being unreliable, a factor usually attributed to age. Traumatized systems are not so easily identified. A computer or telecommunication system may go into an erratic behavior mode which could last from microseconds to months. Sometimes a traumatized system is thought to have software problems when the real problem is spike-related. When analyzed, however, the component parts may not show up as failing or unreliable. Oddly enough, when spiking is eliminated to these systems which have become traumatized, they seem to stabilize and act fully functional again.

Solid-state, microelectronic components are becoming a more common part of everyone's daily life in manufacturing, data transmission, data acquisition, communications, health care and research, finance, etc. Components have become so minute and delicate that as many as 20,000 or more transistors and resistors are compressed into a space of approximately 1/4" x 1/4". And, a computer may have hundreds of these elements. Anytime a new building is being erected in the future, it will be necessary to consider a rigid electrical requirement which will accommodate future generations of yet undeveloped computers, microprocessors, and telecommunication equipment.

What are the many causes of high-speed, overvoltage transients, spikes, and surges? If you can imagine any shunting or switching activity, no matter what the cause, you've got half the answer. Lightning, power company switching, inductive motor start-ups, i.e., air conditioning systems, elevators, SCR switching, arcing contactors, X-ray machines, arc welding, and even circuit breakers tripping. Heavy inductive loads which may be nearby your power lines or even your neighbor's power lines...the causes are so many and so varied that they are only limited by your ability to imagine them.

How does one identify the problem? One method of identifying the problem is to monitor the power lines at the problem location. There are few very fine power line monitors which will be fast enough to record spikes, but one should be cautious to have up-to-date equipment for monitoring. Traditional equipment used by power companies is not fast enough to catch spikes. Another area for caution is that even though you monitor the power lines which are to

feed your facilities in question, you may not monitor long enough to cover all contingencies. The major consideration has to do with what the future holds in store. Equipment requirements for the future will be getting more critical, and the quality of the power being supplied by power companies will be getting worse.

Another method of identifying the problem is through laboratory evaluation of failed parts. Yet another method is deductive reasoning after the fact, i.e., component failure has taken place or logic disruption has occurred. But, with this particular failure or disruption, there has not been a blown out fuse or a tripped circuit breaker. One could, therefore, safely conclude that whatever caused the failure had to be caused by something very fast and high-powered, and that is the nature of a spike. Apart from someone deliberately causing a failure, one must conclude that a spike caused the damage or disruption under these circumstances.

By definition, a surge or spike is a high-amplitude, overvoltage variation of short duration. In the case of the spike, the culprit can rise to very high levels, 5600 volts or more over line voltage, and disappear in less than one microsecond. As little as one nanojoule (1×10^{-9}) of energy applied to the I.C. can cause a shutdown of operations. Figure 1.[1]

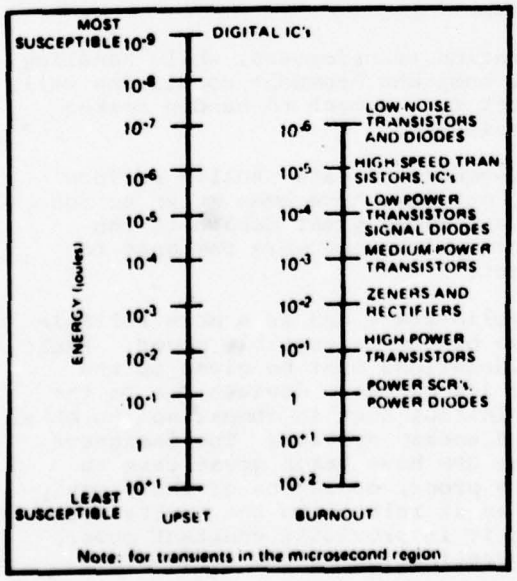

FIGURE 1. UPSET AND BURNOUT ENERGIES FOR VARIOUS SEMICONDUCTORS

With prospects of integrated circuit technology becoming even more delicate and power problems and demands exceeding the limits of what a power company may be able to supply properly, one is left with the task of recommending a proper expedient for new and old electrical systems alike. What, then, does one look for to protect and prevent the contamination of delicate electronic equipment and computers?

SIX MAJOR CONSIDERATIONS FOR ELECTRONIC EQUIPMENT PROTECTION

1. One of the primary characteristics of a suppression system is speed of reaction time, i.e., how fast does the system sense and destroy or neutralize the spike? In order to be effective in preventing the disruption of logic, a system must react and suppress in 50 nanoseconds or faster.

2. The second most important characteristic of an adequate suppression system is its clamping level, i.e., the peak voltage which will be allowed to pass through the system with the suppressor active. For 120 VAC power systems, a maximum allowable level is usually $\leq$ 50%, i.e., turn on at 200V peak with a maximum suppression voltage of 300V peak. This gives a 1:1.5 clamping ratio which is 50%.

3. Another important characteristic is the energy suppression capability (joules) of the suppressor system--how much of the transient energy the suppressor can handle. To be effective, a system must be able to handle as much excessive energy as may come in a given application. A central city office building may be just as troublesome as a rural industrial site. In high lightning areas, one should have as much protection as budget will allow. In industrial environs, requirements vary according to application, but one should allow for the worst of all possible contingencies.

4. Another major consideration in the selection of a transient suppression system is how it affects the continuity of electrical energy while it is performing as a suppressor. Does it cause any distortion of the sine wave, short the line, or cause discontinuity, for however brief a period, in the flow of energy?

5. Perhaps the next most important consideration is whether or not the system is self-resetting, automatic, and self-maintaining.

6. The final consideration is product reliability. Will the system work when you need it to work? Solid-state systems have, to date, been the most reliable and durable yet developed. Within the limits of their engineering specifications, they may be capable of easily allowing the equipment they are assigned to protect to grow obsolete long before either would otherwise wear out.

Once all six factors have been considered, one must look at where the voltage will be at maximum power dissipation. For example, dissipating 100 joules, a Transtector Transient Suppressor (ACP2000) will not allow the voltage to exceed 300 volts peak. Where a metal oxide varistor would dissipate 100 joules, the voltage would rise to over 1000 volts peak. If this happened on 120 VAC service, your equipment would fail using the metal oxide varistor.

WHAT TYPES OF TRANSIENT SUPPRESSORS ARE AVAILABLE?

1. Carbon blocks and spark gaps are the earliest forms of transient suppressors and may work well for nonelectronic or nonsolid-state, microelectronic applications. They can handle large quantities of energy but have a high clamping ratio, relative slow response, and "crowbar" the A.C. line.

2. Thyristors and resistors, more sophisticated forms of suppression, handle very high energy but are too slow to be effective and short the A.C. power line like the gas tube does.

3. Gas-discharge tubes are effective on some communications equipment but not for solid-state, microelectronic applications. Similar problem as 1.

4. Metal-oxide varistors (MOV's) are a recent development which may be used on some solid-state equipment but are not good for computer and solid-state, microelectronic applications. Although the speed with which a varistor operates may be nearly good enough, the peak voltages achieved are not generally low enough to prevent disruption or breakdown of solid-state, microelectronic elements. A varistor's breakdown characteristics are less than desirable for many applications. There use on A.C. power lines without some limiting impedance is extremely dangerous due to the ability to explode when overstressed. Their applications are contactors, relays, solenoid coils, and in some places on the secondary of power supply transformers. In practice, their life expectancy is very short.

5. The silicon, solid-state circuit protectors are generally the fastest and most reliable of all systems for long life, speed, and durability. Variations in circuit design make this method of transient suppression (no gas tube or MOV's) the most reliable and fastest on the market by adding high-speed circuitry to the system with high energy capabilities. Systems designed with gas tubes and MOV's, with a series inductor, initially appear to be adequate, but a great number of failures of these systems have been seen in the field.[2] The reason for this is that when the gas tube finally fails, it usually blows a fuse in the gas tube line producing a very large inductive kick across the inductor which fails the MOV and the equipment. In practice, the initial cost may be low, but the reliability and life is also low.

6. Other forms of transient protection, which are not necessarily transient suppressors, include isolation and regulation transformers, motor-generator sets, and UPS (uninterruptible power systems). The main design function of this category is to electrically isolate and/or provide a continuous flow of power. These systems do have their limits and may not deliver the proper regulation suppression fast enough.

Isolation transformers may reach a saturation level and actually accelerate a spike.

Regulation transformers, while handling power bump and brownout conditions well, are not fast enough to handle spikes (transients).

Motor-generator sets usually perform well, but some have been known to run away and cause great damage to the systems which they were designed to protect.

The solid-state UPS is a more reliable source of uninterruptible power. Basic considerations must be given to the economics of these devices due to the high initial cost in comparison to other stored energy systems. The designers of the UPS have taken great care to insure proper operation of their equipment as it relates to the device for which it is providing constant power. An investigation of the solid-state

circuitry in the control portion of the UPS will show very careful consideration given to providing bypass switch-gear that allows an electrical noise-free transfer from the UPS to the backup power system in case of UPS failure. The control portion of the UPS is made up of solid-state integrated circuits. Transients cause damage to these circuits due to the fact that the UPS is fed by an unfiltered A.C. power line. Additionally, the alternate power source is usually the same unfiltered A.C. power line that feeds the UPS. In the case of UPS failure where the UPS is interfaced with computer hardware, the switch to alternate power allows for a direct pathway by which transients will enter the computer circuitry. It should be noted here that it is not necessary for the UPS to fail before the computer is connected to the unfiltered A.C. power line. The static load transfer switch-gear is devised from noise-free electronic switches (SCR's). These SCR's can be caused to misfire by transients, thus resulting in an unnecessary and potentially damaging transfer to the unfiltered A.C. power source.

Cost considerations are part of making a selection as well as technical ability to perform. Side-by-side comparisons will reveal that even though the solid-state systems appear to cost the most initially, they are the least expensive when the value of the systems being protected is considered as well as the cost of repair and downtime to the systems being protected. Value received, in this case, is far more important than the initial outlay of monies for protection.

When dealing with a computer installation, the primary considerations are the accuracy of data on the computer as well as the operational uptime, as opposed to downtime costs, plus the cost of repair and replacement. With many computers costing over $1,000,000, it's easy to understand the importance of reliable protection. Literally thousands of man-hours can be lost in an instant as a spike does its dirty work. Logic errors and broken down computers are but two of the many problems which develop as a result of spikes. In telecommunication/radar tracking systems, misfired logic can cause outage or worse errors which can cause air crashes.

It is clear that there is an enormous need for a dynamic transient protection device that will identify these high-speed overvoltages and shunt them to ground. This device must incorporate both an extremely fast response time in order to provide adequate protection for logic and memory circuitry as well as a design that allows simultaneous transient suppression on all phases of the power source.

Transtector Systems has had a long-standing reputation as the world's leader in solid-state, transient protection systems. Their use of silicon junction, solid-state devices in a multiple stage circuit has proven to be totally successful in applications of secondary arrestors for computers and all solid-state electronic equipment.

IEEE/SPD WORKING GROUPS[3]

The SPD (Surge Protection Devices) sub-group of IEEE society is divided into several working groups. The writer is participating in two sub-groups. The first is sub-group (3.3.6.3) solid-state devices. This sub-group has the responsibility to write specification standards for semiconductor devices. The three standards are:

1. Metal-oxide varistors.
2. Silicon avalanche suppressors.
3. Two-terminal, multiple component devices.

When these three standards are completed, the "end user" will be able to compare, using common definitions and test circuits, between several suppressor manufacturers and determine which suppressor is the best to fit his needs. It will offer methods of comparing reliability of different suppressors within a particular category.

The second sub-group (3.4.4) is presently writing a guideline entitled, "Guideline on Surge Voltages in A.C. Power Circuits Rated Up To 600V," (P587.1/D1) dated October, 1978. The first draft has been completed.

The scope of the guideline primarily addresses lightning and surges appearing at the A.C. power entrance to facilities and residential buildings. It covers all A.C. voltages up to 600V.

It is to complement such standards as IEEE 472, "Guide for Surge Withstand Capability (SWC) Tests," and IEEE 28, "Standard for Surge Arrestors for A.C. Power Circuits," covering primarily the

utilities environment.

This guideline intends to present a practical proposal for the selection of voltage and current tests to be applied in evaluating the surge withstand capability of equipment connected to these power circuits, primarily in industrial and residential applications. It provides how to proceed from the environment description to the selection of "standard" test waves.

The surge voltages considered are those exceeding twice the peak operating voltage and having duration ranging from a fraction of a microsecond to a millisecond. Voltages of less than twice the operating voltage are not covered here. In addition, transients of longer duration resulting from power company surges are not considered in this guideline.

Other subjects discussed in this guideline are listed below:

1. The origin of surge voltages.
2. Occurrences and voltage levels in unprotected circuits.
3. Wave shape of representative surge voltages.
4. Energy and source impedance.

The guideline group has proposed the following approach because of the wide range of possible source impedances and the difficulty of selecting a specific value. Three broad categories of building locations are proposed to represent the vast majority of locations, from those near the service entrance to those remote from it. The source impedance of the surge increases from the outside to locations well within the building. Open-circuit voltages, on the other hand, show little variation within a building because the wiring provides little attenuation. Figure 2 illustrates the application of the three categories to the wiring of a building.

A. Outside and Service Entrance
Service drop from pole to building entrance. Run between meter and distribution panel. Overhead line to detached buildings. Underground lines to well pumps.

B. Major Feeders and Short Branch Circuits
Distribution panel devices. Bus and feeder systems in industrial plants. Heavy appliance outlets with "short" connections to the service entrance. Lighting systems in commercial buildings.

C. Outlets and Long Branch Circuits
All outlets at more than 10m (30 ft.) from Category B with wires #14-10. All outlets at more than 20m (60 ft.) from Category A with wires #14-10.

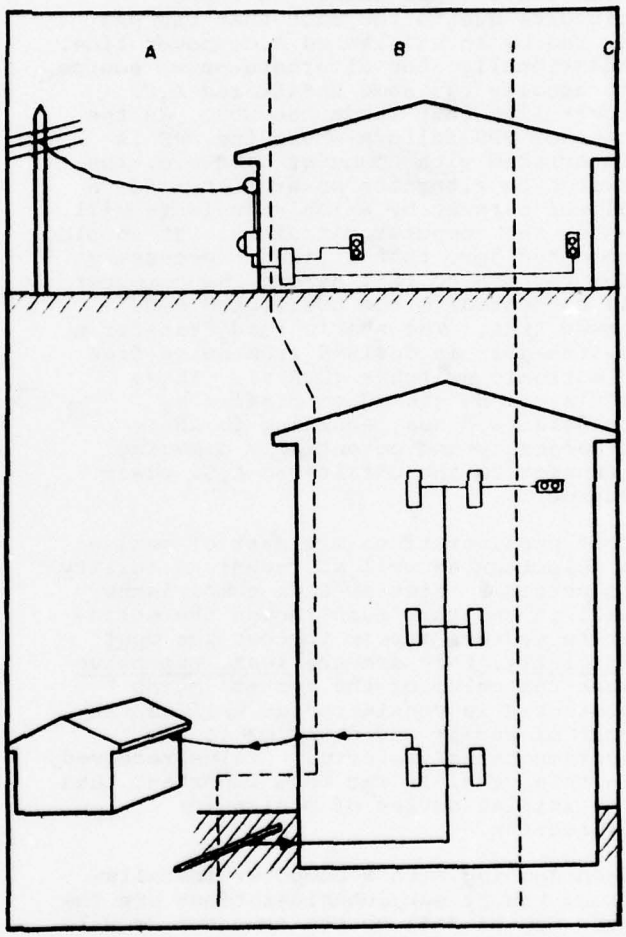

FIGURE 2. LOCATION CATEGORIES

Table I, "Matrix of Surge Voltages Versus Facility Location," shows open-circuit voltages and short-circuit currents for each of the three categories. The energy deposited in a 500V suppressor has been computed and is shown for each of the categories.

Location	Maximum Impulse	Energy In a 500V Suppressor (Joules)
A. Outdoor and Service Entrance	10kV 1.2 x 50 µs 10kA 8 x 20 µs	150
B. Major Feeders and Short Branch Circuits	6kV 1.2 x 50 µs 3kA 8 x 20 µs	40
	6kV 0.5 µs x 100kHz 500 A short circuit	2
C. Long Branch Circuits and Outlets	6kV 0.5 µs x 100kHz 200 A short circuit	0.8

TABLE I. MATRIX OF SURGE VOLTAGES VERSUS FACILITY LOCATION

The values shown in the table represent the maximum range, corresponding to an "High Exposure" situation. For less exposed systems, or when the prospect of a failure is not highly objectionable, one could specify lower values of open-circuit voltages with corresponding reductions in the currents.

SUMMARY

In conclusion, the major factors to be considered for facility and equipment protection are:

1. Response time is to be in the low nanosecond region.
2. The voltage suppression and clamping ratio must be low enough to protect the equipment at the required power level (Reference 3).
3. The power suppression capability is to be large enough to handle the application with concern for what happens if the device fails.
4. No distortion of the sine wave when the suppressor operates.
5. Automatic or resettable operation is important for human life applications as well as maintenance and cost factors.
6. Reliability is most important when human life is at stake and for low-cost maintenance and operation.

REFERENCES

1. Intelcon Rad Tech, Intel-RT-8090-013, September, 1974.
2. Transtector Systems Test Report and Analysis, 78AB-LEA-2, September, 1978.
3. IEEE/SPD Working Group (3.3.4) Guideline No. P587.1/D1, October, 1978, FIRST DRAFT.

INITIAL CURRENTS ASSOCIATED WITH LIGHTNING TRIGGERED BY A ROCKET

RONALD B. STANDLER
Department of Electrical Engineering
University of Florida
Gainesville, FL 32611

CHARLES B. MOORE
Department of Physics
New Mexico Institute of
Mining and Technology
Socorro, NM 87801

BIOGRAPHIES

Ronald B. Standler is a visiting assistant professor of electrical engineering at the University of Florida. He received his B.Sc. in physics in 1971 from the University of Denver and the M.Sc. and Ph.D. degrees in physics in 1975 and 1977 from the New Mexico Institute of Mining and Technology. He does research on the physics of lightning, electronic instrumentation, and atmospheric electricity.

Charles B. Moore is a professor of atmospheric physics at New Mexico Institute of Mining and Technology. He does research principally on cloud electrification processes, precipitation formation, and balloon and airplane instrumentation for atmospheric physics measurements.

ABSTRACT

We measured the charge transferred between ground and a wire-trailing rocket that triggered lightning. The current has two kinds of behavior: there is a current which increases linearly with time during the 2.1 seconds before the lightning strike. Superimposed on this smooth current is a series of 18 pulses each of which transfer between 4 and 200 μC of charge during a period of less than a few milliseconds. The amount of charge transferred by the six largest pulses is approximately described by an exponentially increasing function of time. As the rocket ascends the electric field near its nose will increase due to the enhancement of field about an elevated, grounded conductor. When the field at the nose attains the breakdown field strength, corona discharge will produce space charge which limits the field at the rocket's surface to the breakdown value. As the rocket continues to rise the increased enhancement of the field near the rocket causes the corona discharge current to increase. We think the linearly increasing current that we measured is corona current. The current pulses probably represent streamers which propagate from the rocket to the surrounding air. As the rocket rises, and the field strength near it increases, the streamers will tend to propagate farther and transfer more charge. We think the last streamer developed into an upward propagating lightning.

INTRODUCTION

Launching wire-trailing rockets toward a thundercloud is a proven technique for triggering lightning (Newmann, et al., 1967; Fieux, Gary, Hubert, 1975). We describe here our measurement of the charge transfer between ground and a rocket which triggered lightning.

INSTRUMENTATION

We launched modified "ENTAC 58" rockets from a mountain ridge near Langmuir Laboratory in central New Mexico. These rockets were originally designed for military anti-tank use: the gunner guided the rocket to its target by sending electrical signals through two 0.26 mm diameter steel wires which unwound from a bobbin inside the rocket. We modified the rocket for our application by gluing the fins in a fixed position and by replacing the warhead with an aluminum nose 13 mm in diameter, 140 mm in length whose tip was fashioned into a hemispherical cap. We launched the rockets at a 68° elevation angle so we expect their upward speed was somewhat less than the 80 m s^{-1} value specified for level flight.[3] A rocket was launched when the surface electric field approached the value at which lightning had occurred during several previous local discharges.

We isolated the launcher from earth with plastic blocks of approximately 5 cm thickness. We connected the rocket's wires to ground through a 0.5 ohm wirewound resistor and integrated the voltage across this resistor. The complete circuit is shown in Fig. 1. In this way we were able to measure the charge that flowed between the earth and the rocket. The rocket current integrator output was recorded on a CEC oscillograph recorder with galvanometers with a constant response (within ± 5%) from DC to at least 140 Hz. We used the same oscillograph to also record the outputs from an electric field change meter

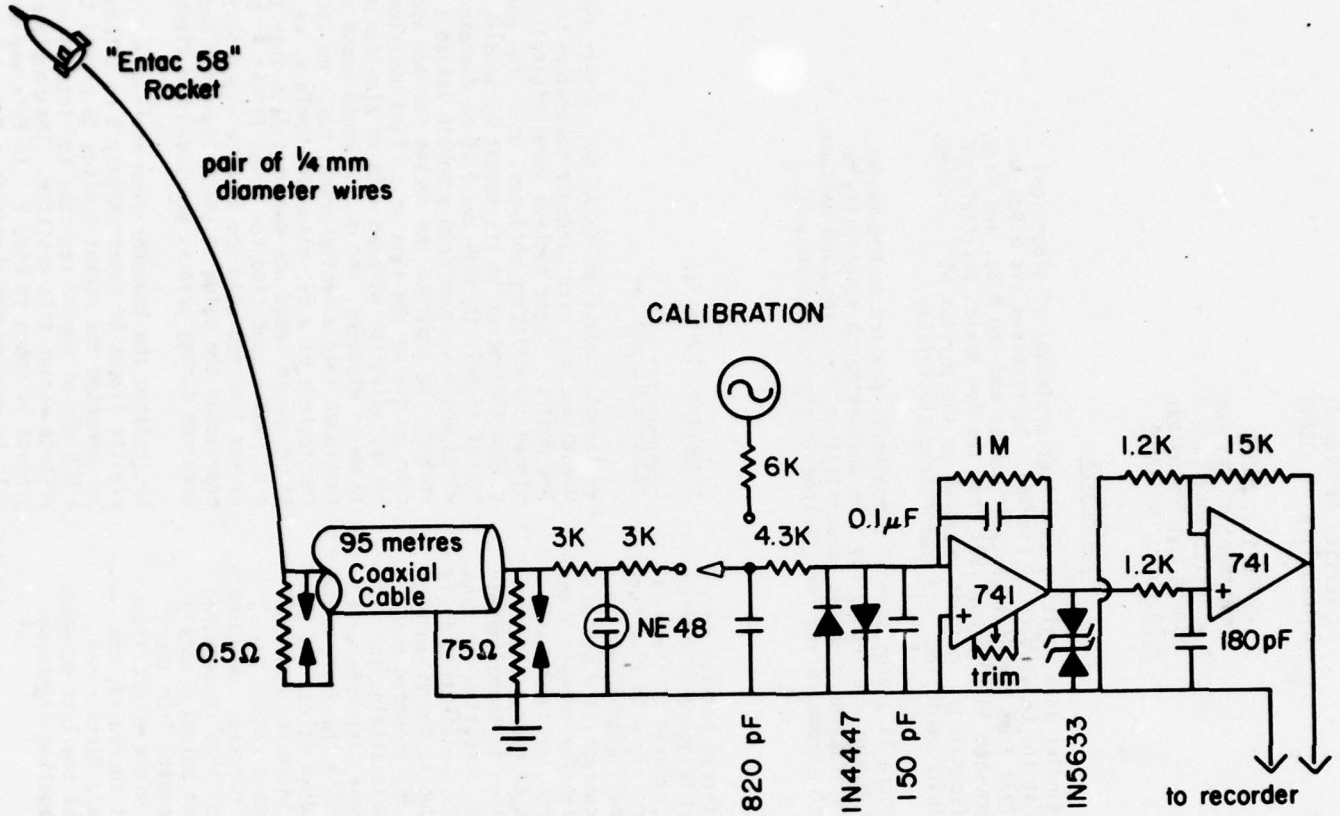

Figure 1. Circuit digram for measurement of charge transfer between rocket and earth. The rocket launcher was isolated from local ground by plastic blocks of a least 5 cm thickness.

(located 60 m southeast of the rocket launcher), a field mill (located 120 m south of the rocket launcher), and a nearby microphone to detect thunder. We digitized the original record to a resolution of 10 milliseconds and 3 millivolts out of the integrator. The presence of the resistor in parallel with the integrator's feedback capacitor makes the integrator's output voltage proportional to the low frequency components of the input current. We removed this effect during the preparation of the plots for the charge transfer between rocket and earth and the electric field by use of the transfer functions of the feedback loop of the integrators.

OBSERVATIONS

We launched a rocket at 11 h 11 m 16.2 s MST on 20 August 1974 when a thundercloud was above our laboratory. Several eyewitnesses reported that the rocket was struck by lightning shortly after its launch. Plots of the electric field at ground level, the deconvoluted charge transfer between rocket and ground, and average current between rocket and ground are shown in Fig. 2.

Examination of the record shows that the rocket current rose above the 0.05 mA threshold for detection at about 5.4 seconds after launch. The current generally tended to increase linearly with time during the next 2.1 seconds. During this time the electric field at the ground decreased. From 6.7 to 7.5 seconds after launch there is a series of 18 discontinuities in the record of the rocket current integrator. These discontinuities represent rapid changes in charge transfer due to current pulses. A plot of the charge transferred during these pulses is shown in Fig. 3. The six largest pulses each transferred an amount of charge which can be described approximately by $\Delta Q = 6.3 \times 10^{-5} \exp(1.19\ t)$ where ΔQ is in coulombs and t is in seconds after the first pulse. The reported value of the charge transferred in the pulses is probably an underestimate because the rocket current integrator circuit was not capable of responding to pulses of duration less than 10 μsec.

At approximately 7.5 seconds after launch the electric field data shows an abrupt change due to lightning at the same time (within the 10 millisecond resolution of our record) as the rocket current integrator abruptly saturated. Hence we have no measurement of the charge transferred by this lightning stroke. The person who fired the rocket from a protective shelter about 10 metres from the launcher reported that the launcher was covered with a white glow, so not all the lightning current passed through our measurement circuit. The output of the field change meter was saturated for 60 ms during the lightning. The output of another field change meter, less sensitive and farther from the rocket than the one used to produce the electric field record shown in Fig. 2, varied rapidly during the lightning. This variation was too rapid to produce a discernible trace on the photosensitive paper in our recorder. The bandwidth of the field mill was too narrow to respond to rapid field changes. We do not have a continuous record of the electric field during the lightning. The value of the electric field at the ground 120 metres from the launcher immediately after the lightning is more negative than -15 KV m^{-1}.

DISCUSSION

We interpret the linear increase in rocket current from 5.4 to 7.5 seconds after launch as corona current from the rocket and its wires. The electric field at the top of an elevated and grounded conductor is enhanced by the shape of the elevated structure. As the rocket ascends we expect the electric field strength at the nose of the rocket will increase approximately linearly with altitude. When the field at the nose exceeds the breakdown field strength of air, about 2000 kV m^{-1} at this mountain top laboratory, corona discharge will produce a space charge which will limit the field strength at the nose. However, the space charge layer continually needs to be replaced since the rocket is moving. This process makes the rocket's corona current larger than the corona current of a stationary structure of the same shape. The decline in the electric field at the ground, shown in Fig. 2, is owing partly to the shielding effect of the elevated, grounded wire near the field change meter and partly to the emission of positive space charge from corona discharge from the rocket.

We believe the current pulses represent positive streamers which propagated from the rocket-wire system to the surrounding air. Since the field near the rocket's nose is enhanced by the elevation and curvature of the surface, we expect that streamers propagated a short distance in the enhanced fields, but terminated a few centimetres from the rocket. As the rocket ascended, the field strength near the rocket increased and the streamers propagated farther and transferred more charge before they died. We think the last streamer developed into the lightning stroke that was seen. We estimate the rocket's altitude was between 300 and 500 metres when the lightning occurred. The rocket was still rising in the clear air below the thundercloud when the lightning occurred.

Unfortunately there are no photographs of this lightning stroke and the eyewitnesses who observed branching did not notice the direction, so we can not determine whether the lightning was upward or downward propagating. However, records from a microphone 60 metres from the rocket launcher show the thunder amplitude was slightly less than that from lightning 2 km away. Weak thunder follows upward propagating lightning(McEachron, 1939) because there is no return stroke with rapidly changing current (Uman, 1969).

We think the weak thunder recorded during our triggered lightning suggests that the lightning propagated upward from the rocket to the cloud. If this is true, the earlier current pulses shown in Fig. 3 may represent "unsuccessful streamers".

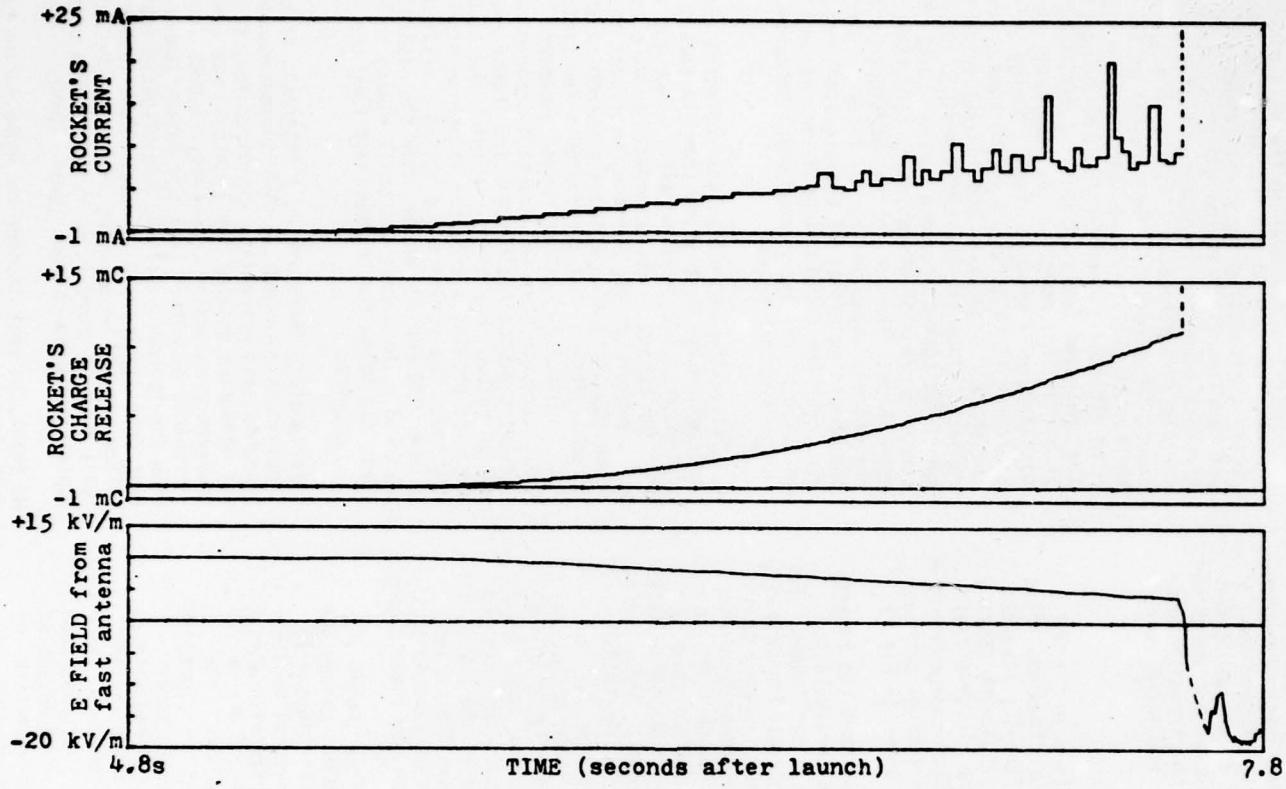

Figure 2

DECONVOLUTED DATA FROM ROCKET LAUNCHED AT 1111:16.2 MST, 20 AUGUST 1974

The charge transferred between rocket and ground as a function of time (middle plot), the average current that flowed between rocket and ground in time intervals of about 20 milliseconds (upper plot), and the electric field at the ground 60 meters from the rocket launcher (lower plot).

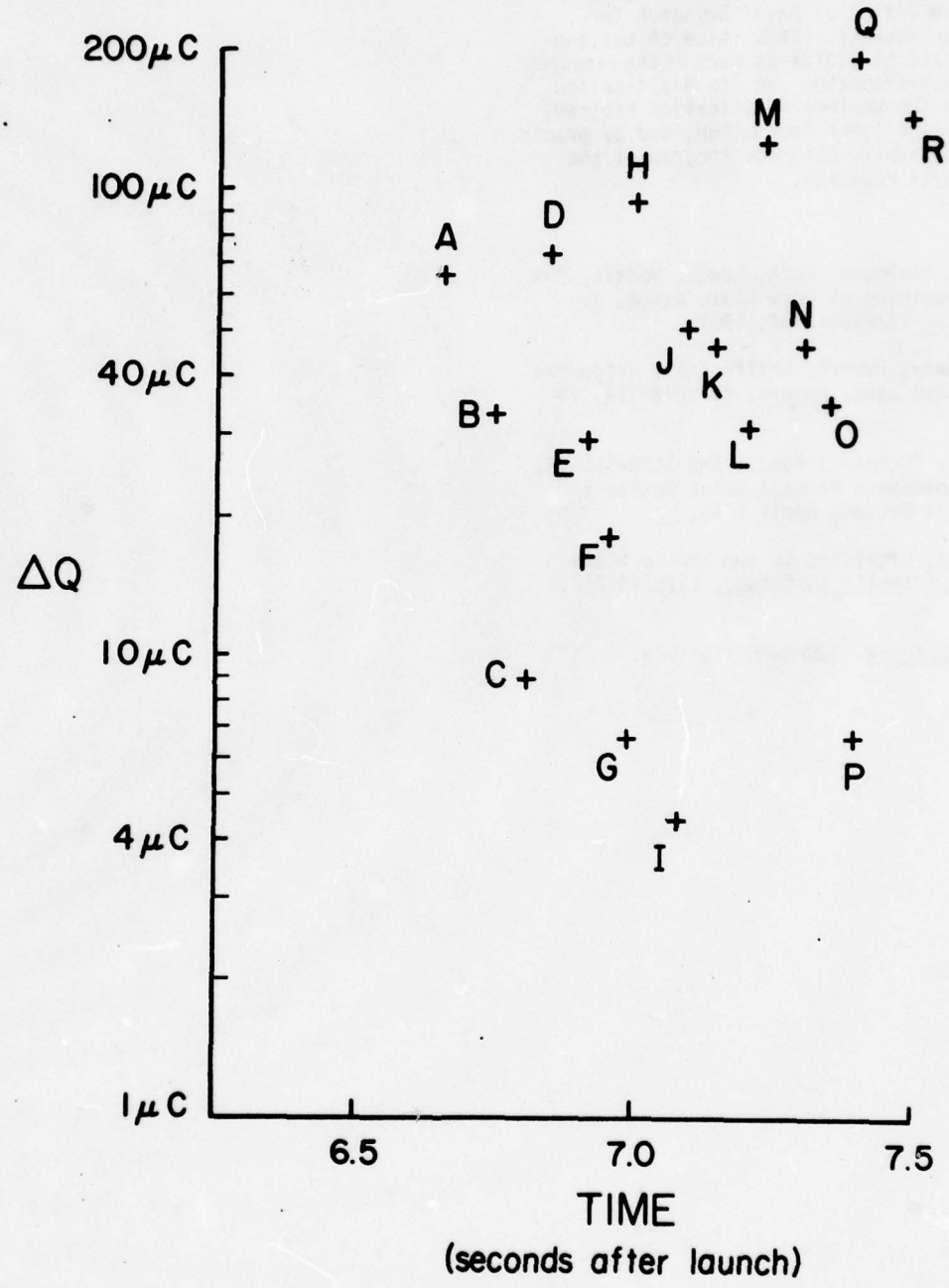

Figure 3. Charge transferred per current pulse vs. time from launch. The first pulse is "B", etc., up to the eighteenth pulse: "R".

ACKNOWLEDGEMENTS

We thank Steven Hunyady and Jack Cobb for assistance in modifying the rockets and launcher and for firing the rockets. We also thank James Hughes of the Office of Naval Research for supplying the rockets. This research was supported by Grant GI-33372X as part of the research on Cloud Electrification and its Modification sponsored by the Weather Modification Program, RANN, National Science Foundation; and by grants from the Atmoshperic Sciences Program of the Office of Naval Research.

REFERENCES

1. Newmann, Stahmann, Robb, Lewis, Martin, Zinn, Triggered Lightning at very Close Range, J. Geophys. Res., 72:4761-4764, 1967.

2. Fieux, Gary, Hubert, Artificially Triggered Lightning above Land, Nature, 257:212-214, 18 Sept. 1975.

3. U.S. Army Technical Manual TM9-1400-455-12, Operator Maintenance Manual: Entac Antitank Guided Missile System, April 1963.

4. McEachron, Lightning to the Empire State Building, J. Franklin Institute, 227:149-217, 1939.

5. Uman, Lightning, McGraw-Hill, 1969.

LIGHTNING PROTECTION DESIGN OF THE SPACE SHUTTLE

M. S. Amsbary
Member, SPS
Space Systems Group
Rockwell International
Downey, CA 90241

G. R. Read
Member, IEEE
Space Systems Group
Rockwell International
Downey, CA 90241

B. L. Giffin
Member, IEEE
Space Systems Group
Rockwell International
Downey, CA 90241

BIOGRAPHIES

Ms. Amsbary is a Member of the Technical Staff in Avionics Systems for the Space Shuttle at Rockwell International. She received her B.S. in Physics from Montana State University in 1976 and joined Rockwell the same year.

Mr. Giffin is Supervisor of Avionics Systems and Electromagnetic Effects for the Space Shuttle at Rockwell International. He received his B.S.E.E. in 1944 and M.S.E.E. in 1946 from Oregon State University. Before joining Rockwell in 1952, he worked for Bonneville Power Administration, Pacific Transformer Company, and Allis Chalmers. At Allis Chalmers, he was in charge of Impulse Testing of High Voltage Transformers. His master's thesis was on a lightning detection for power transmission lines.

Mr. Read is a Member of the Technical Staff in Avionics Systems for the Space Shuttle at Rockwell International. He received his B.S.E.E. in 1956 from Oklahoma University and his M.S.E.E. in 1965 from the University of New Mexico. Before joining Rockwell in 1973, he spent four years in reliability engineering at Sandia Laboratories, ten years in Minuteman, Apollo, and F-111 electrical and project engineering at Rockwell, and three years in Skylab Electrical Power Integration at Martin Marietta. His master's thesis was on thermal battery response to pulse loads.

ABSTRACT

The Space Shuttle lightning design program evaluates direct effects for exterior mounted equipments and restrike probabilities. The prediction of indirect effects on critical circuits is the major effort. This effort involves predicting the internal electromagnetic fields, the energy levels induced in the cables, and the margins between component failure levels and induced energy levels.

INTRODUCTION

The Space Shuttle lightning protection design is based on the NASA criteria that requires the survival of the crew and vehicle in the event of a lightning strike during ascent or descent. The orbiter analysis and test program has been implemented to ensure compliance with this requirement for both direct and indirect effects from a lightning strike.

Shuttle lightning requirements are defined in JSC 07636[1] and impose the lightning waveform shown in Figure 1 as the design baseline. Models of the Shuttle were tested to determine the attach points for lightning in both ascent and descent[2]. These attach points are defined in the lightning criteria document[1] and were derived from tests as in Figure 2, which shows a picture of corona from the high stress points.

DIRECT STRIKE DESIGN

The design requirements for the orbiter to withstand the direct effects of lightning are the same as those required by an aircraft[1]. The orbiter has the advantage that only a small portion of its operations are at altitudes where clouds form and, therefore, the design implementation must consider the probability that the vehicle will not be exposed to lightning. Other environmental factors, such as wind stresses, could do as much damage and abort a flight as easily as lightning. Another important factor is that the orbiter is protected from some of the lightning environment by other elements of the Space Shuttle during launch.

The orbiter is protected by the external tank (ET), which extends 16.2 meters ahead of the orbiter nose. Also, the conductive nature of the solid rocket booster (SRB) plumes makes them the most probable entry point from the rear. Thus any direct strike involvement on an ascent would most probably be a restrike after striking the nose of the external tank and exiting the plume of the solid rocket booster.

Exposure time during a launch would be approximately 80 seconds, of which half might result in a full-scale lightning stroke of 200,000 amperes due to a cloud-to-ground stroke.

In the descent mode, the orbiter could be struck by lightning during a portion of the five minutes it is exposed to the lower atmosphere. This phase is the most probable for lightning involvement, since, with an unpowered vehicle, there is relatively little maneuvering ability. A storm could develop in the landing pattern area after commitment to the landing site.

To assess the proper lightning protection design, it is necessary to examine the protection of each entry point. The nose and leading edge of the wings are thermally insulated with reinforced carbon-carbon (RCC), which has been demonstrated to withstand a 200,000-ampere stroke with only minor damage[3]. The other attach points, the eyebrow, the vertical tail, and wing tips, are covered with reusable

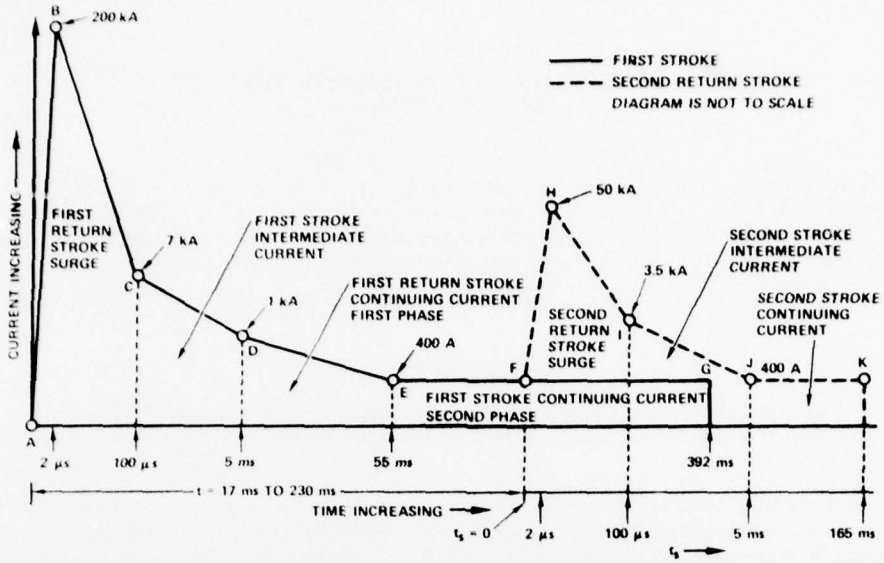

FIGURE 1. DIAGRAMMATIC REPRESENTATION OF LIGHTNING MODEL

FIGURE 2. CORONA FROM HIGH STRESS POINTS

surface insulation, RSI-900, as a thermal protection system (TPS). The TPS can withstand 50,000 amperes[4] with only surface-cracking damage, but with a 100,000-ampere strike, two or three tiles may be blown off (Figure 3).

The protection provided by the external tank and the solid rocket booster plumes lowers the risk of this damage. In the event of a severe strike and major tile damage, an extravehicular activity to repair the tile before reentry is a possibility. The TPS will have performed its function prior to any lightning

FIGURE 3. TPS TILE REMOVAL AT 100,000 AMPS

involvement during descent, and a strike at this time would not result in anything more than replacement of the tiles prior to the next flight.

Other external equipment that could be involved in a restrike of 50,000 amperes are antennas, ducts, reaction control jet nozzles, vent doors, star tracker doors, egress doors, payload bay doors, and windows[1]. These are exposed during both ascent and descent. The air data probe is on a hinged door that allows the probe to be extended during descent only.

The air data probe is similar to the B-1 bomber air data probe, which was tested at 200,000 amperes. Analysis has shown that it will meet the requirements of the Space Shuttle during the descent phase.

The antennas are all flush-mounted and are structurally designed to withstand the burning and distortion damage of a full 200,000-ampere strike. The antenna has a 500-volt

peak-coupled voltage design requirement, which is based on the antenna being bonded with a 2.5-milliohm bond to the orbiter skin. The antennas are mounted with a special corrosion-prevention bonding process, called the KA process, which lowers these resistances to measured values that range from 0.014 to 0.098 milliohm. This provides an adequate margin for a strike near the antenna.

The antenna radome material, polyimide glass, was previously tested[5] to determine the surface flashover distance versus the puncture distance. The test data showed the failure mechanism to be by surface flashover; thus the lightning current will not be directly coupled into the antenna receiver system. The effects of the TPS material on the surface of the radome material were neglected, since it very closely approximates the breakdown strength of air at sea level. This would tend to cause the strike to enter through one of the gaps between the tile surrounding the antenna, rather than to penetrate the tile and cause a surface flashover.

The RCS jets are designed to operate at temperatures of 2500°F but the slurry coating on the surface of the columbium nozzle is thin and its reaction to a lightning strike will be determined early in 1979. If the coating is removed, firing the jets could burn a hole in the nozzle, which could allow reentry heat inside the outer shell and cause serious damage to the vehicle.

The vent ducts have all been analyzed and found to be structurally strong enough to withstand a lightning strike without damage. Analysis has also shown that these ducts will not couple lightning current into any critical component that could be damaged and cause loss of the vehicle.

The vent doors, star tracker doors, egress doors, and payload bay doors have all been analyzed and bonded to ensure that a lightning restrike will not cause welding that would prevent operation of critical vents and doors.

The window glass was sample-tested[4] to determine the effects of lightning; the triple-layer glass construction is such that surface flashover would occur prior to failure of the glass itself.

The remaining exterior structures that have not been discussed are the orbital maneuvering subsystem (OMS) pods, which are mounted on each side of the vertical stabilizer. These pods contain all of the fuel tanks and controls for the OMS engines and the reaction control subsystem (RCS) jets. For strikes attaching to the tail, lightning current will flow under the removable pods, as they cannot be adequately bonded to the orbiter skin. The indirect effects will be discussed in the next section, but the structural configuration needs to be defined in order to analyze the direct strike effects. The fuel tanks are within 0.15 meter of the skin of the OMS pod. The skin is graphite epoxy and it was tested[6] in a configuration representing the pod design. A 50,000-ampere stroke punctured the skin (Figure 4) and evaporated the aluminum on one side of a double thermal blanket, but did not reach the hypergolic fuel tank. Therefore, the only concern is whether the hole will cause too severe a reentry heating problem.

Direct Strike Summary

Thus, by analysis and test, the direct strike lightning characteristics of the orbiter have been evaluated. The design is not impervious to lightning, but the risk has been minimized to the point where it is acceptable for the Shuttle program.

INDIRECT EFFECTS

The indirect effects analysis evaluates the electromagnetic fields, produced by either a direct strike or a near miss, that couple into the orbiter through apertures or diffusion. The analysis then determines the energy levels induced in the cables. To determine the internal fields, it is necessary to establish the skin current density and the resultant aperture fields.

Field Analysis

The maximum current density at each aperture in the fuselage was determined for the worst-case combinations of entry and exit points. For each case, the orbiter surface was mapped into a two-dimensional region and then the skin current density variation over the surface was found by the graphical mapping technique, assuming quasi-static behavior. The skin current distributes itself according to the Laplace equation, subject to proper boundary conditions[7]. The

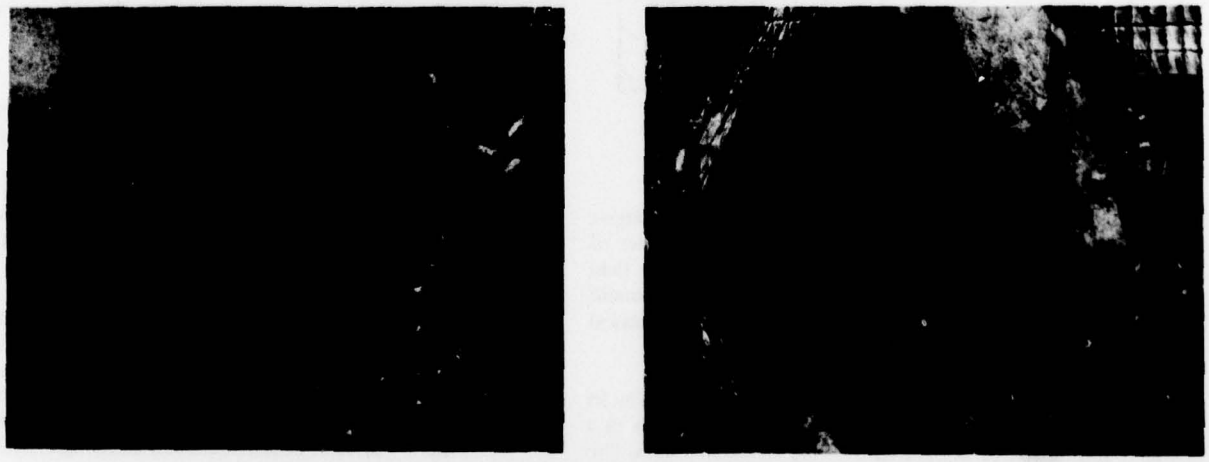

FIGURE 4. OMS POD GRAPHITE EPOXY TEST

current flow lines satisfy the Neumann condition (i.e., no current flows across the boundary) and the equipotential lines satisfy the Dirichlet condition (i.e., they are perpendicular to the boundary), forming an orthogonal set.

With the skin current density established at each aperture, the internally coupled fields due to each aperture were evaluated using Bethe's small-hole coupling theory[8]. The current flowing along the edge of a hole generates a magnetic dipole field in the hole that acts as a transmitting antenna. The field intensity falls off as $1/R^3$, where R is the far-field distance from the aperture (Figure 5). Fields from multiple

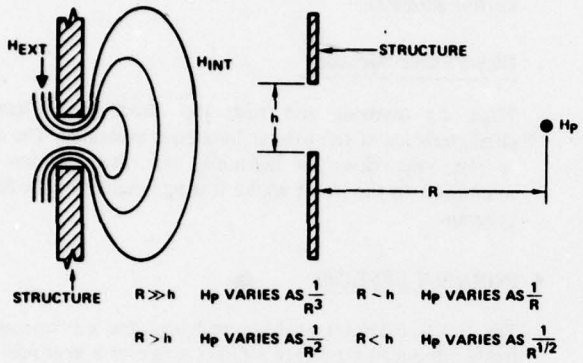

FIGURE 5. APERTURE FIELDS

apertures were added linearly, for a worst case estimate. The field data were prepared in the form of field intensity profiles (Figure 6) for ease of presentation and use.

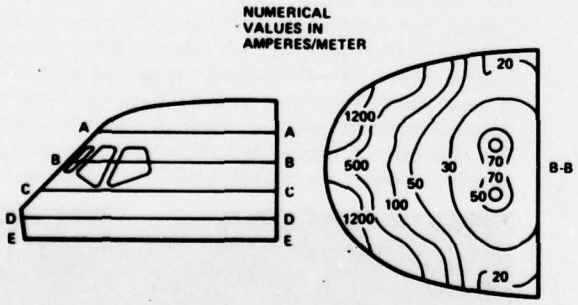

FIGURE 6. EXAMPLE OF ORBITER MAGNETIC FIELD MAPPING

Two areas were analyzed by different methods. The largest aperture, the electromagnetic gap around the perimeter of the payload bay doors, was analyzed by a modal field matching method. The approach was to obtain a resonant mode expansion of the coupled field in the cylindrical payload cavity.

The second area was the aft fuselage cryogenic fuel lines. In the launch phase, all likely attach points would result in a large proportion of the current flowing on the fuel lines. The aperture around the fuel lines could not be totally shielded due to cryogenic temperatures (-423°F or 20.3°K for LH_2), vibration, pressure, material properties, relative motion, separation, and other requirements. At these temperatures and lightning frequencies, the resistivity of aluminum decreases by more than three orders of magnitude, and the skin depth decreases to less than 0.2 mils (3.5×10^{-6} meters). A current-diverting curtain (Figure 7) was installed to make

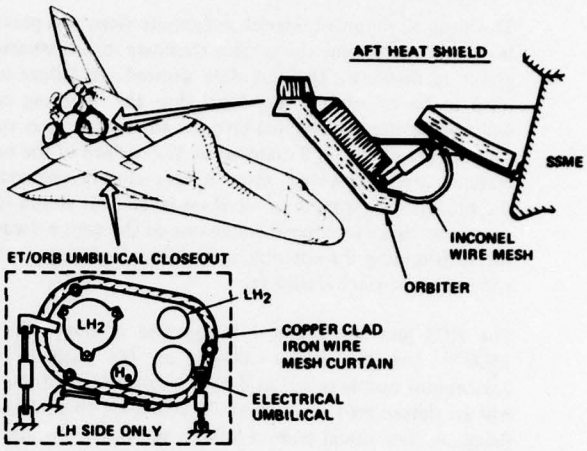

FIGURE 7. BONDING AND APERTURE CLOSEOUT

contact with the periphery of the fuel line and to present a low impedance path to the orbiter skin. The fields in the aft fuselage were based on the 99 percent estimated efficiency of this curtain. It is assumed that only 1 percent of the current on the fuel lines would not be diverted by the curtain, but would continue into the aft fuselage and out the engine thrust structure.

Potential problems due to high field levels in several areas were eliminated or minimized in the early design phase. An example is shown in Figure 7 for the aft heat shield. Other examples are:

1. The wiring harnesses in the wing-elevon gap were relocated forward of the rear spar (i.e., inside the skin) except for short exposed runs that were covered by plastic convoluted tubing with metallic overbraid.

2. All wires were routed as close to the skin as practical throughout the orbiter.

3. A wire mesh was included in the outer layer of the payload bay graphite epoxy doors. They were bonded at all available points and sliding contacts were installed across the expansion joints.

4. The wire harnesses inside the OMS pod graphite epoxy skin were constructed of shielded wire with an overbraid/foil wrap combination.

5. The flight deck wiring was protected by a combination of methods. The objective was to isolate the wiring and hardware volume from the crew volume. All of the primary and secondary structure is bonded. All panels are bonded to the secondary structure. The method and degree of bonding is a function of basic design and location. (Hinges, 360-degree peripheral bonding, mounting point bonding, wire-covered foam rubber for sealing joints and gaps, meters and switches bonded to panels, were some of the techniques employed.)

6. In the aft area of the flight deck, payload panel interchangeability considerations resulted in adding a metallic layer to the overhead observation window covers to totally close these apertures. The covers are used during launch and reentry phases and the windows are used on orbit.

Cable Analysis

Electromagnetic fields, described in the previous section, couple energy into the electrical circuits, producing voltage and current transients that could damage critical electrical equipment. The contribution due to the electric fields and diffusion-coupled magnetic fields can be neglected in the calculation of the voltage and current transients, which could upset or damage critical electrical equipment. This assumption has been verified by test during the Apollo-Soyuz Test Program (ASTP)[9]. Only the magnetic fields coupled through apertures make a significant contribution to the induced transient levels (Figure 8).

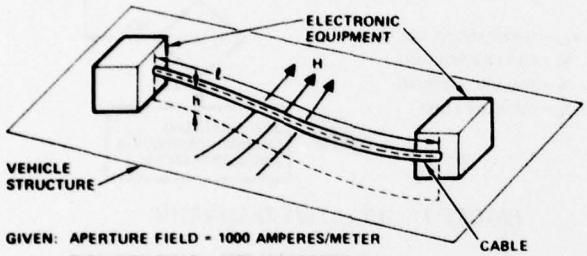

GIVEN: APERTURE FIELD = 1000 AMPERES/METER
DIFFUSION FIELD = 1000 AMPERES/METER
AREA = $\ell \times h = 1\ M^2$
VOLTAGE = K (AREA) $\left(\frac{\text{AMPERES/METER}}{\text{RISE TIME}}\right)$
APERTURE VOLTAGE = $1.26\left(\frac{1000}{2}\right) = 630V$
DIFFUSION VOLTAGE = $1.26\left(\frac{1000}{300}\right) = 4.2V$
CONCLUSION: DIFFUSION FIELDS CAN USUALLY BE NEGLECTED

FIGURE 8. SAMPLE VOLTAGE CALCULATION

The method used for determining the open circuit voltage (Voc), short circuit current (Isc), and self-inductance (L) of a wire above a ground plane is described in Appendix F to Ref. 1. A changing magnetic field linking a wire produces an open circuit voltage given by

$$Voc = \frac{d\phi}{dt} = \mu_o A \frac{dH}{dt} \qquad (1)$$

where

ϕ = the total flux linking the circuit in webers
$\mu_o = 4\pi \times 10^{-7}$ henry/meter, the permeability of free space
A = the area of the circuit loop in square meters (i.e., the length of the circuit times its height above the ground plane)
H = the magnetic field intensity in amperes/meter
t = the pulse time in seconds

The short circuit current is calculated using

$$Voc = L\frac{dIsc}{dt} \text{ or } Isc = \frac{1}{L}\int Voc\ dt \qquad (2)$$

where L has units of henries and Isc has units of amperes. An expression for the self-inductance of a wire over a ground plane is

$$L = 2 \times 10^{-7} \log_e \left[\frac{4h}{d}\right] \text{ henries/meter} \qquad (3)$$

where h is the height of the wire above the ground plane and d is the wire diameter.

For a worst-case analysis, a simple black box-to-black box analysis is done (Figure 8). Open-circuit voltages and short-circuit currents induced in the cable between the two boxes are compared with the voltage and current failure levels of all circuits within each box. The failure levels are calculated by NASA JSC using the method described in Appendix D to Ref. 1. If this initial analysis does not provide a sufficient safety margin, a more detailed analysis must be completed, as discussed later.

To simplify the transient analysis calculations, while still providing accuracy for a worst-case situation, several assumptions were made:

1. The orbiter was divided into several characteristic zones so that the magnetic fields could be mapped in each zone (Figure 9). The fields in each zone will vary according to the type of lightning strike and the attach points. The field used in all calculations for each zone was the maximum, regardless of the type of strike (Table 1).

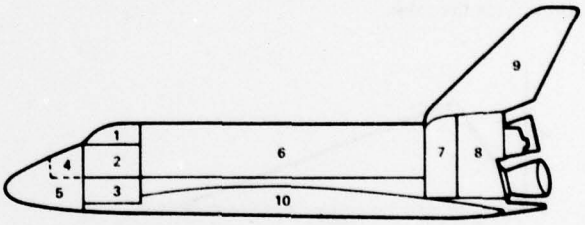

SHUTTLE ZONES

1 FLIGHT DECK	6 PAYLOAD BAY
2 CENTER EQUIPMENT BAY	7 AFT EQUIPMENT BAY
3 LOWER EQUIPMENT BAY	8 ENGINE COMPARTMENT
4 FORWARD TOP	9 VERTICAL STABILIZER
5 FORWARD CENTER	10 WING

FIGURE 9. SHIELDED ZONES WITHIN ORBITER STRUCTURE

2. The waveform of the internal magnetic field follows the lightning current waveform and is triangular. The induced voltage waveform is a square pulse, since it is proportional to the time derivative of the magnetic field, as in Equation (1) (Figure 10). The pulse width is defined as five microseconds in Appendix D to Ref. 1, based on the Apollo-Soyuz Test Program (ASTP) lightning test.

3. For all circuits crossing the orbiter interfaces to exterior equipment, the voltage waveshape is triangular, having a pulse width of 100 microseconds, with a two-microsecond rise time (Figure 10). It is proportional to the lightning current waveform, as Voc = Isc Z_T, where Z_T is the transfer impedance between the cable and its shield.

4. For convenience of calculation, each cable is divided into several segments, based on the field levels of the zones in

TABLE 1. MAGNETIC FIELDS IN DIFFERENT ZONES OF THE STRUCTURE

Zone	Maximum Aperture Coupled Field (amperes/meter)
1	1,200
2	10
3	1
4	100
5	100
6	75
7	200
8	600
9	1,000
10	30,000

which it is located and also on the height of the cable above the ground plane. The open circuit voltage and the self-inductance is calculated for each cable segment using Equations (1) and (3). These are then summed to determine the total open circuit voltage and the short circuit current (Equation 2) for the cable.

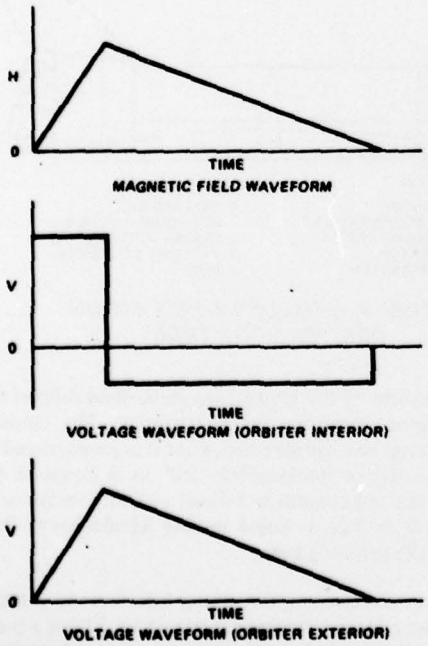

FIGURE 10. VOLTAGE RESPONSE TO MAGNETIC FIELD

NASA JSC has calculated component damage levels for all Lightning Criticality I circuits. These are then compared to the sum of the calculated induced levels, the operating level, and the voltage induced on the power buses, where applicable. If the margin is adequate to prevent failure, no further analysis of the circuit is needed. For little or no margin, a detailed end-to-end analysis is done to determine whether the sum of the cable impedance and the terminating circuit impedances is adequate to prevent failure by limiting the current in the cable (Figure 11).

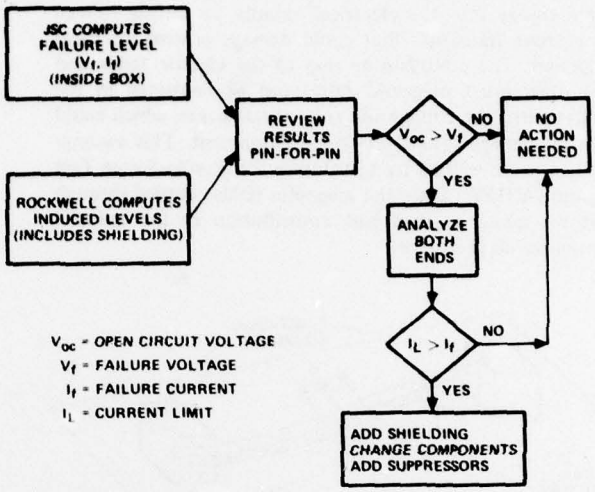

FIGURE 11. ANALYSIS TECHNIQUE

In performing the end-to-end analysis, the total circuit is analyzed, including all terminating impedances, all branch circuit induced voltages, and all interconnected circuits that feed through from another box. Hand calculations of the transient effects are done for simple circuits. More complicated circuits are modeled for time domain transient computer analysis using the Rockwell Electronic Design Analysis Codes Program (REDAC). The transient voltage and current levels versus time across all components can be plotted to provide excellent data for distributed voltages and currents.

If the end-to-end analysis still indicates the probable failure of a Criticality I circuit, measures must be taken to protect the circuit. These methods include multipoint grounded shielding of the wires, adding a dedicated return line, replacing a component with a harder component, adding a transient suppressor or a current limiter, rerouting the wires, or redesigning the circuit.

Multipoint grounded shields provide a path for circulating current that reduces the magnetic field around the wire inside the shield, thereby reducing the open circuit voltage induced in the wire. The most effective shield is a solid conduit or cable tray. A braided shield can also provide adequate shielding effectiveness in most applications with proper grounding procedures. The best methods of grounding are with either a 360-degree connector or a very short external pigtail. Grounding the shield at points other than both ends is necessary on long runs to maintain the shielding effectiveness.

The addition of a dedicated return line, in effect, moves the ground plane nearer to the signal wire. This greatly reduces

the differential loop area of the circuit and the differential induced voltage, as well. The common mode voltage between the total circuit and the ground plane will not be changed by the addition of a dedicated return, however.

A probable circuit failure is often due to one particularly susceptible component. This component can sometimes be replaced by a similar device that is better able to withstand the transient effects of lightning.

A transient suppressor, such as a zener diode, shunting the line immediately inside the box, can protect the circuit by holding the voltage at its zener rating. A current limiting device, such as a resistor, is also effective for limiting the current to a level the circuit can tolerate. The addition of a resistor is particularly useful in the protection of CMOS devices, which can tolerate only low voltages and currents.

If none of the preceding methods are sufficient to protect a circuit from the transients due to lightning, it may be possible to reroute the wires either through a zone with a lower field level or closer to the vehicle structure. As a last alternative, the circuit may need an isolation or protection device inserted in the circuit, or may have to be redesigned.

Recommendations

The lightning design for indirect effects was originally planned to employ a brute-force shielding technique and to verify the design by black-box testing. The first was deleted when the weight impact on the orbiter became excessive. The black-box testing was deleted in favor of a rigorous analysis program. If such analysis were instigated at the start of a program, many dollars would be saved, particularly in the area of testing. It is recommended that the techniques outlined by this paper be used, but that the analysis effort be accomplished by the suppliers of the electronic/electrical equipment. To reduce the cost impact associated with the word "lightning," the analysis should be specified as a square wave pulse input with the voltage levels estimated from a zoned vehicle such as Figure 9. For a worst-case condition in the orbiter, the maximum voltage would be 375 volts for any internal wire run. The OMS pod circuits, being external, could be exposed to more than 50,000 volts, if the wires were not shielded. Other external wiring, such as the elevons and landing gear, could also be subjected to high fields.

CONCLUSIONS

The analysis of the indirect effects of lightning in the orbiter has shown that circuits can be designed to be immune to lightning by using good circuit design techniques, balanced differential circuits, control of wire routing, or addition of components to obtain an adequate margin between the induced energy and failure levels.

Particular care must be used in state-of-the-art circuits, such as CMOS, to identify them early and insure adequate hardness from electrostatic voltages and lightning pulses by short wire runs or high-impedance input circuits.

ACKNOWLEDGMENTS

The authors are indebted to members of the Space Shuttle Lightning Committee, and especially to R.L. Blount, D.L. Suiter, and R.D. Gadbois of NASA JSC, for their technical advice.

REFERENCES

1. Space Shuttle Lightning Protection Criteria Document, JSC 07636, Revision B, National Aeronautics and Space Administration, Lyndon B. Johnson Space Center, Houston, Texas, August 30, 1978.

2. Simulated Lightning Test Shuttle .03 Scale Model, McDonnell Douglas Report MDC A3155, December 1974.

3. Preliminary Evaluation of Space Shuttle Thermal Protection System (TPS) Response to Lightning Strikes, McDonnell Douglas Report, May 11, 1973.

4. Swept Stroke Simulated Lightning Tests, Space Shuttle Thermal Protection System, Lightning and Transients Research Institute, St. Paul, Minn., Report No. 595, December 1974.

5. Artificial Lightning Tests of B-1 Dielectric Composite Panels, Lightning and Transients Research Institute, St. Paul, Minn., Report No. 543, June 1972.

6. APS Graphite Epoxy Skin Panel Lightning Strike Development Test, McDonnell Douglas Test Request No. 073-016.08, February 18, 1976.

7. Ramo, S., Whinnery, J. R., and Van Duzer, T., Fields and Waves in Communication Electronics, John Wiley & Sons, Inc., New York, 1965.

8. Bethe, H. A., "Theory of Diffraction by Small Holes," Phys. Rev., October 1944, pp 163-182.

9. ASTP Simulated Lightning Test Report, JSC 09221, National Aeronautics and Space Administration, Lyndon B. Johnson Space Center, Houston, Texas, November 1974.

A NEW STANDARD FOR LIGHTNING QUALIFICATION TESTING OF AIRCRAFT: TECHNICAL OVERVIEW, DEFINITIONS AND BASIC WAVEFORMS

J. Anderson Plumer
Lightning Technologies, Inc.
560 Hubbard Avenue
Pittsfield, Massachusetts 01201
U.S.A.

SUMMARY

The imperfect lightning-safety record of present-day aircraft, plus the appearance in new aircraft of advanced composite materials and solid state electronic systems that may be even more vulnerable to lightning strikes has led to a demand, from all quarters, for incorporation of improved lightning protection in new aircraft. This may be accomplished, for a new aircraft, in six steps which include: determination of strike zones, establishment of lightning environment, identification of vulnerable components and protection criteria, design of protective measures, and verification of their adequacy by test. The degree of protection achieved is dependent, in part, upon the lightning environment and qualification test criteria employed. In an effort to provide widely accepted criteria representative of a severe environment, Society of Automotive Engineers (SAE) Committee AE4-L (on lightning) and a similar group in UK have prepared documents defining lightning waveforms and testing techniques for aerospace vehicles and hardware. Agreement exists on the criteria to be employed for qualification testing, and the U.S. Committee has drafted a U.S. military standard for lightning qualification testing based on this criteria. This paper summarizes the scope, lightning strike zone definitions and test waveforms presented in the draft standard.

Background

The imperfect lightning-safety record of present-day aircraft, plus the appearance of advanced composite materials and solid state electronic systems that may be even more vulnerable to lightning strikes in the future has led to a demand for incorporation of improved lightning protection in new aircraft. This may be achieved by the following steps:

1. Determine the Lightning Strike Zones

   Determine the aircraft surfaces, or zones, where lightning strike attachment to the aircraft is probable, and the portions of the airframe through which lightning currents must flow between these attachment points.

2. Establish the Lightning Environment

   Establish the component(s) of the total lightning flash current to be expected in each lightning strike zone. These are the currents that must be protected against.

3. Identify Vulnerable Systems or Components

   Identify systems and components that might be vulnerable to interference or damage from either the direct effects (physical damage) or indirect effects (electromagnetic coupling) produced by lightning.

4. Establish Protection Criteria

   Determine the systems and/or components that need to be protected, and those that need not be protected, based upon importance to safety-of-flight, mission reliability or maintenance factors. Establish lightning protection pass-fail criteria for those items to be protected.

5. Design Lightning Protection

   Design lightning protection measures for each of the systems and/or components in need of protection.

6. Verify Protection Adequacy by Test

   Verify the adequacy of the protection designs by laboratory qualification tests simulating the lightning environments established in step 2 using the pass-fail criteria of step 4.

The lightning strike zones (step 1) are usually determined by comparison of the new aircraft with lightning strike experience of earlier aircraft of the same general shape; or by performance of simulated lightning tests on model aircraft. The lightning strike zones of one aircraft determined from a model test (Reference 1) are shown on Figure 1.

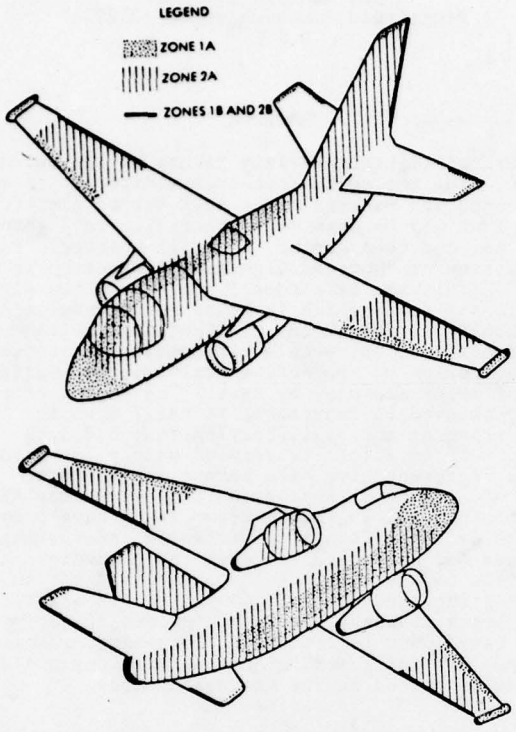

Figure 1 - Typical Lightning Strike Zones.

Until recently, in the absence of a widely accepted standard, the lightning environment expected within each zone (step 2) was designated by individual procuring organizations, or by the lightning laboratory performing the tests, with the result that the degree of protection obtained varied widely from place to place. This was particularly true in the United States, where a number of agencies and laboratories were at work designing lightning protection and performing verification tests.

Identification of potentially vulnerable systems or components (step 3) and protection criteria (step 4) has always been the responsibility of the aircraft designer, although often in consultation with regulatory authorities or lightning laboratory personnel. Design of lightning protective measures (step 5) has also been accomplished by the aircraft designers, with frequent help from specialists in lightning laboratories where potential solutions can be evaluated.

The number and severity of verification tests (step 6) were, like the environment (of step 2) also left for the procuring organization, regulatory authority or lightning laboratory to designate, with the result that laboratory capabilities (and not the natural environment) determined the severity of the tests that would be performed. Inevitably, some disagreement existed among laboratories as to what constituted an appropriate test.

The appearance in the late '60's of advanced composites and microelectronics in aircraft applications placed much greater importance on lightning protection, and emphasized the need for improved, and more widely accepted verification criteria. Prompted by this, a large amount of research was initiated into the nature of lightning and its effects upon the new composite materials and solid-state electronics. A greater understanding of lightning effects resulted, together with improved test and protective techniques. Forums such as the series of Lightning and Static Electricity Conferences beginning in 1968 (References 2, 3, 4 and 5) were created for review of results and exchange of ideas.

The need, however, for widely-accepted criteria with which to verify protection adequacy remained. Accordingly, efforts were begun in the US and the UK toward development of standardized criteria defining lightning voltage and current waveforms, severities, and test techniques for verifying the adequacy of protective measures. In the US, this effort was begun in 1972 with the formation of "Special Task F" under the auspices of the Society of Automotive Engineers (SAE) Committee AE4 on Electromagnetic Compatibility. Special Task F was comprised of 15 individuals from US lightning simulation laboratories, government agencies and aircraft manufacturers with experience in lightning simulation and testing. Beginning with a survey of the extensive literature that had become available, this committee proceeded to define the possible lightning strike zones, the lightning

environment to be experienced in each, and the techniques for simulating this environment in the laboratory. Three years later, the committee published its recommendations in a report entitled, "Lightning Test Waveforms and Techniques for Aerospace Vehicles and Hardware" dated 5 May 1976 (Reference 6). This report (sometimes called the "red book" after its cover) has been in use since 1976 by procuring organizations and lightning test laboratories in the US.

A similar effort was undertaken in the UK, culminating in publication of a "Recommended Practice for Lightning Simulation and Testing Techniques for Aircraft" by J. Phillpott of the Culham Laboratory Lightning Studies Unit in May, 1977 (Reference 7). The current waveforms described in this document have been accepted in the UK for testing aircraft systems, structures and equipment for airworthiness purposes, and are in agreement with the lightning current test criteria in the US "red book". Agreement on this important set of tests resulted from a desire to have mutually acceptable criteria and was achieved from continuing discussion among members of each group over a period of years while these documents were being formulated.

A disparity remained between the US and UK recommendations with respect to model aircraft testing, and also with respect to certain other tests utilized mainly to obtain engineering design data; areas in which some difference among US opinion remained as well. Thus, continuing discussions have been underway among both groups in an effort to resolve the remaining differences and to clarify a few ambiguities turned up during two years of use of the "red book". As a result, the US committee (now designated SAE Committee AE4-L) revised its "red book" as of June 20, 1978 and will shortly publish this document under a blue cover. This "blue book" (Reference 8) will replace the "red book" in the US.

The principal change incorporated in the US "blue book" was the establishment of two categories of tests: qualification testing and engineering testing, and inclusion of all of the protection verification (airworthiness certification) tests within the qualification test category.

The remaining tests, which included the scale model lightning attachment point test, swept stroke test and full vehicle induced voltage test, provide data useful in achieving a qualifiable design but are not considered necessary for protection verification. They are therefore placed within the engineering category. Discussion continues on the validity of several of these engineering tests, and improvements may be possible as research continues. Separation of the tests in this way eases the airworthiness authorities' task of specifying the proper qualification tests, and provides a set of tests upon which wide agreement exists.

The New Military Standard

Upon achievement of this widespread agreement on the lightning environment and test techniques for qualification purposes, the US Dept. of Defense requested SAE Committee AE4-L to draft a military standard incorporating the "blue book" qualification test criteria. This draft, entitled "Lightning Qualification Test Techniques for Aerospace Vehicles and Hardware" (Reference 9) was completed on 20 June 1978.

This new standard defines the lightning strike zones, lightning voltages and currents applicable to each zone, and the methods to be used to test components located in each zone. It is important to note that neither the standard nor the "blue book" that preceded it provide the following:

1. The location of lightning strike zones on a particular aircraft
2. The systems or components that must be tested
3. Protection techniques
4. The pass-fail criteria

These items depend upon the mission and characteristics of the particular aircraft, and should be established and agreed upon by the procuring agency, airworthiness authority and aircraft manufacturer for each new aircraft. Guidance in some of these areas will be provided in a "Users Guide" to be published as an appendix to the new standard in 1979. Further guidance is available in the literature (Reference 10).

The following are excerpts taken directly from the new standard, and discussions, where appropriate, of the definitions and lightning test waveforms incorporated in it.

"3.0 DEFINITIONS

3.1 Lightning Attachment Zones

Aerospace vehicle surfaces are divided into three zones, with each zone having different lightning attachment and/or transfer characteristics. These are defined as follows:

Zone 1: Surfaces of the vehicle for which there is a high probability of initial lightning flash attachment.

Zone 2: Surfaces of the vehicle across which there is a high probability of a lightning flash being swept by the airflow from a Zone 1 point of initial flash attachment."

"Zone 3: Zone 3 includes all of the vehicle areas other than those covered by Zone 1 and Zone 2 regions. In Zone 3 there is a low probability of any direct attachment of the lightning flash arc. Zone 3 areas may carry substantial amounts of electric current but only by conduction between some pair of initial or swept stroke attachment points.

Zones 1 and 2 are further divided into A and B regions depending on the probability that the flash will hang on for any protracted period of time. An A type region is one in which there is low probability that the arc will remain attached and a B type region is one in which there is a high probability that the arc will remain attached. Examples of zones are as follows:

Zone 1A: Initial attachment point with low probability of flash hang-on, such as a leading edge.

Zone 1B: Initial attachment point with high probability of flash hang-on, such as a trailing edge.

Zone 2A: A swept stroke zone with low probability of flash hang-on, such as a wing mid-span.

Zone 2B: A swept stroke zone with high probability of flash hang-on, such as a wing inboard trailing edge."

Note that the above definitions define each zone, but do not provide dimensions or other description of where the zones are located on particular aircraft. Thus the former "18 inch" rule for zone 1 (Reference 11) and similar guidelines have been omitted from the new definitions. The 18-inch dimension may be appropriate for some aircraft, but experience has shown that it is not applicable to all aircraft. Establishment of the zone locations is therefore the first step in design of protection for a new aircraft. Other definitions provided in the new standard are:

"3.2 Direct and Indirect Lightning Effects

The lightning effects to which aerospace vehicles are exposed and the effects which are reproduced through laboratory testing with simulated lightning waveforms are divided into DIRECT EFFECTS and INDIRECT EFFECTS. The DIRECT EFFECTS of lightning are the burning, eroding, blasting, and structural deformation caused by lightning arc attachment, as well as the high-pressure shock waves and magnetic forces produced by the associated high currents. The INDIRECT EFFECTS are predominantly those resulting from the interaction of the electromagnetic fields accompanying lightning, with electrical apparatus in the aircraft. Hazardous indirect effects could in principle be produced by a lightning flash that did not directly contact the aircraft and hence was not capable of producing the direct effects of burning and blasting. However, it is currently believed that most indirect effects of importance will be associated with a direct lightning flash. In some cases both direct and indirect effects may occur to the same component of the aircraft. An example would be a lightning flash to an antenna which physically damages the antenna and also sends damaging voltages into the transmitter or receiver connected to that antenna. In this document the physical damage to the antenna will be discussed as a direct effect and the voltages or currents coupled from the antenna into the communications equipment will be treated as an indirect effect."

Some of the qualification tests address direct effects, whereas others address indirect effects. These definitions clarify the intent of each.

The lightning waveforms presented in the standard are described in terms of time to crest, rate of rise, etc. Definitions of these parameters are also included, as follows:

"3.3 Waveform Parameters

Definitions of the rise time, rate of rise, decay time and other parameters utilized in the waveform definitions that follow are consistent with Paragraphs 2.4 and 2.6 of USA Standard C68.1/IEEE Standard No. 4 Standard Techniques for Dielectric Tests (1978) and High Voltage Test Techniques, IEC 60-2 (1973), Sections 4 and 6.

Average Rate of Rise Voltage

The average rate of rise, dv/dt, of a voltage waveform is defined as the slope of a straight line drawn between the points where the voltage is 30% and 90% of its peak value, as shown in Figure 3-1."

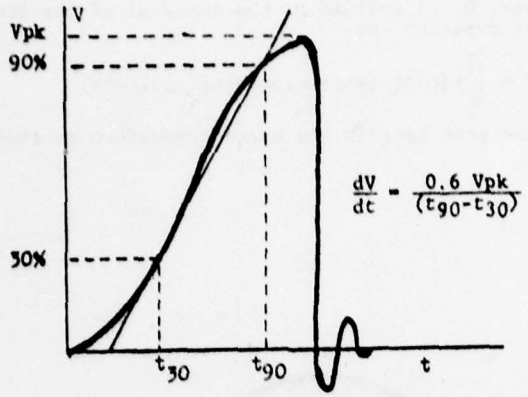

Figure 3-1 Average Rate of Rise of Voltage

Time to Crest

The time to crest, T_1, of a voltage waveform is defined as 1.67 times the time interval between the instants when the voltage is 30% and 90% of its peak value as shown in Figure 3-2.

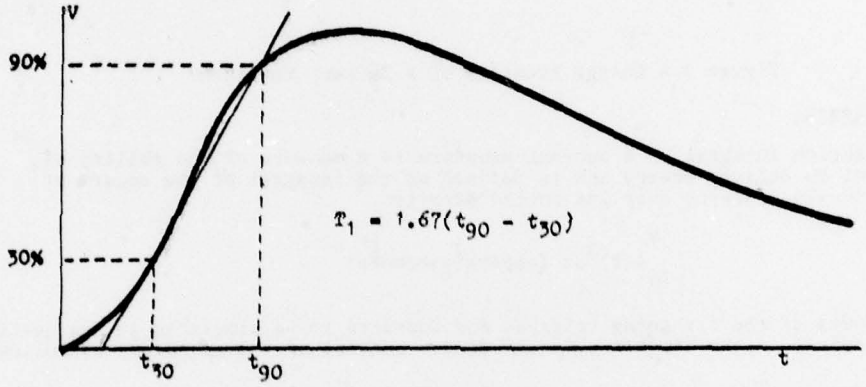

Figure 3-2 Time to Crest of a Voltage Waveform

Decay Time

The decay time, T_2, of a voltage waveform is defined as the time interval between the intersect with the abcissa of a line drawn through the points where the voltage is 30% and 90% of its peak value during its rise, and the instant when the voltage has decayed to 50% of its peak value, as shown on Figure 3-3.

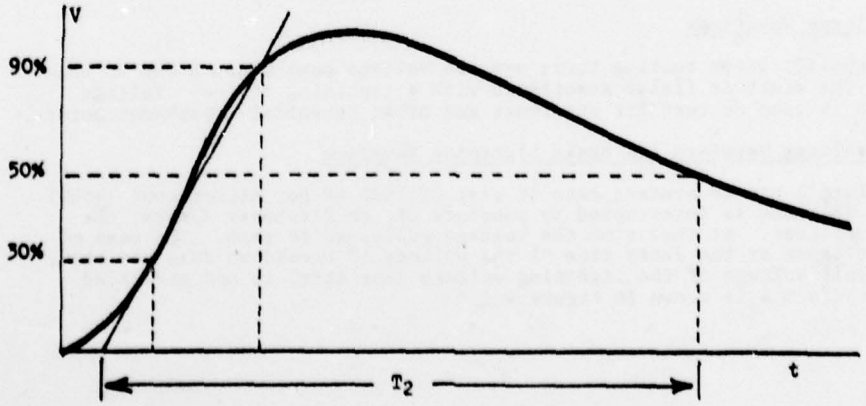

Figure 3-3 Decay Time of a Voltage Waveform

"Charge Transfer

The charge transfer, Q, is defined as the integral of the time-varying current over its entire duration, or

$$Q = \int_0^T i(t)dt \text{ (amp-seconds or coulombs)}$$

and is equivalent to the area beneath the current waveform as shown on Figure 3-4.

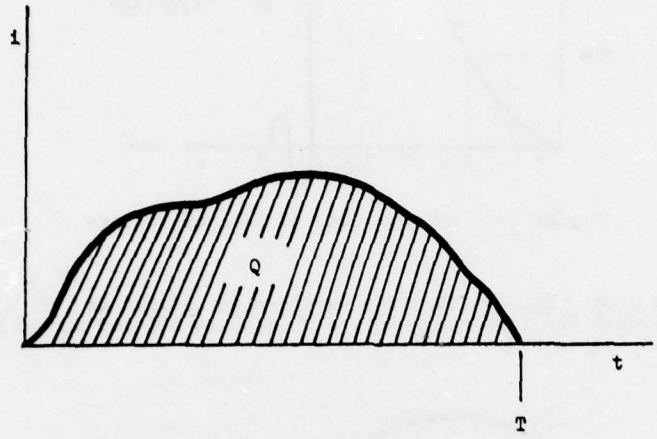

Figure 3-4 Charge Transfer of a Current Waveform.

Action Integral

The action integral of a current waveform is a measure of the ability of the current to deliver energy and is defined as the integral of the square of the time-varying current over its entire duration.

$$\int_0^T i(t)^2 dt \text{ (ampere}^2\text{-seconds)}"$$

The waveforms of the lightning voltages and currents to be simulated in the qualification tests appear in the "Specific Requirements" section of the standard, as follows:

"4.2 Specific Requirements

Waveforms of the simulated lightning currents and voltages to be used in these tests are presented in this section.

4.2.1 Test Waveforms

The waveforms and components depicted in Figures 4-1, 4-2 and 4-3 are idealized representations and need not be simulated exactly. Only the numerical parameters specified in the following paragraphs need be produced.

4.2.2 Voltage Waveforms

For qualification testing there are two voltage waveforms, A and B, which represent the electric fields associated with a lightning strike. Voltage waveform B is used to test for streamers and other potential attachment points.

4.2.2.1 Voltage Waveform A - Basic Lightning Waveform

Waveform A has an average rate of rise of 1000 kV per microsecond (±50%) until its increase is interrupted by puncture of, or flashover across, the object under test. At that time the voltage collapses to zero. The rate of voltage collapse or the decay time of the voltage if breakdown does not occur (open circuit voltage of the lightning voltage generator) is not specified. Voltage waveform A is shown in Figure 4-1."

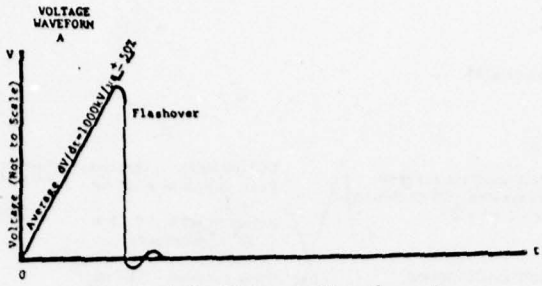

Figure 4-1 Voltage Waveform A

4.2.2.2 Voltage Waveform B - Full Wave

Waveform B rises to crest in 1.2 (±20%) microseconds. Time to crest and decay time refer to the open circuit voltage of the lightning voltage generator, and assume that the waveform is not limited by puncture or flashover of the object under tests. This waveform is shown in Figure 4-2.

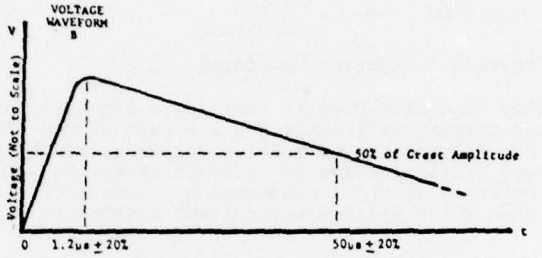

Figure 4-2 Voltage Waveform B

4.2.3 Current Waveforms and Components

For qualification testing, there are four components, A, B, C and D, used for determination of direct effects, and test waveform E used for determination of indirect effects. Components A, B, C and D each simulate a different characteristic of the current in a natural lightning flash and are shown in Figure 4-3. They are applied individually or as a composite of two or more components together in one test. Current waveform E, also shown on Figure 4-3, is intended to determine indirect effects.

4.2.3.1 Component A - Initial High Peak Current

Component A has a peak amplitude of 200 kA (±10%) and an action integral ($\int i^2 dt$) of 2×10^6 amp^2-second (±20%) with a total time duration not exceeding 500 microseconds. This component may be unidirectional or oscillatory.

4.2.3.2 Component B - Intermediate Current

Component B has an average amplitude of 2 kA (±10%) flowing for a maximum duration of 5 milliseconds and a maximum charge transfer of 10 coulombs. The waveform shall be unidirectional, e.g. rectangular, exponential or linearly decaying.

4.2.3.3 Component C - Continuing Current

Component C transfers a charge of 200 coulombs (±20%) in a time of between 0.25 and 1 second. The waveform shall be unidirectional, e.g. rectangular, exponential or linearly decaying.

4.2.3.4 Component D - Restrike Current

Component D has a peak amplitude of 100 kA (±10%) and an action integral of 0.25×10^6 amp^2-second (±20%). This component may be either unidirectional or oscillatory with a total time not exceeding 500 microseconds.

4.2.3.5 Current Waveform E - Fast Rate of Rise Stroke Test for Full-Size Hardware

Current waveform E has an instantaneous rate of rise of at least 25 kA per microsecond for at least 0.5 microsecond, as shown in Figure 4-3. Current waveform E has a minimum amplitude of 50 kA. Alternatively, components A or D may be applied with a 25 kA per microsecond rate of rise for at least 0.5 microsecond and the direct and indirect effects evaluation conducted simultaneously."

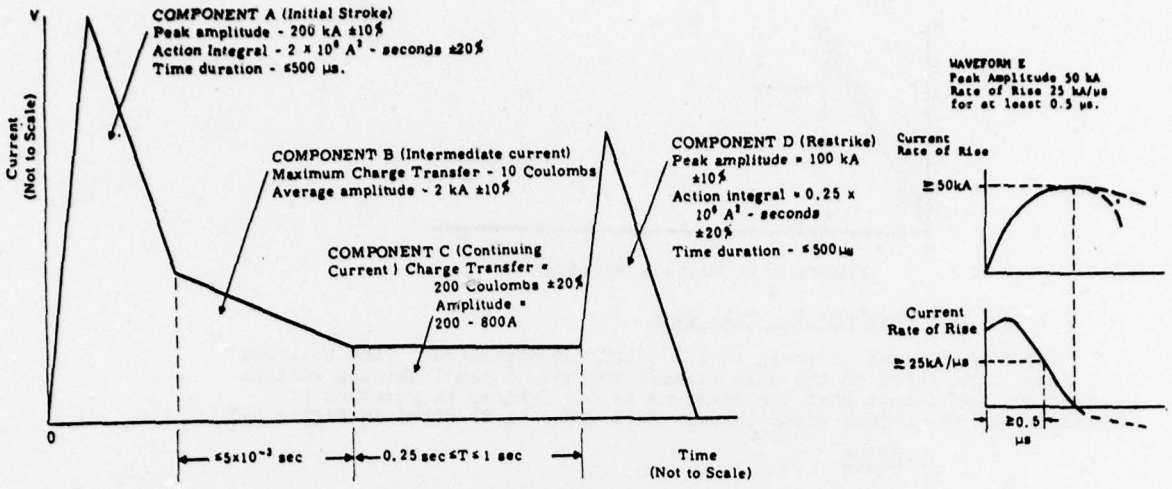

Figure 4-3 Current Waveforms

Since the aircraft is usually in motion when it receives a lightning strike, not all components of the lightning flash current will enter the aircraft at the same point. Surfaces in zone 2A, for example, can be expected to receive only a re-strike and a portion of the continuing current, whereas trailing edges of extremities may be struck initially and have to receive all of the currents as the flash hangs on there until it dies. Accordingly, a table is presented to show which voltage and current components are required in each zone:

Table I - Application of Waveforms for Qualification Tests

		Voltage Waveforms		Current Waveforms/Components					Test
Test	Zone	A	B	A	B	C	D	E	Method
Full size hardware attachment point	1A, B	X							102
Direct effects-structural	1A			X	X				301
"	1B			X	X	X	X		301
"	2A				X[1]	X[1]	X		301
"	2B				X	X	X		301
"	3			X		X			301
Direct effects-combustible vapor ignition	Same current components as for structural tests								302
Direct effects-streamers			X						303
Indirect effects-external electrical hardware								X[2]	401

Note 1: Use an average current of 2 kA ± 10% for the actual dwell time up to 5 msec, and an average current of 400 amps for the remaining dwell time.

Note 2: Indirect effects should also be measured with current components A, B, C or D as appropriate to the test zone."

The test methods (identified by number 102, 301, etc.) in which these waveforms are applied are also listed in Table I.

Severity

Current Components A, B, C, D and E, taken together represent a severe lightning flash, one that is exceeded in action integral only about 1% of the time (Reference 12). It is akin to the "Severe (applied) model" of a lightning flash proposed by Cianos and Pierce (Reference 13). The statistical data against which this comparison is made, of course, was derived from measurements of lightning currents entering grounded objects. There is some reason to believe that, statistically, current amplitudes and action integrals would be somewhat lower at flight altitudes due to branching and higher source impedances. If this is so, the probability of encountering a flash of greater severity than the new-standard criteria would be even less than 1%.

Superseded Documents

If adopted by the US Dept. of Defense, the lightning test criteria in the standard will supersede those in present US military procurement specifications and test standards. These include:

MIL-B-5087B (ASG) - Bonding, Electrical, and Lightning Protectior for Aerospace Systems

MIL-A-9094D (ASG) - Arrester, Lightning General Specification For

MIL-C-38373A (ASG) - Cap, Fluid Filler

Future editions of these and specifications for other hardware in need of lightning tests will make reference to the new standard for lightning tests. It is expected that a similar situation will apply to US Civil (FAA) airworthiness certifiction requirements.

Conclusion

Preparation of the "blue book" and "green book" criteria for lightning testing of aircraft, achievement of widespread US and UK agreement on its validity, and preparation of the new standard that resulted from it represent a significant advancement in the resources available to provide reliable lightning protection for aircraft. This advancement did not come about quickly nor was it accomplished by only a few individuals. It was instead the product of a cooperative effort of many individuals on both sides of the Atlantic. This author wishes to thank all who participated in this effort, and looks forward to continued cooperation in the future.

References

1. H. Knoller and J.A. Plumer, "S-3A Lightning Protection Program: Lightning Effects Analysis", paper included in the 1975 Lightning and Static Electricity Conference Proceedings,. Culham Laboratory, England, April 1975.

2. 1968 Lightning and Static Electricity Conference Proceedings, Miami Beach, Florida, U.S. Air Force Avionics Laboratory TR-68-290, Part II, May 1969.

3. 1970 Lightning and Static Electricity Conference Proceedings, San Diego, California, USA, December 1970.

4. 1972 Lightning and Static Electricity Conference Proceedings, Las Vegas, Nevada, U.S. Air Force Avionics Laboratory TR-72-325, December 1972.

5. 1975 Lightning and Static Electricity Conference Proceedings, Culham Laboratory, England, April 1975.

6. "Lightning Test Waveforms and Techniques for Aerospace Vehicles and Hardware", report of Society of Automotive Engineers (SAE) Committee AE4 on Electromagnetic Compatibility, Special Task F, May 1976.

7. J. Phillpott, "Recommended Practice for Lightning Simulation and Testing Techniques for Aircraft", United Kingdom Atomic Energy Authority Report, CLM-R163, May 1977.

8. "Lightning Test Waveforms and Techniques for Aerospace Vehicles and Hardware", report of SAE Committee AE4L, June 1978

9. "Lightning Qualification Test Techniques for Aerospace Vehicles and Hardware", proposed military standard, SAE Committee AE4L, 20 June 1978.

10. F.A. Fisher and J.A. Plumer, "Lightning Protection of Aircraft", National Aeronautics and Space Administration Reference Publication 1008, October 1977.

11. "Protection of Aircraft Fuel Systems Against Lightning", Federal Aviation Advisory Circular No. AC 20-53.

12. N. Cianos and E.T. Pierce, "A Ground-Lightning Environment for Engineering Use", Technical Report 1, prepared by the Stanford Research Institute for McDonnell Douglas Company, August 1972, p. 91.

13. Cianos and Pierce, pp. 82-93.